REPORT DOCUMENTATION PAGE

Form Approved
OMB No. 0704-0188

PLEASE DO NOT RETURN YOUR FORM TO THE ABOVE ADDRESS.

1. REPORT DATE *(DD-MM-YYYY)*	2. REPORT TYPE	3. DATES COVERED *(From - To)*
08-08-2007	Biannual Technical Report	12/08/2006 - 6/30/2007

4. TITLE AND SUBTITLE

Bi-annual (12/8/2006--6/30/2007) Performance/Technical Report
for ONR Award under Grant N00014-07-1-0395
Studies on Radar Sensor Networks

5a. CONTRACT NUMBER

5b. GRANT NUMBER
N00014 – 07 –1 –0395

5c. PROGRAM ELEMENT NUMBER

6. AUTHOR(S)
Liang, Qilian

5d. PROJECT NUMBER

5e. TASK NUMBER

5f. WORK UNIT NUMBER

7. PERFORMING ORGANIZATION NAME(S) AND ADDRESS(ES)
University of Texas at Arlington
Office of Sponsored Projects
PO Box 19145
Arlington, TX 76019

8. PERFORMING ORGANIZATION REPORT NUMBER

9. SPONSORING/MONITORING AGENCY NAME(S) AND ADDRESS(ES)
Office of Naval Research
875 N. Randolph St.
One Liberty Center
Arlington, VA 22203-1995

10. SPONSOR/MONITOR'S ACRONYM(S)
ONR

11. SPONSOR/MONITOR'S REPORT NUMBER(S)

12. DISTRIBUTION/AVAILABILITY STATEMENT
Approved for Public Release; Distribution is Unlimited.

13. SUPPLEMENTARY NOTES

14. ABSTRACT

During the period of 12/8/2006 -- 6/30/2007, we performed the following studies in radar sensor network:
1. Sense-through-foliage target detection using UWB radar sensor network based on real-world data; 2. Foliage clutter modeling using UWB radars; 3. Outdoor UWB channel modeling based on field data; 4. Multi-target detection using radar sensor networks (theoretical studies); 5. SVD-QR and graph theory for MIMO channel selection; 6. Image fusion using radar sensor network; 7. Performance analysis of energy detection for cognitive radio wireless networks; 8. Superimposed code based channel assignment in multi-radio multi-channel wireless mesh networks.

15. SUBJECT TERMS

Radar Sensor Network, UWB Radar, Sense through foliage, Automatic Target Recognition, outdoor UWB channel, clutter modeling.

16. SECURITY CLASSIFICATION OF:			17. LIMITATION OF ABSTRACT	18. NUMBER OF PAGES	19a. NAME OF RESPONSIBLE PERSON
a. REPORT	b. ABSTRACT	c. THIS PAGE			Qilian Liang
U	U	U	UU	144	19b. TELEPHONE NUMBER *(Include area code)* 817-272-1339

Bi-annual (12/8/2006–6/30/2007) Performance/Technical Report for ONR Award under Grant N00014-07-1-0395 Studies on Radar Sensor Networks

Qilian Liang
Department of Electrical Engineering
University of Texas at Arlington
Arlington, TX 76019-0016 USA
Phone: 817-272-1339, Fax: 817-272-2253
E-mail: liang@uta.edu

Abstract

During the period of 12/8/2006 – 6/30/2007, we performed the following studies in radar sensor network:

1. Sense-through-foliage target detection using UWB radar sensor network based on real-world data;
2. Foliage clutter modeling using UWB radars;
3. Outdoor UWB channel modeling based on field data;
4. Multi-target detection using radar sensor networks (theoretical studies);
5. SVD-QR and graph theory for MIMO channel selection;
6. Image fusion using radar sensor network;
7. Performance analysis of energy detection for cognitive radio wireless networks;
8. Superimposed code based channel assignment in multi-radio multi-channel wireless mesh networks.

1 Sense-through-Foliage Target Detection using UWB Radar Sensor Network

In [1], we proposed a Discrete-Cosine-Transform (DCT)-based approach for sense-through-foliage target detection when the echo signal quality is good, and a Radar Sensor Network (RSN) and DCT-based approach when the echo signal quality is poor. A RAKE structure which can combine the echos from different cluster-members was proposed for clusterhead in the RSN. We compared our approach with the ideal case when both echos are available, i.e., echos with target and without target. We also compared our approach against the scheme in which 2-D image was created via adding voltages with the appropriate time offset. Simulation results show that our DCT-based scheme works much better than the existing approach, and our RSN and DCT-based approach can be used for target detection successfully while even the ideal case fails to do it. In [3], we generalized the RAKE structure and propose waveform diversity combining and maximum likelihood (ML)-ATR algorithms for nonfluctuating target as well as fluctuating target. In [4], a differential based approach was proposed for sense-through-foliage target detection.

2 Foliage Clutter Modeling Using UWB Radars

In [5], we proved that the amplitude of foliage clutter follows log-logistic model using maximum likelihood (ML) parameter estimation as well as the root mean square error (RMSE) on PDF curves between original clutter and statistical model data. We not only investigate log-logistic model, but compare it with other popular clutter models, namely log-normal, weibull and nakagami. It shows that log-logistic model not only achieves the smallest standard divination (STD) error on estimated model parameters, but also the best goodness-of-fit and smallest RMSE for both poor and good clutter signals.

3 Outdoor UWB Channel Modeling Based on Field Data

In [2], we studied the statistical modeling for outdoor Ultra-WideBand (UWB) channel in rich scattering and time-varying environment based on extensive data collected using UWB radar. We validated that UWB echo signals (within a burst) dont hold self-similarity, which means the future signals cant be forecasted based on the current received signals and channel modeling is necessary from statistical point of view. In outdoor UWB channel, the multipath contributions arrive at the receiver are grouped into clusters. The time of arrival of clusters can be modeled as a Poisson arrival process, while within each cluster, subsequent multipath contributions or rays also arrive according to a Poisson process. At different field (near field, medium field, and far field), we observe that the Poisson process parameters are quite different. We also observe that the amplitude of channel coefficient at each path follows Rician distribution for medium and far field, and its non-stationary for paths from near field (one of two Rician distributions), and these observations are quite different with the IEEE indoor UWB channel model and S-V model.

4 Multi-target Detection Using Radar Sensor Networks

In many military and civilian applications, estimating the number of targets in a region of interest plays a primary role in performing important tasks such as target localization, classification, recognition, tracking, etc. Such an estimation problem is however very challenging since the number of targets is time-varying, targets state is fluctuating, and many kinds of targets might appear in the field of interest. In [6], we developped a framework for estimating the number of targets in a sensing area using Radar Sensor Networks (RSNs): (1) we formulated the multi-target detection problem; (2) we modelled signals, interference (e.g., clutter, jamming, and interference between radars), and noise at radar sensors; (3) we proposed a Maximum Likelihood Multi-Target Detection (MLMTD) algorithm to combine received measurements and estimate the number of targets present in the sensing area. We evaluated multi-target detection performance using RSNs in terms of the probability of miss detection PMD and the root mean square error (RMSE). Simulation results showed that multi-target detection performance of the RSNs is much better than that of single radar systems.

In [7], we investigated the problem of jointly classifying and identifying multiple targets in radar sensor networks where the maximum number of categories and the maximum number of targets in each category are obtained a priori based on statistical data. However, the actual number of targets in each category and the actual number of target categories being present at any given time are assumed unknown. It is assumed that a given target belongs to one category and one identification number. The target signals are modeled as zero-mean complex Gaussian processes. We propose a joint multi-target identification and classification (JMIC) algorithm for radar surveillance using

cognitive radars. The existing target categories are first classified and then the targets in each category are accordingly identified. Simulation results are presented to evaluate the feasibility and effectiveness of the proposed JMIC algorithm in a query surveillance region.

5 SVD-QR and Graph Theory for MIMO Channel Selection

In [8], we presented Singular-Value Decomposition- QR with Threshold (SVD-QR-T) algorithm to select a subset of channels in virtual MIMO wireless sensor networks (WSN) in order to reduce its complexity and cost. SVD-QR-T selects best subset of transmitters while keeping all receivers active. The threshold is adaptive by means of Fuzzy C-Mean (FCM). Under the constraint of the same total transmission power, this approach is compared against the case without channel selection in terms of capacity, bit error rate (BER) and multiplexing gain in the presence of water-filling as well without. It is shown that in spite of less multiplexing gain, when water-filling is applied, SVD-QR-T FCM provides lower BER at moderate to high SNR; in case of equal transmission power allocation, SVD-QR-T FCM achieves higher capacity at low SNR and lower BER. In general, it provides satisfying performances compared to the case without channel selection but reduced cost and resource. In [9], we propsed Maximum Spanning Tree Searching (MASTS) algorithm on a basis of graph theory to select a set of subchannels, which consequently reduce the complexity and cost of full virtual MIMO while providing network layer connection for all sensors. The performances are analyzed through Monte Carlo simulation in terms of capacity with/without water-filling, diversity gain and multiplexing gain. It is shown that MASTS virtual MIMO can achieve satisfying performances compared to those of full virtual MIMO.

In [10], the above two approaches were compared against the case without channel selection in terms of capacity, bit error rate (BER) and multiplexing gain in the presence of water-filling as well as the circumstance of without water-filling under the same total transmission power constraint. Despite less multiplexing gain, when water-filling is applied, MASTS achieves higher capacity and lower BER than virtual MIMO without channel selection at moderate to high SNR while SVD-QR-T FCM provides the lowest BER at high SNR; in case of no water-filling and equal transmission power allocation, MASTS still offers the highest capacity at moderate to high SNR but SVD-QR-T FCM achieves the lowest BER. Both algorithms provide satisfying performances compared to the case without channel selection but reduced cost and resource.

6 Image Fusion Using Radar Sensor Network

Owning to Rician fading and white gaussian noise, the scattered back image signal of radar sensors would be distorted to some extend. In [11], we applied two schemes named Equal Gain Combination (EGC) and Maximal Ration Combination (MRC) respectively for RSN image fusion. Simulation results show that image fusion by means of MRC can provide much better image quality based on both minimum mean squared error (MMSE) and the mean of structural similarity (MSSIM) index if the channel estimation offers satisfying channel side information at receiver (CSIR). However, EGC itself does not require any channel estimation scheme and thus more simple to implement. In [12], we considerred cross-layer design for image transmission in wireless sensor networks. We combined application layer, MAC layer and physical layer together. According to analysis and simulation, high priority service will achieve better PSTR performance. Low priority service achieve better performance at the first stage, and it become worse later. The application level QoS is a tradeoff with the energy consumption between high priority service and low priority service.

7 Some Other Studies on Non-Radar Sensor Networks

7.1 Performance Analysis of Energy Detection for Cognitive Radio Wireless Networks

While energy detection has been extensively studied in the past, hidden terminal and exposed node problems are ignored through assuming that the environment is same for transmitters and receivers. In [13], this paper, considering hidden terminal and exposed node problems, we make a theoretical analysis on the performance of commonly used energy detection methods, such as ideal method, transmitter-independent method and transmitter/receiver-cooperated method, in terms of detection probability. Corresponding ana- lytical models are provided. Performance theoretical curves are acquired to compare the characteristics for individual energy detection methods under various scenarios. Moreover the upper bound for detection probability is achieved and is compared under various system traffic intensity and sensing capability. From the theoretical results, we found that it is easy to correctly detection the channel status when primary systems are heavily occupied for ideal energy detection method and tansmitter/receiver-cooperated energy detection method. Otherwise, transmitter-independent method is a better scheme to monitor the primary systems. Commonly, increasing the sensitivity of secondary users can upgrade the detection performance. However, in our analysis, it is not true for transmitter-independent method and transmitter/receriver-cooperated method under certain situations. We have concluded those special cases in this paper. Therefore, the theoretical results can supply a reference on the choosing of energy detection method according to system scenario, such as traffic load, sensing capability, etc.

7.2 Superimposed Code based Channel Assignment in Multi-radio Multi-channel Wireless Mesh Networks

Motivated by the observation that channel assignment for multiradio multi-channel mesh networks should support both unicast and local broadcast1, should be interference-aware, and should result in low overall switching delay, high throughput, and low overhead, in [14], we proposed two flexible localized channel assignment algorithms based on s-disjunct superimposed codes. These algorithms support the local broadcast and unicast effectively, and achieve interference-free channel assignment under certain conditions. In addition, under the primary interference constraints2, the channel assignment algorithm for unicast can achieve 100% throughput with a simple scheduling algorithm such as the maximal weight independent set scheduling, and can completely avoid hidden/exposed terminal problems under certain conditions. Our algorithms make no assumptions on the underlying network and therefore are applicable to a wide range of MR-MC mesh network settings. We conduct extensive theoretical performance analysis to verify our design.

References

[1] Q. Liang, S. Samn, "Sense-through-Foliage Target Detection Using DCT and UWB Radar Sensor Networks," to be submitted to *IEEE Trans on Aerospace and Electronic Systems.*

[2] Q. Liang, S. Samn, "Outdoor UWB Channel Modeling in Rich Scattering and Time-Varying Environment," to be submitted to *IEEE Trans on Wireless Communications.*

[3] Q. Liang, "NEW-CATR: Network-enabled Electronic Warfare for Collaborative Automatic Target Recognition," accepted by *IEEE Military Communication Conference*, Oct 2007, Orlando, FL.

[4] J. Liang, Q. Liang, and S. Samn, "A Differential Based Approach for Through-Foliage Target Detection using UWB Radar Sensor Networks," to be submitted to *IEEE ICASSP 2008.*

[5] J. Liang, Q. Liang, and S. Samn, "Foliage Clutter modeling Using UWB Radar," to be submitted to *IEEE Trans on Aerospace and Electronic Systems.*

[6] H. Ly, Q. Liang, "Collaborative Multi-Target Detection in Radar Sensor Networks," accepted by *IEEE Military Communication Conference*, Oct 2007, Orlando, FL.

[7] H. Le, Q. Liang, "Joint Multi-target Identification and Classification in Cognitive Radar Sensor Networks," to be submitted to *IEEE ICASSP 2008.*

[8] J. Liang and Q. Liang, "SVD-QR-T FCM Approach for Virtual MIMO Channel Selection in Wireless Sensor Networks," presented at *IEEE International Conference on Wireless Algorithms, Systems, and Applications*, August 2008, Chicago, IL.

[9] J. Liang and Q. Liang, "A Graph Theory Algorithm for Virtual MIMO Channel Selection in Wireless Sensor Networks," to be submitted to *IEEE ICC 2008.*

[10] J. Liang and Q. Liang, "Channel Selection Algorithms in Virtual MIMO Wireless Sensor Networks," submitted to *IEEE Trans on Wireless Communications.*

[11] J. Liang and Q. Liang, "Image Fusion on Radar Sensor Networks," accepted by *International Conference on Heterogeneous Networking for Quality, Reliability, Security and Robustness (Qshine), Workshop on Mobile Content Quality of Experience*, Vancouver, Canada, August 2007.

[12] X. Xia and Q. Liang, "Cross-Layer Design for Image Transmission in Wireless Sensor Networks," to be submitted to *IEEE ICC 2008.*

[13] Q. Ren and Q. Liang, "Performance Analysis of Energy Detection for Cognitive Radio Wireless Networks," presented at *IEEE International Conference on Wireless Algorithms, Systems, and Applications*, August 2008, Chicago, IL.

[14] K. Xing, X. Cheng, L. Ma, and Q. Liang, "Superimposed Code Based Channel Assignment in Multi-Radio Multi-Channel Wireless Mesh Networks," accepted by *ACM MobiCom 2007*, Montreal, QC, Canada, Sept 2007.

Sense-through-Foliage Target Detection Using DCT and UWB Radar Sensor Networks

Qilian Liang
Department of Electrical Engineering
University of Texas at Arlington
Arlington, TX 76019-0016, USA
E-mail: liang@uta.edu

Sherwood W. Samn
Air Force Research Laboratory/HEX
Brooks City Base
San Antonio, TX 78235, USA
E-mail: Sherwood.samn@brooks.af.mil

Abstract— **In this paper, we propose a Discrete-Cosine-Transform (DCT)-based approach for sense-through-foliage target detection when the echo signal quality is good, and a Radar Sensor Network (RSN) and DCT-based approach when the echo signal quality is poor. A RAKE structure which can combine the echos from different cluster-members is proposed for clusterhead in the RSN. We compared our approach with the ideal case when both echos are available, i.e., echos with target and without target. We also compared our approach against the scheme in which 2-D image was created via adding voltages with the appropriate time offset. Simulation results show that our DCT-based scheme works much better than the existing approach, and our RSN and DCT-based approach can be used for target detection successfully while even the ideal case fails to do it.**

I. Introduction and Motivation

Forests and buildings favor asymmetric threats because the warfighter has a limited sensing capability. Forest and buildings provide excellent concealment from observation, ambush, and escape, as well as provide secure bases for enemy Command & Control (C2), weapons caches, and Improvised Explosive Device (IED)/ Weapon of Mass Destruction (WMD) assembly. These have become "the high ground" in fourth-generation warfare, providing a significant strategic advantage. We believe that solving the sense-through-foliage target detection will significantly benefit sense-through-wall and other subsurface sensing problems. The objective of this paper is to develop measurable advances in improving the understanding of intelligence for the forest conflict using UWB radar. The key focus of this study is to develop advanced technologies that make foliage transparent, thereby eliminating the safe harbor that forest provides to hostile forces and their malicious activities. Sense-through-foliage target detection resulting from this research will benefit emerging Department of Defense (DoD) net-centric warfare programs.

In this paper, we will apply our expertise in signal processing, data fusion, sensor networks, etc to achieve effective sense-through-foliage technology using ultra-wideband (UWB) radar. UWB radar emissions are at a relatively low frequency-typically between 100 MHz and 3 GHz. Additionally, the fractional bandwidth of the signal is very large (greater than 0.2). Such radar sensor has exceptional range resolution that also has an ability to penetrate many common materials (e.g., walls). Law enforcement personnel have used UWB ground penetrating radars (GPRs) for at least a decade. Like the GPR, sense-through-foliage radar takes advantage of UWB's very fine resolution (time gating) and low frequency of operation. In the existing works on UWB radar/sensor based target detection, Time Domain Inc has invented UWB radars, and some algorithms for target detection were overviewed in [11]; these are mainly based on target response signal strength (1-D) and different copies of signals to construct 2-D features. The Adaptive Polarization-Difference Imaging (APDI) algorithm and PDI technique [8][9] were originally developed for optical imaging and in many situations can provide significant enhancements in target detection and feature extraction over conventional methods. In [12], these two techniques were applied to transient time-domain microwave signals with particular applications in through-wall microwave imaging (TWMI). In [10], a chaos-based high-resolution imaging technique was applied to through-the-wall imaging, but no detection algorithm was presented. In this paper, we are interested in investigating more features from sense through foliage signals and extracting as much information as possible for data fusion.

The rest of this paper is organized as follows. In Section II, we summarize the measurement and collection of data we used in this paper. In Section III, we propose a discrete-cosine-transform (DCT) based approach for sense-through-foliage target detection with good signal quality. In Section IV, we propose a radar sensor network (RSN) and DCT-based approach for sense-through-foliage target detection when the signal quality is poor. We conclude this paper and discuss some future research topics in Section V.

II. Sense-through-Foliage Data Measurement and Collection

Our work is based on the sense-through-foliage data collected by Virtual Machines LLC supported by Air

Force [3]. The foliage penetration measurement effort began in August 2005 and continued through December 2005. The measurements were taken on the grounds of Virtual Machines Company in Holliston, Massachusetts. Working in August through the fall of 2005, the foliage measured included late summer foliage and fall and early winter foliage. Late summer foliage, because of the limited rainfall, involved foliage with decreased water content. Late fall and winter measurements involved largely defoliated but dense forest.

The foliage experiment was constructed on a seven-ton man lift, which had a total lifting capacity of 450 kg. The limit of the lifting capacity was reached during the experiment as essentially the entire measuring apparatus was placed on the lift. The principle pieces of equipment secured on the lift are: Barth pulser, Tektronix model 7704 B oscilloscope, dual antenna mounting stand, two antennas, rack system, IBM laptop, HP signal Generator, Custom RF switch and power supply and Weather shield (small hut). The target is a trihedral reflector (as shown in Fig. 1). Throughout this work, a Barth pulse source (Barth Electronics, Inc. model 732 GL) was used. The pulse generator uses a coaxial reed switch to discharge a charge line for a very fast rise time pulse outputs. The model 732 pulse generator provides pulses of less than 50 picoseconds (ps) rise time, with amplitude from 150 V to greater than 2 KV into any load impedance through a 50 ohm coaxial line. The generator is capable of producing pulses with a minimum width of 750 ps and a maximum of 1 microsecond. This output pulse width is determined by charge line length for rectangular pulses, or by capacitors for 1/e decay pulses.

Fig. 1. The target (a trihedral reflector) is shown on the stand at 300 feet from the lift.

For the data we used in this paper, each sample is spaced at 50 picosecond interval, and 16,000 samples were collected for each collection for a total time duration of 0.8 microseconds at a rate of approximately 20 Hz. We considered two sets of data from this experiment. Initially, the Barth pulse source was operated at low amplitude and 35 pulses reflected signal were averaged for each collection. Significant pulse-to-pulse variability was noted for these collections. The scheme for the sense-through-foliage target detection with "poor" signal quality will be presented in Section IV. Later, good signal quality data were collected using higher amplitude pulses and 100 pulses reflected signals were averaged for each collection. The scheme for target detection with "good" signal quality will be presented in Section III.

III. Sense-through-Foliage Target Detection with Good Signal Quality: A DCT-based Approach

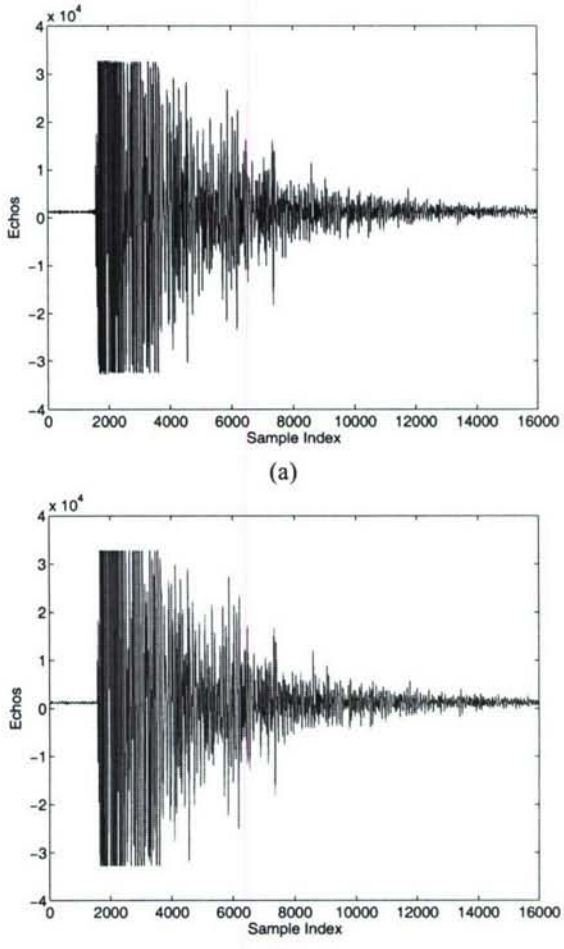

Fig. 2. Measurement with very good signal quality and 100 pulses average. (a) No target on range, (b) with target on range (target appears at around sample 14,000).

In Fig. 2, we plot two collections with good signal quality, one without target on range (Fig. 2a) and the

other one with target on range (Fig. 2b and target appears at around sample 14,000). To make it more clear to the readers, we provide expanded views of traces (with target) from sample 13,001 to 15,000 for the above two collections in Figs. 3a and 3b. Since there is no target in Fig. 3a, it can be treated as the response of foliage clutter. It's quite straightfoward that the target response will be the echo difference between Fig. 3b and Fig. 3a, which is plotted in Fig. 3c. However, it's impossible to obtain Fig. 3a (clutter echo) in practical situation if there is target on range. The challenge is how to make target detection based on Fig. 3b (with target) or Fig. 3a (no target) only?

Observe Fig. 3b, for samples where target appears (around sample 14,000), the sample strength changes much abruptly than that in Fig. 3a, which means echo from target contains more AC values than that without target. Motivated by this, we applied Discrete Cosine Transform (DCT) to the echos $x(iM+n)$ $(n = 0, 1, 2, \cdots, N-1)$ where N is the DCT window length, M is the step size of each DCT window, and i is the window index. Let $x(n,i) \triangleq x(iM+n)$

$$X(K,i) = \sum_{n=0}^{N-1} x(n,i) \cos(\frac{2\pi}{N} nK) \tag{1}$$

then we cumulate the power of AC values (for $K > 2$)

$$P(i) = \sum_{K=3}^{N-1} X(K,i)^2 \tag{2}$$

For $N = 100$ and $M = 10$, we plot the power of AC values $P(i)$ versus iM (time domain sample index) in Figs. 4a and 4b for the above data sets in Figs. 3a and 3b respectively. Observe that in Fig. 4b, the power of AC values (around sample 14,000) where the target is located is non-fluctuating (monotonically increase then decrease). Although some other samples also have very high AC power values, it is very clear that they are quite fluctuating and the power of AC values behave like random noise because generally the clutter has Gaussian distribution in the frequency domain [2].

We compared our DCT-based approach to the scheme proposed in [11]. In [11], 2-D image was created via adding voltages with the appropriate time offset. In Figs. 5a and 5b, we plot the 2-D image created based on the above two data sets (from samples 13,800 to 14,200). However, it's not clear which image shows there is target on range.

IV. Sense-through-Foliage Target Detection with Poor Signal Quality: A Sensor Network and DCT-based Approach

As mentioned in Section II, when the Barth pulse source was operated at low amplitude and the sample values are not obtained based on sufficient pulse response averaging (averaged over 35 pulses for each collection), significant pulse-to-pulse variability was noted and the return signal quality is poor. In Figs. 6a and 6b, we plot two collections with poor signal quality. Fig. 6a has no target on range, and Fig. 6b has target at samples around 14,000. We plot the echo differences between Figs. 6a and 6b in Fig. 6c. However, it is impossible to identify whether there is any target and where there is target based on Fig. 6c. We observed the DCT-based approach failed to detect target based on one collection. Since significant pulse-to-pulse variability exists in the echos, this motivate us to explore the spatial and time diversity using Radar Sensor Networks (RSN).

In RSN, the radar sensors are networked together in an ad hoc fashion. They do not rely on a preexisting fixed infrastructure, such as a wireline backbone network or a base station. They are self-organizing entities that are deployed on demand in support of various events surveillance, battlefield, disaster relief, search and rescue, etc. Scalability concern suggests a hierarchical organization of radar sensor networks with the lowest level in the hierarchy being a cluster. As argued in [6] [5] [4] [7], in addition to helping with scalability and robustness, aggregating sensor nodes into clusters has additional benefits:

1) conserving radio resources such as bandwidth;
2) promoting spatial code reuse and frequency reuse;
3) simplifying the topology, e.g., when a mobile radar changes its location, it is sufficient for only the nodes in attended clusters to update their topology information;
4) reducing the generation and propagation of routing information; and,
5) concealing the details of global network topology from individual nodes.

In RSN, each radar can provide their pulse parameters such as timing to their clusterhead radar, and the clusterhead radar can combine the echos (RF returns) from the target and clutter. In this paper, we propose a RAKE structure for combining echos, as illustrated by Fig. 7. The integration means time-average for a sample duration T and it's for general case when the echos are not in discrete values. It is quite often assumed that the radar sensor platform will have access to Global Positioning Service (GPS) and Inertial Navigation Unit (INU) timing and navigation data [1]. In this paper, we assume the radar sensors are synchronized in RSN. In Fig. 7, the echo, i.e., RF response by the pulse of each cluster-member sensor, will be combined by the clusterhead using a weighted average, and the weight w_i is determined by the power of each echo $x_i(n)$ (n is the sample index),

$$w_i = \frac{E_i}{\sum_{i=1}^{M} E_i} \tag{3}$$

and

$$E_i = \text{var}(x_i(n)) + [\text{mean}(x_i(n))]^2 \quad (4)$$

We ran simulations for $M = 30$, and plot the power of AC values in Figs. 8a and 8b for the two cases (with target and without target) respectively. Observe that in Fig. 4b, the power of AC values (around sample 14,000) where the target is located is non-fluctuating (monotonically increase then decrease). Although some other samples also have very high AC power values, it is very clear that they are quite fluctuating and the power of AC values behaves like random noise because generally the clutter has Gaussian distribution in the frequency domain.

V. Conclusions and Future Works

In this paper, we proposed a DCT-based approach for sense-through-foliage target detection when the echo signal quality is good, and a sensor network and DCT-based approach when the echo signal quality is poor. A RAKE structure which can combine the echos from different cluster-members is proposed for clusterhead in the RSN. We compared our approach with ideal case when both echos are available, i.e., echos with target and without target. We also compared our approach against the scheme in which 2-D image was created via adding voltages with the appropriate time offset. Simulation results show that our DCT-based scheme works much better than the existing approach, and our RSN and DCT-based approach can be used for target detection successfully while the ideal case fails to do it. For future works, we will collect more data with different targets and perform automatic target recognition besides target detection.

Acknowledgement

This work was supported by ONR under Grant N00014-07-1-0395 and N00014-03-1-0466 and AFOSR Summer Faculty Fellowship Program Award.

References

[1] ONR BAA 07-017, "NET-SENTRIC Surveillance," http://www.onr.navy.mil/02/baa/.

[2] D. K. Barton, *Radar System Analysis and Modeling*, Artech House, Boston, MA, 2006.

[3] C. Dill, "Foliage Penetration (Phase II) Field Test: Narrowband versus Wideband Foliage Penetration," *Final Report of Contract Number F41624-03-D-7001/04*, July 2005 to Feb 2006.

[4] T.-C. Hou and T-J. Tsai, " An access-based clustering protocol for multihop wireless ad hoc networks," *IEEE J. Selected Areas in Communications*, vol. 19, no. 7, pp. 1201-1210, July 2001.

[5] A. Iwata, C. C. Chiang, G. Pei, M. Gerla, and T. W. Chen, " Scalable routing strategies for ad hoc networks," *IEEE J. Selected Areas in Communications*, vol. 17, pp. 1369-1379, 1999.

[6] C. R. Lin and M. Gerla, "Adaptive clustering in mobile wireless networks," *IEEE J. Selected Areas in Communications*, vol. 16, pp. 1265-1275, 1997.

[7] C. E. Perkins, "Chapter 4, Cluster-Based Networks," *Ad Hoc Networking*, Edited by C. E. Perkins, pp. 75-138, Addison-Wesley, 2001.

[8] M. P. Rowe, E. N. Pugh, Jr., J. S. Tyo, and N. Engheta, "Polarization-difference imaging: a biologically inspired technique for observation through scattering media," *Optics Letters*, Vol. 20, pp. 608-610, 1995.

[9] J. S. Tyo, M. P. Rowe, E. N. Pugh, Jr., N. Engheta, "Target detection in optically scattering media by polarization difference imaging," *Applied Optics*, Vol. 35, pp. 1855-1870, 1996.

[10] V. Venkatasubramanian and Henry Leung, "A Novel Chaos-Based High-Resolution Imaging Technique and Its Application to Through-the-Wall Imaging," *IEEE Signal Proc Letters*, Vol. 12, No. 7, July 2005.

[11] P. Withington , H. Fluhler, and S. Nag , "Enhancing homeland security with advanced UWB sensors," *IEEE Microwave Magazine*, Sept 2003.

[12] K. M. Yemelyanov, J. A. McVay, N. Engheta, A. Hoorfar, "Adaptive Polarization-Difference Imaging Algorithms for Through-the-Wall Microwave Imaging Scenarios," *Proc. IEEE AP-S Int. Symposium and USNC/URSI National Radio Science Meeting*, July 3-6, 2005, Washington DC, USA.

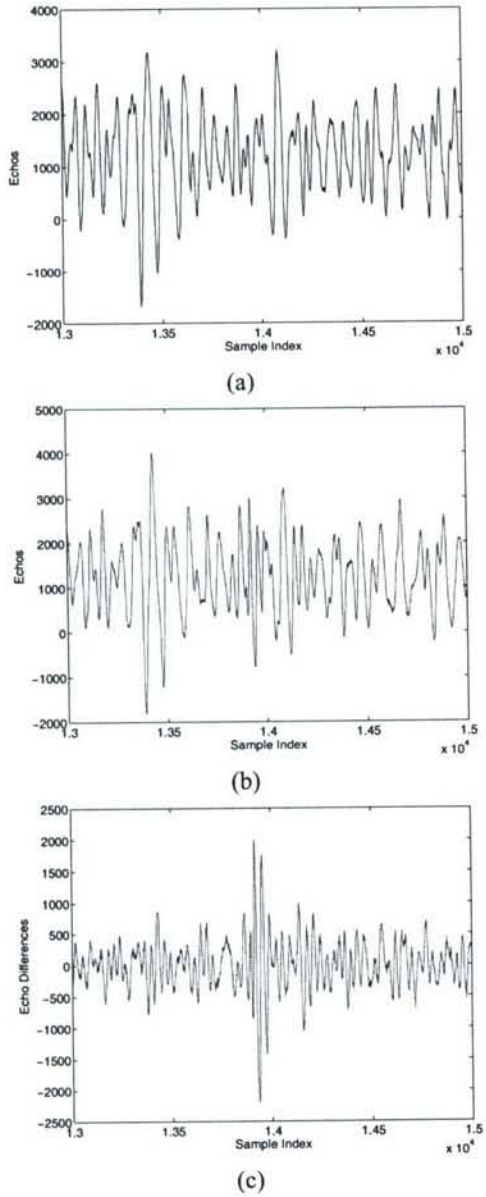

Fig. 3. Measurement with very good signal quality and 100 pulses average. (a) Expanded view of traces (with target) from samples 13,001 to 15,000. (b) Expanded view of traces (without target) from samples 13,001 to 15,000. (c) The differences between (a) and (b).

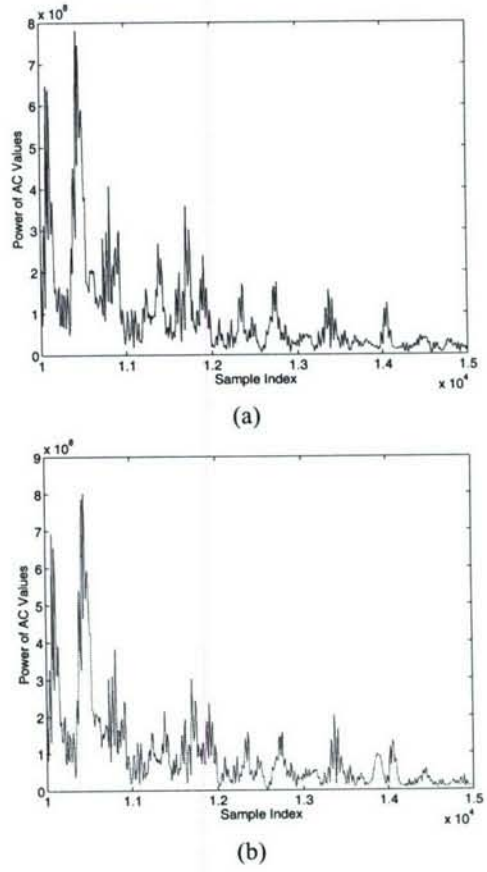

Fig. 4. The power of AC values versus sample index. (a) No target (b) With target in the field.

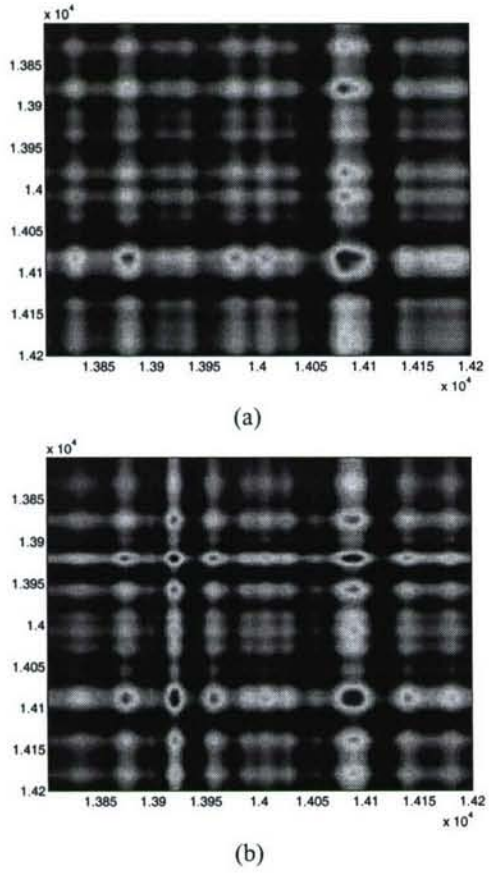

(a)

(b)

Fig. 5. 2-D image created via adding voltages with the appropriate time offset. (a) No target (b) With target in the field.

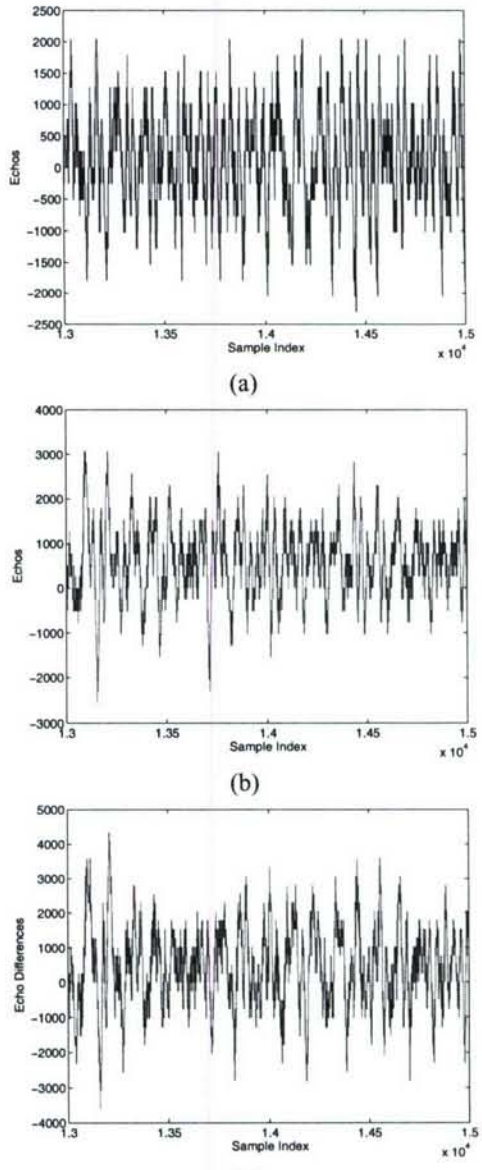

(a)

(b)

(c)

Fig. 6. Measurement with poor signal quality and 35 pulses average. (a) Expanded view of traces (no target) from sample 13,001 to 15,000. (b) Expanded view of traces (with target) from sample 13,001 to 15,000. (c) The differences between (a) and (b).

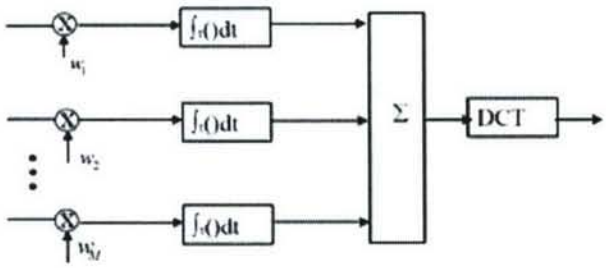

Fig. 7. Echo combining by clusterhead in RSN.

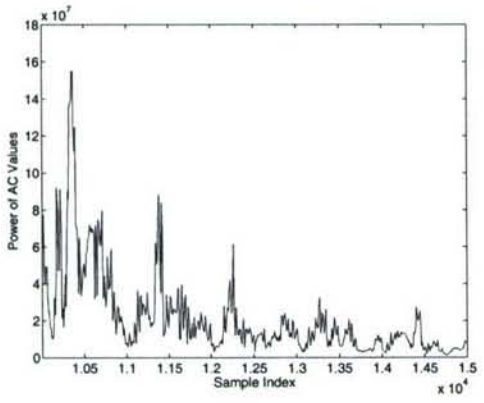

(a)

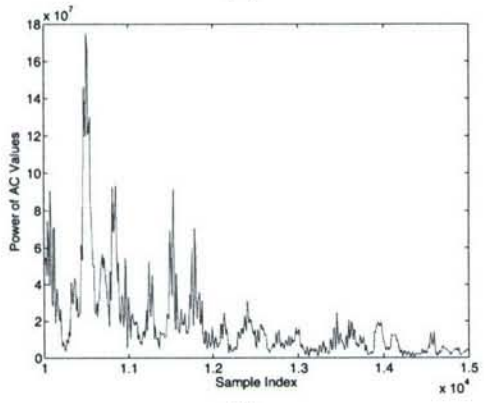

(b)

Fig. 8. Power of AC values based on UWB radar sensor networks and DCT based approach. (a) No target (b) With target in the field.

Outdoor UWB Channel Modeling in Rich Scattering and Time-Varying Environment

Qilian Liang
Department of Electrical Engineering
University of Texas at Arlington
Arlington, TX 76019-0016, USA
E-mail: liang@uta.edu

Sherwood W. Samn
Air Force Research Laboratory/HEX
Brooks City Base
San Antonio, TX 78235, USA
E-mail: Sherwood.samn@brooks.af.mil

Abstract— **In this paper, we study the statistical modeling for outdoor Ultra-WideBand (UWB) channel in rich scattering and time-varying environment based on extensive data collected using UWB radar. We validate that UWB echo signals (within a burst) don't hold self-similarity, which means the future signals can't be forecasted based on the current received signals and channel modeling is necessary from statistical point of view. In outdoor UWB channel, the multipath contributions arrive at the receiver are grouped into clusters. The time of arrival of clusters can be modeled as a Poisson arrival process, while within each cluster, subsequent multipath contributions or rays also arrive according to a Poisson process. At different field (near field, medium field, and far field), we observe that the Poisson process parameters are quite different. We also observe that the amplitude of channel coefficient at each path follows Rician distribution for medium and far field, and it's non-stationary for paths from near field (one of two Rician distributions), and these observations are quite different with the IEEE indoor UWB channel model and S-V model.**

I. Introduction and Motivation

In July 2003, the Channel Modeling sub-committee of study group IEEE 802.15.SG3a published the final report regarding the UWB indoor multipath channel model [4]. It is a modified version of the indoor Saleh and Valenzuela (S-V) channel model [6]. The IEEE suggested an initial set of values for the indoor UWB channel model which has range less than 10 meters. However, lots of applications of UWB are for outdoor activities such as sense-through-foliage target detection. Forests favor asymmetric threats because the warfighter has a limited sensing capability. Forests provide excellent concealment from observation, ambush, and escape, as well as provide secure bases for enemy Command & Control (C2), weapons caches, and Improvised Explosive Device (IED)/ Weapon of Mass Destruction (WMD) assembly. These have become "the high ground" in fourth-generation warfare, providing a significant strategic advantage. Unfortunately, no work has been done on the outdoor UWB channel modeling.

In this paper, we will model the outdoor UWB channel model in rich scattering and time-varying environment such as in sense-through-foliage application using UWB radar. UWB radar emissions are at a relatively low frequency-typically between 100 MHz and 3 GHz. Additionally, the fractional bandwidth of the signal is very large (greater than 0.2). Such radar sensor has exceptional range resolution that also has an ability to penetrate many common materials (e.g., walls). Law enforcement personnel have used UWB ground penetrating radars (GPRs) for at least a decade. Like the GPR, sense-through-foliage radar takes advantage of UWB's very fine resolution (time gating) and low frequency of operation.

The rest of this paper is organized as follows. In Section II, we summarize the measurement and collection of data we used in this paper. In Section III, we demonstrate that the UWB reflected signal in foliage environment does not hold self-similarity, and validate that outdoor channel modeling is necessary. In Section IV, we give an overview on indoor UWB channel model. In Section V, we present our outdoor UWB channel model in rich scattering and time-varying environment. We conclude this paper in Section VI.

II. Experiment Setup and Data Collection

Our work is based on the UWB radar-based sense-through-foliage data collection by Virtual Machines LLC supported by Air Force [2]. The foliage penetration measurement effort began in August 2005 and continued through December 2005. The measurements were taken on the grounds of Virtual Machines Company in Holliston, Massachusetts. Working in August through the fall of 2005, the foliage measured included late summer foliage and fall and early winter foliage. Late summer foliage, because of the limited rainfall, involved foliage with decreased water content. Late fall and winter measurements involved largely defoliated but dense forest, so it's a rich scattering environment. Because of wind or different temperature in dense forest, it's also a time-varying environment.

The UWB radar-based experiment was constructed on a seven-ton man lift, which had a total lifting capacity

of 450 kg. The limit of the lifting capacity was reached during the experiment as essentially the entire measuring apparatus was placed on the lift (as shown in Fig. 1). The principle pieces of equipment secured on the lift are: Barth pulser, Tektronix model 7704 B oscilloscope, dual antenna mounting stand, two antennas, rack system, IBM laptop, HP signal Generator, Custom RF switch and power supply and Weather shield (small hut). Throughout this work, a Barth pulse source (Barth Electronics, Inc. model 732 GL) was used. The pulse generator uses a coaxial reed switch to discharge a charge line for a very fast rise time pulse outputs. The model 732 pulse generator provides pulses of less than 50 picoseconds (ps) rise time, with amplitude from 150 V to greater than 2 KV into any load impedance through a 50 ohm coaxial line. The generator is capable of producing pulses with a minimum width of 750 ps and a maximum of 1 microsecond. This output pulse width is determined by charge line length for rectangular pulses, or by capacitors for 1/e decay pulses.

Fig. 1. This figure shows the lift with the experiment. The antennas are at the far end of the lift from the viewer under the roof that was built to shield the equipment from the elements. This picture was taken in September with the foliage largely still present. The cables coming from the lift are a ground cable to an earth ground and one of 4 tethers used in windy conditions.

For the data we used in this paper, each sample is spaced at 50 picosecond interval, and 16,000 samples were collected for each collection for a total time duration of 0.8 microseconds at a rate of approximately 20 Hz. The Barth pulse source was operated at low amplitude and 35 pulses reflected signal were averaged for each collection. Significant pulse-to-pulse variability was noted for these collections. We plot the transmitted pulse (one realization) in Fig. 2a) and the received echos in one collection in Fig. 2b (averaged over 35 pulses).

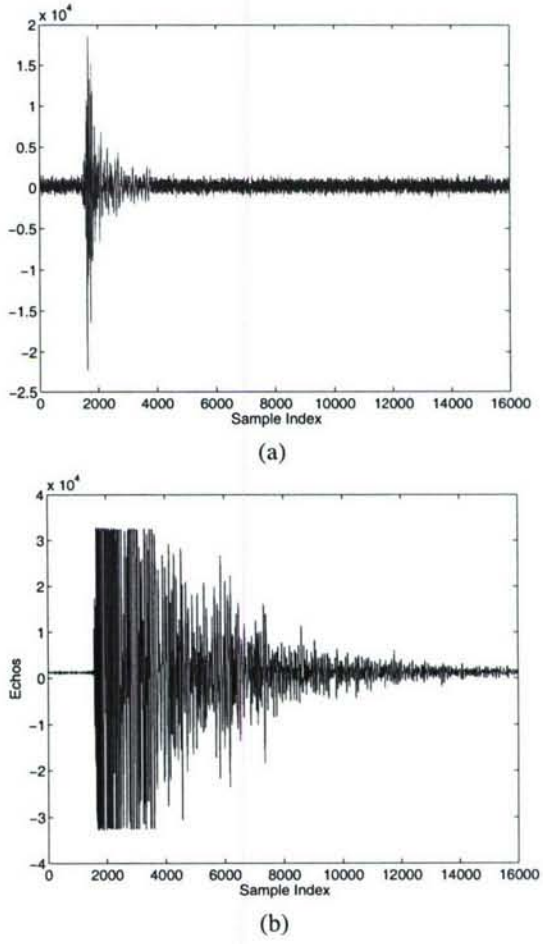

Fig. 2. Transmitted pulse and received echos in one experiment. (a) Transmitted pulse. (b) Received echos.

III. Self-Similarity Properties of UWB Reflected Signals

Recently, it has been observed that ethernet video/voice/data traffic have self-similarity [5] [3] [8]. According to Stallings [7], "Self-similarity is such an important concept that, in a way, it is surprising that only recently has it been applied to data communications traffic analysis.", and "Since 1993, a number of studies reported in the literature have documented that the pattern of data traffic is well modeled by self-similar processes in a wide variety of real-world networking situations." Such self-similarity is quite common in both natural and human-made phenomena [7] such as the distribution of earthquakes, ocean waves, fluctuation of the stock market. But the self-similarity of UWB signals has not been studied.

For a detailed discussion on self-similarity in time-series, see [8] [7]. Here we briefly present its definition [1]. Given a zero-mean, stationary time-series $X = (X_t; t = 1, 2, 3, \cdots)$, we define the m-aggregated series $X^{(m)} = (X_k^{(m)}; k = 1, 2, 3, \cdots)$ by summing the original series X over nonoverlapping blocks of size m. Then it's said that X is H-self-similar, if, for all positive m, $X^{(m)}$ has the same distribution as X rescaled by m^H. That is,

$$X_t \stackrel{\Delta}{=} m^{-H} \sum_{i=(t-1)m+1}^{tm} X_i \quad \forall m \in N \tag{1}$$

If X is H-self-similar, it has the same autocorrelation function $r(k) = E[(X_t - \mu)(X_{t+k} - \mu)]/\sigma^2$ as the series $X^{(m)}$ for all m, which means that the series is distributionally self-similar: the distribution of the aggregated series is the same as that of the original.

Self-similar processes can show *long-range dependence*. A process with long-range dependence has an autocorrelation function $r(k) \sim k^{-\beta}$ as $k \to \infty$, where $0 < \beta < 1$. The degree of self-similarity can be expressed using *Hurst* parameter $H = 1 - \beta/2$. For self-similar series with long-range dependence, $1/2 < H < 1$. As $H \to 1$, the degree of both self-similarity and long-range depence increases.

One method that has been widely used to verify self-similarity is the *variance-time plot*, which relies on the slowly decaying variance of a self-similar series. The variance of $X^{(m)}$ is plotted against m on a log-log plot, and a straight line with slope $(-\beta)$ greater than -1 is indicative of self-similarity, and the parameter H is given by $H = 1 - \beta/2$. We use this method in this paper. In Fig. 3, we plot the variance of $X^{(m)}$ against m on a log-log plot for 10 different UWB data collections. From this figure, it's very clear that **the UWB signal does not has self-similarity** because its trace has slope lower than -1. This conclusion means that we can't use current received signals to forecast future reflected signals within one collection, so channel modeling is very important to UWB outdoor channel because the charateristics of the future reflected signal could be known in advance if its channel can be modelled.

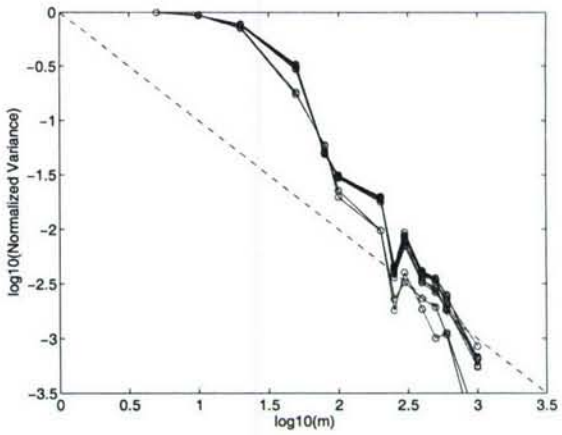

Fig. 3. The *variance-time* plot of 10 UWB data collections, which demonstrates that UWB reflected signals are not self-similar within each collection.

IV. Introduction to Channel Modeling for Indoor UWB Channel

In the S-V model [6], the arrival of clusters is modelled as a Poisson arrival process with a rate Λ, while within each cluster, subsequent multipath contributions or rays also arrive according to a Poisson process with a rate λ (see Fig. 4). In the S-V model, the magnitude of the k-th path within the l-th cluster follows a Rayleigh distribution, and the phase of each path is assumed to be a statistically independent random variable over $[0, 2\pi)$. Besides, the average Power Decay Profile (PDP) is characterized by an exponential decay of the amplitude of the clusters, and a different exponential decay for the amplitude of the received pulses within each cluster, as shown in Fig. 5. In the IEEE UWB indoor channel model [4], the cluster approach was adopted (same as S-V model), but a log-normal distribution was suggested for characterizing the multi-path gain amplitude, and an additional log-normal variable was introbuced for representing the fluctuations of the total multipath gain. Besides, the phase of each path is assumed to be either 0 or π with equal probability.

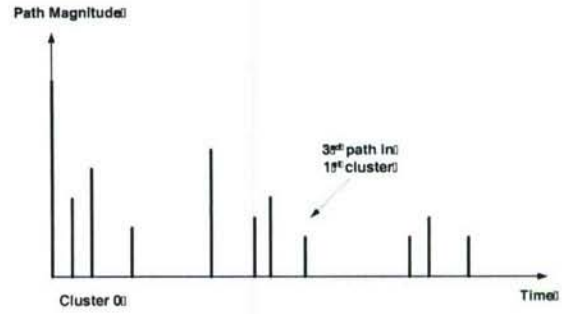

Fig. 4. An illustration of the channel impulse response in S-V model.

V. Outdoor UWB Channel Modeling

A. Cluster Arrival and Power Decay Profile

We study the outdoor UWB signal propagation in three cases: near field (less than $55m$), medium field ($55m$–$85m$), and far field (above $85m$ and up to $120m$ in this study). In the data collection, each sample is spaced at 50 picosecond interval, so these cases are corresponding to samples 1–7333 for near field, samples 7333–11333 for

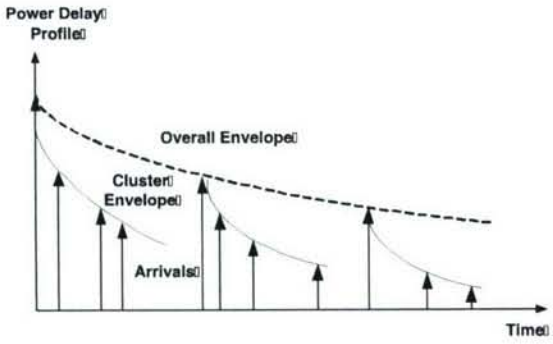

Fig. 5. An illustration of the double exponential decay of the mean cluster power and the ray power within clusters in S-V model.

medium field, and samples 11334–16000 for far field. In Fig. 6, we plot the power profile of the received echos (averaged over 30 collections to eliminate the effect of random noise and each collection was averaged based on 35 pulses) for the three different cases. Since the transmitted pulse (as plotted in Fig. 2a) is a very narrow impulse pulse (like a delta function in time domain), we analyzed the channel property based on the received echos power profile plotted in Fig. 6, and similar methodology was also used in S-V model studies [6].

Observe Fig. 6, multi-path contributions arrive at the receiver grouped into clusters. The time of arrival of clusters can be modeled as a Poisson arrival process with a rate Λ, while within each cluster, subsequent multipath contributions or rays also arrive according to a Poisson process with a rate λ (see Fig. 4). We define:

- T_l = the arrival time of the first path of the l-th cluster;
- $\tau_{k,l}$ = the delay of the k-th path within the l-th cluster relative to the first path arrival time T_l;
- Λ = the cluster arrival rate;
- λ = the ray arrival rate, i.e., the arrival rate of the paths within each cluster.

By definition, we have $\tau_{0l} = T_l$. The distributions of the cluster arrival time and the ray arrival time are given by

$$p(T_l|T_{l-1}) = \Lambda \exp\left(-\Lambda(T_l - T_{l-1}), l > 0\right)$$
$$p(\tau_{k,l}|\tau_{(k-1),l}) = \lambda \exp\left(-\lambda(\tau_{k,l} - \tau_{(k-1),l})\right), k > 0 \quad (2)$$

The above observations are very similar as that for the indoor UWB channel. Specifically, we also observed the Λ and λ are quite different for three different cases.

- Observe Fig. 6a for near field, Λ (1/ns) is around 0.02 (one cluster in every $50ns$ or 1000 samples), and λ (1/ns) is around 0.4 (one path in every $2.5ns$ or 50 samples). Perhaps it's because some major scatters in near field (such as tree stems) reflected signals, so some paths are quite dominant.
- Observe Fig. 6b for medium field, clusters arrive quite often. Λ (1/ns) is around 0.05 (one cluster in every $20ns$ or 400 samples), and λ (1/ns) is around 1 (one path in every $1ns$ or 20 samples).
- Observe Fig. 6c for far field, clusters almost always arrive (because of rich scattering), so Λ (1/ns) is around 0.5 (one cluster in every $2ns$ or 20 samples), and λ (1/ns) is around 4 (one path in every $250ps$ or 5 samples). Perhaps it's because of rich scattering, every path has very similar power level.

Besides, the average PDP can be represented by an exponential decay of the amplitude of the clusters, and a different exponential decay for the amplitude of the received pulses within each cluster, as shown in Fig. 5.

B. Statistical Distribution of Channel Coefficients

We also study the statistical distributions of each given path. We plot the histogram for some sample values of the above three cases based on 30 collections and each collection is averaged over 35 pulses. Near field samples are based on samples 5001–6000; medium field samples are based on samples 8001–9000; and far field samples are based on samples 12001–13000. Since the samples are very close (within 7.5m distance), so their path-loss effect can be ignored. For each case, we have 30000 samples, and we plot their histogram in Fig. 7.

First, observe Fig. 7c for far field, the histogram can be almost perfectly modelled by a non-zero-mean Gaussian distribution, which means the amplitude of the channel coefficient follows a Rician distribution,

$$p_\alpha(x) = \frac{x}{\sigma^2} \exp\{-\frac{x^2 + s^2}{2\sigma^2}\} I_0(\frac{xs}{\sigma^2}) \quad x \geq 0 \quad (3)$$

where s is the mean value of Gaussian and $I_0(\cdot)$ is the zero order modified Bessel function. This kind of channel is known as Rician fading channel. A Rician channel is characterized by two parameters, Rician factor K which is the ratio of the direct path power to that of the multipath, i.e., $K = s^2/2\sigma^2$, and the Doppler spread (or single-sided fading bandwidth) f_d. Similarly, Fig. 7b for medium field, the histogram can be approximately modelled by a non-zero-mean Gaussian distribution, which means the amplitude of the channel coefficient follows a Rician distribution. Observe Fig. 7a for near field, the histogram can be approximately modelled by two non-zero-mean Gaussian distributions, which means it's non-stationary, and the amplitude of the channel coefficient follows one of two Rician distributions. **The above observations are quite different with the indoor UWB channel model (log-normal distribution) and S-V model (Rayleigh distribution)**. The sign of channel coefficient is either +1 or -1, i.e., its phase is either 0 or π, which matches the IEEE indoor UWB channel model.

VI. Conclusions

In this paper, we studied the statistical modeling for outdoor UWB channel in rich scattering and time-varying environment based on extensive data collected using UWB radar. We validated that UWB echo signals (within a burst) don't hold self-similarity, which means the future signals can't be forecasted based on the received signals and channel modeling is necessary from statistical point of view. In outdoor UWB channel, the multi-path contributions arrive at the receiver are grouped into clusters. The time of arrival of clusters can be modeled as a Poisson arrival process, while within each cluster, subsequent multipath contributions or rays also arrive according to a Poisson process. At different field (near field, medium field, and far field), we observed that the Poisson process parameters are quite different. We also observed that the amplitude of channel coefficient at each path follows Rician distribution for medium and far field, and it's non-stationary for paths from near field (one of two Rician distributions), and these observations are quite different with the IEEE indoor UWB channel model and S-V model.

Acknowledgement

This work was supported by ONR under Grant N00014-07-1-0395 and N00014-03-1-0466 and AFOSR Summer Faculty Fellowship Program Award.

References

[1] M. E. Crovella and A. Bestavros, "Self-similarity in world wide web traffic: evidence and possible causes," *IEEE Trans. on Networking*, vol. 5, no. 6, pp. 835-846, Dec 1997.

[2] C. Dill, "Foliage Penetration (Phase II) Field Test: Narrowband versus Wideband Foliage Penetration," *Final Report of Contract Number F41624-03-D-7001/04*, July 2005 to Feb 2006.

[3] M. W. Garrett and W. Willinger, "Analysis, modeling and generation of self-similar VBR video traffic," *SIGCOMM'94*, pp. 269-280, Aug. 1994, London, UK.

[4] IEEE 802.15.SG3a, "Channel modeling sub-committee report final," *IEEE P802.15-02/490r1-SG3a*, Feb 2003.

[5] W. E. Leland, M. S. Taqqu, W. Willinger, and D. V. Wilson, " On the self-similar nature of ethernet traffic," *IEEE Trans. on Networking*, vol. 2, no. 1, pp. 1-15, Feb 1994.

[6] A. A. Saleh and R. A. Valenzuela, "A statistical model for indoor multipath propagation," *IEEE J. on Selected Areas in Communications*, vol. 5, no. 2, pp. 128-137, Feb 1987.

[7] W. Stallings, *High-Speed Networks: TCP/IP and ATM Design Principles*, Upper Saddle River, NJ, 1998.

[8] W. Willinger, M. S. Taqqu, R. Sherman, and D. V. Wilson, "Self-similarity through high-variability: statistical analysis of ethernet LAN traffic at the source level," *IEEE Trans. on Networking*, vol. 5, no. 1, pp. 71-86, Feb 1997.

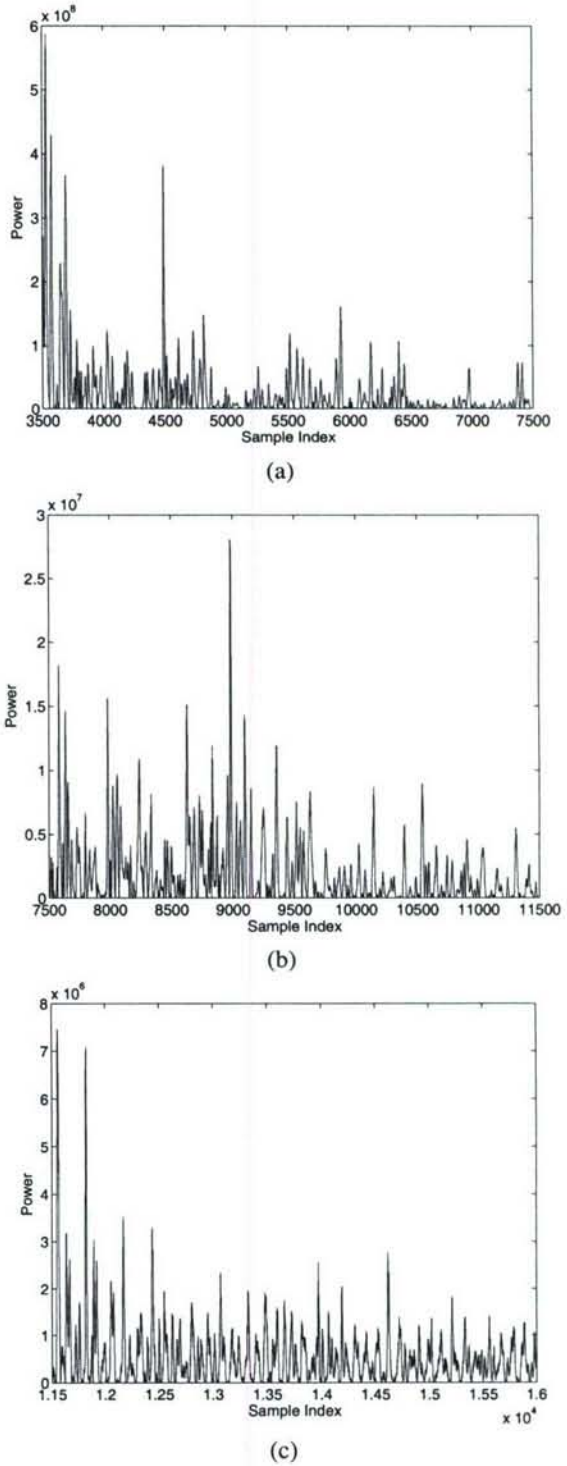

Fig. 6. The power profile for three different cases: (a) near field, (b) medium field, and (c) far field.

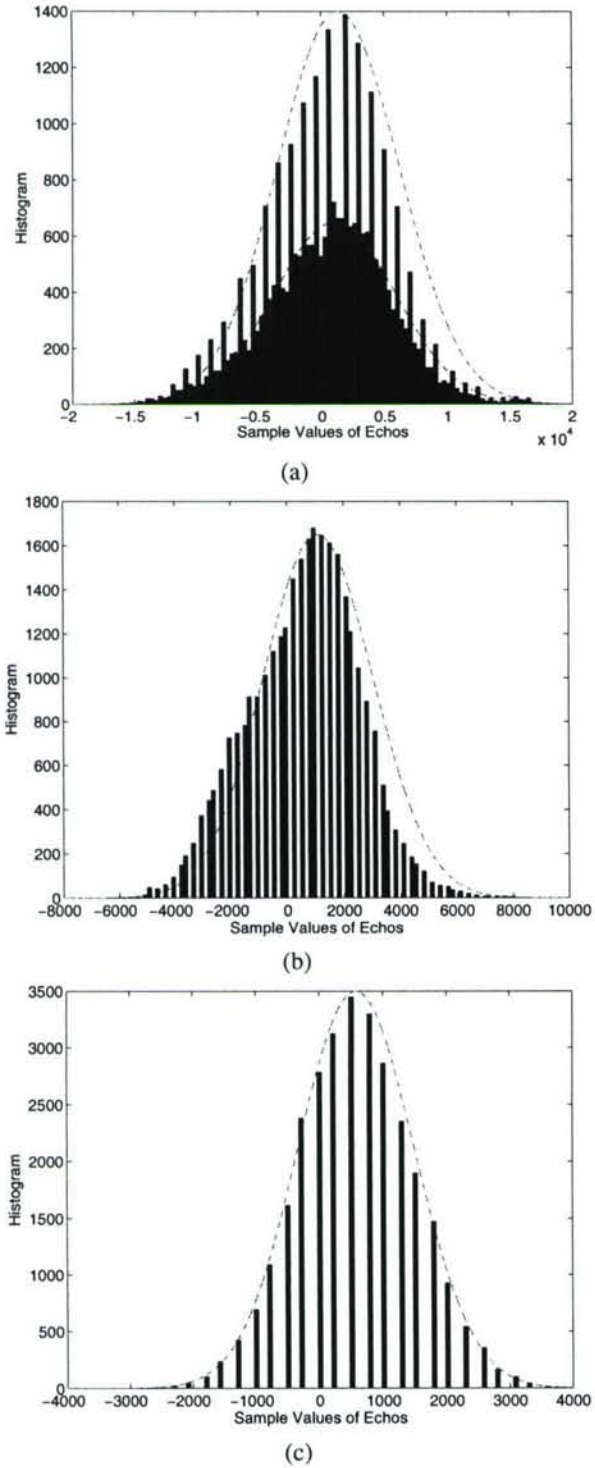

Fig. 7. The histograms and their approximation using Gaussian distributions (dashed lines). The histograms are based on 30 collections and each collection is averaged over 35 pulses. (a) near field samples, (b) medium field samples, and (c) far field samples.

NEW-CATR: Network-enabled Electronic Warfare for Collaborative Automatic Target Recognition

Qilian Liang
Dept of Electrical Engineering
University of Texas at Arlington
Arlington, TX 76019-0016, USA
E-mail: liang@uta.edu

Abstract— **Network-enabled Electronic Warfare (NEW) is to develop modeling and simulation efforts to explore the advantages and limitations of network-enabled electronic warfare concepts. The advantages of linking multiple electronic support measures (ESM) and electronic attack (EA) assets to achieve improved capabilities across a networked battleforce have yet to be quantified. In this paper, we will use radar sensors as ESM and EA assets to demonstrate the advantages of NEW in Collaborative Automatic Target Recognition (CATR). We apply the NEW to CATR via waveform diversity combining and and propose maximum-likehood (ML)-ATR algorithms for nonfluctuating target as well as fluctuating target. Simulation results show that our NEW-CATR performs much better than single sensor-based ATR algorithm for nonfluctuating targets or fluctuating targets. Conclusions are drawn based on our analysis and simulations and future research works on this research topic are discussed.**

Index Terms : Network-enabled electronic warfare, radar sensor networks, waveform diversity, collaborative automatic target recognition, maximum-likelihood, interferences.

I. Introduction and Motivation

In current and future military operational environments, such as Global War on Terrorism (GWOT) and Maritime Domain Awareness (MDA), warfighters require technologies evolved to support information needs regardless of location and consistent with the users level of command or responsibility and operational situation. To support this need, the U.S. Department of Defense (DoD) has developed the concept of Network Centric Warfare (NCW), defined as "*military operations that exploit state-of-the-art information and networking technology to integrate widely dispersed human decision makers, situational and targeting sensors, and forces and weapons into a highly adaptive, comprehensive system to achieve unprecedented mission effectiveness*" [1]. The goal of electronic warfare is to control the electromagnetic (EM) spectrum by exploiting, disrupting, or denying enemy use of the spectrum while ensuring its use by friendly forces [2].

Network-enabled Electronic Warfare (NEW) is to develop modeling and simulation efforts to explore the advantages and limitations of network-enabled electronic warfare concepts. The advantages of linking multiple electronic support measures (ESM) and electronic attack (EA) assets to achieve improved capabilities across a networked battleforce have yet to be quantified [2]. In this paper, we will use radar sensors as ESM and EA assets to demonstrate the advantages of NEW in Collaborative Automatic Target Recognition (CATR). The network of radar sensors should operate with multiple goals managed by an intelligent platform network that can manage the dynamics of each radar to meet the common goals of the platform, rather than each radar to operate as an independent system. Therefore, it is significant to perform signal design and processing and networking cooperatively within and between platforms of radar sensors and their communication modules. This need is also testified by recent solicitations from U.S. Office of Naval Research [2][3]. For example, in [3], it is stated that "Algorithms are sought for fused, and or, coherent cross-platform Radio Frequency (RF) sensing. The focus of this effort is to improve surveillance utilizing a network, not fusion of disparate sensor products. The algorithms should be capable of utilizing RF returns from multiple aspects in a time-coordinated sensor network." In this paper, we will study waveform design and diversity algorithms for radar sensor networks. Waveform diversity is the technology that will allow one or more sensors on board a platform to automatically change operating parameters, e.g., frequency, gain pattern, and pulse repetition frequency (PRF) to meet the varying environments. It has long been recognized that judicious use of properly designed waveforms, coupled with advanced receiver strategies, is fundamental to fully utilizing the capacity of the electromagnetic spectrum. However, it is only relatively recent advances in hardware technology that are enabling a much wider range of design freedoms to be explored. As a result, there are emerging and compelling changes in system requirements such as more efficient spectrum usage, higher sensitivities, greater information content, improved robustness to errors, reduced interference emissions, etc. The combination of these is fuelling a worldwide interest in the subject of

waveform design and the use of waveform diversity techniques.

In the existing works on waveform design and selection, Fitzgerald [8] demonstrated the inappropriateness of selection of waveform based on measurement quality alone: the interaction between the measurement and the track can be indirect, but must be accounted for. Bell [6] used information theory to design radar waveform for the measurement of extended radar targets exhibiting resonance phenomena. In [5], singularity expansion method was used to design some discriminant waveforms such as K-pulse, E-pulse, and S-pulse. Sowelam and Tewfik [24] developed a signal selection strategy for radar target classification, and a sequential classification procedure was proposed to minimize the average number of necessary signal transmissions. Intelligent waveform selection was studied in [4][12], but the effect of doppler shift was not considered. In [15], the performance of constant frequency (CF) and linear frequency modulated (LFM) waveform fusion from the standpoint of the whole system was studied, but the effects of clutter was not considered. In [23], CF and LFM waveforms were studied for sonar system, but it was assumed that the sensor is nonintelligent (i.e., waveform can't be selected adaptively). All the above studies and design methods were focused on the waveform design or selection for a single active radar or sensor. In [21], cross-correlation properties of two radars are briefly mentioned and the binary coded pulses using simulated annealing [7] are highlighted. However, the cross-correlation of two binary sequences such as binary coded pulses (e.g. Barker sequence) are much easier to study than that of two analog radar waveforms. In this paper, we will focus on the waveform diversity and design for radar sensor networks using constant frequency (CF) pulse waveform.

The rest of this paper is organized as follows. In Section II we propose a RAKE structure for waveform diversity combining and propose maximum-likelihood (ML) algorithms for CATR. In Section II we propose another RAKE structure for UWB radar diversity combining. In Section IV, we conclude this paper and provide some future works.

II. NEW FOR COLLABORATIVE AUTOMATIC TARGET RECOGNITION

In NEW, the radar sensors are networked together in an ad hoc fashion. They do not rely on a preexisting fixed infrastructure, such as a wireline backbone network or a base station. They are self-organizing entities that are deployed on demand in support of various events surveillance, battlefield, disaster relief, search and rescue, etc. Scalability concern suggests a hierarchical organization of radar sensor networks with the lowest level in the hierarchy being a cluster. As argued in [14] [10] [9] [17], in addition to helping with scalability and robustness, aggregating sensor nodes into clusters has additional benefits:

1) conserving radio resources such as bandwidth;
2) promoting spatial code reuse and frequency reuse;
3) simplifying the topology, e.g., when a mobile radar changes its location, it is sufficient for only the nodes in attended clusters to update their topology information;
4) reducing the generation and propagation of routing information; and,
5) concealing the details of global network topology from individual nodes.

In RSN, each radar can provide their waveform parameters such as δ_i to their clusterhead radar, and the clusterhead radar can combine the waveforms from its cluster members. In this paper, we propose a RAKE structure for waveform diversity combining, as illustrated by Fig. 1. According to this structure, the received $r_1(u,t)$ is processed by a bank of matched filters.

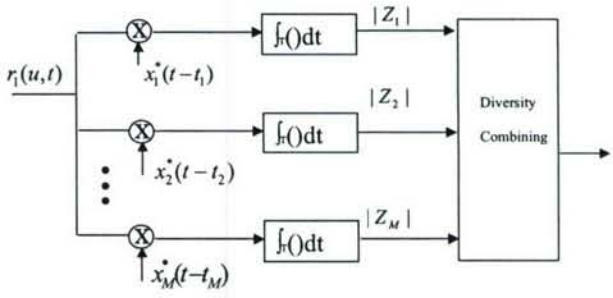

Fig. 1. Waveform diversity combining by clusterhead in RSN.

How to combine all the Z_m's ($m = 1, 2, \cdots, M$) are very similar to the diversity combining in communations to combat channel fading, and the combination schemes may be different for different applications. In this paper, we are interested in applying RSN waveform diversity to CATR, e.g., recognition that the echo on a radar display is that of an aircraft, ship, motor vehicle, bird, person, rain, chaff, clear-air turbulence, land clutter, sea clutter, bare montains, forested areas, meteors, aurora, ionized media, or other natural phenomena via collaborations among different radars. Early radars were "blob" detectors in that they detected the presence of a target and gave its location in range and angle, and radar began to be more than a blob detector and could provide recognition of one type of target from another[21]. It is known that small changes in the aspect angle of complex (multiple scatter) targets can cause major changes in the radar cross section (RCS). This has been considered in the past as a means of target recognition,

and is called *fluctuation of radar cross section with aspect angle*, but it has not had much success[21]. In this paper, we propose a maximum likelihood collaborative automatic target recognition (ML-CATR) algorithm for RSN. We will study non-fluctuating target as well as fluctuating target.

A. ML-CATR for Non-fluctuating Targets

In some sources, the non-fluctuating target is identified as "Swerling 0" or "Swerling 5" model [22]. For non-fluctuating target, the RCS $\alpha_m(u)$ is just a constant α for a given target. Noise $n(u,\tau)$ is a zero-mean Gaussian random variable for given τ, so $|Z_m|$ follows Rician distribution because signal $E\alpha(u)$ is a positive constant $E\alpha$ for non-fluctuating target. Let $y_m \triangleq |Z_m|$, then the probability density function (pdf) of y_m is

$$f(y_m) = \frac{2y_m}{\sigma^2}\exp[-\frac{(y_m^2+\lambda^2)}{\sigma^2}]I_0(\frac{2\lambda y_m}{\sigma^2}) \quad (1)$$

where

$$\lambda = E\alpha, \quad (2)$$

σ^2 is the noise power (with I and Q sub-channel power $\sigma^2/2$), and $I_0(\cdot)$ is the zero-order modified Bessel function of the first kind. Let $\mathbf{y} \triangleq [y_1, y_2, \cdots, y_M]$, then the pdf of $\mathbf{y}$ is

$$f(\mathbf{y}) = \prod_{m=1}^{M} f(y_m) \quad (3)$$

Our CATR is a multiple-category hypothesis testing problem, i.e., to decide a target category (e.g. aircraft, ship, motor vehicle, bird, etc) based on $r_1(u,t)$. Assume there are totally N categories and category n target has RCS α_n, so the ML-CATR algorithm to decide a target category C can be expressed as,

$$\begin{aligned} C &= \arg\max_{n=1}^{N} f(\mathbf{y}|\lambda = E\alpha_n) \quad (4)\\ &= \arg\max_{n=1}^{N} \prod_{m=1}^{M} \frac{2y_m}{\sigma^2}\exp[-\frac{(y_m^2+E^2\alpha_n^2)}{\sigma^2}]I_0(\frac{2E\alpha_n y_m}{\sigma^2}) \quad (5)\end{aligned}$$

B. ML-CATR for Fluctuating Targets

Fluctuating target modeling is more realistic in which the target RCS is drawn from either the Rayleigh or chi-square of degree four pdf. The Rayleigh model describes the behavior of a complex target consisting of many scatters, none of which is dominant. The fourth-degree chi-square models targets having many scatters of similar strength with one dominant scatter. Based on different combinations of pdf and decorrelation characteristics (scan-to-scan or pulse-to-pulse decorrelation), four Swerling models are used[19]. In this paper, we will focus on "Swerling 2" model which is Rayleigh distribution with pulse-to-pulse decorrelation. The pulse-to-pulse decorrelation implies that each individual pulse results in an independent value for RCS α.

For Swerling 2 model, the RCS $|\alpha(u)|$ follows Rayleigh distribution and its I and Q subchannels follow zero-mean Gaussian distributions with variance γ^2. Assume

$$\alpha(u) = \alpha_I(u) + j\alpha_Q(u) \quad (6)$$

and $n(u) = n_I(u) + jn_Q(u)$ follows zero-mean complex Gausian distribution with variance σ^2 for the I and Q subchannels. Z_m is a zero-mean Gaussian random variable with variance $E^2\gamma^2 + \sigma^2$ for the I and Q subchannels, which means $y_m \triangleq |Z_m|$ follows Rayleigh distribution with parameter $\sqrt{E^2\gamma^2+\sigma^2}$,

$$f(y_m) = \frac{y_m}{E^2\gamma^2+\sigma^2}\exp(-\frac{y_m^2}{E^2\gamma^2+\sigma^2}) \quad (7)$$

The mean value of y_m is $\sqrt{\frac{\pi(E^2\gamma^2+\sigma^2)}{2}}$, and variance is $\frac{(4-\pi)(E^2\gamma^2+\sigma^2)}{2}$. The variance of signal is $\frac{(4-\pi)E^2\gamma^2}{2}$ and the variance of noise is $\frac{(4-\pi)\sigma^2}{2}$.

Let $\mathbf{y} \triangleq [y_1, y_2, \cdots, y_M]$, then the pdf of $\mathbf{y}$ is

$$f(\mathbf{y}) = \prod_{m=1}^{M} f(y_m) \quad (8)$$

Assume there are totally N categories and category n target has RCS $\alpha_n(u)$ (with variance γ_n^2), so the ML-ATR algorithm to decide a target category C can be expressed as,

$$\begin{aligned} C &= \arg\max_{n=1}^{N} f(\mathbf{y}|\gamma = \gamma_n) \quad (9)\\ &= \arg\max_{n=1}^{N} \prod_{m=1}^{M} \frac{y_m}{E^2\gamma_n^2+\sigma^2}\exp(-\frac{y_m^2}{E^2\gamma_n^2+\sigma^2}) \quad (10)\end{aligned}$$

C. Simulations

Radar sensor networks will be required to detect a broad range of target classes. Too often, the characteristics of objects that are not of interest (e.g., bird) will be similar to those of threat objects (e.g., missile). Therefore, new techniques to discriminate threat against undesired detections (e.g. birds, etc.) are needed. We applied our ML-CATR to this important application, to recognize a target from many target classes. We assume that the domain of target classes is known a priori (N in Sections II-A and II-B), and that the RSN is confined to work only on the known domain.

For non-fluctuating target recognition, our targets have 5 classes with different RCS values, which are summarized in Table I[21]. We applied the ML-CATR algorithms in Section II-A (for nonfluctuating target case) to classify an unknown target as one of these 5 target classes. At each average SNR value, we ran Monte-Carlo simulations

for 10^5 times for each target. The average SNR value is based on the average power from all targets (signal variance), so the actual SNRs for bird and missile are much lower than the average SNR value. For example, at the average SNR=16dB, the bird target SNR=-33.1646dB, and missile target SNR=0.8149dB; and at average SNR=20dB, the bird target SNR=-29.1646dB, and missile target SNR=4.8149dB. In Fig. 2(a)(b), we plotted the probability of ATR error in bird and missile recognition when they are assumed as nonfluctuating targets. Observe both figures, single radar system can't perform well in both recognitions, and their probability of ATR error is above 10%, which can't be used for real-world ATR. However, the 5-radar RSN and 10-radar RSN can maintain very low ATR errors. In Fig. 2(c), we plotted the average probability of ATR error for all 5 targets recognition. Since the other 3 targets (different aircrafts) have much higher SNRs, so their ATR error is lower, which makes the average probability of ATR error lower.

For fluctuating target recognition, we assume the fluctuating targets follow "Swerling 2" model (Rayleigh with pulse-to-pulse decorrelation), and assume the RCS value listed in Table I to be the standard deviation (std) γ_n of RCS $\alpha_n(u)$ for target n. We applied the ML-CATR algorithm in Section II-B (for fluctuating target case) for target recognition within the 5 targets domain. Similarly we ran Monte-Carlo simulations at each SNR value. In Fig. 3(a)(b)(c), we plot the ATR performance for fluctuating targets and compared the performances of single radar system, 5-radar RSN, and 10-radar RSN. Observe that the two RSNs perform much better than the single radar system. The ATR error for missile is higher than that of bird because Rayleigh distribution of missile has lots of overlap with its neighbor targets (aircrafts). Comparing Fig. 2(a)(b)(c) to Fig. 3(a)(b)(c), it is clear that higher SNRs are needed for fluctuating target recognition comparing to nonfluctuating target recognition. According to Skolnik[21], radar performance with probability of recognition error (p_e) less than 10% is good enough. Our RSN with waveform-diversity can have probability of ATR error much less than 10% for each target ATR as well as the average ATR for all targets. However, the single radar system has probability of ATR error much higher than 10%. Observe Fig. 3(c), the average probability of ATR error of single-radar is impossible to be less than 10% even at extreme high SNR. Our RSN with waveform diversity is very promising to be used for real-world ATR.

III. Sense-through-Foliage Target Detection Using Radar Sensor Network

In Figs. 4a and 4b, we plot two collections using UWB radars. Fig. 4a has no target on range, and Fig. 4b has target at samples around 14,000. We plot the echo differences between Figs. 4a and 4b in Fig. 4c. However, it is impossible to identify whether there is any target and where there is target based on Fig. 4c. Since significant pulse-to-pulse variability exists in the echos, this motivate us to explore the spatial and time diversity using Radar Sensor Networks (RSN).

TABLE I
RCS values at microwave frequency for 5 targets.

Index n	Target	RCS
1	Bird	0.01
2	Conventional unmanned winged missile	0.5
3	Small single-engine aircraft	1
4	Small flighter aircraft or 4 passenger jet	2
5	Large flighter aircraft	6

In Fig. 5, the echo, i.e., RF response by the pulse of each cluster-member sensor, will be combined by the clusterhead using a weighted average, and the weight w_i is determined by the power of each echo $x_i(n)$ (n is the sample index),

$$w_i = \frac{E_i}{\sum_{i=1}^{M} E_i} \tag{11}$$

and

$$E_i = \text{var}(x_i(n)) + [\text{mean}(x_i(n))]^2 \tag{12}$$

We ran simulations for $M = 30$, and plot the power of AC values in Figs. 6a and 6b for the two cases (with target and without target) respectively. Observe that in Fig. 6b, the power of AC values (around sample 14,000) where the target is located is non-fluctuating (monotonically increase then decrease). Although some other samples also have very high AC power values, it is very clear that they are quite fluctuating and the power of AC values behaves like random noise because generally the clutter has Gaussian distribution in the frequency domain.

IV. Conclusions and Future Works

We have studied constant frequency pulse waveform design and diversity in radar sensor networks. We proposed a RAKE structure for waveform diversity combining in RSN. As an application example, we applied the waveform design and diversity to CATR in RSN and proposed ML-CATR algorithms for nonfluctuating target as well as fluctuating target. Simulation results show that RSN using our waveform diversity-based ML-ATR algorithm performs much better than single radar system for nonfluctuating targets and fluctuating targets recognition.

In our future works, we will investigate the CATR when multiple targets co-exist in RSN, and the number of targets are time-varying. In this paper, we used spatial diversity combining. For multi-target ATR, we will further investigate spatial-temporal-frequency combining for waveform diversity in RSN.

ACKNOWLEDGEMENT

This work was supported by the U.S. Office of Naval Research (ONR) under Grant N00014-07-1-0395 and ONR Young Investigator Program Award under Grant N00014-03-1-0466.

REFERENCES

[1] ONR BAA 06-016, "Command and Control and Combat Systems (C2 and CS)", http://www.onr.navy.mil/02/baa/expired.asp.

[2] ONR BAA 07-009, "Electronic Warfare Discovery and Invention (D&I)," http://www.onr.navy.mil/02/baa/.

[3] ONR BAA 07-017, "NET-SENTRIC Surveillance," http://www.onr.navy.mil/02/baa/.

[4] P. Baggenstoss, "Adaptive pulselength correction (APLECORR): a strategy for waveform optimization in ultrawideband active sonar," *IEEE Trans on Oceanic Engineering*, vol. 23, no. 1, pp. 1-11, 1998.

[5] C. E. Baum, et al, "The singularity expansion method and its application to target identification", *Proc. of the IEEE*, vol 79, no. 10, Oct 1991.

[6] M. R. Bell, "Information theory and radar waveform design", *IEEE Trans on Information Theory*, vol. 39, no. 5, pp. 1578-1597, Sept 1993.

[7] H. Deng, "Synthesis of binary sequences with good correlation and cross-correlation properties by simulated annealing," *IEEE Trans on Aerospace and Electronic Systems*, vol. 32, no. 1, Jan 1996.

[8] R. Fitzgerald, "Effects of range-doppler coupling on chirp radar tracking acuracy," *IEEE Trans on Aerospace and Eletronic Systems*, vol. 10, pp. 528-532, July 1974.

[9] T.-C. Hou and T-J. Tsai, " An access-based clustering protocol for multihop wireless ad hoc networks," *IEEE J. Selected Areas in Communications*, vol. 19, no. 7, pp. 1201-1210, July 2001.

[10] A. Iwata, C. C. Chiang, G. Pei, M. Gerla, and T. W. Chen, " Scalable routing strategies for ad hoc networks," *IEEE J. Selected Areas in Communications*, vol. 17, pp. 1369-1379, 1999.

[11] R. A. Johnson and E. L. Titlebaum, "Range Doppler Uncoupling in the Doppler Tolerant Bat Signal", *Proc. of IEEE Ultrasonics Symposium*, New York, pp. 64-67, 1972.

[12] D. Kershaw and R. Evans, "Optimal waveform selection for tracking system", *IEEE Trans on Information Theory*, vol. 40, no. 5, pp. 1536-1550, 1994.

[13] Q. Liang, X. Cheng, " KUPS: Knowledge-based Ubiquitous and Persistent Sensor Networks for Threat Assessment", submitted to *IEEE Trans on Aerospace and Electronic Systems*.

[14] C. R. Lin and M. Gerla, "Adaptive clustering in mobile wireless networks," *IEEE J. Selected Areas in Communications*, vol. 16, pp. 1265-1275, 1997.

[15] R. Niu, P. Willett, and Y. Bar-Shalom, "Tracking consideration in selection of radar waveform for range and range-rate measurements", *IEEE Transactions on Aerospace and Electronic Systems*, Vol. 38, No. 2, 2002.

[16] A. Papandreou, G. F. Boudreaux-Bartels, and S. M. Kay, "Detection and estimation of generalized chirps using time-frequency representations", *Twenty-Eighth Asilomar Conference on Signals, Systems and Computers*, vol. 1, pp. 50-54, Oct. 1994.

[17] C. E. Perkins, "Chapter 4, Cluster-Based Networks," *Ad Hoc Networking*, Edited by C. E. Perkins, pp. 75-138, Addison-Wesley, 2001.

[18] J. Roman, M. Rangaswamy, D. Davis, Q. Zhang, B. Himed, and J. Michels, "Parametric adaptive matched filter for airborne radar applications," *IEEE Trans. Aerosp. Electron. Syst.*, vol. 36, no. 2, pp. 677-692, 2000.

[19] M. A. Richards, *Fundamentals of Radar Signal Processing*, McGraw-Hill Companies, New York, 2005.

[20] T.K. Sarkar and N. Sangruji, "An adaptive nulling system for a narrow-band signal with a look-direction constraint utilizing the conjugate gradient method," *IEEE Trans. Antennas Propagat.*, vol. 37, no. 7, pp. 940-944, July 1989.

[21] M. I. Skolnik, *Introduction to Radar Systems*, 3rd ed, New York, McGraw Hill, 2001.

[22] P. Swerling, "Probability of detection for fluctuating targets", *IRE Trans on Information Theory*, vol. 6, pp. 269-308, April 1960.

[23] Y. Sun, P. Willett, and R. Lynch, "Waveform fusion in sonar signal processing", *IEEE Transactions on Aerospace and Electronic Systems*, Vol. 40, No. 2, 2004

[24] S. Sowelam and A. Tewfik, "Waveform selection in radar target classification," *IEEE Trans on Information Theory*, vol. 46, no. 3, pp. 1014-1029, 2000.

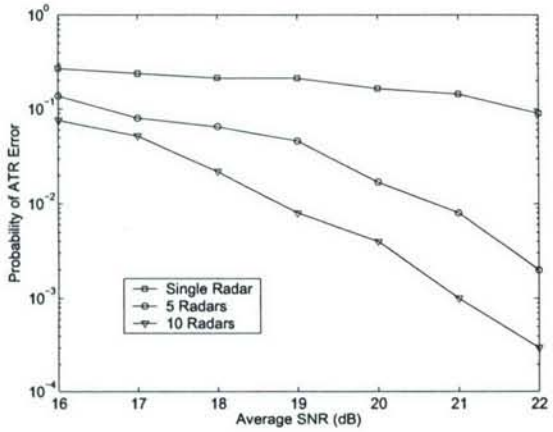

(a)

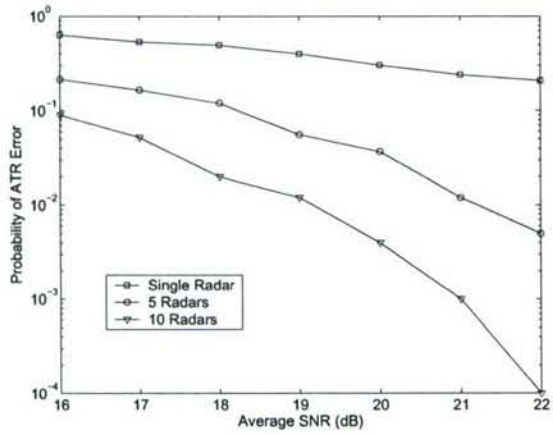

(b)

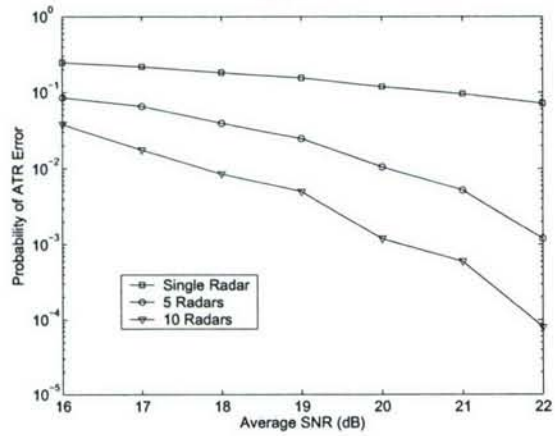

(c)

Fig. 2. Probability of ATR error for *nonfluctuating* targets at different average SNR (dB) values. (a) bird, (b) missile, (c) the average probability of ATR error for 5 targets.

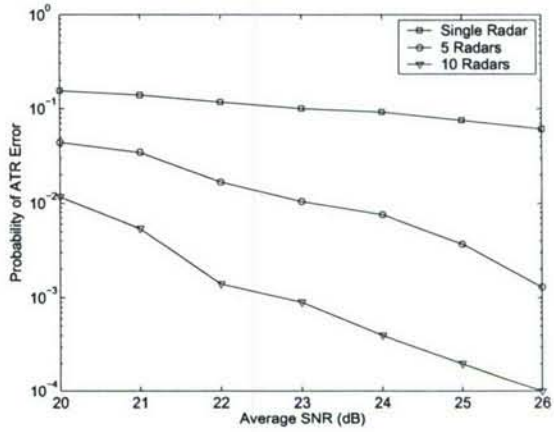

(a)

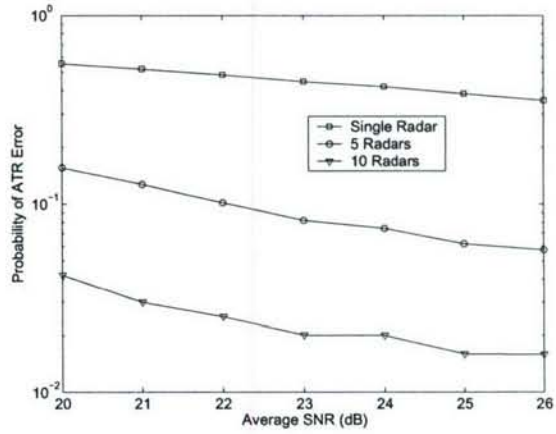

(b)

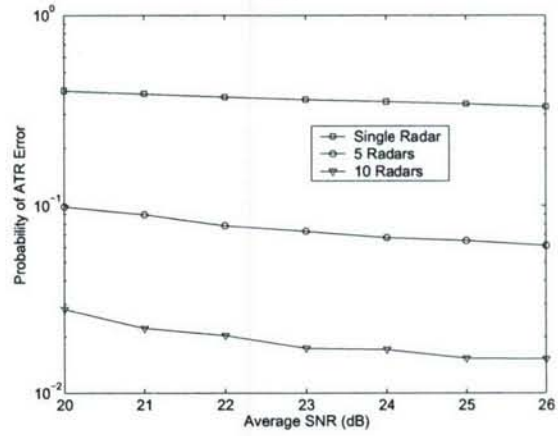

(c)

Fig. 3. Probability of ATR error for *fluctuating* targets at different average SNR (dB) values. (a) bird, (b) missile, (c) the average probability of ATR error for 5 targets.

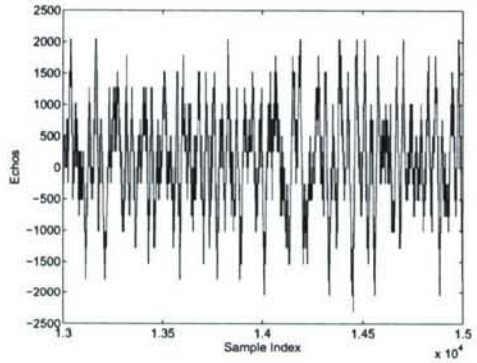

(a)

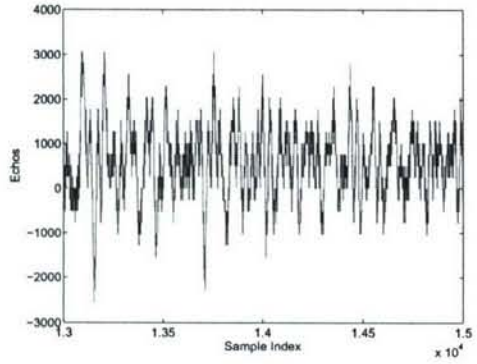

(b)

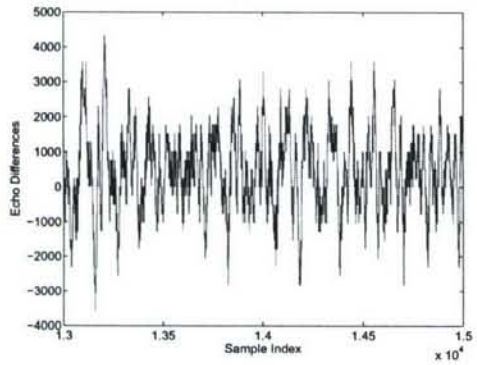

(c)

Fig. 4. Measurement with poor signal quality and 35 pulses average. (a) Expanded view of traces (no target) from sample 13,001 to 15,000. (b) Expanded view of traces (with target) from sample 13,001 to 15,000. (c) The differences between (a) and (b).

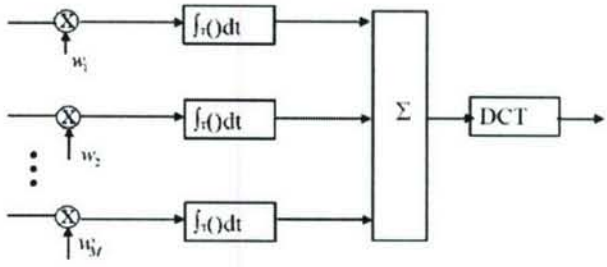

Fig. 5. Echo combining by clusterhead in RSN.

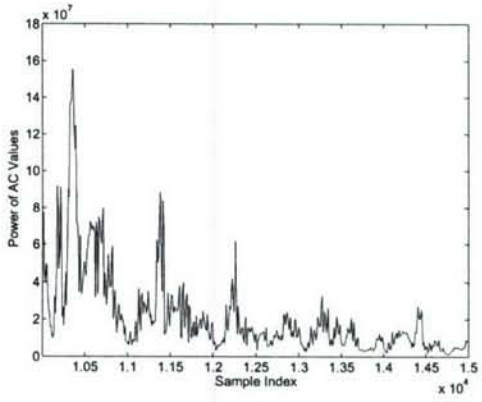

(a)

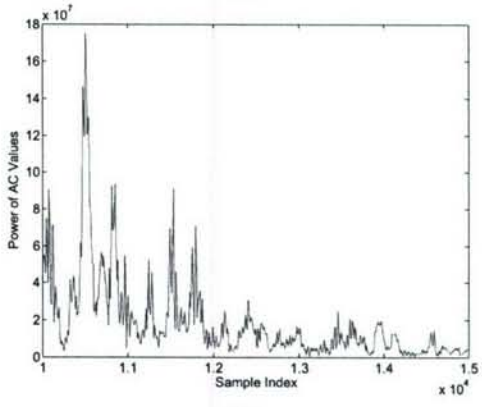

(b)

Fig. 6. Power of AC values based on UWB radar sensor networks and DCT based approach. (a) No target (b) With target in the field.

A Differential Based Approach for Through-Foliage Target Detection using UWB Radar Sensor Networks

Jing Liang, Qilian Liang
Department of Electrical Engineering
University of Texas at Arlington
Arlington, TX 76019-0016, USA
Email: jliang@wcn.uta.edu, liang@uta.edu

Sherwood W. Samn
Air Force Research Laboratory/HEX
Brooks City Base
San Antonio, TX 78235, USA
Email: Sherwood.samn@brooks.af.mil

Abstract— **In this paper, the foliage penetration measurements were taken in Holliston, Massachusetts. When radar echoes are in good quality, the detection of target can be achieved by applying our differential based technology on received single UWB radar waveform. We compared our approach in case of no target as well as with target against the scheme in which 2-D image was created via adding voltages with the appropriate time offset. Results show that our approach can work much better. When radar echoes are in poor condition and single radar is unable to carry out detection, we employ both Radar Sensor Networks (RSN) and RAKE structure to combine the echoes from different radar members and successfully detect the target.**

I. Introduction

Detection and identification of military equipment in a strong clutter background, such as foliage, soil cover or building leads has been a long-standing subject of intensive study. It is believed that solving the target detection through foliage will significantly benefit sense-through-wall and many other subsurface sensing problems. However, to this date, the detection of foliage-covered military targets, such as artillery, tanks, trucks and other weapons with the required probability of detection and false alarm still remains a challenging issue. This is due to the following facts:

1) Given certain low radar cross section(RCS), scattering from tree trunk and ground reflectivity may overwhelm the returned target signals of interest
2) Very high multiple fading severely corrupt the amplitude and phase of the echoes
3) Even if target is stationery, tree leaves and branches are likely to swing in result of gust, which will generate doppler shift of clutters.

Therefore, our main goal is to account for the above effects and better analyze the "defoliated" signal and thus improve the probability of target detection.

Over the past two decades, experimental and theoretical research have been studied to examine the performance on target detection covered by foliage employing imaging radars working at following 3 types signals:

1) Traditional sinusoidal waveforms at VHF through UHF bands [1], as the lower is the radar frequency, the lower is the attenuation and scattering from branches and trees, and thus better penetration through foliage. However, these approaches result in low resolution and low RCS.
2) Millimeter-Wave (MMW) radars are used in [2] [3] and [4]. Results demonstrate the potential for satisfying performance but need further investigation.
3) Relatively low frequency Ultra-wide band (UWB) radars between 100 MHZ and 3 GHz are frequently employed in recent years owning to the characteristics provided by their high resolutions as well as the very good ability of penetration, such as penetrating walls etc. [5] [6]. Despite comparatively short detection range, UWB signal would have advantages over a narrowband signal with limited frequency content.

In this paper, we will apply our expertise in signal processing, data fusion, sensor networks, etc to achieve effective through-foliage technology using ultra-wideband (UWB) radar and extracting as much information as possible to improve the probability of target detection.

The remainder of this paper is organized as follows. In Section II, we summarize the measurement and collection of data we used in this paper. In Section III, we propose a differential based approach for through-foliage target detection with good signal quality. In Section IV, we propose a radar sensor network (RSN) and RAKE structure for through-foliage target detection when the signal quality is poor. We conclude this paper and discuss some future research topics in Section V.

II. Through-Foliage Data Measurement and Collection

Our work is based on the through-foliage data collected by Virtual Machines LLC supported by Air Force [7]. The foliage penetration measurement effort began in August 2005 and continued through December 2005. The measurements were taken on the grounds of Virtual Machines Company in Holliston, Massachusetts. Working in August through the fall of 2005, the foliage measured included late summer foliage and fall and early winter foliage. Late summer foliage, because

of the limited rainfall, involved foliage with decreased water content. Late fall and winter measurements involved largely defoliated but dense forest.

The foliage experiment was constructed on a seven-ton man lift, which had a total lifting capacity of 450 kg. The limit of the lifting capacity was reached during the experiment as essentially the entire measuring apparatus was placed on the lift. The principle pieces of equipment secured on the lift are: Barth pulser, Tektronix model 7704 B oscilloscope, dual antenna mounting stand, two antennas, rack system, IBM laptop, HP signal Generator, Custom RF switch and power supply and Weather shield (small hut). The target is a trihedral reflector (as shown in Fig. 1). Throughout this work, a Barth pulse source (Barth Electronics, Inc. model 732 GL) was used. The pulse generator uses a coaxial reed switch to discharge a charge line for a very fast rise time pulse outputs. The model 732 pulse generator provides pulses of less than 50 picoseconds (ps) rise time, with amplitude from 150 V to greater than 2 KV into any load impedance through a 50 ohm coaxial line. The generator is capable of producing pulses with a minimum width of 750 ps and a maximum of 1 microsecond. This output pulse width is determined by charge line length for rectangular pulses, or by capacitors for 1/e decay pulses.

Fig. 1. The target (a trihedral reflector) is shown on the stand at 300 feet from the lift.

For the data we used in this paper, each sample is spaced at 50 picosecond interval, and 16,000 samples were collected for each collection for a total time duration of 0.8 microseconds at a rate of approximately 20 Hz. We considered two sets of data from this experiment. Initially, the Barth pulse source was operated at low amplitude and 35 pulses reflected signal were averaged for each collection. Significant pulse-to-pulse variability was noted for these collections. The scheme for the sense-through-foliage target detection with "poor" signal quality will be presented in Section IV. Later, good signal quality data were collected using higher amplitude pulses and 100 pulses reflected signals were averaged for each collection. The scheme for target detection with "good" signal quality will be presented in Section III.

III. Target Detection with Good Signal Quality: A Differential-Based Approach

In Fig. 2, we plot two collections with good signal quality, one without target on range (Fig. 2a) and the other one with target on range (Fig. 2b and target appears at around sample 14,000). To make it more clear to the readers, we provide expanded views of traces (with target) from sample 13,001 to 15,000 for the above two collections in Figs. 3a and 3b. Since there is no target in Fig. 3a, it can be treated as the response of foliage clutter. It's quite straightforward that the target response will be the echo difference between Fig. 3b and Fig. 3a, which is plotted in Fig. 3c. However, in practical situation we either obtain Fig. 3a (clutter echo without target) or Fig. 3b (target on range). The challenge is how to make target detection based on Fig. 3b (with target) or Fig. 3a (no target) only?

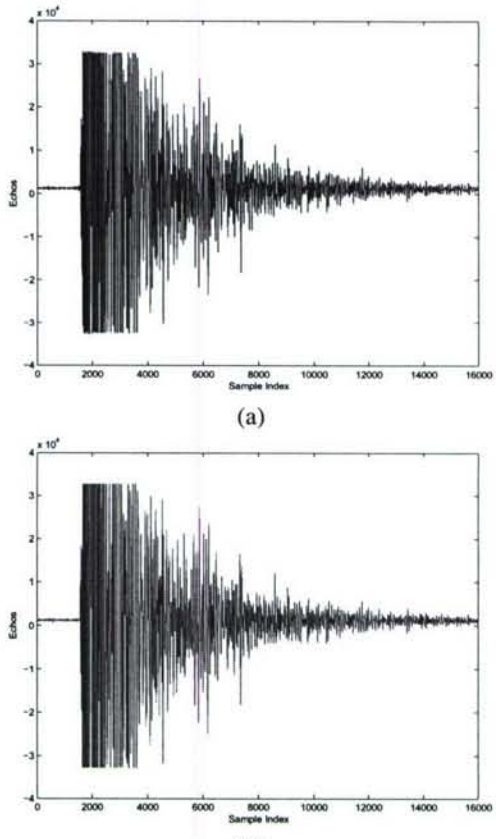

Fig. 2. Measurement with very good signal quality and 100 pulses average. (a) no target on range (b) with target on range (target appears at around sample 14000)

The block diagram of our approach is dawn in Fig.4.

The waveforms in Fig. 2a and 2b imply the synthesized effect of large-scale path loss and small-scale fading and multipath scattering. We believe if UWB propagation channel at foliage can be approximately estimated based on received echoes with good quality, we may reduce the "foliage-based"

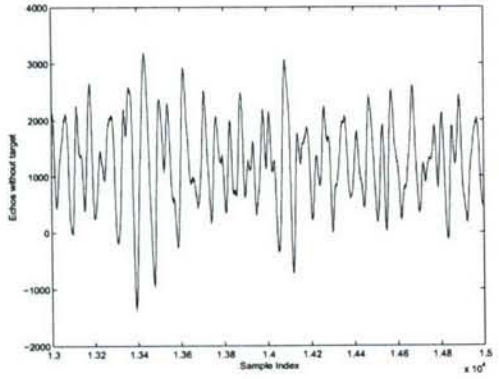

(a)

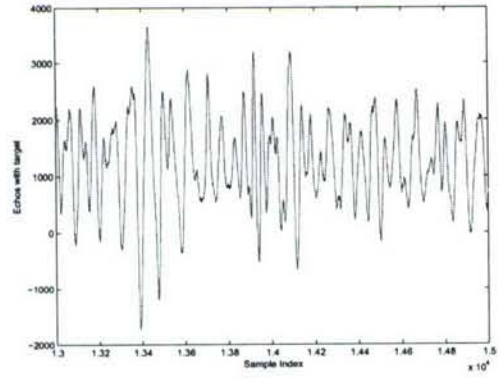

(b)

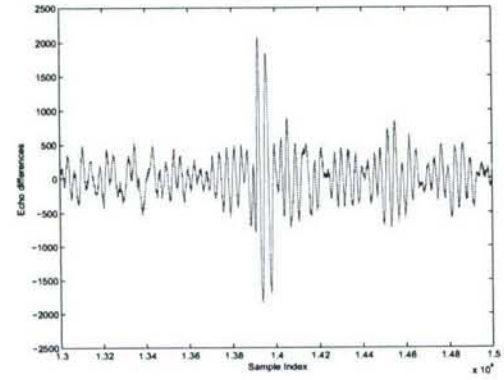

(c)

Fig. 3. Measurement with good signal quality and 100 pulses integration (a) Expanded view of traces (no target) from samples 13001 to 15000 (b) Expanded view of traces (with target) from samples 13001 to 15000 (c) Expanded view of traces difference between with and without target

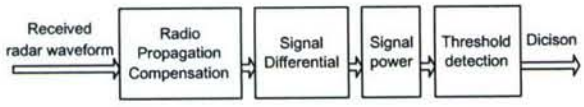

Fig. 4. Block diagram of differential based approach for single radar

UWB channel effect on received waveforms and better detect the target under foliage. However, this channel estimation is an open problem. For simplicity, we apply the following model to defoliate the scene.

$$\hat{y} = \begin{cases} Ae^{-Bx} & y > 0 \\ -Ae^{-Bx} & \text{otherwise} \end{cases} \quad (1)$$

where $\hat{y}$ is the amplitude of estimated clutter echo. x is sample index. y is the amplitude of original measurement. A and B are constants. Although it deserves much further study on the estimation problem, we shall see later that as the target appears at a relative tail part, this simple estimation is applicable.

Observe Fig. 3b, for samples where target appears (around sample 14,000), the waveform changes much abruptly than that in Fig. 3a. As differential value represents the changing rate of a function, it is quite intuitively that the amplitude of differential value at around sample 14,000 should be large. We plot the power of clutter-accounted and differentiated echoes in Fig. 5. It is quite straightforward to see there is no target in Fig. 5a and there is target in Fig. 5b.

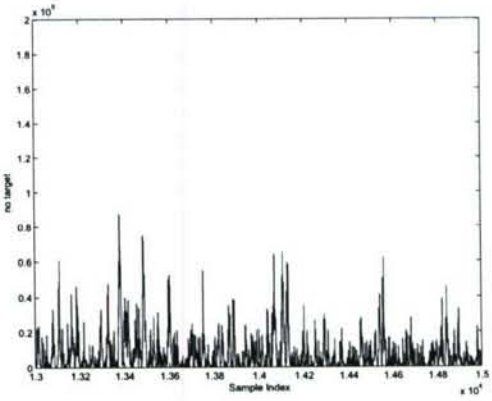

(a)

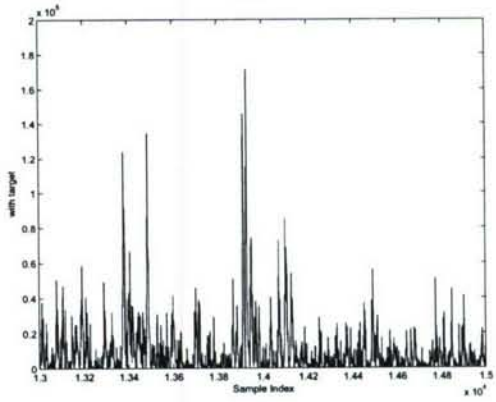

(b)

Fig. 5. The power of processed waveforms (a) no target (b) with target in the field

We compared our differential based approach to the scheme proposed in [8]. In [8], 2-D image was created via adding voltages with the appropriate time offset. In Figs. 6a and 6b,

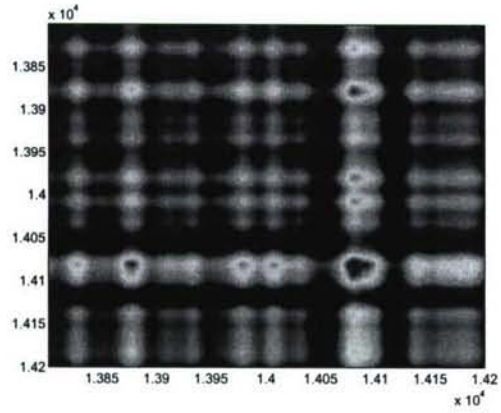

(a)

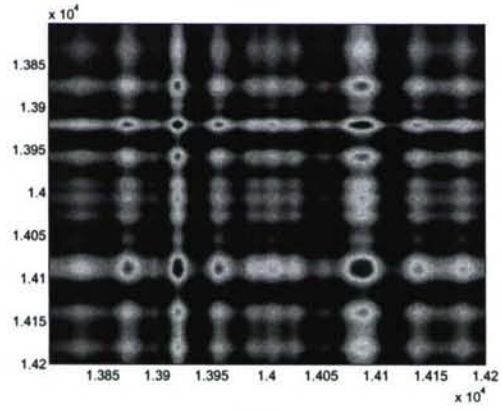

(b)

Fig. 6. 2-D image created via adding voltages with the appropriate time offset (a) no target (b) with target in the field

we plot the 2-D image created based on the above two data sets (from samples 13,800 to 14,200). However, it's not clear which image shows there is target on range.

IV. Target Detection with Poor Signal Quality: Radar Sensor Network and Differential-Based Approach

As mentioned in Section II, when the Barth pulse source was operated at low amplitude and the sample values are not obtained based on sufficient pulse response averaging (averaged over 35 pulses for each collection), significant pulse-to-pulse variability was noted and the return signal quality is poor. Fig. 8a illustrate the received echoes in this situation. Even with the application of our proposed differential-based scheme, we can not tell whether there is target or not in the range based on Fig. 8b. Since significant pulse-to-pulse variability exists in the echos, this motivate us to explore the spatial and time diversity using Radar Sensor Networks (RSN).

In nature, a network of multiple radar sensors can been utilized to combat performance degradation of single radar [9]. These radar sensors are managed by an intelligent clusterhead that combines waveform diversity in order to satisfy the common goals of the network other than each radar operate substantively. As radar sensors are environment dependent [10], it may provide better signal quality if different neighboring radars work collaboratively to perform data fusion. For example, consider a system of two radars. When the signal of either radar unfortunately experience a severe fading, if two radars are spaced sufficiently far apart, it is not likely that both of the radars experience deep fade at the same time. By selecting better waveform from the two radar waveforms, the data is less likely to be lost.

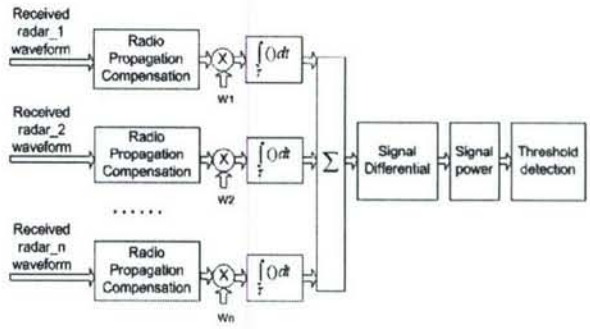

Fig. 7. Block diagram of differential based approach and diversity combination in RSN

In this paper, we assume the radar sensors are synchronized in RSN. In Fig. 7, the echo, i.e., RF response by the pulse of each cluster-member sensor, will be combined by the clusterhead using a weighted average, and the weight w_i is determined by the power of each echo $x_i(m)$ (m is the sample index),

$$w_i = \frac{E_i}{\sum_{i=1}^{n} E_i} \tag{2}$$

and

$$E_i = \text{var}(x_i(m)) + [\text{mean}(x_i(m))]^2 \tag{3}$$

We ran simulations for n = 35 and plot the power of combined signal obtained through differential based approach in Fig. 8c. Compare this figure with Fig. 8a and Fig. 8b, it is quite obvious to see that there is a target around sample 14,000.

V. Conclusion and Future Works

In this paper, we propose a differential-based signal processing approach on received UWB Radar waveforms to improve through-foliage target detection. The foliage penetration measurements were taken in Holliston, Massachusetts. When radar echoes are in good quality, the detection of target can be achieved by applying differential-based technology to single radar waveform. We compared our approach in case of no target as well as with target against the scheme in which 2-D image was created via adding voltages with the appropriate time offset. Results show that our approach can work much better. When radar echoes are in poor condition and single radar is unable to carry out detection, we employe both Radar Sensor Networks (RSN) and RAKE structure to combine the echoes from different radar members and finally successfully

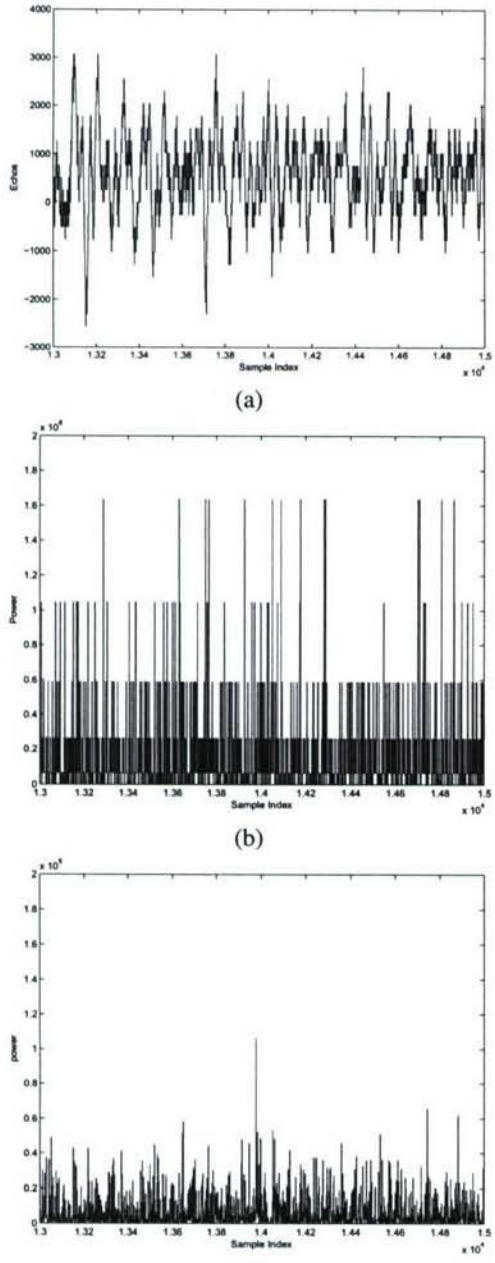

Fig. 8. Measurement with poor signal quality (with target) and 35 pulses integration (a) Expanded view of traces with target from samples 13001 to 15000 (b) Power of single radar after differential based approach (c) Power after both differential based approach and echoes combination in RSN

detect the target. For future works, we will collect more data with different targets and perform automatic target recognition besides target detection.

ACKNOWLEDGEMENT

This work was supported by the Office of Naval Research (ONR) Grant N00014-03-1-0466, N00014-07-1-0395 and AFOSR Summer Faculty Fellowship Program Award.

REFERENCES

[1] S. Ayasli and L. Bessette, " UHF & VHF SAR phenomenology, presented at the Proc. PIERS, Workshop on Advances in Radar Mathods, Baveno, Italy, July 20-22, 1998"

[2] F. K. Schwering, E. J. Violette and R. H. Espeland, "Millimeter-wave propagation in vegetation: Experiments and theory", *IEEE Trans. Geosci. Remote Sensing*, vol.26, pp. 355-367, May 1988

[3] F. T. Ulaby, T. E. Van Deventer, J. R. East, T. F. Haddock and M. E. Coluzzi, "Millimeter-wave bistatic scaterring from ground and vegetation targets" , *IEEE Trans. Geosci. Remote Sensing*, vol.26, pp. 229-243, May 1988

[4] A. Y. Nashashibi, k. Sarabandi, S. Oveisgharan *et al.*, "Millimeter-Wave Measurement of Foliage Attenuation and Ground Reflectivity of Tree Stands at Nadir Incidence", *IEEE Trans. Antennas Propagat.*, vol.52, pp.1211-2004, May, 2004

[5] B. Ferrell "Ultrawideband foliage penetration measurement", in *Proc. IEEE Nation Radar Conf.*, Mar. 29-31, pp.80-84, 1994

[6] X. Xu; R. M. Narayanan, "FOPEN SAR imaging using UWB step-frequency and random noise waveforms ", *IEEE Trans. Aerospace and Electronic Systems*, vol.37, pp.1287-1300, Oct. 2001

[7] C. Dill, "Foliage Penetration (Phase II) Field Test: Narrowband versus Wideband Foliage Penetration," *Final Report of Contract Number F41624-03-D-7001/04*, July 2005 to Feb 2006.

[8] P. Withington , H. Fluhler, and S. Nag, "Enhancing homeland security with advanced UWB sensors," *IEEE Microwave Magazine*, Sept 2003.

[9] S. Haykin, "Cognitive radar networks" , *2005 1st IEEE International Workshop on Computational Advances in Multi-Sensor Adaptive Processing*, pp.1-3, Dec 2005.

[10] R. A. Johnson and E. L. Titlebaum, "Range Doppler Uncoupling in the Doppler Tolerant Bat Signal", *Proc. of IEEE Ultrasonics Symposium* , New York, pp.64-67, 1972.

Foliage Clutter modeling Using UWB Radar

Jing Liang and Qilian Liang, *Senior Member, IEEE*
Department of Electrical Engineering
University of Texas at Arlington
Arlington, TX 76019-0016, USA
E-mail: jliang@wcn.uta.edu, liang@uta.edu

Sherwood W. Samn
Air Force Research Laboratory/HEX
Brooks City Base
San Antonio, TX 78235, USA
Sherwood.samn@brooks.af.mil

Abstract

In this paper, we prove that the amplitude of foliage clutter follows log-logistic model using maximum likelihood (ML) parameter estimation as well as the root mean square error (RMSE) on PDF curves between original clutter and statistical model data. The measured clutter data is provided by Air Force Office of Scientific Research (AFOSR). We not only investigate log-logistic model, but compare it with other popular clutter models, namely log-normal, weibull and nakagami. It shows that log-logistic model not only achieves the smallest standard divination (STD) error on estimated model parameters, but also the best goodness-of-fit and smallest RMSE for both poor and good clutter signals.

Index Terms : foliage clutter, log-logistic, log-normal, weibull, nakagami, goodness-of-fit

1 Introduction and Motivation

Detection and identification of military equipment in a strong clutter background, such as foliage, soil cover or building leads has been a long-standing subject of intensive study. It is believed that solving the target detection through foliage will significantly benefit sense-through-wall and many other subsurface sensing problems. However, to this date, the detection of foliage-covered military targets, such as artillery, tanks, trucks and other weapons with the required probability of detection and false alarm still remains a challenging issue. Recent

investigations on scattering behavior of tree canopies have shown that both signal backscattering and attenuation are significantly influenced by tree architecture [1]. Therefore use the return signal from foliage to establish the clutter model that accounts for environment effects is crucial for the sense-through-foliage radar detection.

clutter is a term used to define all unwanted echoes from natural environment [2]. The nature of clutter may necessarily varies on a basis of different application and radar parameters. Most previous study have investigated in land clutter and sea clutter intensively and some conclusions have been reached, such as log-normal, weibull and K-distributions have proved to be better suited for the clutter than Rayleigh and Rician models in the high resolution radar systems. Fred [3] did statistical comparisons and found that sea clutter at low grazing angles and high range resolution is spiky based on the data measured from various sites in Kauai and Hawaii. David generalized radar clutter model as noncentral chi-square density by allowing the noncentrality parameter to fluctuate according to the gamma distribution [4]. Furthermore, Henry *et al.* used a Neural-Network-based approach to predict sea clutter model [5] [6].

As far as clutter modeling in forest is concerned, it is still of great interest and will be likely to take some time to reach any agreement. A team of researchers from MIT [7] and U. S. Army Research Laboratory (ARL) [8] [9] have measured ultrawideband (UWB) backscatter signals in foliage for different polarizations and frequency ranges. The measurements show that the foliage clutter is impulsive corrupted with multipath fading, which leads to inaccuracy of the K-distributions description [10]. The Air Force Office of Scientific Research (AFOSR) has conducted field measurement experiment concerning foliage penetration radar since 2004 and led to the sense that metallic targets may be more easily identified with wideband than with narrowband signals [11].

In this investigation, we will apply ultra-wide band (UWB) radar to model the foliage clutter. UWB radar emissions are at a relatively low frequency-typically between 100 MHz and 3 GHz. Additionally, the fractional bandwidth of the signal is very large (greater than 0.2). Such radar sensor has exceptional range resolution that also has an ability to penetrate many

common materials (e.g., walls). Law enforcement personnel have used UWB ground penetrating radars (GPRs) for at least a decade. Like the GPR, sense-through-foliage radar takes advantage of UWB's very fine resolution (time gating) as well as low frequency of operation.

In our present work, we investigate the log-logistic distribution to model foliage clutter and illustrate the goodness-of-fit to real UWB clutter data conducted by AFOSR. Additionally, we compare the goodness-of-fit with existing popular models namely log-normal, weibull and nakagami by means of maximum likelihood estimation (MLE). The result shows that log-logistic model provides a better fit to the foliage clutter.

The rest of this paper is organized as follows. Section 2 provide a statistical model review on log-logistic, log-normal, weibull and nakagami distributions and discuss their properties and applicability as models for foliage clutter. Section 3 summarize the measurement and collection of clutter data we used in this paper. Section 4 discuss estimation on model parameters and the goodness-of-fit. Finally, section 5 concludes this paper and describe some future research topics.

2 Clutter Models

Many radar clutter models have been proposed in terms of distinct statistical distributions, most of which describe the characteristics of clutter amplitude. Here we discuss the properties and applicability of log-logistic, log-normal, Weibull and Nakagami statistic models, which are designated as "curve fit" models in section 4, since they are more likely to provide good fit to our collections of pragmatic clutter data in general.

2.1 Log-Logistic Model

In spite of intensive application in precipitation and stream-flow data, so far the log-logistic distribution (LLD) [12] statistical model has never been applied to radar foliage clutter model to the best our knowledge. The motivation for considering log-logistic model involves a con-

sideration of how well the model matches our collected foliage clutter statistics and in section 4, we shall prove that this model provides the best curve fit and smaller parameter estimation error than those of lognormal, Weibull and Nakagami.

Here we apply the two-parameter distribution with parameters μ and σ, for 3-parameter Log-Logistic distribution (LLD3), readers may refer to [13]. The PDF for this distribution is given by

$$f(x) = \frac{e^{\frac{lnx-\mu}{\sigma}}}{\sigma x(1+e^{\frac{lnx-\mu}{\sigma}})^2}, \quad x > 0, \ \sigma > 0 \tag{1}$$

where μ is scale parameter and σ is shape parameter. The mean of the the LLD is

$$E\{x\} = e^{\mu}\Gamma(1+\sigma)\Gamma(1-\sigma) \tag{2}$$

The variance is given by

$$Var\{x\} = e^{2\mu}\{\Gamma(1+2\sigma)\Gamma(1-2\sigma) - [\Gamma(1+\sigma)\Gamma(1-\sigma)]^2\} \tag{3}$$

while the moment of order k is

$$E\{x^k\} = \sigma e^{\mu} B(k\sigma, 1-k\sigma), \ k < \frac{1}{\sigma} \tag{4}$$

where

$$B(m,n) = \int_0^1 x^{m-1}(1-x)^{n-1}dx \tag{5}$$

This distribution is a special case of Burr's type-XII distribution [14] as well as a special case of the kappa distribution proposed by Mielke and Jonson [15]. LLD has been applied recently in hydrological analysis. Lee *et al.* employed the LLD for frequency analysis of multiyear drought durations [16], whereas Shoukri *et al.* employed LLD to analyse extensive Canadian precipitation data [17], and Narda & Malik used LLD to develop a model of root growth and water uptake in wheat [18]. This model is intended to be employed on a basis of higher kurtosis and longer tails, as well as its shape similarity to log-normal and Weibull distributions. PDF for LLD on a basis of different of μ and σ are illustrated in Fig. 1.

2.2 Log-Normal Model

Most previous experimental data have resulted in clutter being modeled using a log-normal distribution, which is most frequently used when the radar sees land clutter [19] or sea clutter [20] at low grazing angles ($\leq$ 5 degrees) since it has a long tail. However it is reported that the log-normal model tends to overestimate the dynamic range of the real clutter distribution in [21]. Furthermore, most previous research apply log-normal model to land and sea clutter, but how accurately it models foliage clutter requires detailed analysis.

The log-normal distribution [22] is also a two-parameter distribution with parameters μ and σ. The PDF for this distribution is given by

$$f(x) = \frac{1}{x\sigma\sqrt{2\pi}} e^{-\frac{(lnx-\mu)^2}{2\sigma^2}}, \quad x > 0, \sigma > 0 \tag{6}$$

where μ is the scale parameter and σ is the shape parameter. The mean, variance and the moment of order k are shown below respectively

$$E\{x\} = e^{\mu+\frac{\sigma^2}{2}} \tag{7}$$

$$Var\{x\} = (e^{\sigma^2} - 1)e^{2\mu+\sigma^2} \tag{8}$$

$$E\{x^k\} = e^{k\mu+\frac{k^2\sigma^2}{2}} \tag{9}$$

PDF on a basis of different μ and σ for log-normal distribution is shown in Fig. 2.

2.3 Weibull Model

The Weibull distribution, which is named after Waloddi Weibull, can be made to fit clutter measurements that lie between the Rayleigh and log-normal distribution [23]. It has been applied to land clutter [24] [25], sea clutter [26] [27] and weather clutter [28]. However, in very spiky sea and foliage clutter, the description of the clutter statistics provided by Weibull distributions may not always sufficiently accurate [29].

The Weibull distribution is also a two-parameter distribution with parameters a and b. The PDF for this distribution is given by

$$f(x) = ba^{-b}x^{b-1}e^{-(x/a)^b}, \quad x > 0, a > 0, \ b > 0 \tag{10}$$

where b is the shape parameter and a is the scale parameter. The mean, variance and the moment of order k are shown below respectively

$$E\{x\} = a\Gamma(1 + \frac{1}{b}) \tag{11}$$

$$Var\{x\} = a^2\{\Gamma(1 + \frac{2}{b}) - [\Gamma(1 + \frac{1}{b})]^2\} \tag{12}$$

$$E\{x^k\} = a^k\Gamma(1 + \frac{k}{b}) \tag{13}$$

PDF based on different a and b for Weibull distribution is shown in Fig. 3.

2.4 Nakagami Model

Consider the foliage penetration setting, the target returns are from multipath effects corrupted with fading. As nakagami distribution is used to model scattered fading signals that reach a receiver by multiple paths, we also apply it to analyze how well it fits the foliage clutter statistics.

The PDF for Nakagami distribution is given by

$$f(x) = 2(\frac{\mu}{\omega})^{\mu}\frac{1}{\Gamma(\mu)}x^{(2\mu-1)}e^{-\frac{\mu}{\omega}x^2}, \quad x > 0, \omega > 0 \tag{14}$$

where μ is the shape parameter and ω is the scale parameter. The mean, variance and the moment of order k of Nakagami distribution are shown below respectively

$$E\{x\} = \frac{\Gamma(\mu + \frac{1}{2})}{\Gamma(\mu)}(\frac{\omega}{\mu})^{\frac{1}{2}} \tag{15}$$

$$Var\{x\} = \omega[1 - \frac{1}{\mu}(\frac{\Gamma(\mu + \frac{1}{2})}{\Gamma(\mu)})^2] \tag{16}$$

$$E\{x^k\} = \frac{\Gamma(\mu + \frac{k}{2})}{\Gamma(\mu)}(\frac{\omega}{\mu})^{\frac{k}{2}} \tag{17}$$

The PDF on a basis of different μ and ω for Nakagami distribution is illustrated in Fig. 4.

3 Experiment Setup and Data Collection

Our work is based on the sense-through-foliage data collected by Virtual Machines LLC supported by Air Force [11]. The foliage penetration measurement effort began in August 2005 and continued through December 2005. The measurements were taken on the grounds of Virtual Machines Company in Holliston, Massachusetts. Working in August through the fall of 2005, the foliage measured included late summer foliage and fall and early winter foliage. Late summer foliage, because of the limited rainfall, involved foliage with decreased water content. Late fall and winter measurements involved largely defoliated but dense forest.

The UWB radar-based experiment was constructed on a seven-ton man lift, which had a total lifting capacity of 450 kg. The limit of the lifting capacity was reached during the experiment as essentially the entire measuring apparatus was placed on the lift (as shown in Fig. 5). The principle pieces of equipment secured on the lift are: Barth pulser, Tektronix model 7704 B oscilloscope, dual antenna mounting stand, two antennas, rack system, IBM laptop, HP signal Generator, Custom RF switch and power supply and Weather shield (small hut). Throughout this work, a Barth pulse source (Barth Electronics, Inc. model 732 GL) was used. The pulse generator uses a coaxial reed switch to discharge a charge line for a very fast rise time pulse outputs. The model 732 pulse generator provides pulses of less than 50 picoseconds (ps) rise time, with amplitude from 150 V to greater than 2 KV into any load impedance through a 50 ohm coaxial line. The generator is capable of producing pulses with a minimum width of 750 ps and a maximum of 1 microsecond. This output pulse width is determined by charge line length for rectangular pulses, or by capacitors for 1/e decay pulses.

For the data we used in this paper, each sample is spaced at 50 picosecond interval, and 16,000 samples were collected for each collection for a total time duration of 0.8 microseconds at a rate of approximately 20 Hz. We considered two sets of data from this experiment. Initially, the Barth pulse source was operated at low amplitude and 10 pulses reflected clutter signal were obtained for each collection at the same site but different time, one example of

transmitted pulse and received backscattering are shown in Fig. 6(a) and (b) respectively. Significant pulse-to-pulse variability was noted for these collections. Later, echoes with good signal quality were collected using higher amplitude transmitted pulses, shown in Fig. 6(c). To make them clearer to readers, we provide expanded views of received traces from sample 10,000 to 12,000 in Fig. 7.

4 Statistical Analysis of the Foliage Clutter Data

4.1 Maximum Likelihood Estimation

On a basis of collected clutter data, we apply Maximum Likelihood Estimation (MLE) approach to estimate the parameters for log-logistic, log-normal, weibull and nakagami models respectively. MLE is often used when the sample data are known and parameters of the underlying probability distribution are to be estimated [31] [32]. It is generalized as follows:

Let $y_1, y_2, \cdots, y_N$ be N independent samples drawn from a random variable $\mathbf{Y}$ with m parameters $\theta_1, \theta_2, \cdots, \theta_m$, where $\theta_i \in \theta$, then the joint PDF of $y_1, y_2, \cdots, y_N$ is

$$L_N(\mathbf{Y}|\theta) = f_{Y|\theta}(y_1|\theta_1, \theta_2, \cdots, \theta_m) f_{Y|\theta}(y_2|\theta_1, \theta_2, \cdots, \theta_m) \cdots f_{Y|\theta}(y_n|\theta_1, \theta_2, \cdots, \theta_m) \tag{18}$$

When expressed as the conditional function of $\mathbf{Y}$ depends on the parameter θ, the likelihood function is

$$L_N(\mathbf{Y}|\theta) = \prod_{k=1}^{N} f_{Y|\theta}(y_k|\theta_1, \theta_2, \cdots, \theta_m) \tag{19}$$

The maximum likelihood estimate of $\theta_1, \theta_2, \cdots, \theta_m$ is the set of values $\hat{\theta}_1, \hat{\theta}_2, \cdots, \hat{\theta}_m$ that maximize the likelihood function $L_N(\mathbf{Y}|\theta)$.

As the logarithmic function is monotonically increasing, maximizing $L_N(\mathbf{Y}|\theta)$ is equivalent to maximizing $\ln(L_N(\mathbf{Y}|\theta))$. Hence, it can be shown that a necessary but not sufficient condition to obtain the ML estimate $\hat{\theta}$ is to solve the likelihood equation

$$\frac{\partial}{\partial \theta} \ln(L_N(\mathbf{Y}|\theta)) = 0 \tag{20}$$

On a basis of collected clutter radar, we apply MLE to obtain $\hat{\mu}$ and $\hat{\sigma}$ for log-logistic, $\hat{\mu}$ and $\hat{\sigma}$ for log-normal, $\hat{a}$ and $\hat{b}$ for weibull and $\hat{\mu}$ and $\hat{\omega}$ for nakagami respectively, which are shown in table 1. We also explore the standard deviation (STD) error of each parameter. These descriptions are also shown in table 1 in the form of ε_x, where x denotes different parameter for each model. As there are 10 data sets for poor clutter signal and 2 for good ones, we also calculate the average values of estimated parameters and their STD error.

From table 2, we can see STD error for log-logistic and log-normal parameters are less than 0.02 and their estimated parameters vary little from data to data compared to Weibull and nakagami. It is obvious that log-logistic model provides the smallest STD error and nakagami the largest. Therefore, in the view of statistics, log-logistic model fits the collected data best compared to log-normal, weibull and nakagami.

4.2 Goodness-of-fit in curve and RMSE

We may also observe that to what extend does the PDF curve of the statistic model match that of clutter data by root mean square error (RMSE). Let i (i=1, 2, $\cdots$, n) be the sample index of clutter amplitude, c_i is the corresponding PDF value whereas $\hat{c}_i$ is the PDF value of the statistical model with estimated parameters by means of MSE. RMSE is obtained through

$$\texttt{RMSE} = \sqrt{\frac{1}{n}\sum_{i=1}^{n}(c_i - \hat{c}_i)^2} \tag{21}$$

Here we apply n=101 for each model.

The goodness-of-fit in curve and RMSE of each model for both collected poor and good clutter signals are illustrated in Fig. 8 and 9 respectively.

Consider the poor signal of clutter, the PDF of absolute amplitude of one-time poor clutter data is presented by means of histogram bars. In Fig. 8, it can be seen obviously that log-logistic model with MLE parameters provides best goodness-of-fit compared to other models since it provides the most suitable kurtosis, slope and tail. As for the maximum PDF value, log-logistic is about 1×10^{-3}, while that of other models are over 1.2×10^{-3}. For the slope part which

connected kurtosis and tail, which is in the range from 0.1×10^4 to 0.5×10^4 in view of x axes, log-logistic provides the smallest skewness whereas nakagami provides the largest. Observation of the tails show that log-logistic and log-normal provides very close-valued tails, while the tail of weibull and nakagami is lager than the collected data. Meanwhile, we obtain that $\texttt{RMSE}_{log-logistic} = 2.5425 \times 10^{-5}$, $\texttt{RMSE}_{log-normal} = 3.2704 \times 10^{-5}$, $\texttt{RMSE}_{weibull} = 3.7234 \times 10^{-5}$, $\texttt{RMSE}_{nakagami} = 5.4326 \times 10^{-5}$. This sufficiently shows that log-logistic is more accurate then log-normal, weibull and nakagami models.

Similarly, in Fig. 9 histogram bars denote the PDF of absolute amplitude of one-time good clutter data. Compared to Fig. 8, log-logistic and lognormal provides quite similar extend of goodness-of-fit, weibull is worse since it can not fit well in both kurtosis and tail, while nakagami is the worst and unacceptable. Also, we obtain $\texttt{RMSE}_{log-logistic} = 2.739 \times 10^{-5}$, $\texttt{RMSE}_{log-normal} = 3.1866 \times 10^{-5}$, $\texttt{RMSE}_{weibull} = 3.6361 \times 10^{-5}$, $\texttt{RMSE}_{nakagami} = 4.4045 \times 10^{-5}$, which illustrates that for clutter backscattering with good quality, log-logistic still fits best.

5 Conclusion

On a basis of 2 groups of foliage clutter data using UWB radar, we prove that it is more accurate to describe foliage clutter using log-logistic statistic model other than log-normal, weibull or nakagami. Log-normal is also acceptable whereas nakagami provides the worst goodness-of-fit. Future research will investigate how to design the radar receiver to reduce the false alarm and improve the probability of detection based on the foliage clutter model we proposed.

Acknowledgement

This work was supported by the Office of Naval Research (ONR) Grant N00014-07-1-0395, N00014-07-1-1024, N00014-03-1-0466, and AFOSR Summer Faculty Fellowship Program Award.

References

[1] Imhoff, M. L., "A theoretical analysis of the effect of forest structure on SAR backscatter and the remote sensing of biomass," *IEEE Trans. Geosci. Remote Sensing*, vol. 33, pp. 341C352, Mar. 1995.

[2] Skolnik, M. I.,*Introduction to Radar Systems*, 3rd ed, New York, McGraw Hill, 2001.

[3] Posner, F. L., *IEEE Trans. on Aerosp. Electron. Syst.*, vol. 38, no. 1, pp. 58-73, Jan 2002.

[4] David, A. Shnidman, "Generalized Radar Clutter Model", *IEEE Trans. on Aerosp. Electron. Syst*, vol. 35, no. 3, July 1999.

[5] Hennessey, G. and Leung, H., "Sea-Clutter Modeling Using a Radial-Basis-Function Neural Network", *IEEE Journal of Oceanic Engineering*, vol. 26, no. 3, pp. 358-372, July, 2001.

[6] Xie, N. and Leung, H., "A Multiple-Model Prediction Approach for Sea Clutter Modeling", *IEEE Trans. on Geoscience and Remote Sensing*, vol. 41, no. 6, pp. 1491-1502, June, 2003.

[7] Fleischman, J. G., Ayasli, S., Adams, E. M., and Gosselin, D. R., Foliage penetration experiment: Part I: Foliage attenuation and backscatter analysis of SAR imagery, *IEEE Trans. on Aerosp. Electron. Syst.*, 32, 1, part 1 of 3 (1996), 134-144.

[8] Mccorkle, J. W., "Early results from the ARL UWB Foliage attenuation (FOPEN) SAR", Presented at the SPIE International Symposium on Optical Engineering and Photonics in Aerospace and Remote Sensing, Conference 1942, Underground and Obscured Object Detection, Apr. 1993.

[9] Sheen, D. R., Malinas, N. P., Kletzli, D. W., Lewis, T. B., and Roman, J. F., "Foliage transmission meassurement using a ground-based ultrawideband (UWB) (300-1300MHz) SAR system", *IEEE Trans. on Geoscience and Remote Sensing*, 32, 1(1994).

[10] Watts, S., "Radar detection prediction in K-distribution sea clutter and thermal noise", *IEEE Trans. on Aerosp. Electron. Syst.*, AES-23, 1, 1987, pp. 40-45.

[11] Dill, C., "Foliage Penetration (Phase II) Field Test: Narrowband versus Wideband Foliage Penetration," Final Report of Contract Number F41624-03-D-7001/04, July 2005 to Feb 2006.

[12] Gupta, R. C., Akman, O. and Lvin, S., "A Study of Log-Logistic Model in Survival Analysis", *Biometrical Journal*, 41, pp. 431-443, 1999

[13] Singh, V. P., Guo, H. and Yu, F. X., "Parameter estimation for 3-parameter log-logistic distribution (LLD3) by Pome", *Parameter estimation for 3-parameter log-logistic distribution (LLD3) by Pome*, vol.7, no.3, pp. 163-177, 2005

[14] Burr, I. W.,"Cumulative frequency functions." *Ann. Math. Statist.*, 13, 215-232, 1942.

[15] Mielke, P. W. and Johnson. E. S.,"Three-parameter kappa distribution maximum likelihood estimates and likelihood ratio tests," *Monthly Weather Rev.*, 101, 701-709, 1973.

[16] Lee, K. S., Sadeghipour, J. and Dracup, J. A., "An approach for frequency analysis of multiyear dought duration.", *Wat. Resour. Res.* 22(5), 655-662, 1986.

[17] Shoukri, M. M., Mian, I. U. H. and Tracy, D. S., " Sampling properties of estimators of the log-logistic distribution with application to Canadian precipitation data.", *Can. J. Statist.* 16(3), 223-236, 1988.

[18] Narda, N. K. and Malik, R. K., "Dynamic model of root growth and water uptake in wheat.", *Indian J. Agric. Engng* 3(3&4), 147-155, 1993.

[19] Warden, M., "An experimental study of some clutter characteristics.", in *AGARD Conf. Proc. 66-Advanced Radar Systems*, May 1970.

[20] Trunk, G. and George, S., "Detection of targets in non-Gaussian sea clutter", *IEEE Trans. on Aerosp. Electron. Syst.*, vol. AES-6, Sept. 1970

[21] Schleher, D. C., "Radar Detection in Weibull Clutter", *IEEE Trans. on Aerosp. Electron. Syst.*, vol. AES-12, No. 6, Nov. 1976

[22] Limpert, E., Stahel, W. and Abbt, M., "Log-normal Distributions across the Sciences: Keys and Clues.", *BioScience*, 51 (5), pp. 341C352, 2001.

[23] Weibull, W. "A statistical distribution function of wide applicability", J. Appl. Mech.-Trans. ASME 18(3), 293-297, 1951.

[24] Boothe, R. R., "The Weibull distribution applied to the ground clutter backscatter coefficient.", U.S. Army Missile Command Report No. RE-TR-69-15, June, 1969.

[25] Sekine, M., *et al*, "Weibull distributed ground clutter.", *IEEE Trans. on Aerosp. Electron. Syst.*, AES-17 pp. 596-598, July 1981.

[26] Fay, F. A., Clarke, J. and Peters, R. S, "Weibull distributed applied to sea clutter", *Radar 77, IEE Conf. Publ.*, 155, pp. 101-104, 1977.

[27] Sekine, M., *et al*, "Weibull distributed sea clutter.", *IEE Proceedings, Part F - Communications, Radar and Signal Processing*, vol. 130, no. 5, Aug. 1983.

[28] Sekine, M., *et al*, "On Weibull distributed weather clutter.", *IEEE Trans. on Aerosp. Electron. Syst.*, AES-15, pp. 824-830.

[29] Tsihrintzis, G. A. and Nikias, C. L., "Evaluation of fractional lower-order statistics-based detection algorithms on real sea-clutter data.", *IEE Proc-Radar, Sonar Navig.*, vol. 144, no.1, Feb., pp. 29-37, 1997.

[30] M. Nakagami, "The m-Distribution, a general formula of intensity of rapid fading". In W. G. Hoffman, editor, *Statistical Methods in Radio Wave Propagation: Proceedings of a Symposium held at the University of California*, pp 3-36. Permagon Press, 1960.

[31] Devore, Probability and Statistics for Engineering and the Sciences. Monterey, CA: BrooksiCole, 1982.

[32] Barkat, M., Signal deteciton and estimation, 2nd, London: Artech house, 2005.

List of Tables

Table 1: Estimated Parameters for Poor Signal

PDF	Log-Logistic	Log-normal	Weibull	Nakagami
data 1	$\hat{\mu} = 7.24161$ $\hat{\sigma} = 1.06483$ $\varepsilon_\mu = 0.0141212$ $\varepsilon_\sigma = 0.00724181$	$\hat{\mu} = 7.0455$ $\hat{\sigma} = 2.20761$ $\varepsilon_\mu = 0.0174527$ $\varepsilon_\sigma = 0.0123415$	$\hat{a} = 2975.33$ $\hat{b} = 0.594979$ $\varepsilon_a = 41.6157$ $\varepsilon_b = 0.00356925$	$\hat{\mu} = 0.177062$ $\hat{\omega} = 9.09663e+007$ $\varepsilon_\mu = 0.00150615$ $\varepsilon_\omega = 1.70907e+006$
data 2	$\hat{\mu} = 6.9716$ $\hat{\sigma} = 1.2126$ $\varepsilon_\mu = 0.014747$ $\varepsilon_\sigma = 0.00773723$	$\hat{\mu} = 6.72573$ $\hat{\sigma} = 2.33617$ $\varepsilon_\mu = 0.0184691$ $\varepsilon_\sigma = 0.0130602$	$\hat{a} = 2285.13$ $\hat{b} = 0.563747$ $\varepsilon_a = 33.7127$ $\varepsilon_b = 0.00337485$	$\hat{\mu} = 0.162375$ $\hat{\omega} = 7.4776e+007$ $\varepsilon_\mu = 0.00137422$ $\varepsilon_\omega = 1.46679e+006$
data 3	$\hat{\mu} = 7.00554$ $\hat{\sigma} = 1.10741$ $\varepsilon_\mu = 0.0145728$ $\varepsilon_\sigma = 0.0076303$	$\hat{\mu} = 6.76262$ $\hat{\sigma} = 2.31258$ $\varepsilon_\mu = 0.0182825$ $\varepsilon_\sigma = 0.0129283$	$\hat{a} = 2341.52$ $\hat{b} = 0.57073$ $\varepsilon_a = 34.1207$ $\varepsilon_b = 0.00341448$	$\hat{\mu} = 0.164695$ $\hat{\omega} = 7.46366e+007$ $\varepsilon_\mu = 0.001395$ $\varepsilon_\omega = 1.45459e+006$
data 4	$\hat{\mu} = 7.03055$ $\hat{\sigma} = 1.07858$ $\varepsilon_\mu = 0.0142027$ $\varepsilon_\sigma = 0.00741556$	$\hat{\mu} = 6.80711$ $\hat{\sigma} = 2.25973$ $\varepsilon_\mu = 0.0178647$ $\varepsilon_\sigma = 0.0126329$	$\hat{a} = 2395.85$ $\hat{b} = 0.579381$ $\varepsilon_a = 34.4066$ $\varepsilon_b = 0.00345156$	$\hat{\mu} = 0.167391$ $\hat{\omega} = 7.4926e+007$ $\varepsilon_\mu = 0.0014916$ $\varepsilon_\omega = 1.44727e+006$
data 5	$\hat{\mu} = 7.16226$ $\hat{\sigma} = 1.10132$ $\varepsilon_\mu = 0.014605$ $\varepsilon_\sigma = 0.00750067$	$\hat{\mu} = 6.95712$ $\hat{\sigma} = 2.26592$ $\varepsilon_\mu = 0.0179137$ $\varepsilon_\sigma = 0.0126675$	$\hat{a} = 2806.76$ $\hat{b} = 0.577823$ $\varepsilon_a = 40.4226$ $\varepsilon_b = 0.00347389$	$\hat{\mu} = 0.17112$ $\hat{\omega} = 9.03298e+007$ $\varepsilon_\mu = 0.00145265$ $\varepsilon_\omega = 1.72749e+006$
data 6	$\hat{\mu} = 7.01527$ $\hat{\sigma} = 1.10123$ $\varepsilon_\mu = 0.0144902$ $\varepsilon_\sigma = 0.00758568$	$\hat{\mu} = 6.77515$ $\hat{\sigma} = 2.30286$ $\varepsilon_\mu = 0.0182057$ $\varepsilon_\sigma = 0.012874$	$\hat{a} = 2360.33$ $\hat{b} = 0.572749$ $\varepsilon_a = 34.2753$ $\varepsilon_b = 0.00342376$	$\hat{\mu} = 0.165292$ $\hat{\omega} = 7.50824e+007$ $\varepsilon_\mu = 0.00140035$ $\varepsilon_\omega = 1.46145e+006$
data 7	$\hat{\mu} = 7.14523$ $\hat{\sigma} = 1.09486$ $\varepsilon_\mu = 0.0145132$ $\varepsilon_\sigma = 0.00745994$	$\hat{\mu} = 6.94201$ $\hat{\sigma} = 2.25621$ $\varepsilon_\mu = 0.0178369$ $\varepsilon_\sigma = 0.0126132$	$\hat{a} = 2753.69$ $\hat{b} = 0.578948$ $\varepsilon_a = 39.585$ $\varepsilon_b = 0.00347442$	$\hat{\mu} = 0.170964$ $\hat{\omega} = 8.80474e+007$ $\varepsilon_\mu = 0.00145125$ $\varepsilon_\omega = 1.68382e+006$
data 8	$\hat{\mu} = 6.95411$ $\hat{\sigma} = 1.11486$ $\varepsilon_\mu = 0.0146774$ $\varepsilon_\sigma = 0.00768003$	$\hat{\mu} = 6.71591$ $\hat{\sigma} = 2.31898$ $\varepsilon_\mu = 0.0183331$ $\varepsilon_\sigma = 0.0129641$	$\hat{a} = 2250.66$ $\hat{b} = 0.564989$ $\varepsilon_a = 33.1387$ $\varepsilon_b = 0.0033763$	$\hat{\mu} = 0.162448$ $\hat{\omega} = 7.31436e+007$ $\varepsilon_\mu = 0.00137488$ $\varepsilon_\omega = 1.4338e+006$
data 9	$\hat{\mu} = 7.18561$ $\hat{\sigma} = 1.09854$ $\varepsilon_\mu = 0.0145483$ $\varepsilon_\sigma = 0.00749265$	$\hat{\mu} = 6.9715$ $\hat{\sigma} = 2.27088$ $\varepsilon_\mu = 0.0179529$ $\varepsilon_\sigma = 0.0126952$	$\hat{a} = 2840.72$ $\hat{b} = 0.581219$ $\varepsilon_a = 40.6593$ $\varepsilon_b = 0.0034984$	$\hat{\mu} = 0.172324$ $\hat{\omega} = 8.97304e+007$ $\varepsilon_\mu = 0.00146348$ $\varepsilon_\omega = 1.70923e+006$
data 10	$\hat{\mu} = 7.192$ $\hat{\sigma} = 1.0866$ $\varepsilon_\mu = 0.0144166$ $\varepsilon_\sigma = 0.0073916$	$\hat{\mu} = 6.99196$ $\hat{\sigma} = 2.23975$ $\varepsilon_\mu = 0.0177067$ $\varepsilon_\sigma = 0.0125211$	$\hat{a} = 2869.65$ $\hat{b} = 0.584803$ $\varepsilon_a = 40.837$ $\varepsilon_b = 0.00351294$	$\hat{\mu} = 0.173572$ $\hat{\omega} = 9.01631e+007$ $\varepsilon_\mu = 0.0014747$ $\varepsilon_\omega = 1.71142e+006$

Table 2: Averaged Estimated Parameters for Poor Signal

PDF	Log-Logistic	Log-normal	Weibull	Nakagami
average	$\hat{\mu} = 7.0904$ $\hat{\sigma} = 1.1061$ $\varepsilon_\mu = 0.0145$ $\varepsilon_\sigma = 0.0075$	$\hat{\mu} = 6.8695$ $\hat{\sigma} = 2.2771$ $\varepsilon_\mu = 0.0180$ $\varepsilon_\sigma = 0.0127$	$\hat{a} = 2588$ $\hat{b} = 0.5769$ $\varepsilon_a = 37.4316$ $\varepsilon_b = 0.0035$	$\hat{\mu} = 0.1687$ $\hat{\omega} = 8.218e + 007$ $\varepsilon_\mu = 0.0014$ $\varepsilon_\omega = 1.4905e + 006$

Table 3: Estimated Parameters for Good Signal

PDF	Log-Logistic	Log-normal	Weibull	Nakagami
data 1	$\hat{\mu} = 7.76868$ $\hat{\sigma} = 0.786511$ $\varepsilon_\mu = 0.0107792$ $\varepsilon_\sigma = 0.00521601$	$\hat{\mu} = 7.79566$ $\hat{\sigma} = 1.41771$ $\varepsilon_\mu = 0.011208$ $\varepsilon_\sigma = 0.00792559$	$\hat{a} = 4901.07$ $\hat{b} = 0.743223$ $\varepsilon_a = 55.3011$ $\varepsilon_b = 0.00434465$	$\hat{\mu} = 0.239587$ $\hat{\omega} = 1.16839e + 008$ $\varepsilon_\mu = 0.00207912$ $\varepsilon_\omega = 1.88719e + 006$
data 2	$\hat{\mu} = 7.78096$ $\hat{\sigma} = 0.787426$ $\varepsilon_\mu = 0.0107917$ $\varepsilon_\sigma = 0.0052213$	$\hat{\mu} = 7.8046$ $\hat{\sigma} = 1.41855$ $\varepsilon_\mu = 0.0112147$ $\varepsilon_\sigma = 0.00793033$	$\hat{a} = 4942.48$ $\hat{b} = 0.745233$ $\varepsilon_a = 55.6114$ $\varepsilon_b = 0.0043612$	$\hat{\mu} = 0.240593$ $\hat{\omega} = 1.17237e + 008$ $\varepsilon_\mu = 0.00208848$ $\varepsilon_\omega = 1.88953e + 006$
average	$\hat{\mu} = 7.7748$ $\hat{\sigma} = 0.7870$ $\varepsilon_\mu = 0.0108$ $\varepsilon_\sigma = 0.0052$	$\hat{\mu} = 7.7881$ $\hat{\sigma} = 1.4181$ $\varepsilon_\mu = 0.0112$ $\varepsilon_\sigma = 0.0079$	$\hat{a} = 4921.8$ $\hat{b} = 0.7442$ $\varepsilon_a = 55.4565$ $\varepsilon_b = 0.0044$	$\hat{\mu} = 0.2401$ $\hat{\omega} = 1.1704 + 008$ $\varepsilon_\mu = 0.0021$ $\varepsilon_\omega = 1.8884 + 006$

List of Figures

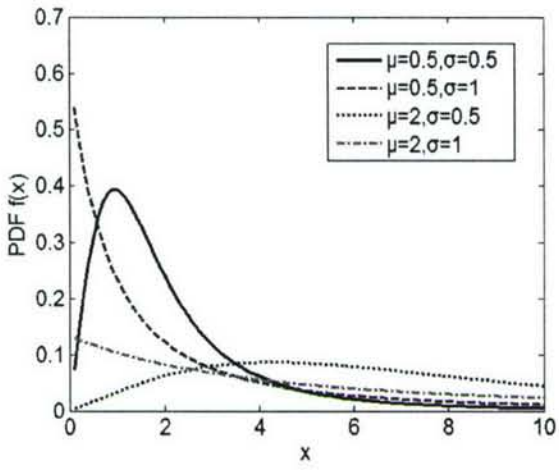

Figure 1: Log-Logistic distribution PDF for $\mu = 0.5$ and $\sigma = 0.5$, $\mu = 0.5$ and $\sigma = 1$, $\mu = 2$ and $\sigma = 0.5$, $\mu = 2$ and $\sigma = 1$

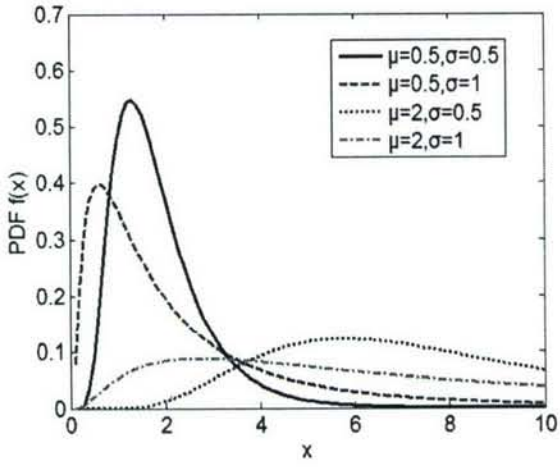

Figure 2: Log-Normal distribution PDF for $\mu = 0.5$ and $\sigma = 0.5$, $\mu = 0.5$ and $\sigma = 1$, $\mu = 2$ and $\sigma = 0.5$, $\mu = 2$ and $\sigma = 1$

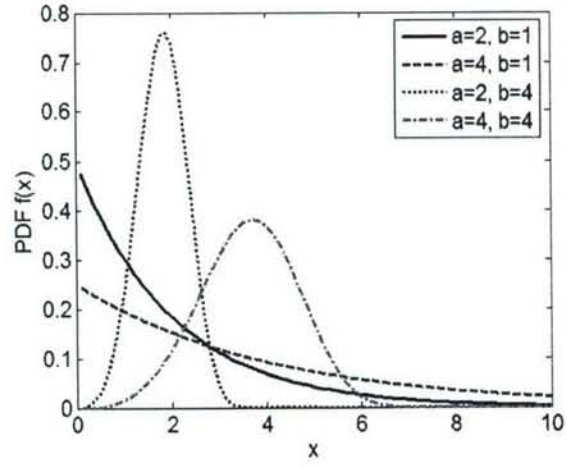

Figure 3: Log-Normal distribution PDF for $a = 2$ and $b = 1$, $a = 4$ and $b = 1$, $a = 2$ and $b = 4$, $a = 4$ and $b = 4$

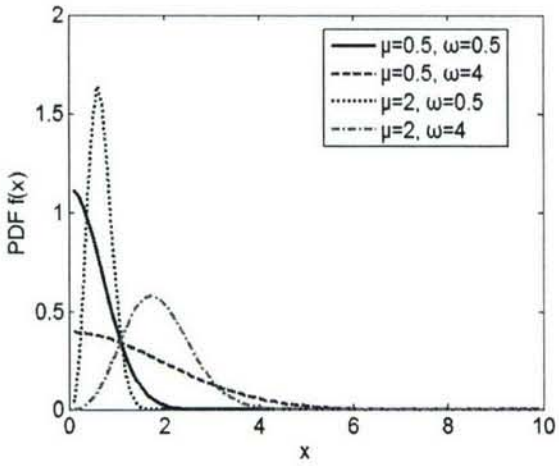

Figure 4: Nakagami distribution PDF for $\mu = 0.5$ and $\omega = 0.5$, $\mu = 0.5$ and $\omega = 4$, $\mu = 2$ and $\omega = 0.5$, $\mu = 2$ and $\omega = 4$

Figure 5: This figure shows the lift with the experiment. The antennas are at the far end of the lift from the viewer under the roof that was built to shield the equipment from the elements. This picture was taken in September with the foliage largely still present. The cables coming from the lift are a ground cable to an earth ground and one of 4 tethers used in windy conditions.

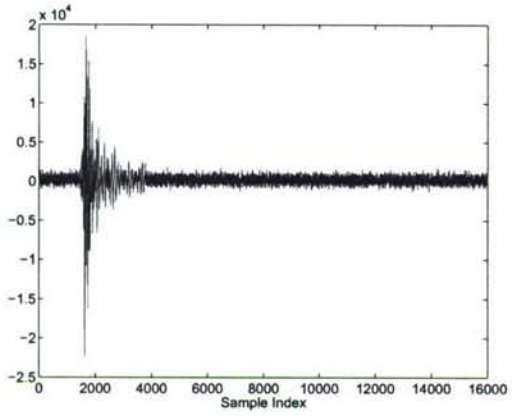

(a)

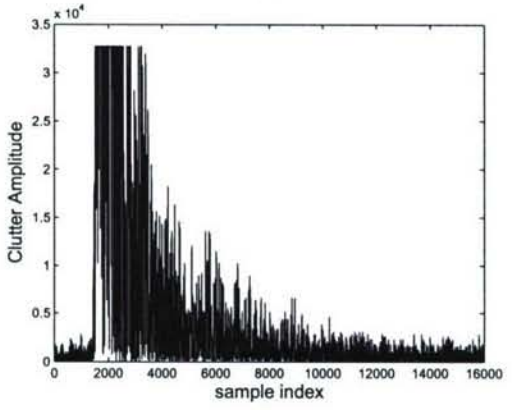

(b)

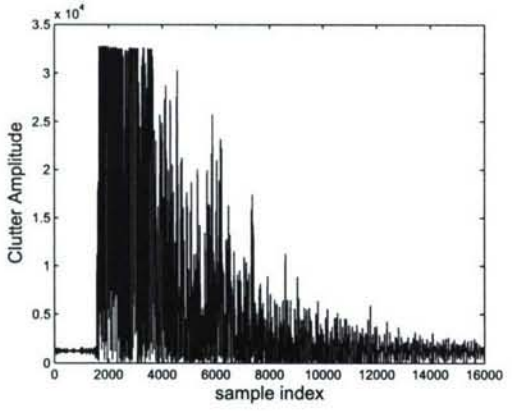

(c)

Figure 6: Clutter data (a)transmitted pulse (b)received echoes with poor quality, and (c)received echoes with good quality

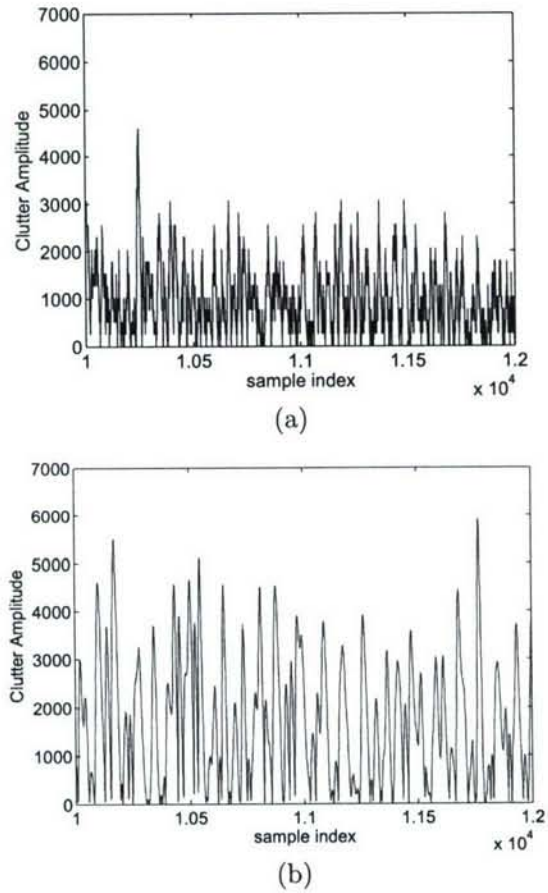

Figure 7: Expanded view from clutter samples 10,000 to 12,000 (a) poor quality, and (b) good quality

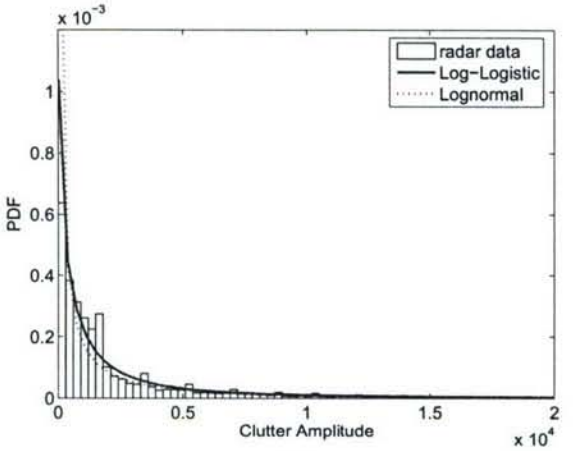

(a)

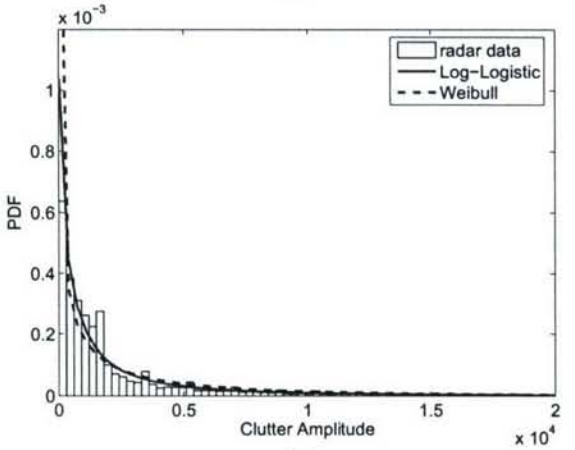

(b)

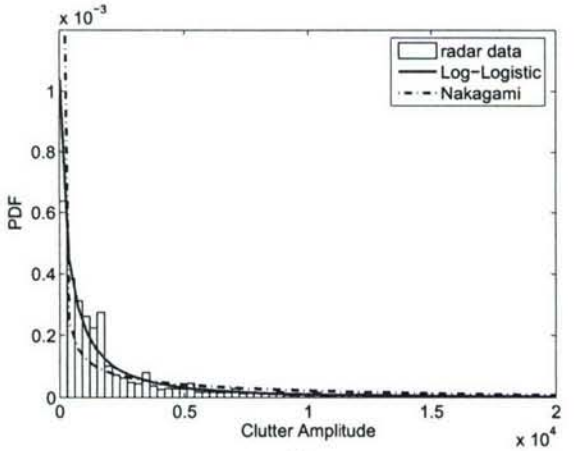

(c)

Figure 8: Clutter model comparison with poor signal quality. (a) log-logistic vs. lognormal, and (b) log-logistic vs. weibull (c) log-logistic vs. nakagami. $\texttt{RMSE}_{log-logistic} = 2.5425 \times 10^{-5}$, $\texttt{RMSE}_{log-normal} = 3.2704 \times 10^{-5}$, $\texttt{RMSE}_{weibull} = 3.7234 \times 10^{-5}$, $\texttt{RMSE}_{nakagami} = 5.4326 \times 10^{-5}$.

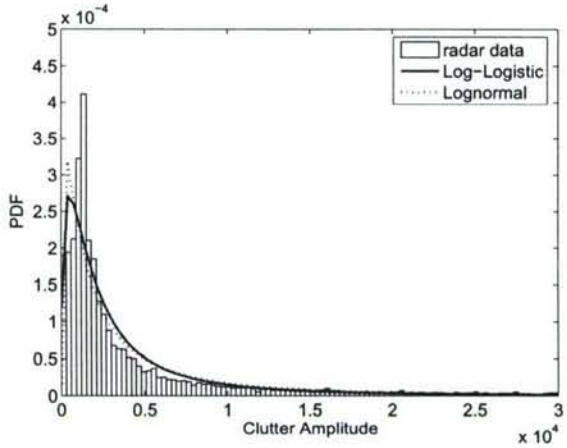

(a)

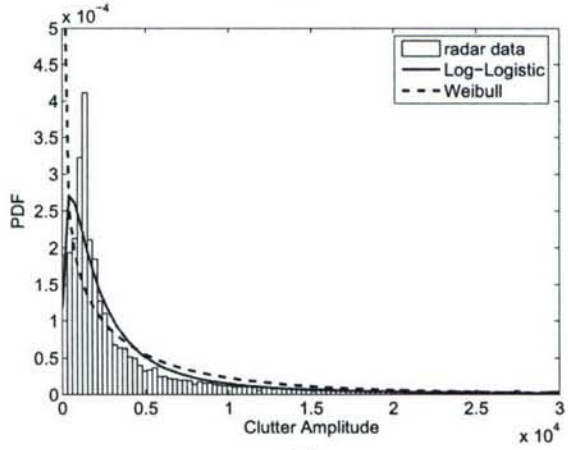

(b)

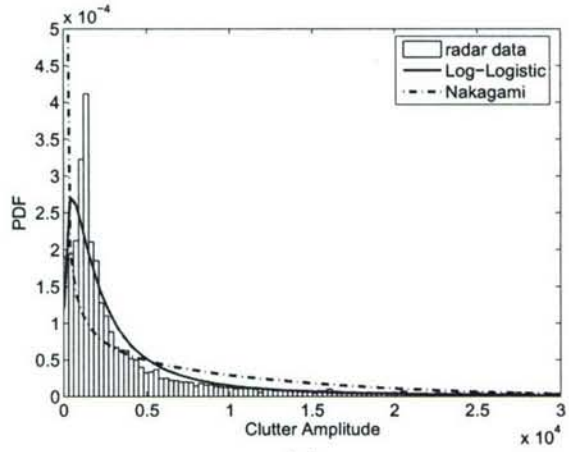

(c)

Figure 9: Clutter model comparison with good signal quality. (a)log-Logistic vs. lognormal, and (b) log-logistic vs. weibull (c) log-logistic vs. nakagami. $\texttt{RMSE}_{log-logistic} = 2.739 \times 10^{-5}$, $\texttt{RMSE}_{log-normal} = 3.1866 \times 10^{-5}$, $\texttt{RMSE}_{weibull} = 3.6361 \times 10^{-5}$, $\texttt{RMSE}_{nakagami} = 4.4045 \times 10^{-5}$.

Collaborative Multi-Target Detection in Radar Sensor Networks

Hung D. Ly and Qilian Liang
Department of Electrical Engineering
The University of Texas at Arlington
Arlington, TX 76019-0016, USA
E-mail: ly@wcn.uta.edu, liang@uta.edu

Abstract— **In many military and civilian applications, estimating the number of targets in a region of interest plays a primary role in performing important tasks such as target localization, classification, recognition, tracking, etc. Such an estimation problem is however very challenging since the number of targets is time-varying, targets' state is fluctuating, and many kinds of targets might appear in the field of interest. In this paper, we develop a framework for estimating the number of targets in a sensing area using Radar Sensor Networks (RSNs): (1) we formulate the multi-target detection problem; (2) we model signals, interference (e.g., clutter, jamming, and interference between radars), and noise at radar sensors; (3) we propose a Maximum Likelihood Multi-Target Detection (ML-MTD) algorithm to combine received measurements and estimate the number of targets present in the sensing area. We evaluate multi-target detection performance using RSNs in terms of the probability of miss detection P_{MD} and the root mean square error (RMSE). Simulation results show that multi-target detection performance of the RSNs is much better than that of single radar systems.**

I. Introduction and Motivations

Radar sensor networks (RSNs) are networks of distributed radar sensors which collaboratively operate and are deployed ubiquitously on airborne, surface, and unmanned vehicles in a large geographical area. Radar sensors have capabilities for radar sensing, signal processing, and wireless communications. In RSNs, radar sensors are networked together in an ad-hoc fashion, i.e., they do not depend on any preexisting infrastructure. In fact, they are self-organizing entities that are deployed on demand to perform various tasks such as surveillance, search and rescue, disaster relief, etc. RSNs have advantages compared to single radar systems in improving the system sensitivity, reducing obscuration effects and vulnerability, and increasing the detection performance [2], [3].

An RSN is organized into clusters, which are independently controlled and dynamically reconfigured as sensors move, to observe targets such as tactical weapons, missiles, aircraft, ships, etc. in the surveillance area. In a cluster, sensors receive the signals backscattered by targets in the presence of interference (e.g., clutter, jamming, interference between radar sensors), and noise. Then, the observed signals from all radar sensors are forwarded to a clusterhead where received data set will be combined to perform fundamental tasks such as detection, localization, identification, classification, and tracking. For target detection problem, there are two primary levels: single target detection and multi-target detection. In the single target scenario, we proposed a diversity scheme in [13] to improve detection performance of RSNs in the presence of strong interference, especially clutters, and noise. We are now interested in using RSNs to estimate the number of targets present in the surveillance area. In practice, multiple moving targets might appear in the sensing area, the number of targets is time-varying, and targets' state is fluctuating. Therefore, the multi-target detection is more challenging and difficult to solve than the single target detection.

Among the existing work on multi-target detection, Yung and Mourad [16] used frequency diversity signaling to estimate the number of moving targets. Kaveh *et al.* [20] applied the information theoretic criteria to detect the number of targets. However, both work only studied the performance of their proposals for the case of two closely spaced targets. A performance analysis for a general case was provided in [19] and [18]. In [15], multiple target detection and estimation by exploiting the amplitude modulation induced by antenna scanning was proposed and a sequential hypothesis test was examined to determine the number of targets. However, all above work studied multi-target detection problem using a single radar. For the sensor network scenario, Wang *et al.* [17] applied Bayesian source number estimation to solve the distributed multiple target detection in sensor networks. Based on their approach, each cluster computed the posterior probability corresponding to each hypothesis on the number of sources and a central processor fused posterior probabilities using Bayes' theorem to select the best hypothesis. Their proposal however did not consider Doppler shifts of the targets and was not suitable for the multi-target detection in RSNs.

In this paper, we develop a framework for estimating the number of targets in the field of interest using RSNs. At the ith sensor, we deploy a receiver with an K element-ULA (Uniform Linear Array) whose spacing between elements is d_i. During the observation time, P pulses are transmitted to track targets. The useful signals backscattered from targets include spatial-temporal snapshots of targets and parameters representing radar cross section of targets. Then, a RSN-clusterhead collects measurements from all radar sensors and combines them to perform detection procedures. To fuse

received measurements and estimate the unknown number of targets in the area of interest, at the RSN-clusterhead, we propose a multi-target detection algorithm which is Maximum Likelihood Multi-Target Detection (ML-MTD) algorithm. We use the probability of miss detection P_{MD} and the root mean square error (RMSE) as metrics to evaluate multi-target detection performance using RSN. Simulation results show that detection performance of the RSN is much better than that of a single radar system.

The rest of this paper is organized as follows. In Section II, we state our multi-target detection problem. In Section III, we model signals, interference, and noise at radar sensors. In Section IV, we propose an ML-MTD algorithm to estimate the number of targets present in the sensing field. Multi-target detection performance of RSN is discussed in Section V while conclusions and open directions are given in Section VI.

II. Multi-Target Detection Problem Statement

In this paper, we address a realistic situation in which the number of targets to be detected is generally unknown and has to be estimated. To handle our problem, an RSN consisting of N radar sensors is deployed. Radar sensors receive signals embedded in interference and forward them to a central processor, e.g., a clusterhead to perform detection tasks. At the RSN-clusterhead, we propose a detection algorithm to estimate the number of targets. To support the rest of the paper, we make some assumptions as follows:

- Targets evolve along independent trajectories and do not leave the surveillance area during the entire observation time of P consecutive pulses.
- Targets are modeled as Swerling II target models whose magnitudes fluctuate independently from pulse to pulse according to a chi-square probability density function.
- The locations of targets are unknown. Besides, Doppler frequencies when targets are moving relatively to radar platforms are uncertain.
- Observation data or measurements from radar sensors, at the RSN-clusterhead, are statistically independent. The measurements furthermore either originate from true targets or clutters.

The estimated number of targets present in the surveillance area is determined as

$$\{\hat{\tau}_1, \hat{\tau}_2, ..., \hat{\tau}_N\} = \arg \min_{\tau_1, \tau_2, ..., \tau_N} \Lambda(\tau). \quad (1)$$

where $\hat{\tau}_i$ is the estimated number of targets at sensor i and $\Lambda(\tau)$ is an utility function derived in IV. Hence, the possible number of targets $\widehat{M}$ that RSN can detect is the average value of $\hat{\tau}_1, \hat{\tau}_2, ...,$ and $\hat{\tau}_N$, i.e.,

$$\widehat{M} = \lceil \frac{1}{N} \sum_{i=1}^{N} \hat{\tau}_i \rceil. \quad (2)$$

where $\lceil \cdot \rceil$ denotes a ceil operation.

III. Signal and Interference Models

A. Signal Models

At radar sensor i, we deploy a receiver with an K-element ULA whose spacing between elements is d_i. If P pulses are processed in a coherent pulse interval, the snapshot of target m is a $KP \times 1$ spatial-temporal steering vector with the following form [1], [9]:

$$\mathbf{e}(\theta_{im}, f_{im}) = \mathbf{b}_t(f_{im}) \otimes \mathbf{a}_s(\theta_{im}). \quad (3)$$

where f_{im} and θ_{im} are the normalized Doppler shift and normalized angle for the target m, respectively. The notation $\otimes$ denotes the Kronecker product, $\mathbf{b}_t(f_{im})$ is a $P \times 1$ Doppler steering vector, and $\mathbf{a}_s(\theta_{im})$ is a $K \times 1$ spatial steering vector. $\mathbf{b}_t(f_{im})$ and $\mathbf{a}_s(\theta_{im})$ are defined as follows:

$$\mathbf{b}_t(f_{im}) = [1 \quad e^{j2\pi f_{im}} \quad ... \quad e^{j2\pi(P-1)f_{im}}]^T. \quad (4)$$

$$\mathbf{a}_s(\theta_{im}) = [1 \quad e^{-j2\pi\theta_{im}} \quad ... \quad e^{-j2\pi(K-1)\theta_{im}}]^T. \quad (5)$$

where T denotes the transpose operation. Let ϕ_{im} be an angle that sensor i observes the mth target, $f_{max,m}$ be the maximum Doppler frequency for target m, and T_p be the pulse duration. The normalized angle θ_{im} for target m and the normalized Doppler shift f_{im} when target m is moving relatively to sensor platform i are computed as [9]

$$\theta_{im} = \frac{d_i \sin \phi_{im}}{\lambda_i} \quad (6)$$

$$f_{im} = 4 f_{max,m} T_p \theta_{im} \quad (7)$$

We now assume that radar sensor i can detect M_i targets during the observation time. The received signal vector $\mathbf{z}_i(u,t)$ at sensor i is the superposition of signals reflected from M_i targets, interference, and noise.

$$\begin{aligned} \mathbf{z}_i(u,t) &= \sum_{m=1}^{M_i} \mathbf{e}(\theta_{im}, f_{im}) \alpha_m(u) s_{mi}(t) + \mathbf{w}_i, \\ &= \mathbf{A}(\theta_i, f_i) \mathbf{s}_i(u,t) + \mathbf{w}_i, \quad i = 1, 2, ..., N. \end{aligned} \quad (8)$$

where

- $\mathbf{A}(\theta_i, f_i) = [\mathbf{e}(\theta_{i1}, f_{i1}), \mathbf{e}(\theta_{i2}, f_{i2}), ..., \mathbf{e}(\theta_{iM_i}, f_{iM_i})]$ is the $PK \times M_i$ target response matrix. $\mathbf{e}(\theta_{im}, f_{im})$ is a spatial-temporal steering vector that models the mth target return at angle θ_{im} and Doppler shift f_{im}.
- $\mathbf{s}_i(u,t) = [\alpha_1(u) s_{1i}(t), \alpha_2(u) s_{2i}(t), ..., \alpha_{M_i}(u) s_{M_i i}(t)]^T$ is the $M_i \times 1$ target signal vector with a random variable $\alpha_m(u)$ that models the radar cross section (RCS) of the target m and $s_{mi}(t)$ is the waveform reflected from target m.
- $\mathbf{w}_i = \mathbf{w}_{ci} + \mathbf{w}_{ji} + \mathbf{w}_{si} + \mathbf{n}_i$ represents the overall interference and noise: a clutter vector $\mathbf{w}_{ci}$, a jamming vector $\mathbf{w}_{ji}$, an interference vector between radar sensors $\mathbf{w}_{si}$, and thermal noise $\mathbf{n}_i$.

Received signals from radar sensors are forwarded to a central controller, e.g., clusterhead. Then, these received signal vectors $\mathbf{z}_i(u,t)$ are fused to make estimation operations. Since $\mathbf{z}_i(u,t)$ is a zero-mean Gaussian vector, the probability density function of $\mathbf{z}_i(u,t)$ can be presented as

$$f(\mathbf{z}_i(u,t)) = \frac{\exp\{-\frac{1}{2}\mathbf{z}_i^H[\mathbf{R}_{z,i}^{(\tau_i)}]^{-1}\mathbf{z}_i\}}{(2\pi)^{\frac{KP}{2}}|\mathbf{R}_{z,i}^{(\tau_i)}|^{\frac{1}{2}}}. \quad (9)$$

where $\mathbf{R}_{z,i}^{(\tau_i)}$ is the covariance matrix of $\mathbf{z}_i(u,t)$, τ_i is the rank of $\mathbf{R}_{z,i}$, and $|\cdot|$ denotes the determinant of the matrix.

B. Interference and Noise Models

As pointed out, at the ith radar sensor, the interference vector $\mathbf{w}_i$ is the sum of clutter $\mathbf{w}_{ci}$, jamming $\mathbf{w}_{ji}$, and interference between sensors $\mathbf{w}_{si}$. We apply the waveform design algorithm proposed in [12] to have waveforms at sensors be orthogonal. By doing so, interference between sensors can be canceled, i.e., $\mathbf{w}_{si} = \mathbf{0}$. Following are characteristics and models of clutter, jamming, and thermal noise at radar sensor i.

1) Clutter: Clutter generates undesired radar returns that may interfere with the desired signal. In RSNs, the signal-to-clutter ratio (SCR) is often more important than the signal-to-noise ratio (SNR). The integrated clutter can be generally approximated as the sum of N_{ci} clutter patches. For clutter patch k, the space-time data vector is modeled as [9]

$$\begin{aligned}\mathbf{p}_{ki} &= \xi_{ki}\mathbf{b}_t(f_{ki}) \otimes \mathbf{a}_s(\theta_{ki}) \\ &= \xi_{ki}\mathbf{u}_{ki}, \quad k = 1,2,...,N_{ci}. \end{aligned} \quad (10)$$

where ξ_{ki} is a complex random variable that accounts for the amplitude and phase of clutter patch k. $\mathbf{u}_{ki} = \mathbf{b}_t(f_{ki}) \otimes \mathbf{a}_s(\theta_{ki})$ where $\mathbf{b}_t(f_{ki})$ and $\mathbf{a}_s(\theta_{ki})$ are temporal vector and spatial vector of clutter patch k, respectively. f_{ki} and θ_{ki} are the normalized Doppler shift and angle of arrival of the kth clutter patch, respectively. Total clutter vector $\mathbf{w}_{ci}$ equals to

$$\begin{aligned}\mathbf{w}_{ci} &= \sum_{k=1}^{N_{ci}} \xi_{ki}\mathbf{b}_t(f_{ki}) \otimes \mathbf{a}_s(\theta_{ki}) \\ &= \sum_{k=1}^{N_{ci}} \xi_{ki}\mathbf{u}_{ki}. \end{aligned} \quad (11)$$

The $KP \times KP$ covariance matrix of the clutter $\mathbf{R}_{ci}$ at the ith radar is given by

$$\begin{aligned}\mathbf{R}_{ci} &= E\{\mathbf{w}_{ci}\mathbf{w}_{ci}^H\} \\ &= \sum_{k=1}^{N_{ci}}\sum_{j=1}^{N_{ci}} E\{\xi_i\xi_j^H\}\mathbf{u}_{ki}\mathbf{u}_{ji}^H, \\ &= \sigma_{ci}^2\mathbf{M}_{ci}. \end{aligned} \quad (12)$$

where H denotes the Hermitian operation, $E\{\cdot\}$ denotes the expectation, and $\mathbf{M}_{ci}$ is the normalized covariance matrix, i.e., all diagonal entries of $\mathbf{M}_{ci}$ are ones.

2) Jamming: Jamming signals are generated by hostile interfering signal sources that seek to degrade the performance of radar sensors by mechanisms such as degrading signal-to-interference-plus-noise ratio (SINR) by increasing the noise level, or generating false detections to overwhelm RSNs with false targets. A model for N_{ji} jamming signals is commonly presented as [1]

$$\mathbf{w}_{ji} = \sum_{l=1}^{N_{ji}} \beta_l \otimes a_{ji}(\theta_l), \quad i = 1,2,...,N. \quad (13)$$

where β_l contains voltage samples of the lth jamming waveform and $a_{ji}(\theta_l)$ is the jamming signal waveform at an angle θ_l. The different jamming waveforms are uncorrelated with each other.

3) Thermal Noise: Among noise existing in RSNs, thermal noise due to ohmic losses at the radar receiver is normally dominant. We model the thermal noise vector $\mathbf{n}_i$ at radar sensor i as a complex white Gaussian vector with zero-mean and covariance σ_{ni}^2. The covariance matrix of noise $\mathbf{R}_{ni} = \sigma_{ni}^2\mathbf{I}$ where $\mathbf{I}$ is the $KP \times KP$ identity matrix.

In RSNs, detection performance is largely affected by clutters. So we will consider the disturbance at the ith radar as a sum of thermal noise and clutter. The disturbance covariance matrix $\mathbf{R}_{wi}$ is given by

$$\begin{aligned}\mathbf{R}_{wi} &= E\{\mathbf{w}_i\mathbf{w}_i^H\} \\ &= \mathbf{R}_{ni} + \varepsilon_{ci}(h)\mathbf{R}_{ci}. \end{aligned} \quad (14)$$

where $\mathbf{R}_{ni}$ and $\mathbf{R}_{ci}$ are the covariance matrices of noise and clutter, respectively. $\varepsilon_{ci}(h)$ is a random variable used to model the clutter power of the hth range cell. $\varepsilon_{ci}(h)$ often follows Weibull distribution for ground clutter or gamma distribution for sea and/or weather clutter [14][21]. In homogeneous environments, the average clutter power does not depend on h, i.e., $\varepsilon_{ci}(h)$ is constant. Therefore, the disturbance covariance matrix is rewritten as

$$\begin{aligned}\mathbf{R}_{wi} &= \sigma_{wi}^2\mathbf{M}_{wi} \\ &= \sigma_{ni}^2\mathbf{I} + \varepsilon_c\sigma_{ci}^2\mathbf{M}_{ci}. \end{aligned} \quad (15)$$

where σ_{wi}^2 is the total disturbance power and $\mathbf{M}_{wi}$ is the normalized disturbance covariance matrix.

$$\mathbf{M}_{wi} = \frac{1}{CNR_i + 1}\mathbf{I} + \frac{CNR_i}{CNR_i + 1}\mathbf{M}_{ci}. \quad (16)$$

with $CNR_i = \frac{\varepsilon_c\sigma_{ci}^2}{\sigma_{ni}^2}$ is the clutter-to-noise power ratio. Then, total interference and noise can be modeled as a complex zero-mean white Gaussian vector with the covariance matrix $\sigma_{wi}^2\mathbf{M}_{wi}$, i.e., $\mathbf{w}_i \sim \mathcal{CN}(0, \sigma_{wi}^2\mathbf{M}_{wi})$.

IV. Maximum Likelihood Multi-Target Detection (ML-MTD) Algorithm

In this section, we develop an algorithm to detect the number of targets in the sensing region. We assume that signals

backscattered from targets and interference are uncorrelated. From the signal model in (8), the covariance matrix of received signal $\mathbf{z}_i(u,t)$ at radar sensor i is given by

$$\begin{aligned}\mathbf{R}_{z,i}^{(\tau_i)} &= E\{\mathbf{z}_i(u,t)\mathbf{z}_i^H(u,t)\},\\ &= \mathbf{A}(\theta_i,f_i)\mathbf{R}_{s,i}\mathbf{A}^H(\theta_i,f_i)+\sigma_{wi}^2\mathbf{M}_{wi},\\ &= \mathbf{\Phi}_i^{(\tau_i)}+\sigma_{wi}^2\mathbf{M}_{wi}. \end{aligned} \quad (17)$$

where $\mathbf{R}_{s,i}$ is a $M_i \times M_i$ positive definite matrix which represents the covariance matrix of the signal $\mathbf{s}_i(u,t)$, σ_{wi}^2 is the disturbance power, and $\mathbf{M}_{wi}$ is the normalized disturbance covariance matrix at radar sensor i. $\mathbf{R}_{s,i}$ and $\mathbf{\Phi}_i^{(\tau_i)}$ are defined:

$$\mathbf{R}_{s,i} = E\{\mathbf{s}_i(u,t)\mathbf{s}_i^H(u,t)\} \quad (18)$$

$$\mathbf{\Phi}_i^{(\tau_i)} = \mathbf{A}(\theta_i,f_i)\mathbf{R}_{s,i}\mathbf{A}^H(\theta_i,f_i) \quad (19)$$

The random variables $\alpha_m(u)$ $(i=1,2,...,M_i)$ in $\mathbf{s}_i(u,t)$ models the RCS of the mth target. In [11], Swerling proposed five target models called Swerling models where Swerling V model is for non-fluctuating targets and Swerling I-IV models are for fluctuating targets. In this paper, we focus our studies on the Swerling II target models. We know that magnitude of the RCS $|\alpha(u)|$ for Swerling II targets fluctuates independently from pulse to pulse according to a chi-square probability density function with two degree of freedom, i.e., a Rayleigh probability density function. Therefore, the RCS of target m can be modeled as a Gaussian random variables. That is,

$$\alpha_m(u) = \alpha_{Im}(u) + j\alpha_{Qm}(u). \quad (20)$$

where $\alpha_{Im}(u)$ and $\alpha_{Qm}(u)$ follow Gaussian distribution with zero mean and variance $\rho_m^2/2$ for each branch I, Q.

From (17), it follows that the rank of matrix $\mathbf{R}_{z,i}^{(\tau_i)}$ is τ_i, which is equal to the number of targets M_i present in the surveillance region, and the smallest $(KP-\tau_i)$ of its eigenvalues are zero, i.e., the received signal contains interference and noise only. Sorting the eigenvalues of $\mathbf{R}_{z,i}^{(\tau_i)}$ in a decreasing order, we obtain

$$\lambda_1 \geq \lambda_2 \geq ... \geq \lambda_{\tau_i} \geq \lambda_{\tau_i+1}. \quad (21)$$

$$\lambda_{\tau_i+1} = \lambda_{\tau_i+2} = ... = \lambda_{KP} = \sigma_{wi}^2. \quad (22)$$

Assume that measurements $\mathbf{z}_i(u,t)$, at the clusterhead, are statistically independent complex Gaussian random vectors with zero mean. The joint probability density function of these random vectors has the form:

$$\begin{aligned} f(\mathbf{z}(u,t)) &= \prod_{i=1}^{N} f(\mathbf{z}_i(u,t)),\\ &= \prod_{i=1}^{N} \frac{\exp\{-\frac{1}{2}\mathbf{z}_i^H[\mathbf{R}_{z,i}^{(\tau_i)}]^{-1}\mathbf{z}_i\}}{(2\pi)^{\frac{KP}{2}}|\mathbf{R}_{z,i}^{(\tau_i)}|^{\frac{1}{2}}}. \end{aligned} \quad (23)$$

Basically, we have to estimate $\hat{\tau}_i$ such that the joint probability density function $f(\mathbf{z}(u,t))$ is maximized. We now define a log-likelihood function $\Gamma(\tau)$ $\{\tau=[\tau_1,\tau_2,...,\tau_N]\}$ in (24). Hence, our mission is to find $\hat{\tau}_i$ such that $\Gamma(\tau)$ is minimized.

$$\begin{aligned}\Gamma(\tau) &= -\ln f(\mathbf{z}(u,t)),\\ &= \frac{N\times KP}{2}\ln(2\pi)+\frac{1}{2}\sum_{i=1}^{N}\log|\mathbf{R}_{z,i}^{(\tau_i)}|+\\ &+ \frac{1}{2}\sum_{i=1}^{N}\mathbf{z}_i^H[\mathbf{R}_{z,i}^{(\tau_i)}]^{-1}\mathbf{z}_i. \end{aligned} \quad (24)$$

Omitting terms that are independent of τ_i, we find the log-likelihood function $\Gamma(\tau)$.

$$\Gamma(\tau) = \sum_{i=1}^{N}\log|\mathbf{R}_{z,i}^{(\tau_i)}| + \sum_{i=1}^{N}\mathbf{z}_i^H[\mathbf{R}_{z,i}^{(\tau_i)}]^{-1}\mathbf{z}_i. \quad (25)$$

From [6], [8], and [7], the utility function $\Lambda(\tau)$ takes the form:

$$\Lambda(\tau) = \Gamma(\tau) + P(N). \quad (26)$$

where $P(N) = \wp(N)[\tau_{avg}(2KP-\tau_{avg})]$ is a bias correction term or penalty function to make estimate unbiased. τ_{avg} is an average value of $\{\tau_i | i=1,2,...,N\}$ and $\wp(N)$ is a penalty coefficient which is a constant function of N. For example, $\wp(N)=1$ for the Akaike information criterion (AIC) and $\wp(N)=\frac{1}{2}\ln N$ for the minimum description length (MDL). $\Lambda(\tau)$ then can be rewritten as

$$\begin{aligned}\Lambda(\tau) &= \sum_{i=1}^{N}\log|\mathbf{R}_{z,i}^{(\tau_i)}| + \sum_{i=1}^{N}\mathbf{z}_i^H[\mathbf{R}_{z,i}^{(\tau_i)}]^{-1}\mathbf{z}_i +\\ &+ \wp(N)\{\tau_{avg}(2KP-\tau_{avg})\}. \end{aligned} \quad (27)$$

Our ML-MTD algorithm to detect the number of targets $\widehat{M}$ present in the sensing field now can be expressed as

$$\widehat{M} = \lceil \frac{1}{N}\sum_{i=1}^{N}\hat{\tau}_i \rceil. \quad (28)$$

where $\hat{\tau} = \{\hat{\tau}_1,\hat{\tau}_2,...,\hat{\tau}_N\}$ is computed as

$$\{\hat{\tau}_1,\hat{\tau}_2,...,\hat{\tau}_N\} = \arg\min_{\tau_1,\tau_2,...,\tau_N}\Lambda(\tau). \quad (29)$$

In practice, sensors can observe the different numbers of targets, i.e., τ_is may not be equal, since targets might not be exposed to all sensors. However, for the sake of simplicity, we assume that all radar sensors can observe the same number of targets, i.e., $\tau_1=\tau_2=...=\tau_N=\tau$ and energy backscattered from targets is similar at radar sensors. Furthermore, we assume that the environment is homogeneous, that is, the average clutter power is a constant. These assumptions imply that $\mathbf{R}_{z,1}^{(\tau)}=\mathbf{R}_{z,2}^{(\tau)}=\mathbf{R}_{z,N}^{(\tau)}=\mathbf{R}_z^{(\tau)}$. For those reasons, our ultimate purpose is to evaluate detection performance improvement achievable by exploiting the networking of multiple radar sensors. Under our assumptions, the utility function $\Lambda(\tau)$ can be simplified as

$$\Lambda(\tau) = N \log|\mathbf{R}_z^{(\tau)}| + N\mathbf{tr}([\mathbf{R}_z^{(\tau)}]^{-1}\mathbf{Y}) + \wp(N)\{\tau(2KP-\tau)\}. \quad (30)$$

where $\mathbf{tr}(\cdot)$ denotes the trace of a matrix and $\mathbf{Y}$ is the sample covariance matrix of $\mathbf{z}_1, \mathbf{z}_2, ..., \mathbf{z}_N$.

$$\mathbf{Y} = \frac{1}{N}\sum_{i=1}^{N} \mathbf{z}_i \mathbf{z}_i^T. \quad (31)$$

Based on (30) and (31), we can observe that the utility function $\Lambda(\tau)$ depends on the number of radar sensors N. Our ML-MTD algorithm is used to determine any non-negative integer τ to minimize the utility function $\Lambda(\tau)$ when the number of radars is changed. Achieved results are analyzed to evaluate the multi-target detection performance in Section V.

V. Multi-Target Detection Performance Analysis

We denote the true number of targets appearing in the observation area and the number of targets we can estimate from received signals as M and $\widehat{M}$, respectively. The probability of miss detection P_{MD} and the root mean square error (RMSE) are used as metrics to evaluate detection performance of the RSN using our proposed algorithm. We define P_{MD} and RMSE as follows:

- P_{MD} is the probability that the estimated number of targets is smaller than the true number of targets. Suppose that ω_{md} is the number of estimations in which the estimated number of targets is smaller than the true number of targets and ω_t is the total number of estimations. P_{MD} is given as

$$\begin{aligned} P_{MD} &= P(\widehat{M} < M) \\ &= \frac{\omega_{md}}{\omega_t}. \end{aligned} \quad (32)$$

- RMSE is used to determine the vibration of the estimated number of targets $\widehat{M}$ around the true number of targets M.

$$RMSE = \sqrt{\frac{1}{\omega_t}\sum_{g=1}^{\omega_t}(M - \widehat{M}_g)^2}. \quad (33)$$

To study the MTD performance, we setup parameters for the RSN and targets as follows.

1) Spacing d_i between elements of the K-element ULA at radar sensor i is chosen to be a half of the wavelength λ_i, i.e., $d_i = \frac{\lambda_i}{2}$.
2) The pulse duration (T_p) is 1 ms.
3) The number of elements (K) in ULA is 5.
4) The number of pulses (P) in a coherent pulse interval is 4.
5) To observe targets, we assume that θ_{im} is a random variable which follows a uniform distribution in an interval [-0.5, 0.5].
6) The maximum Doppler frequencies for targets are similar, e.g., $f_{max} = 5000$Hz. The normalized Doppler shift f_{im} only depends on the random variable θ_{im}.

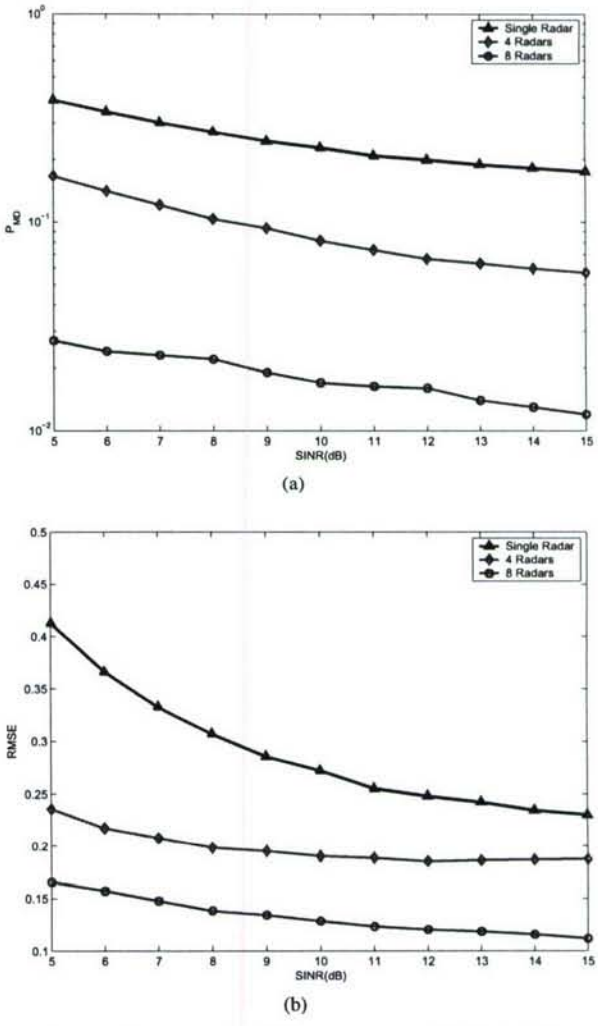

Fig. 1: P_{MD} and RMSE vs. Average SINR, M=3

7) Average Signal-to-Interference-plus-Noise Ratio (SINR) refers to average SINR of all radars in RSN. We examine detection performance of RSN with average SINR in an interval [5dB, 15dB].
8) The MDL criterion is used for the penalty function.
9) 10^5 estimations are performed, i.e., $\omega_t = 10^5$.

We first examine the case in which there are three targets in surveillance region, i.e., $M = 3$. Single radar system, 4-radar RSN, and 8-radar RSN are employed to detect these targets. At each average SINR, the estimated number of targets is compared to the true number of targets to compute P_{MD} and RMSE which are drawn in Fig. 1 for this case. After that, we increase the number of targets into four, i.e., $M = 4$. Using the same RSNs as the previous case, we can get P_{MD} and RMSE as plotted in Fig. 2. Based on achieved results in Fig. 1a and Fig. 2a, we can realize that miss detection probability of 4-radar RSN and 8-radar RSN is much smaller than that of single radar system. This implies that detection

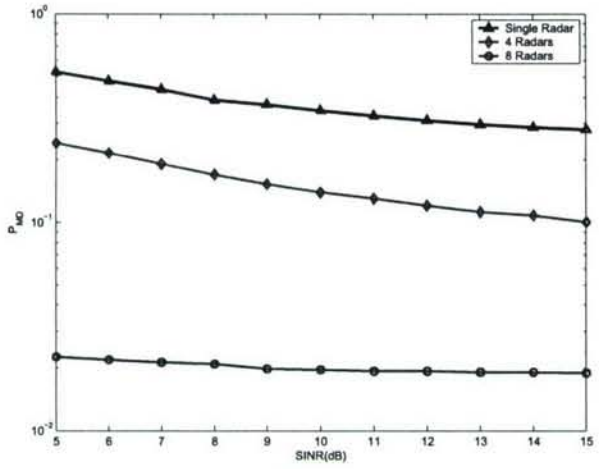

(a)

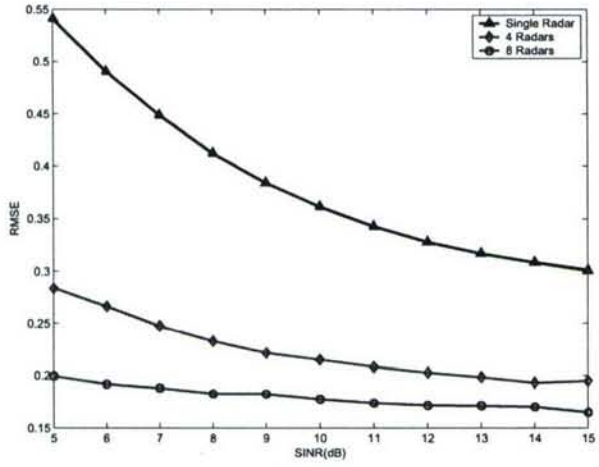

(b)

Fig. 2: P_{MD} and RMSE vs. Average SINR, M=4

performance of 4-radar RSN and 8-radar RSN is improved. For example, to achieve the same $P_{MD} = 10\%$ which is good enough according to Skolnik [4], the average SINR required for 4-radar RSN to detect three targets is about 9dB while the average SINR required for the single radar system is greater than 15dB. This means that detection performance gain of the 4-radar RSN is greater than 6dB. In both cases, moreover, the probability of miss detection is vastly reduced when the 8-radar RSN is used.

Furthermore, we observe that the higher average SINR, the smaller probability of miss detection. The reason is that, at high average SINR, radar sensors radiate signals at a high power level, so the coverage area of radar sensors is large. However, radiating signals at high power levels is costly. Thus tradeoff between cost and detection performance is necessary. We also observe that when we increase the number of targets, the detection performance is slightly reduced. For example, to achieve the same $P_{MD} = 10\%$, the 4-radar RSN to detect four targets requires average SINR around 4dB higher than that to detect three targets. This means that we need increase the transmit power for radar sensors. If the number of sensor radars is however large, e.g. $N = 8$, the detection performance of the RSN does not change much.

Besides the miss detection probability, RMSE is the other metric to examine the detection performance of the RSN. RMSE helps us evaluate the variability of the estimated number of targets around the true number of targets present in the sensing field. From Fig. 1b and Fig. 2b, we note that, to estimate three or four targets, RMSE of a single radar system is very high while RMSE of RSNs is reduced tremendously. For example, at SINR = 9dB, compared to a single radar system, the 4-radar RSN can reduce RMSE by 31.52% for three target case and 42.32% for four target case. Moreover, we can see that RMSE is reduced when we increase the number of sensors and/or average SINR.

VI. Conclusions

We investigate a multi-target detection problem in Radar Sensor Networks. Signal, interference, and noise models at radar sensors are presented and analyzed. We also propose a Maximum Likelihood Multi-Target Detection algorithm to estimate the possible number of targets in a surveillance area. RSN-clusterhead utilizes our algorithm to combine measurements from radar sensors and make decision. Achieved results show that detection performance of our RSN is much better than that of a single radar system in terms of the miss detection probability and the root mean square error. Besides scenarios presented in our work, one can extend our proposal in several directions as follows:

1) For the sake of simplicity, we assumed clutter environment which affects largely the performance of RSNs is homogeneous. Multi-target detection therefore can be examined when heterogeneous clutter environment is considered.
2) We only consider target models as small moving point-like targets. Thus dynamic and state space-based models might be further studied.
3) We only examine the case in which Swerling II target models are present in the sensing area. Naturally, multiple target model types can appear during the observation time, so multi-target detection problem when multiple target models coexist in the sensing region is worth looking into.
4) Our proposal is a primary state for important tasks such as target recognition, classification, tracking, etc. A joint algorithm to combine multi-target detection and one of above tasks can be investigated.

Acknowledgement

This work was supported by the U.S. Office of Naval Research (ONR) Young Investigator Program Award under Grant N00014-03-1-0466 and ONR Award under Grant N00014-07-1-0395.

REFERENCES

[1] William L. Melvin, "A STAP Overview," *IEEE A&E Systems Magazine*, vol 19, no. 1, pp. 19-35, Jan. 2004.

[2] S. Kadambe, "Feature discovery and sensor discrimination in a network of distributed radar sensors for target tracking," HRL Laboratories, LLC, 2001.

[3] C.J. Baker, A.L.Hume, "Netted Radar Sensing," *IEEE A&E Systems Magazine*, Feb. 2002.

[4] Skolnik, *Introduction to Radar Systems*, 3rd ed, McGraw Hill, 2001.

[5] M. Wax and T. Kailath, "Detection of signals by information theoretic criteria," *IEEE Transactions on Acoustics, Speech, and Signal Processing*, vol 33, no.2, pp 387-392, April 1985.

[6] H. Akaike, "A new look at the statistical model identification," *IEEE Transactions on Automatic Control*, vol 19, pp 716-723, Dec. 1974.

[7] G. Schwartz, "Estimating the dimension of a model," *Annals of Statistics*, vol. 6, pp. 497-511, 1978.

[8] J. Rissanen, "A universal prior for intergers and estimation by minimum description length," *Annals of Statistics*, vol. 11, no. 2, pp. 431-466, 1983.

[9] J.R Guerci, *Space-Time Adaptive Processing for Radar*, Artech House, 2003.

[10] Mark A. Richards, *Fundamentals of Radar Signal Processing*, McGraw-Hill Companies, New York 2005.

[11] Swerling, P., "Probability of Detection for Fluctuating Targets," *IRE Transactions on Information Theory*, vol IT-6, pp. 269-308, April 1960.

[12] Q. Liang, "Radar Sensor Networks: Algorithms for Waveform Design and Diversity with Application to ATR with Delay-Doppler Uncertainty," *EURASIP Journal on Wireless Communications and Networking*, Volume 2007, 2007.

[13] Hung D. Ly and Q. Liang, "Spatial-Temporal-Frequency Diversity in Radar Sensor Networks," *Military Communications Conference (MILCOM 2006)*, Oct. 2006, Washington, DC.

[14] R. Nitzberg, "An effect of range-heterogeneous clutter on adaptive doppler filters," *IEEE Transaction on Aerospace and Electronic Systems*, vol 26, no.3, pp 475-480, May 1990.

[15] Fulvio Gini *et al.*, "Multiple target detection and estimation by exploiting the amplitude modulation induced by antenna scanning. Part II: Detection," IEEE ICASSP, pp 533-536, 2003.

[16] Y. D. Huang and M. Barkat, "On estimation of number of moving targets via frequency-diversity signaling," *Proceedings of the 32nd Midwest Symposium on Circuits and Systems*, vol.2, pp 1170-1173, Aug. 1989.

[17] X. Wang, H. Qi, H. Du, "Distributed source number estimation for multiple target detection in sensor networks," *IEEE Workshop on Statistical Signal Processing*, pp 395-398, MO, Sept. 2003.

[18] Q. T. Zhang *et al.*, "Statistical Analysis of the performance of Information Theoretic Criteria in the detection of the number of signals in array processing," *IEEE Trans. on Acoustics, speech, and signal processing*, pp 1557-1565, vol. 37, no.10, Oct. 1989.

[19] W. Xu and M. Kaveh, "Analysis of the performance and sensitivity of Eigendecomposition-based detectors," *IEEE Trans. on signal processing*, vol. 43, no.6, Jun. 1995.

[20] M. Kaveh *et al.*, "On the theoretical performance of a class of estimators of the number of narrow-band sources," *IEEE Trans. on Acoustics, speech, and signal processing*, no.9, Sept. 1987.

[21] William L. Melvin, "Space-time adaptive radar performance in heterogeneous clutter," *IEEE Transaction on Aerospace and Electronic Systems*, vol 36, no.2, pp 621-633, April 2000.

Joint Multi-target Identification and Classification in Cognitive Radar Sensor Networks

Hong-Sam T. Le and Qilian Liang
Department of Electrical Engineering
The University of Texas at Arlington
Arlington, TX 76019, USA
E-mail: le@wcn.uta.edu, liang@uta.edu

Abstract— **We investigate the problem of jointly classifying and identifying multiple targets in radar sensor networks where the maximum number of categories and the maximum number of targets in each category are obtained a priori based on statistical data. However, the actual number of targets in each category and the actual number of target categories being present at any given time are assumed unknown. It is assumed that a given target belongs to one category and one identification number. The target signals are modeled as zero-mean complex Gaussian processes. We propose a joint multi-target identification and classification (JMIC) algorithm for radar surveillance using cognitive radars. The existing target categories are first classified and then the targets in each category are accordingly identified. Simulation results are presented to evaluate the feasibility and effectiveness of the proposed JMIC algorithm in a query surveillance region.**

I. Introduction

The importance of providing multiple target identification and classification (MTIC) capability for military applications is widely recognized nowadays. When the total number of targets being present in tactical battlefields is increased, classifying as well as identifying these targets will become a very challenging task. Measurements received from multiple radar sensors should be collected and processed in an efficient and robust manner to obtain the most meaningful information for identification and classification. Therefore, collaborative processing algorithms at the fusion center are in urgent need to successfully achieve this ultimate goal.

Many algorithms have been suggested to handle the task of multiple target identification and classification. In [5], a Gaussian Mixture Model (GMM) classifier was proposed to distinct target categories in a semi-structured outdoor environment. For radar target identification, a multi-feature decision space approach was discussed in detail in [3]. Other approaches to the problem of target identification were presented in [1] applying two statistical-based techniques, namely Bayesian and Dempster-Shafer, to develop radar target identification algorithms. Distributed multi-class classification with fault-tolerance capability was studied in [2]. Collaborative classification algorithms [6] were applied to single target scenarios and then extended to more complex scenarios of multiple targets.

Multiple target identification and classification have become major concerns in radar surveillance applications. Usually, this task is implemented based on wideband radars or imaging radars [11]. In this paper, we address the problem of MTIC for radar surveillance using cognitive radars. Cognitive radars, as presented in [12] and [7], continuously interact with the environment, intelligently collect data and thereby efficiently adapt to statistical variations in the environment in real-time so as to achieve reliable surveillance where the likelihood of the presence of targets is high. Cognitive radars are showing promise in home health care, rescue and homeland security applications [7], [10]. Such applications were studied in [12], [10].

We consider the scenario wherein the total number of targets K is unknown in a region of interest and a query regarding to the classification of these targets and the identification of the targets in each category is inquired. This is the general surveillance scenario since each target belonging to one distinct category as in [9] is no longer considered. In this work, some targets now share the same target category but possess different identification numbers. In order to perform this higher complexity version of surveillance scenario, we assume that each given target belongs to one distinct pair of one target category and one identification number. Based on statistical data, we then reasonably assume that the maximum number of target categories M and the maximum number of targets N in each category are a priori known parameters. However, the actual number of existing target categories and the actual number of targets being present in each category at any given time are unknown. It is assumed that there are R cognitive radar sensors in the query region.

Within the above-described framework, we propose a joint multi-target identification and classification (JMIC) algorithm for radar surveillance. Firstly, the existing target categories are classified based on $M^\star$-ary hypothesis testing where $M^\star = 2^M$. Note that, $M^\star$ hypotheses correspond to all possibilities we may have regarding to the presence or absence of each category. Thereafter, based on the result obtained from classification specifying which target categories exist, we identify targets belonging to each detected category. Targets in a category are identified based on their identification numbers or identification indices. Therefore, $N^\star$ ($N^\star = 2^N$ - 1) hypotheses are set up corresponding to all scenarios of presence or absence

of each target identification index. Numerical results based on simulated data are finally presented to demonstrate the feasibility and effectiveness of the proposed JMIC algorithm in a query surveillance region.

The rest of the paper is organized as follows. In section II, we provide a framework and formulate the multi-target classification and identification problem in a cognitive radar network. In section III, we propose the joint multi-target identification and classification algorithm. Simulation results are presented in section IV. Finally, section V concludes the paper.

II. System description and problem formulation

The general system architecture for MTIC problem used in this work is shown in Fig. 1. This architecture accommodates the deployment of R cognitive radar sensors (CRSs). These sensors will collect and then send all the target signals to the fusion center. It is assumed that there are K targets in the region of interest. Each target is considered as a point source and target signals are modeled as zero-mean complex Gaussian processes [9]. All measurements from sensors are combined to reduce the impact of target signal variability. At any given time, the measurements in distinct cognitive radar sensors are approximately independent.

We assume that at most M distinct target categories and N targets in each category are present in the surveillance region in the observation duration. However, the actual existing number of target categories is unknown. Therefore, we set up 2^M hypotheses corresponding to all possible scenarios of presence or absence of each target category. We denote these hypotheses by H_k (k = 0, 1, ..., $2^M - 1$). Target categories are denoted by i (i = 1, 2, ..., M) and in each ith category, targets are identified by the identification indices j (j = 1, 2, ..., N). We use the parameter $b_{ij} \in \{0, 1\}$ to denote the event in which target of category i, index j is absent or present. Specifically,

$$b_{ij} = \begin{cases} 0 & \text{if target of category } i, \text{ index } j \text{ is absent} \\ 1 & \text{if target of category } i, \text{ index } j \text{ is present} \end{cases}$$

Classification and identification parameters are given in Table I wherein each row represents one target category and each column represents one target index. The probability of target of category i, index j being absent $P(b_{ij} = 0)$ is denoted by p_{ij}, i.e., $P(b_{ij} = 0) = p_{ij}$. Hence, the probability of presence of this target $P(b_{ij} = 1)$ is: $P(b_{ij} = 1)$ = 1- p_{ij}.

We employ hypothesis H_0 for scenario of no category being present, hypothesis H_1 for scenario of category 1 being present,..., and hypothesis H_{2^M-1} for scenario of all M categories being present. We assume that the total number of targets K in the region of interest is unknown. In the case of K = 0, i.e., there is no target in the surveillance region, hypothesis H_0 is chosen. The prior probability of hypothesis H_0 is given by:

$$\begin{aligned} P(H_0) &= \text{P } \{\text{no category present}\} \\ &= P(\forall b_{1j} = 0; \forall b_{2j} = 0; ...; \forall b_{Mj} = 0), \\ &\qquad \text{for } j = 1, 2, ..., N \end{aligned} \quad (1)$$

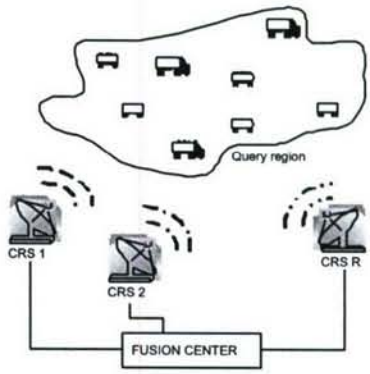

Fig. 1: System architecture for JMIC algorithm

Since the possibilities for presence or absence of targets are independent, we have

$$\begin{aligned} P(H_0) &= P(\forall b_{1j} = 0).P(\forall b_{2j} = 0)...P(\forall b_{Mj} = 0) \\ &= (p_{11}.p_{12}...p_{1N})(p_{21}.p_{22}...p_{2N})...(p_{M1}...p_{MN}) \\ &= \prod_{j=1}^{N} p_{1j} \cdot \prod_{j=1}^{N} p_{2j} \cdots \prod_{j=1}^{N} p_{Mj} \end{aligned} \quad (2)$$

Similarly, the prior probability of H_1 is given by:

$$\begin{aligned} P(H_1) &= \text{P } \{\text{category 1 present}\} \\ &= P(\textit{at least one } b_{1j} = 1; \forall b_{2j} = 0; ...; \forall b_{Mj} = 0) \\ &= P(\exists \textit{ one } b_{1j} = 1).P(\forall b_{2j} = 0)...P(\forall b_{Mj} = 0) \\ &= (1 - \prod_{j=1}^{N} p_{1j}) \cdot \prod_{j=1}^{N} p_{2j} \cdots \prod_{j=1}^{N} p_{Mj} \end{aligned} \quad (3)$$

Generally, we obtain the prior probability of hypothesis H_k in the form as follows:

$$P(H_k) = \prod_{i=1}^{M} [b_i^{(k)}(1 - \prod_{j=1}^{N} p_{ij}) + (1 - b_i^{(k)}) \prod_{j=1}^{N} p_{ij}] \quad (4)$$

where $b_i^{(k)}$ takes the value of 0 when category i is absent, otherwise $b_i^{(k)}$ takes the value of 1 when category i is present under hypothesis H_k.

III. Joint multi-target identification and classification algorithm

Joint multi-target identification and classification algorithm consists of two steps. In the first step, multiple target classification is implemented to investigate which target categories are present within the entire surveillance region. Then, in the second step, based on classification results, targets in each detected category are identified using identification indices. Our JMIC algorithm relies on the framework previously presented in section II.

TABLE I: Classification and Identification Parameters

	Index 1	Index 2	Index 3	...	Index N
Category 1	b_{11}	b_{12}	b_{13}	...	b_{1N}
Category 2	b_{21}	b_{22}	b_{23}	...	b_{2N}
Category 3	b_{31}	b_{32}	b_{33}	...	b_{3N}
⋮	⋮	⋮	⋮	⋮	⋮
Category M	b_{M1}	b_{M2}	b_{M3}	...	b_{MN}

A. Multiple Target Classification

The M^*-ary hypothesis testing problem is given by:

$$H_k : \mathbf{z}_l = \mathbf{s}_l + \mathbf{n}_l, \qquad k = 0, 1, ..., 2^M - 1 \tag{5}$$

where $\mathbf{z}_l$ is a feature vector of dimension D collected by the lth (l = 1,2,..., R) cognitive radar sensor. We assume that target signals have the same energy, i.e., these signals are modeled as zero-mean complex Gaussian vectors with covariance matrix $\mathbf{\Sigma}_m$. Thus,

$$\mathbf{s}_l \sim \mathcal{CN}(0, \mathbf{\Sigma}_{s_{lk}}), \quad \text{where} \quad \mathbf{\Sigma}_{s_{lk}} = \sum_{i=1(i\in H_k)}^{M} \sum_{j=1}^{N} b_{ij} \mathbf{\Sigma}_m \tag{6}$$

Signals are corrupted by zero-mean complex white Gaussian noise.

$$\mathbf{n}_l \sim \mathcal{CN}(0, \sigma_n^2 \mathbf{I}). \tag{7}$$

Under hypothesis H_k, the probability density function of the feature vector $\mathbf{z}_l$ is given by:

$$\begin{aligned} P(\mathbf{z}_l|H_k) &= p_k(\mathbf{z}_l) \\ &= \frac{1}{\pi^D |\mathbf{\Sigma}_{z_{lk}}|} \exp\{-\mathbf{z}_l^H \mathbf{\Sigma}_{z_{lk}}^{-1} \mathbf{z}_l\} \end{aligned} \tag{8}$$

where $\mathbf{\Sigma}_{z_{lk}} = \mathbf{\Sigma}_{s_{lk}} + \sigma_n^2 \mathbf{I}$

We denote $P(H_k)$ by δ_k. The decision rule for the multiple target classifier is therefore given by:

$$\hat{k} = \arg \max_{k=0,1,...,M^*-1} p_k(\mathbf{z}_1, \mathbf{z}_2, ..., \mathbf{z}_R)\delta_k \tag{9}$$

Due to the conditional independence of $\mathbf{z}_l$, (9) can be expressed as:

$$\hat{k} = \arg \max_{k=0,1,...,M^*-1} \prod_{l=1}^{R} p_k(\mathbf{z}_l)\delta_k \tag{10}$$

In term of log-likelihood, we have

$$\begin{aligned} \Delta_k(\mathbf{z}_1, \mathbf{z}_2, ..., \mathbf{z}_R) &= \log \prod_{l=1}^{R} p_k(\mathbf{z}_l)\delta_k \\ &= \sum_{l=1}^{R} \log p_k(\mathbf{z}_l) + \log \delta_k \end{aligned} \tag{11}$$

By substituting $p_k(\mathbf{z}_l)$ from (8) to (11) and omitting constants that do not depend on categories, we then obtain Δ_k in the following form, :

$$\Delta_k(\mathbf{z}_1, \mathbf{z}_2, ..., \mathbf{z}_R) = -R \log |\mathbf{\Sigma}_{z_{lk}}| - \sum_{l=1}^{R} \mathbf{z}_l^H \mathbf{\Sigma}_{z_{lk}}^{-1} \mathbf{z}_l + \log \delta_k \tag{12}$$

The information about $\mathbf{z}_l$ is then sent from the lth (l = 1, 2,..., R) cognitive radar sensor to the fusion center. The classifier at the fusion center then makes the final classification decision in the form:

$$\begin{aligned} \hat{k} &= \arg \max_{k=0,1,...,M^*-1} \Delta_k(\mathbf{z}_1, \mathbf{z}_2, ..., \mathbf{z}_R) \\ &= \arg \min_k \{R \log |\mathbf{\Sigma}_{z_{lk}}| + \sum_{l=1}^{R} \mathbf{z}_l^H \mathbf{\Sigma}_{z_{lk}}^{-1} \mathbf{z}_l - \log \delta_k\} \end{aligned} \tag{13}$$

From (13), we map the integer value of $\hat{k}$ to binary value to obtain a category vector $\mathbf{c} = [c_1, c_2, ..., c_M]$ where c_i (i = 1, 2, ..., M) takes value of 1 corresponding to category i being present or takes value of 0 corresponding to category i being absent in the area of interest. The total number of target categories being present in the surveillance region is given by:

$$N_C = \sum_{i=1}^{M} c_i \tag{14}$$

For example, if $\hat{k}$ = 5, then we get $\mathbf{c}$ = [1, 0, 1, 0, ...,0], i.e., only categories 1 and 3 are present within the surveillance region. Therefore, the total number of target categories being present N_C is 2.

B. Multiple Target Identification

Based on the estimated value $\hat{k}$, we realize which target categories have shown up in the surveillance region. However, we still have no information about the number of targets belonging to each category. Therefore, the second step of the JMIC algorithm is repeatedly applied to each detected category to identify targets in the surveillance region. We aim at searching all the targets using their jth indices. For each category i, we denote $H_{h,\hat{k}}^i$ to represent the hypothesis h (h = 0, 1, ..., 2^N - 1), given category $i \in \mathbf{S}$ being present under hypothesis $H_{\hat{k}}$. Note that, $\mathbf{S}$ is a set of all categories i being present in hypothesis $H_{\hat{k}}$.

$$\mathbf{S} = \{i \text{ present in } H_{\hat{k}}\} \tag{15}$$

Since category i is estimated to be present, i.e, at least one target index j shows up in this category, thus, the scenario of no target index of category i being present is eliminated, i.e., P($H_{0,\hat{k}}^i$) = 0. Thus, we only have $N^* = 2^N$ - 1 hypotheses corresponding to h = 1, 2, ..., N^*. We choose $H_{1,\hat{k}}^i$ to represent the hypothesis of target index ♯1 of category $i \in \mathbf{S}$ being present, $H_{2,\hat{k}}^i$ to represent the hypothesis of target index ♯2 of category $i \in \mathbf{S}$ being present, ..., $H_{N^*,\hat{k}}^i$ to represent the hypothesis of all targets index ♯1, ♯2, ..., ♯N of category $i \in \mathbf{S}$ being present.

TABLE II: Classification and Identification Example

	Index 1	Index 2	Index 3	Index 4
Category 1	0	1	0	1
Category 2	1	1	0	1
Category 3	1	1	0	0

We have

$$\begin{aligned} P(H^i_{h,\hat{k}}) &= P(H^i_h, H_{\hat{k}}) \\ &= P(H^i_h|H_{\hat{k}})P(H_{\hat{k}}) \end{aligned} \quad (16)$$

The conditional probability of hypothesis $H^i_{1,\hat{k}}$ is given by:

$$\begin{aligned} P(H^i_1|H_{\hat{k}}) &= \text{P } \{\text{target index } \sharp 1 \text{ category } i \text{ present}\} \\ &= P(b_{i1}=1; b_{i2}=0; ...; b_{iN}=0) \end{aligned} \quad (17)$$

Because the possibilities for presence or absence of targets are independent, we have

$$\begin{aligned} P(H^i_1|H_{\hat{k}}) &= P(b_{i1}=1).P(b_{i2}=0)...P(b_{iN}=0) \\ &= (1-p_{i1}).p_{i2}...p_{iN} \end{aligned} \quad (18)$$

Similarly, the conditional probability of hypothesis $H^i_{2,\hat{k}}$ is:

$$\begin{aligned} P(H^i_2|H_{\hat{k}}) &= \text{P } \{\text{target index } \sharp 2 \text{ category } i \text{ present}\} \\ &= P(b_{i1}=0; b_{i2}=1; ...; b_{iN}=0) \\ &= P(b_{i1}=0).P(b_{i2}=1)...P(b_{iN}=0) \\ &= p_{i1}.(1-p_{i2})...p_{iN} \end{aligned} \quad (19)$$

In general, we obtain the conditional probability of hypothesis $H^i_{h,\hat{k}}$ as follows:

$$P(H^i_h|H_{\hat{k}}) = \prod_{j=1}^{N}[b^{(h)}_{ij}(1-p_{ij}) + (1-b^{(h)}_{ij})p_{ij}] \quad (20)$$

where $b^{(h)}_{ij}$ takes the value of 0 when target index j of category i is absent, otherwise $b^{(h)}_{ij}$ takes the value of 1 when target index j of category i is present under hypothesis H^i_h given hypothesis $H_{\hat{k}}$.

We now set up $N^\star$ hypotheses:

$$H^i_{h,\hat{k}} : \mathbf{z}^i_l = \mathbf{s}^i_l + \mathbf{n}^i_l, \qquad h = 1, 2, ..., N^\star \quad (21)$$

where $\mathbf{z}^i_l$ is collected by lth (l = 1, 2, ..., R) cognitive radar sensor regarding to ith category. Target signals of ith category are given by:

$$\mathbf{s}^i_l \sim \mathcal{CN}(0, \mathbf{\Sigma}_{s^i_{l,h}}), \quad \text{where} \quad \mathbf{\Sigma}_{s^i_{l,h}} = \sum_{j=1(j\in H^i_{h,\hat{k}})}^{N} b_{ij}\mathbf{\Sigma}_m \quad (22)$$

Signals are corrupted by zero-mean complex white Gaussian noise.

$$\mathbf{n}^i_l \sim \mathcal{CN}(0, \sigma^2_n\mathbf{I}) \quad (23)$$

Under hypothesis $H^i_{h,\hat{k}}$, the probability density function of the feature vector $\mathbf{z}^i_l$ of category i is given by:

$$\begin{aligned} P(\mathbf{z}^i_l|H^i_{h,\hat{k}}) &= p_{h,\hat{k}}(\mathbf{z}^i_l) \\ &= \frac{1}{\pi^D|\mathbf{\Sigma}_{z^i_{l,h}}|}\exp\{-(\mathbf{z}^i_l)^H\mathbf{\Sigma}^{-1}_{z^i_{l,h}}\mathbf{z}^i_l\} \end{aligned} \quad (24)$$

where $\mathbf{\Sigma}_{z^i_{l,h}} = \mathbf{\Sigma}_{s^i_{l,h}} + \sigma^2_n\mathbf{I}$.

We denote $P(H^i_h|H_{\hat{k}})$ by α^i_h. From (16) and due to the conditional independence of $\mathbf{z}^i_l$, the identification decision rule is hence given by:

$$\hat{h} = \arg\max_{h=1,2,...,N^\star}\prod_{l=1}^{R} p_{h,\hat{k}}(\mathbf{z}^i_l)\alpha^i_h\delta_{\hat{k}} \quad (25)$$

In term of log-likelihood, we have

$$\begin{aligned} \Delta^i_k &= \log\prod_{l=1}^{R} p_{h,\hat{k}}(\mathbf{z}^i_l)\alpha^i_h\delta_{\hat{k}} \\ &= \sum_{l=1}^{R}\log p_{h,\hat{k}}(\mathbf{z}^i_l) + \log\alpha^i_h + \log\delta_{\hat{k}} \end{aligned} \quad (26)$$

By substituting $p_{h,\hat{k}}(\mathbf{z}^i_l)$ from (24) to (26) and omitting constants that do not depend on target indices in each category, we have Δ^i_k in the following form:

$$\Delta^i_k = -R\log|\mathbf{\Sigma}_{z^i_{l,h}}| - \sum_{l=1}^{R}(\mathbf{z}^i_l)^H\mathbf{\Sigma}^{-1}_{z^i_{l,h}}\mathbf{z}^i_l + \log\alpha^i_h + \log\delta_{\hat{k}} \quad (27)$$

The information about $\mathbf{z}^i_l$ is sent from the lth cognitive radar sensor to the fusion center. The identifier at the fusion center then makes the final identification decision:

$$\begin{aligned} \hat{h} &= \arg\max_{h=1,2,...,N^\star}\Delta^i_k \\ &= \arg\min_h\{R\log|\mathbf{\Sigma}_{z^i_{l,h}}| + \sum_{l=1}^{R}(\mathbf{z}^i_l)^H\mathbf{\Sigma}^{-1}_{z^i_{l,h}}\mathbf{z}^i_l - \log\alpha^i_h \\ &\qquad - \log\delta_{\hat{k}}\} \end{aligned} \quad (28)$$

From (28), we map the integer value of $\hat{h}$ to binary value to obtain a index vector $\mathbf{b}_i = [b_{i1}, b_{i2}, ..., b_{iN}]$ where every component of $\mathbf{b}_i$ takes the value of 1 or 0. Component $\sharp j$ takes value of 1 corresponding to the scenario of target index $\sharp j$ of category i being present. The total number of targets N_i in each category i is calculated by:

$$N_i = \sum_{j=1}^{N} b_{ij} \quad (29)$$

Following the example previously described in classification step, for i = 1, if $\hat{h}$ = 7, then we get $\mathbf{b}_1$ = [1, 1, 1, 0, ...,0]. Therefore, only targets with indices 1, 2 and 3 of category 1 are present within the surveillance region. The total number of targets of category 1 being present N_1 is 3. Repeatedly implementing this step, for i = 3, if $\hat{h}$ = 3, we obtain $\mathbf{b}_3$ = [1, 1, 0, 0, ..., 0]. So, targets with indices 1 and 2 of category 3

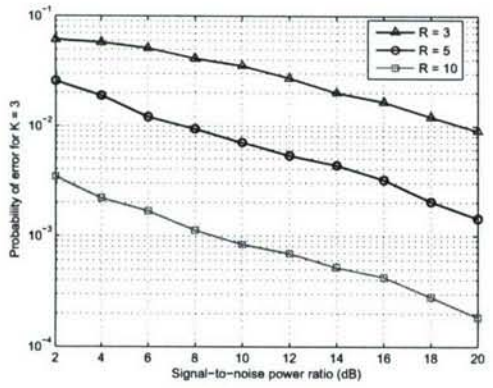

Fig. 2: Probability of error using JMIC algorithm for K = 3

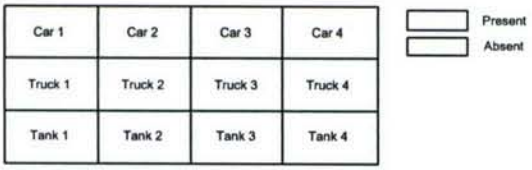

Fig. 3: Surveillance scenario of K = 3

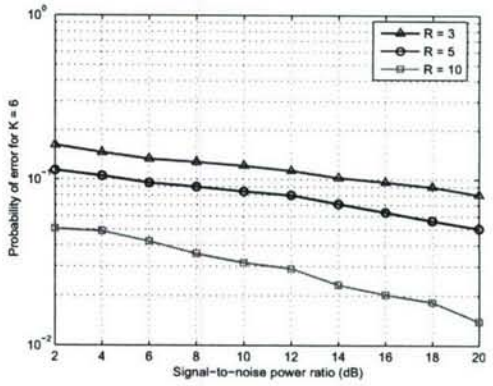

Fig. 4: Probability of error using JMIC algorithm for K = 6

Fig. 5: Surveillance scenario of K = 6

are present. The total number of targets of category 3 being present N_3 is 2.

The total number of targets K in the surveillance region is finally given by:

$$K = \sum_{i=1}^{M} N_i = \sum_{i=1}^{M} \sum_{j=1}^{N} b_{ij} \tag{30}$$

In the example, the total number of targets within the surveillance region K is 5.

IV. Simulation Results

We perform simulations to illustrate the performance of the proposed JMIC algorithm. An encounter of unknown K targets in the region of query was simulated. A set of R cognitive radar sensors was deployed. A cognitive radar sensor may detect more than one target at any given time. Therefore, a more accurate estimation about target categories and the total number of targets being present in each category can be obtained by fusion of several radar sensors. The maximum number of categories M = 3 and the maximum number of targets in each category N = 4 were assumed in this region of interest.

An example using JMIC for K = 7 targets in the region of interest is given in Table II. We use JMIC algorithm to obtain $\hat{k}$ = 7 which specifies that categories 1, 2, 3 are present and thus N_c = 3. The number of targets of category 1 is 2 (target index ♯2 and ♯4) corresponding to $\hat{h}$ = 10. The number of targets of category 2 is 3 (target index ♯1, ♯2, and ♯4) corresponding to $\hat{h}$ = 11. The total number of targets of category 3 is 2 (target index ♯1 and ♯2) corresponding to $\hat{h}$ = 3.

To evaluate the performance of the proposed JMIC algorithm, we conduct a Monte-Carlo simulation of 10^5 runs. The probability of error of the proposed JMIC algorithm given in the form of function of signal-to-noise power ratio is shown in Fig. 2, Fig. 4, and Fig. 6. The scenarios of R = 3, 5 and 10 cognitive radar sensors were used in the simulations. From Fig. 2, we realize that a sufficiently low probability of error can be obtained with a small number of cognitive radar sensors R = 5 in the surveillance scenario of K = 3 targets as shown in Fig. 3. Comparison of probability of error for the different number of cognitive radar sensors in the scenario of K = 3 targets was shown in Fig. 2. The simulation results demonstrate our algorithm in the surveillance scenarios of K = 6 as described in Fig. 5 and K = 8 as in Fig. 7 are, correspondingly, given in Fig. 4 and Fig. 6. From Fig. 2, Fig. 4 and Fig. 6, we also observe that for a given number of targets K in the surveillance region, the performance of JMIC using R = 5 or R = 10 radar sensors is better than that using R = 3 radar sensors. Besides, for a given number of R radar sensors, the identification and classification performance is reduced when we notice an increasing number of targets in the surveillance region. The probability of JMIC error is inversely proportional to signal-to-noise power ratio. At high SNR, the probability of error is rather small. The simulation results validate the robustness and effectiveness of our proposed JMIC algorithm.

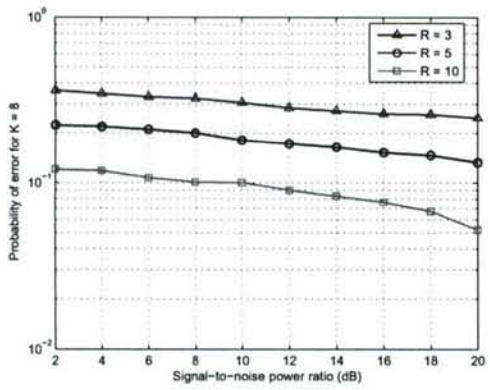

Fig. 6: Probability of error using JMIC algorithm for K = 8

Fig. 7: Surveillance scenario of K = 8

V. Conclusion

We have demonstrated that K targets in a query region can be classified and identified efficiently by a network of R cognitive radar sensors using our JMIC algorithm. A computer simulation with simulated radar data was used to investigate the accuracy of classification and identification algorithm in the variations of the target signals in the network. Using JMIC algorithm, we show that a sufficiently low probability of error can be achieved with a fairly small number of radar sensors for a given common number of targets. The unprecedented desire of knowing not only the number of target categories, but also the total number of targets in each category in a surveillance region is making JMIC algorithm an attractive choice in practice for military applications.

Acknowledgement

This work was supported by the U.S. Office of Naval Research (ONR) Young Investigator Program Award under Grant N00014-03-1-0466, and ONR Award under Grant N00014-07-1-0395.

References

[1] Henry Leung and Jiangfeng Wu, "Bayesian and Dempster-Shafer target identification for radar surveillance", *IEEE Trans. on Aerospace and Electronic Systems*, vol. 36, no. 2, pp. 432-447, Apr. 2000.

[2] Tsang-Yi Wang, Y. S. Han, Pramod K. Varshney, and Po-Ning Chen, "Distributed fault-tolerant classification in wireless sensor networks", *IEEE Journal on Selected Areas in Communications*, vol. 23, no. 4 , pp. 724-734, Apr. 2005.

[3] J. G. Teti, JR., R. P. Gorman, and W. A. Berger, "A multifeature decision space approach to radar target identification", *IEEE Trans. on Aerospace and Electronic Systems*, vol. 32, no. 1, pp. 480-487, Jan. 1996.

[4] S. M. Kay, *Fundamentals of Statistical Signal Processing: Detection Theory*, PTR Prentice-Hall Inc., vol. 2, 1993.

[5] C. Premebida, "A multi-target tracking and GMM-classifier for intelligent vehicles", in *2006 IEEE Proc. Intelligent Transportation Systems, Toronto, Cananda*, pp. 313-318, Sept. 2006.

[6] C. Meesookho, S. Narayanan, C. S. Raghavendra, "Collaborative classification applications in sensor networks", *Sensor Array and Multichannel Signal Processing Workshop Proceedings, 2002*, pp. 370-374, Aug. 2002.

[7] S. Haykin, "Cognitive radar networks", *Fourth IEEE Workshop on Sensor Array and Multichannel Processing, 2006*, pp. 1-24, Jul. 2006.

[8] T. Vercauteren, D. Guo, and X. Wang, "Joint multiple target tracking and classification in collaborative sensor networks", *IEEE Journal on Selected Areas in Communications*, vol. 23, no. 4 , pp. 714-723, Apr. 2005.

[9] J. H. Kotecha, V. Ramachandran, and A. M. Sayeed, "Distributed multitarget classification in wireless sensor networks", *IEEE Journal on Selected Areas in Communications*, vol. 23, no. 4 , pp. 703-713, Apr. 2005.

[10] Yifan Chen, E. Gunawan, K. S. Low, Y. Kim, C. B. Soh, A. R. Leyman, and L. L. Thi, "Non-invasive respiration rate estimation using ultra-wideband distributed cognitive radar system", in *Proc. of the 28th IEEE Engineering in Medicine and Biology Society Annual International Conference, New York City, USA*, pp. 920-923, Aug. 2006.

[11] V. G. Nebabin, *Methods and techniques of radar recognition*, Artech House, 1994.

[12] S. Haykin, "Cognitive radar: A way of the future", *IEEE Signal Processing Mag.*, vol. 23, no. 1, pp. 30-40, Jan. 2006.

SVD-QR-T FCM Approach for Virtual MIMO Channel Selection in Wireless Sensor Networks

Jing Liang and Qilian Liang, Senior Member, IEEE
Department of Electrical Engineering
University of Texas at Arlington
Arlington, TX 76019-0016 USA
E-mail: jliang@wcn.uta.edu, liang@uta.edu

Abstract

In this paper, we present Singular-Value Decomposition-QR with Threshold (SVD-QR-T) algorithm to select a subset of channels in virtual MIMO wireless sensor networks (WSN) in order to reduce its complexity and cost. SVD-QR-T selects best subset of transmitters while keeping all receivers active. The threshold is adaptive by means of Fuzzy C-Mean (FCM). Under the constraint of the same total transmission power, this approach is compared against the case without channel selection in terms of capacity, bit error rate (BER) and multiplexing gain in the presence of water-filling as well without. It is shown that in spite of less multiplexing gain, when water-filling is applied, SVD-QR-T FCM provides lower BER at moderate to high SNR; in case of equal transmission power allocation, SVD-QR-T FCM achieves higher capacity at low SNR and lower BER. In general, it provides satisfying performances compared to the case without channel selection but reduced cost and resource.

1 Introduction

1.1 Channel selection in virtual MIMO

Virtual multiple-input-multiple-output (MIMO) has been studied intensively in recent years in order to improve the energy-efficiency in wireless sensor networks (WSN) [1][2][3]. Constrained by its physical size and limited battery, individual sensor is allowed to contain only one antenna. Numerical results show that if these individual sensors jointly form the MIMO system, tremendous energy will be saved while satisfying the required performance. However, a natural drawback of virtual MIMO is the increased complexity and the cost of multiple radio frequency (RF) chains. One technique to reduce the complexity and cost while providing similar capacity and performance is channel selection, or antenna selection.

The knowledge of channels can be obtained by various channel estimation techniques, such as reciprocity principle and feedback channel [4]. When channel side information (CSI) is known to transmitters or receivers, antenna selection can be applied through subset selection algorithms by switchers either at transmitters or receivers, or jointly working at both ends. Therefore the best set of channels are selected to be active while remaining ones are not employed. These switchers typically cost much less than RF chains so that low-cost and low-complexity can be achieved with the benefits of multiple antennas [5] [6]. This system is illustrated in Fig. 1.

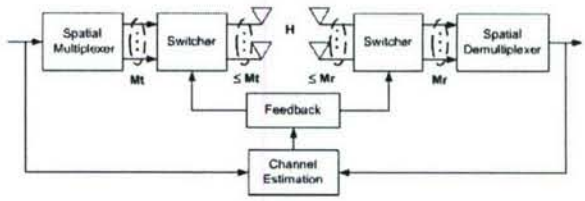

Figure 1. system diagram for virtual MIMO channel selection

Recent years have seen an explosion of interest in MIMO antenna selection and various criteria have been used:

1. Capacity Maximization: In the previous work of [7] [8] [9], channel capacity is used as the optimality criterion, i.e., antennas that achieve the largest capacity are active. [7] demonstrated that in case of no CSI at transmitter (CSIT) but receiver (CSIR), close capacity to that of the MIMO system can be achieved as far as the number of selected receivers is no less than the number of transmitters. [8] and [9] considered CSI

at transmitter and proposed an exhaustive search algorithm.

2. Minimum Error rate: Apart from maximization of capacity based on Shannon theory, [10] derived another criteria from the respect of minimum error rate when coherent receivers, either maximum likelihood (ML), zero-forcing (ZF) or the minimum mean-square error (MMSE) linear receiver is employed.

3. SNR Maximization: In [11], antenna selection is performed only at the receiver on a basis of largest instantaneous SNR using space-time coding. It is analytically shown that full diversity advantage promised by MIMO can be fully exploited using this criteria as long as the space-time code employed has full spatial diversity.

Although there have been dazzling mathematical studies on antenna selection criteria, practical algorithms of joint transmit and receive antenna selection, i.e., *channel selection* is still open and the problem of corresponding performance analysis require more investigations.

1.2 Contributions and Organization of This Paper

In this paper, under the assumption of quasi-static Rayleigh fading, we propose a practical algorithm to perform channel selection: singular-value decomposition-QR with threshold (SVD-QR-T) employing Fuzzy C-Mean (FCM) to virtually provide adaptive threshold. This algorithm selects rt (see section 3) best subset of transmitters while keeping all receivers active. An example is presented to illustrate each step. Under the constraint of the same total transmission power, this approach is compared against the case without channel selection in terms of capacity, bit error rate (BER) and multiplexing gain. it is shown that in spite of less multiplexing gain, when water-filling is applied, SVD-QR-T FCM provides lower BER at moderate to high SNR; in case of no water-filling and equal transmission power allocation, SVD-QR-T FCM achieves higher capacity at low SNR and lower BER. In general, it provides satisfying performances compared to the case without channel selection but reduced cost and resource.

We organize the remainder of this paper as follows. In Section 2, we introduce our virtual MIMO channel model. Section 3 proposes SVD-QR-T FCM algorithm. Section 4 compares the performances of virtual MIMO after channel selection with those without. Section 5 draws the conclusion and presents future work.

2 Channel Model

Virtual MIMO channel model with M_t transmitters and M_r receivers ($M_t + M_r$ sensors) is illustrated in Fig. 2, where each receiver observes a superposition of the M_t transmitted signals corrupted by Rayleigh flat fading and additive white gaussian noise. Each h_{ji}, $i = 1, 2, \cdots, M_t$ and $j = 1, 2, \cdots, M_r$ represents the channel gain from transmitter i to receiver j [12], which is assumed to be Rayleigh independent and identically distributed (i.i.d.). The additive noise also has i.i.d entries $n_j \sim \mathcal{CN}(0, \sigma^2)$.

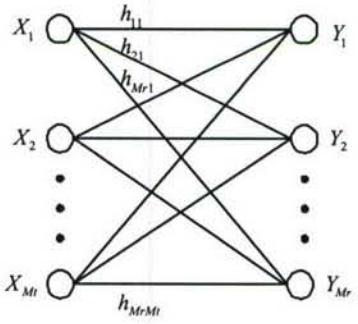

Figure 2. Graphic channel model for virtual MIMO

We may denote this virtual MIMO channel graph with discrete time model:

$$\begin{bmatrix} Y_1 \\ Y_2 \\ \vdots \\ Y_{Mr} \end{bmatrix} = \begin{bmatrix} h_{11} & h_{12} & \cdots & h_{1Mt} \\ h_{21} & h_{22} & \cdots & h_{2Mt} \\ \vdots & \vdots & \vdots & \vdots \\ h_{Mr1} & h_{Mr2} & \cdots & h_{MrMt} \end{bmatrix} \begin{bmatrix} X_1 \\ X_2 \\ \vdots \\ X_{Mt} \end{bmatrix} + \begin{bmatrix} n_1 \\ n_2 \\ \vdots \\ n_{Mr} \end{bmatrix} \quad (1)$$

The above equation can be simplified as $\mathbf{Y} = \mathbf{HX} + \mathbf{n}$, where $\mathbf{H}$ is a $Mr \times Mt$ independent Rayleigh random matrix and $\mathbf{n}$ denotes random noise.

3 SVD-QR-T Virtual MIMO

3.1 SVD-QR-T in virtual MIMO channel selection

SVD has been applied to MIMO channel decomposition in [12], [14], and sensor node selection in [15]. However,

these studies are on theoretical analysis only and no algorithm has been proposed on which channels will be physically selected in practice.

We propose SVD-QR-T as follows:

1. Given channel gain matrix $\mathbf{H} \in R^{Mr \times Mt}$ and $r = rank(\mathbf{H}) \leq \min(Mt, Mr)$, determine a numerical estimate rt of the rank r by calculating the singular value decomposition
$$\mathbf{H} = \mathbf{U}\Sigma\mathbf{V}^T, \tag{2}$$
where $\mathbf{U}$ is an $Mr \times Mr$ matrix of orthonormalized eigenvectors of $\mathbf{H}\mathbf{H}^T$, $\mathbf{V}$ is an $Mt \times Mt$ matrix of orthonormalized eigenvectors of $\mathbf{H}^T\mathbf{H}$, and Σ is the diagonal matrix $\Sigma = diag(\sigma_1, \sigma_2, \ldots, \sigma_i, \sigma_r)$, where $\sigma_i = \sqrt{\lambda_i}$ and λ_i is the ith eigenvalue of $\mathbf{H}\mathbf{H}^T$ and $\sigma_1 \geq \sigma_2 \geq \cdots \geq \sigma_r > 0$. σ_i is the singular value of $\mathbf{H}$. In many practical cases, σ_1, σ_1, $\cdots$, σ_{rt} are much larger than $\sigma_{rt+1}, \cdots, \sigma_r$; thus we may set threshold to pick up valuable $\sigma_i, i = 1, 2, \cdots, \sigma_{rt}$ and discard those trivial singular values in order to save resource but maintain satisfying performance. Sometimes rt can be chosen much smaller than the rank r, even 1. In this paper, we propose to use fuzzy c-means (FCM) to determine rt. Details will be discussed in section 3.2.

2. Partition
$$\mathbf{V} = \begin{bmatrix} \mathbf{V}_{11} & \mathbf{V}_{12} \\ \mathbf{V}_{21} & \mathbf{V}_{22} \end{bmatrix} \tag{3}$$
where $\mathbf{V}_{11} \in R^{rt \times rt}$, $\mathbf{V}_{12} \in R^{rt \times (Mt-rt)}$, $\mathbf{V}_{21} \in R^{(Mt-rt) \times rt}$, and $\mathbf{V}_{22} \in R^{(Mt-rt) \times (Mt-rt)}$.

3. Using QR decomposition with column pivoting, determine $\mathbf{E}$ such that
$$[\mathbf{V}_{11}^T, \mathbf{V}_{21}^T]\mathbf{E} = \mathbf{QR}, \tag{4}$$
where $\mathbf{Q}$ is a unitary matrix, and $\mathbf{R} \in R^{rt \times Mt}$ forms an upper triangular matrix with decreasing diagonal elements; and $\mathbf{E}$ is the permutation matrix. The positions of 1 in the first rt columns of $\mathbf{E}$ correspond to the rt ordered *most-significant* transmitters.

3.2 Fuzzy C-Means – Unsupervised Clustering for Adaptive Threshold

In order to keep the balance between performances and cost, we propose FCM clustering approach to divide singular value $(\sigma_1, \sigma_2, \ldots, \sigma_r)$ into two clusters, and thus provides virtual adaptive threshold, so the cluster with higher center would remain for active channels.

FCM clustering is a data clustering technique where each data point belongs to a cluster to a degree specified by a membership grade. This technique was originally introduced by Bezdek [16] as an improvement on earlier clustering methods. Here we briefly summarize it.

Definition 1 (Fuzzy c-Partition) *Let $\mathbf{X} = x_1, x_2, \cdots, x_n$ be any finite set, $\mathbf{V}_{cn}$ be the set of real $c \times n$ matrices, and c be an integer, where $2 \leq c < n$. The* Fuzzy c-partition space *for $\mathbf{X}$ is the set*
$$M_{fc} = U \in V_{cn} | u_{ik} \in [0, 1] \ \forall i, k; \tag{5}$$
where $\sum_{i=1}^{c} u_{ik} = 1 \ \forall k$ and $0 < \sum_{k=1}^{n} u_{ik} < n \ \forall i$. The row i of matrix $U \in M_{fc}$ contains values of the ith membership function, u_i, in the fuzzy c-partition U of $\mathbf{X}$.

The row i of matrix $U \in M_{fc}$ contains values of the ith membership function, u_i, in the fuzzy c-partition U of $\mathbf{X}$.

Definition 2 (Fuzzy c-Means Functionals) *[16] Let $J_m : M_{fc} \times \mathcal{R}^{cp} \rightarrow \mathcal{R}^+$ be*
$$J_m(\mathbf{U}, \mathbf{v}) = \sum_{k=1}^{n} \sum_{i=1}^{c} (u_{ik})^m (d_{ik})^2 \tag{6}$$
where $\mathbf{U} \in M_{fc}$ is a fuzzy c-partition of X; $\mathbf{v} = (\mathbf{v}_1, \mathbf{v}_2, \cdots, \mathbf{v}_c) \in \mathcal{R}^{cp}$, where $\mathbf{v}_i \in \mathcal{R}^p$, is the cluster center of prototype u_i, $1 \leq i \leq c$;
$$(d_{ik})^2 = ||\mathbf{x}_k - \mathbf{v}_i||^2 \tag{7}$$
where $||\cdot||$ is any inner product induced norm on $\mathcal{R}^p$; weighting exponential $m \in [1, \infty)$; and, u_{ik} is the membership of $\mathbf{x}_k$ in fuzzy cluster u_i. $J_m(\mathbf{U}, \mathbf{v})$ represents the distance from any given data point to a cluster weighted by that point's membership grade.

The solutions of
$$\min_{\mathbf{U} \in M_{fc}, \mathbf{v} \in \mathcal{R}^{cp}} J_m(\mathbf{U}, \mathbf{v}) \tag{8}$$
are least-squared error stationary points of J_m. An infinite family of fuzzy clustering algorithms — one for each $m \in (1, \infty)$ — is obtained using the necessary conditions for solutions of (8), as summarized in the following:

Theorem 1 *[16] Assume $||\cdot||$ to be an inner product induced norm: fix $m \in (1, \infty)$, let $\mathbf{X}$ have at least $c < n$ distinct points, and define the sets ($\forall k$)*
$$I_k = \{i | 1 \leq i \leq c; d_{ik} = ||\mathbf{x}_k - \mathbf{v}_i|| = 0\} \tag{9}$$
$$\tilde{I}_k = \{1, 2, \cdots, c\} - I_k \tag{10}$$
Then $(\mathbf{U}, \mathbf{v}) \in M_{fc} \times \mathcal{R}^{cp}$ is globally minimal for J_m only if (ϕ denotes an empty set)
$$I_k = \phi \Rightarrow u_{ik} = 1 \Big/ [\sum_{j=1}^{c} (\frac{d_{ik}}{d_{jk}})^{2/(m-1)}] \tag{11}$$

or

$$I_k \neq \phi \Rightarrow u_{ik} = 0 \ \forall i \in \tilde{I}_k \ and \ \sum_{i \in I_k} u_{ik} = 1, \quad (12)$$

and

$$\mathbf{v}_i = \sum_{k=1}^{n} (u_{ik})^m \mathbf{x}_k \Big/ \sum_{k=1}^{n} (u_{ik})^m \ \forall i \quad (13)$$

Bezdek proposed the following iterative method [16] to minimize $J_m(\mathbf{U}, \mathbf{v})$:

1. Fix c, $2 \leq c < n$; choose any inner product norm metric for $\mathcal{R}^p$; and fix m, $1 \leq m < \infty$. Initialize $\mathbf{U}^{(0)} \in M_{fc}$ (e.g., choose its elements randomly from the values between 0 and 1). Then at step l $(l = 1, 2, \cdots)$:
2. Calculate the c fuzzy cluster centers $\mathbf{v}_i^{(l)}$ using (13) and $\mathbf{U}^{(l)}$.
3. Update $\mathbf{U}^{(l)}$ using (11) or (12).
4. Compare $\mathbf{U}^{(l)}$ to $\mathbf{U}^{(l-1)}$ using a convenient matrix norm, i.e., if $||\mathbf{U}^{(l)} - \mathbf{U}^{(l-1)}|| \leq \varepsilon_L$ stop; otherwise, return to step 2.

3.3 Example of SVD-QR-T with FCM in virtual MIMO channel selection

We use the following example to illustrate the SVD-QR-T with FCM application in MIMO-WSN channel selection.

1. *Step 1.* Assume the estimated channel gain is

$$\mathbf{H} = \begin{bmatrix} 0.6211 & 0.7536 & 0.6595 \\ 0.5602 & 0.6596 & 0.1834 \\ 0.2440 & 0.2141 & 0.6365 \\ 0.8220 & 0.6021 & 0.1703 \\ 0.2632 & 0.6049 & 0.5396 \end{bmatrix}$$

By matrix computation, we get:

$$\mathbf{V} = \begin{bmatrix} -0.5856 & -0.5075 & -0.6321 \\ -0.6574 & -0.1589 & 0.7366 \\ -0.4743 & 0.8469 & -0.2406 \end{bmatrix}$$

$diag(\Sigma) = (2.0017, 0.6347, 0.2572)$. Use FCM to divide $diag(\Sigma)$ into 2 clusters, we get

$$\mathbf{v} = \begin{bmatrix} 2.0010 \\ 0.4445 \end{bmatrix}$$

$$\mathbf{U} = \begin{bmatrix} 1.0000 & 0.0190 & 0.0114 \\ 0.0000 & 0.9810 & 0.9886 \end{bmatrix}$$

where entry 1.0000 at $\mathbf{U}$ is the membership that 2.0017 belongs to the cluster with center 2.0010. Therefore, the cluster with higher center is composed of only 2.0017, then 2.0017 is chosen and $rt = 1$.

2. *Step 2.* Obtain $\mathbf{V}_{11}$ and $\mathbf{V}_{21}$ from $\mathbf{V}$:

$$\mathbf{V}_{11} = -0.5856$$

$$\mathbf{V}_{21} = \begin{bmatrix} -0.6574 \\ -0.4743 \end{bmatrix}$$

Based on $[\mathbf{V}_{11}^T \mathbf{V}_{21}^T]$ get $\mathbf{E}$ by QR:

$$\mathbf{E} = \begin{bmatrix} 0 & 1 & 0 \\ 1 & 0 & 0 \\ 0 & 0 & 1 \end{bmatrix}$$

As $rt = 1$, choose the first column of $\mathbf{E}$

$$\mathbf{E}(:, rt) = \begin{bmatrix} 0 \\ 1 \\ 0 \end{bmatrix}$$

3. *Step 3.* Analyze $\mathbf{E}(:, rt)$, 1 appears on the $2nd$ row, and thus the $2nd$ column of $\mathbf{H}$ is selected to construct $\mathbf{H}_s$, which is:

$$\mathbf{H}_s = \begin{bmatrix} 0 & 0.7536 & 0 \\ 0 & 0.6596 & 0 \\ 0 & 0.2141 & 0 \\ 0 & 0.6021 & 0 \\ 0 & 0.6049 & 0 \end{bmatrix}$$

This implies that the channel to be selected are those that connect $2nd$ transmitter and all receivers, i.e., transmitter 2 and all the receivers are selected to be active while other transmitters are not employed to save their battery.

As we may see, the row index in which 1 appears in $\mathbf{E}(:, rt)$ particularly decide which transmitters to be selected, so with regard to SVD-QR-T, $rt \times M_r$ channels are selected to be active.

4 Performance Analysis

Due to the randomness of channel gain matrix, we employ Monte Carlo simulations to analyze the performances

on our algorithms in terms of capacity, multiplexing gain and bit error rate (BER). Following steps are applied:

1. Use Jake's Model [19] to randomly generate independent $M_t \times M_r$ Rayleigh channels, take their channel gains at a particular the same time as entries for matrix $\mathbf{H}$.
2. Follow the SVD-QR-T FCM and channel selection algorithm respectively to select channels.
3. Obtain eigenvalue λ_{is} and its rank r_s for $\mathbf{H}_s$. Note that λ_{is} is totally different with λ_i of $\mathbf{H}$.
4. Here we assume $B = 1Hz$. Through 10,000 times Monte Carlo simulations to obtain capacity, BER for QPSK modulation and multiplexing gain with and without water-filling.

4.1 Channel Known At the Transmitter: Water-Filling

When both of CSIT and CSIR are known, water-filling technique can be utilized to optimally allocate power P_i at independent parallel channel i. The sum of capacities on each of these independent parallel channels is the maximal capacity of virtual MIMO [12]. This capacity can be expressed as

$$C = \max_{\sum P_i \leq P} \sum_{i=1}^{r} B \log_2(1 + \frac{P_i}{\sigma^2}\lambda_i) \qquad (14)$$

where P is total power constraint for transmitters, r is the rank of $\mathbf{H}$ and λ_i is the eigenvalue of $\mathbf{H}\mathbf{H}^T$. Since the SNR at the ith channel at full power is $SNR_i = \lambda_i P/\sigma^2$, the capacity (14) can also be given in terms of the power allocation P_i as

$$C = \max_{\sum P_i \leq P} \sum_{i=1}^{r} B \log_2(1 + \frac{P_i}{P} SNR_i) \qquad (15)$$

where

$$\frac{P_i}{P} = \begin{cases} 1/SNR_0 - 1/SNR_i & SNR_i \geq SNR_0 \\ 0 & SNR_i < SNR_0 \end{cases} \qquad (16)$$

for some cutoff value SNR_0. The final capacity is given as

$$C = \sum_{SNR_i \geq SNR_0} B \log_2(\frac{SNR_i}{SNR_0}) \qquad (17)$$

The value of SNR_0 must be found numerically, owning to no existence of closed-form solution for continues distributions of SNR [21]. This results in Monte Carlo simulations to analyze the capacity performances on SVD-QR-T FCM, which is illustrated in Fig. 3. It is shown that the capacity of 4x4 virtual MIMO is 4 bps/Hz while it becomes 3.4 bps/Hz if SVD-QR-T FCM channel selection is applied. This difference grows up to around 2.2 bps/Hz when SNR reaches 20dB.

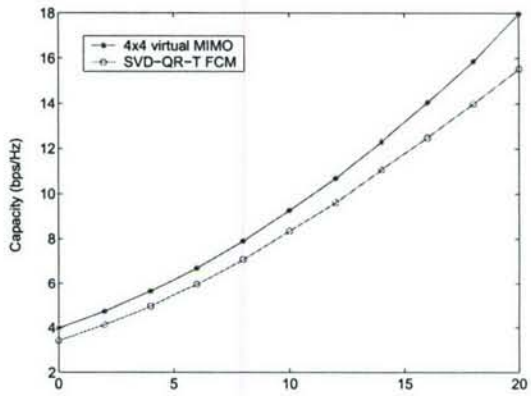

Figure 3. Capacity of SVD-QR-T FCM vs. virtual MIMO with water-filling

Although SVD-QR-T FCM does not seem to provide any advantage in the above figure, it offers lower BER than virtual MIMO without channel selection when SNR is higher than 7dB, which is shown in Fig. 4. This is because SVD-QR-T FCM chooses the best subset of equivalent parallel channels so that SNR allocated at each parallel is larger than that of virtual MIMO as P/σ^2 grows larger. Here we employ QPSK modulation with multiplexing but no space-time coding (STC). Since no diversity gain is obtained, maximal multiplexing does exist.

Maximal multiplexing gain is the number of equivalent multiple parallel spatial channels [22], and also it is referred to as degrees of freedom to communicate [23], which is related with the row and column number of $\mathbf{H}$ and $\mathbf{H}_s$. It has been derived in [23] that the maximal multiplexing gain provided by $M_r \times M_t$ MIMO is $\min(M_t, M_r)$. However, the accurate multiplexing gain is $r = rank(\mathbf{H})$ since it is possible that $\mathbf{H}$ is not full rank. As SVD-QR-T FCM select rt transmitters and all receivers, the maximal multiplexing gain offered by SVD-QR-T FCM is $\min(rt, M_r)$. Note that $rt \leq r \leq M_r$, therefore the accurate multiplexing gain for SVD-QR-T FCM is rt. However, this values are applicable only for no water-filling. If water-filling are applied, less multiplexing gain will be offered as some singular values with SNR lower than SNR_0 will be cut off.

Under the premise that $\mathbf{H}$ is full rank, we obtain the multiplexing gain on SVD-QR-T FCM and virtual MIMO in Fig. 5.

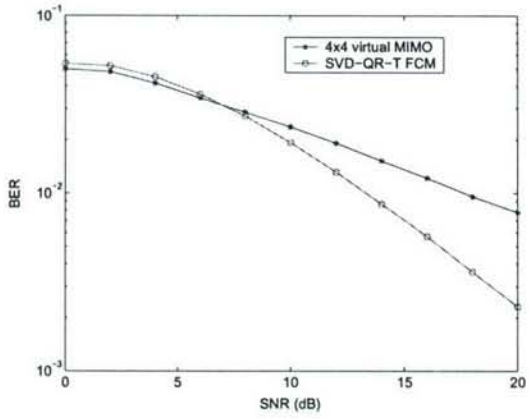

Figure 4. BER of SVD-QR-T vs. 4×4 virtual MIMO with water-filling

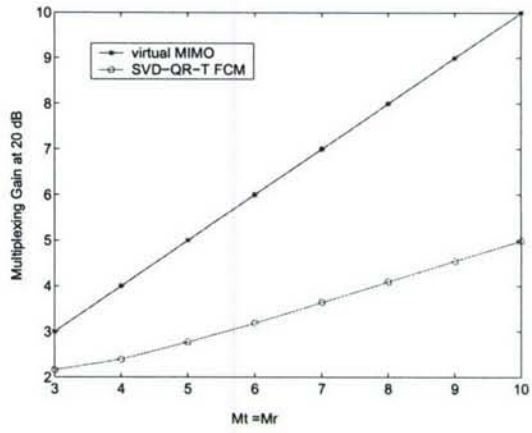

Figure 5. Multiplexing gain of SVD-QR-T FCM vs. virtual MIMO with water-filling at SNR=20dB

4.2 Channel Unknown At Transmitter: Uniform Power Allocation

it is not always the case that both CSIT and CSIR are known. In case of only CSIR, water-filling power optimization can not be applied and people simply allocate equal power to each transmitters, therefore its capacity becomes

$$C = \sum_{i=1}^{r} B \log_2(1 + \frac{SNR_i}{M_t}) \qquad (18)$$

Here we also apply 10,000 time Monte Carlo simulations to obtain the expectation of capacity for SVD-QR-T FCM and 4×4 virtual MIMO at different SNR in Fig. 6. It is shown that SVD-QR-T FCM provides higher capacity than that of virtual MIMO without channel selection if SNR is less than 10dB.

The BER performance is illustrated in Fig. 7. We can see that as SNR increase, BER after SVD-QR-T FCM channel selection become much lower than that of virtual MIMO.

In the mean time, Fig. 8 illustrates that virtual MIMO can achieve larger multiplexing gain than that of SVD-QR-T FCM but that implies more transmitters and RF chains consumption, which is the same situation as in case of water-filling. As no-water-filling is used, here multiplexing gain is not associate with SNR.

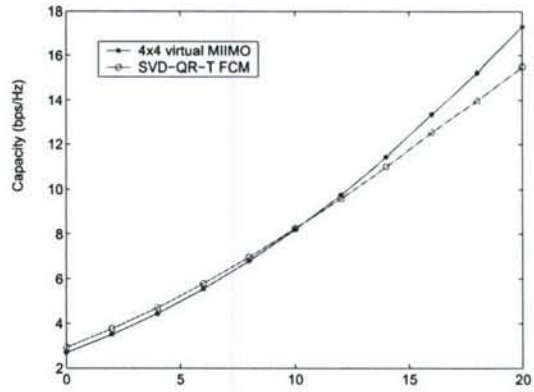

Figure 6. Capacity of SVD-QR-T FCM vs. virtual MIMO without water-filling

5 Conclusions

This paper is a preliminary work on virtual MIMO channel selection problem in practice. SVD-QR-T FCM approach with concrete example is proposed. We not only present the channel selection algorithms, but also provide the detailed approach on performance analysis with Monte Carlo simulations. We demonstrate that with the same total transmission power constraint, SVD-QR-T FCM can offer higher capacity at low SNR without waterfilling and much lower BER at high SNR no matter water-filling is applied or not. Future research tracks might concern the extension of the proposed algorithm to integrate with space time coding (STC) so as to further optimize the system performances.

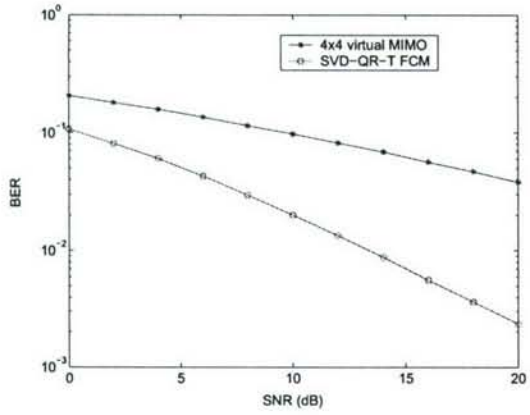

Figure 7. BER of SVD-QR-T vs. 4×4 virtual MIMO without water-filling

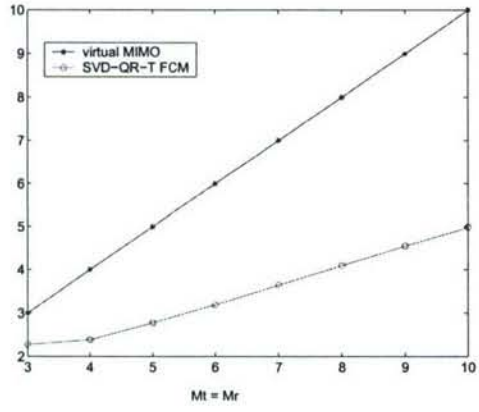

Figure 8. Multiplexing gain of SVD-QR-T FCM vs. virtual MIMO without water-filling

Acknowledgement

This work was supported by the Office of Naval Research (ONR) Young Investigator Award under Grant N00014-03-1-0466, and ONR Award under Grant N00014-07-1-0395.

References

[1] S. Cui and A. Goldsmith "Energy-efficiency of MIMO and Cooperative MIMO Techniques in Sensor Networks" , *IEEE Journal on selected areas in communications*, vol. 22, Aug 2004, pp. 1089-1098

[2] S. K. Jayaweera "Virtual MIMO-based cooperative communication for energy-constrained wireless sensor networks" , *IEEE Transactions on Wireless Communications*, vol. 5, May 2006, pp. 984 - 989

[3] Y. Yuan; Z. He and M. Chen "Virtual MIMO-based cross-layer design forwireless sensor networks" , *IEEE Transactions on Vehicular Technology*, vol. 55, May 2006, pp. 856 - 864

[4] M. Bengtsson and B. Ottersten, "Optimal and suboptimal transmit beamforming", *Handbook of Antennas in Wireless Communications*, L. C. Godara, Ed. Boca Raton, Fl, CRC, 2001

[5] D. A. Gore and A. J. Paulraj, "MIMO antenna subset selection with space-time coding", *IEEE Transactions on Signal Processing*, vol. 50, Oct. 2002

[6] A. Gorokhov, D. A. Gore and A. J. Paulraj, "Receive antenna selection for MIMO flat-fading channels: theory and algorithms", *IEEE Transactions on Information Theory*, vol. 49, Oct. 2003

[7] A. F. Molisch, M. Z. Win and J. H. Winters, "Capacity of MIMO systems with antenna selection", in *Proc. Int. Conf. Communications*, 2001, pp. 570-574

[8] D. A. Gore, R. U. Nabar and A. Paulraj, "Selecting an optimal set of transmit antennas for a low rank matrix channel", in *Proc. Int. Conf. Acoustics, Speech, and Signal Processing*, 2000, pp. 2785-2788

[9] S. Sandhu, R. U. Nabar, D. A. Gore and A. Paulraj, "Near optimal antenna selection of transmit antennas for a MIMO channel based on Shannon capacity", in Proc. 34th Asilomar Conf., Nov. 1999, pp. 567-571

[10] R. W. Heath Jr. and A. Paulraj, "Antenna Selection for spatial multiplexing systems based on minimum error rate", in *Proc. IEEE Int. Control Conf.*, 2001, pp. 2276-2280

[11] I. Bahceci, T. M. Duman and Y. Altunbasak "Antenna Selection for Multiple-Antenna Transmission Systems: Performance Analysis and Code Construction *IEEE Transctions on Information Theory*, vol. 49, oct. 2003

[12] A. Goldsmith, *Wireless Communications*, Cambridge University Press, NJ 2001.

[13] D. B. West, *Introduction to Graph Theory (2 Ed.)*, Prentice-Hall of India, NY 2005.

[14] Chen, S., S. A. Billings and W. Luo, "Orthogonal Least Squares Methods and their Application to Non-linear System Identification," *Int. J. Control*, vol. 50, 1989, pp. 1873-1896.

[15] Q. Liang and L. Wang, "Redundancy Reduction in Wireless Sensor Networks Using Singular-Value-QR Decomposition" , *IEEE Military Communication Conference*, Oct. 2005, Atlantic City, NJ.

[16] J. C. Bezdek, *Pattern Recognition with Fuzzy Objective Function Algorithms*, Plenum Press, New York, 1981.

[17] "Xiuzhen Cheng, et al, Strong Minimum Energy Topology: NP-Completeness and Heuristics , IEEE Transaction on Mobile Computing", Vol. 2, No. 3, pp. 248-256, July-September 2003.

[18] Xiuzhen Cheng, et al, "Polynomial-Time Approximation Scheme for Minimum Connected Dominating Set in Ad Hoc Wireless Networks", Networks, Vol. 42, No. 4, pp. 202-208, 2003.

[19] G. Stüber, *Mobile Communications*, 2nd ed., Kluwer Academic Publishers, 2001

[20] M. K. Simon and M. S. Alouini, *Digital Communication over fading channels*, 2nd ed., John Wiley & Sons, 2005

[21] M.-S. Alouini and A. J. Goldsmith, " Capacity of Rayleigh fading channels under different adaptive transmission and diversity combining techniques", *IEEE Trans. Veh. Tech*, pp. 1165-1181, July. 1999

[22] Jr. R. Heath and A. Paulraj, "Switching between multiplexing and diversity based on constellation distance", in *Proc. Allerton Conf. Communication, Contril and Computing*, Oct 2000

[23] L. Zheng, D. N. C. Tse, "Diversity and multiplexing: a fundamental tradeoff in multiple-antenna channels", *IEEE Trans. on Information Theory*, vol. 49, pp. 1073-1096, May 2003

A Graph Theory Algorithm for Virtual MIMO Channel Selection in Wireless Sensor Networks

Jing Liang and Qilian Liang, Senior Member, IEEE
Department of Electrical Engineering
University of Texas at Arlington
Arlington, TX 76019-0016 USA
E-mail: jliang@wcn.uta.edu, liang@uta.edu

***Abstract*— In virtual multiple input multiple output wireless sensor networks (MIMO-WSN), sensors are likely to be densely deployed, which gives rise to the open problem of channel selection. In respect of cross-layer design, we propse Maximum Spanning Tree Searching (MASTS) algorithm on a basis of graph theory to select a set of subchannels, which consequently reduce the complexity and cost of full virtual MIMO while providing network layer connection for all sensors. The performances are analyzed through Monte Carlo simulation in terms of capacity with/without water-filling, diversity gain and multiplexing gain. It is shown that MASTS virtual MIMO can achieve satisfying performances compared to those of full virtual MIMO.**

I. Introduction and Motivation

A. Channel selection in virtual MIMO

Virtual multiple-input-multiple-output (MIMO) has been studied intensively in recent years in order to improve the energy-efficiency in wireless sensor networks (WSN) [1][2][3]. Constrained by its physical size and limited battery, individual sensor is allowed to contain only one antenna. Numerical results show that if these individual sensors jointly form the MIMO system, tremendous energy will be saved while satisfying the required performance. However, a natural drawback of virtual MIMO is the increased complexity and the cost of multiple radio frequency (RF) chains. One technique to reduce the complexity and cost while providing similar performances is antenna selection, or channel selection. The latter is joint antenna selection at both transmitter and receiver and requires channel side information at both transmitter (CSIT) and receiver (CSIR).

The knowledge of channels can be obtained by various channel estimation techniques, such as reciprocity principle and feedback channel [4]. When CSIR or CSIR is obtained, antenna selection can be applied through subset selection algorithms by switchers either at transmitters or receivers, or jointly working at both ends. Therefore the best set of channels are selected to be active while remaining ones are not employed. These switchers typically cost much less than RF chains so that low-cost and low-complexity can be achieved with the benefits of multiple antennas [5] [6]. This system is illustrated in Fig. 1.

Recent years have seen an explosion of interest in MIMO antenna selection and various criteria have been used:

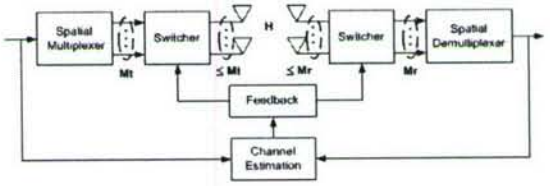

Fig. 1. system diagram for virtual MIMO channel selection

1) Capacity Maximization: In the previous work of [7] [8] [9], channel capacity is used as the optimality criterion, i.e., antennas that achieve the largest capacity are active. In [7], it is demonstrated that in case of no CSIT but CSIR, close capacity to that of the full-MIMO system can be achieved as far as the number of selected receivers is no less than the number of transmitters. [8] and [9] considered CSIT and proposed an exhaustive search algorithm.
2) Minimum Error rate: Apart from maximization of capacity based on Shannon theory, [10] derived another criteria from the respect of minimum error rate when coherent receivers, either maximum likelihood (ML), zero-forcing (ZF) or the minimum mean-square error (MMSE) linear receiver is employed.
3) Cross-layer optimal scheduling: Besides physical layer, some related works have adopted graph theory approach to consider cross-layer design. [11] performed the optimal antenna assignment for spatial multiplexing by Hungarian algorithm using weighted bipartite matching graph, and [12] took into account users' QoS requirement with clique-searching algorithm for antenna selection.

Although there have been dazzling mathematical studies on antenna selection criteria, practical algorithms of channel selection require more investigations and the problem of corresponding performance analysis is still open [13] .

B. Contributions and Organization of This Paper

In this paper, under the assumption of quasi-static channels and both CSIT and CSIR, we propose Maximum Spanning Tree Searching (MASTS) algorithm on a basis of Kruskal's

theory [14] to perform channel selection, which potentially provide a path connecting all sensors. Concrete example is presented to illustrate each step. We not only employ graph theory into virtual MIMO study in view of cross-layer design, but analyze its performance by means of Monte Carlo simulations, which is an efficient approach to illustrate the tendency of results in practice. We employ 10000 times of Monte Carlo simulation to estimate capacity, diversity gain, and multiplexing gain. The result shows that at high SNR, MASTS can achieve higher capacity than that of full virtual MIMO.

We organize the remainder of this paper as follows. In Section II, we introduce virtual MIMO channel model. Section III proposes MASTS algorithm step by step. Section IV compares the performances of MASTS with that of full virtual MIMO and Section V draws the conclusion.

II. Channel Model

Based on CSIT and CSIR, the estimated virtual MIMO channel model with M_t transmitters and M_r receivers ($M_t + M_r$ sensors) is illustrated in Fig. 2, where each receiver observes a superposition of the M_t transmitted signals corrupted by flat fading and additive white gaussian noise. Each h_{ji}, $i = 1, 2, \cdots, Mr$ and $j = 1, 2, \cdots, Mt$ represents the transmission channel gain from transmitter i to receiver j [15], which is assumed to be independent and identically distributed (i.i.d.). The additive noise also has i.i.d entries $n_j \sim \mathcal{CN}(0, \sigma^2)$.

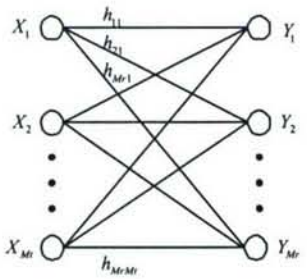

Fig. 2. Channel Graph for virtual MIMO

We may denote this virtual MIMO channels with discrete time model:

$$\begin{bmatrix} Y_1 \\ Y_2 \\ \vdots \\ Y_{Mr} \end{bmatrix} = \begin{bmatrix} h_{11} & h_{12} \cdots h_{1Mt} \\ h_{21} & h_{22} \cdots h_{2Mt} \\ \vdots & \vdots \\ h_{Mr1} & h_{Mr2} \cdots h_{MrMt} \end{bmatrix} \begin{bmatrix} X_1 \\ X_2 \\ \vdots \\ X_{Mt} \end{bmatrix} + \begin{bmatrix} n_1 \\ n_2 \\ \vdots \\ n_{Mr} \end{bmatrix} \quad (1)$$

We may simplify the above equation as $\mathbf{Y} = \mathbf{HX} + \mathbf{n}$, where $\mathbf{H}$ is a $Mr \times Mt$ independent zero mean random matrix and $\mathbf{n}$ denotes random noise.

From the respect of graph theory, Fig. 2 is a connected graph [16], i.e., there is an edge connecting any two vertex with sensors and transmission channels forming vertex set and edge set respectively, h_{ji} denoting edge weight. This gives rise to the graph theoretical approach to virtual MIMO study. However, the integration of graph theory into communication systems is still neonatal and deserves more attention and development.

Our purpose is to replace $\mathbf{H}$ with an approximate matrix $\hat{\mathbf{H}}$ with lower dimensions but satisfying performances and basic network layer connections.

III. MASTS Virtual MIMO

A. Introduction of MASTS

As mentioned in section II, we may use a graph of vertices and edges to represent the virtual MIMO communication scenario. From this aspect, essentially channel selection is to remove some of vertices and edges while keep those remaining. Spanning tree [16] suggests such an algorithm that in an arbitrary graph, all the vertices are connected with the minimum necessary edges, i.e., there is no isolated vertices under the condition of the least possible edge number. For example, when $Mt = 3$ and $Mr = 5$, some of the possible spanning trees are drawn in Fig. 3.

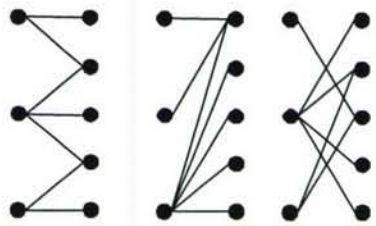

Fig. 3. Examples of spanning trees for 5×3 MIMO

In general, MASTS algorithm is to compute a spanning tree with the maximum sum of weight of edge, i.e., to select the maximum sum of channel gain while realizing the connectivity of all the sensors on a basis of maximum spanning tree algorithm. Our contribution is to apply the graph theoretical concept on maximum spanning tree into virtual MIMO channel selection and program the algorithm.

Note that for an arbitrary graph of n vertices, its spanning tree is of n vertices and $n - 1$ edges [16]. Since there are $Mt + Mr$ vertices, the number of edges to be selected by MASTS algorithm is a fixed $Mt + Mr - 1$, which means MASTS always chooses $Mt + Mr - 1$ channels.

B. MASTS in virtual MIMO channel selection

MASTS algorithm is:

1) *Step 1*: Select 3 edges with the largest weight at first (including their vertices).
2) *Step 2*: Enlarge the subgraph by edges with large weight in decreasing manner and make sure no cycles are formed.
3) *Step 3*: Continue *Step 2* until the edge number of enlarged subgraph is equal to $Mt + Mr - 1$. This final

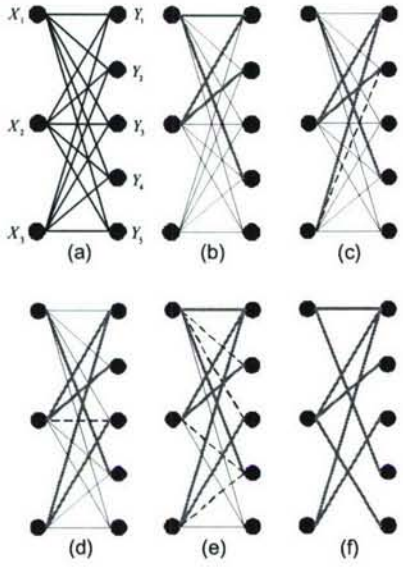

Fig. 4. MASTS algorithm

subgraph is the spanning tree with the maximum sum of weight.

As virtual MIMO graph contains the same information as that of channel gain matrix $\mathbf{H}$, we illustrate MASTS algorithm by matrix entry selection procedure using Fig. 4 and matrix $\mathbf{H}_b$ $\mathbf{H}_c$ $\mathbf{H}_d$ $\mathbf{H}_e$ $\hat{\mathbf{H}}$.

Fig. 4 (a) is the original virtual MIMO graph. Fig. 4 (b) shows the subgraph with 3 largest weight. These edges are denoted by $\langle\rangle$ in matrix $\mathbf{H}_b$. This is *Step 1*.

$$\mathbf{H}_b = \begin{bmatrix} 0.6211 & \langle 0.7536\rangle & 0.6595 \\ 0.5602 & \langle 0.6596\rangle & 0.1834 \\ 0.2440 & 0.2141 & 0.6365 \\ \langle 0.8220\rangle & 0.6021 & 0.1703 \\ 0.2632 & 0.6049 & 0.5396 \end{bmatrix}$$

Note that among the selected 3 entries, 0.8220 have the different row index either with 0.7536 or 0.6595, so enlarging this subgraph with any of the remaining edges will absolutely not form a cycle.

Thus, the second step starts with selecting the edge with the fourth largest weight, which is shown in Fig. 4 (c) and Matrix $\mathbf{H}_c$.

$$\mathbf{H}_c = \begin{bmatrix} 0.6211 & \langle 0.7536\rangle & \langle 0.6595\rangle \\ 0.5602 & \langle 0.6596\rangle & 0.1834\times \\ 0.2440 & 0.2141 & 0.6365 \\ \langle 0.8220\rangle & 0.6021 & 0.1703 \\ 0.2632 & 0.6049 & 0.5396 \end{bmatrix}$$

Note that after selection of entry 0.6595, the entry 0.1834 will no longer be selected, or there is going to form a cycle $X_2Y_1X_3Y_2$, so we note the entry 0.1834 with "$\times$" and use dash line to represent the unavailability of corresponding edge in Fig. 4(c). This implies following criteria:

Any four entries with index (i,j) (i,q) (p,j) (p,q), where $i, p \leq Mr$, $i \neq p; j, q \leq Mt$, $j \neq q$ form a cycle. If any three have been selected, the remaining one should be eliminated.

Based on this criteria, we continuously select entries as shown in Fig. 4 (d) (e) (f) and matrix $\mathbf{H}_d$ $\mathbf{H}_e$ $\mathbf{H}_f$. As we only have to select $3 + 5 - 1 = 7$ edges. Edges in graph (f) represented by none-zero entries in matrix $\hat{\mathbf{H}}$ are the channels finally selected.

$$\mathbf{H}_d = \begin{bmatrix} 0.6211 & \langle 0.7536\rangle & \langle 0.6595\rangle \\ 0.5602 & \langle 0.6596\rangle & 0 \\ 0.2440 & 0.2141\times & \langle 0.6365\rangle \\ \langle 0.8220\rangle & 0.6021 & 0.1703 \\ 0.2632 & 0.6049 & 0.5396 \end{bmatrix}$$

$$\mathbf{H}_e = \begin{bmatrix} \langle 0.6211\rangle & \langle 0.7536\rangle & \langle 0.6595\rangle \\ 0.5602\times & \langle 0.6596\rangle & 0 \\ 0.2440\times & 0 & \langle 0.6365\rangle \\ \langle 0.8220\rangle & 0.6021\times & 0.1703\times \\ 0.2632 & 0.6049 & 0.5396 \end{bmatrix}$$

$$\hat{\mathbf{H}} = \begin{bmatrix} 0.6211 & 0.7536 & 0.6595 \\ 0 & 0.6596 & 0 \\ 0 & 0 & 0.6365 \\ 0.8220 & 0 & 0 \\ 0 & 0.6049 & 0 \end{bmatrix}$$

IV. Performance Analysis

A. Capacity

When the channel matrix $\mathbf{H}$ / $\hat{\mathbf{H}}$ is known at both transmitters and receivers, water-filling technique can be utilized to optimally allocate power P_i at independent parallel channel i. The sum of capacities on each of these independent parallel channels is the maximal capacity of virtual MIMO [15]. The capacity on full virtual MIMO can be expressed as

$$C = \max_{\sum P_i \leq P} \sum_{i=1}^{r} B \log_2(1 + \frac{P_i}{\sigma^2}\lambda_i) \tag{2}$$

where P is total power constraint for transmitters, r is the rank of $\mathbf{H}$ and λ_i is the eigenvalue of $\mathbf{H}\mathbf{H}^T$. Since the SNR at the ith channel at full power is $SNR_i = \lambda_i P/\sigma^2$, the capacity (2) can also be given in terms of the power allocation P_i as

$$C = \max_{\sum P_i \leq P} \sum_{i=1}^{r} B \log_2(1 + \frac{P_i}{P} SNR_i) \tag{3}$$

where

$$\frac{P_i}{P} = \begin{cases} 1/SNR_0 - 1/SNR_i & SNR_i \geq SNR_0 \\ 0 & SNR_i < SNR_0 \end{cases} \tag{4}$$

for some cutoff value SNR_0. The final capacity is given as

$$C = \sum_{SNR_i \geq SNR_0} B \log_2(\frac{SNR_i}{SNR_0}) \tag{5}$$

The value of SNR_0 must be found numerically, owning to no existence of closed-form solution for continues distributions of SNR [23]. This results in Monte Carlo simulation to analyze the capacity performance on MASTS virtual MIMO. We take following steps to do each experiment:

1) For simplicity, we apply Matlab "rand" to generate channel gain matrix $\mathbf{H}$.
2) Follow the MASTS channel selection algorithm to obtain the new channel gain matrix $\hat{\mathbf{H}}$.
3) Employ "svd" to obtain $\hat{\lambda}_i$ and its rank $\hat{r}$ for $\hat{\mathbf{H}}$. Note that $\hat{\lambda}_i$ is different with λ_i of $\mathbf{H}$.
4) Use water-filling power allocation to find out the cutoff value SNR_0 and the resulting capacity for MASTS virtual MIMO based on (3) (4) and (5). Here we assume $B = 1Hz$.

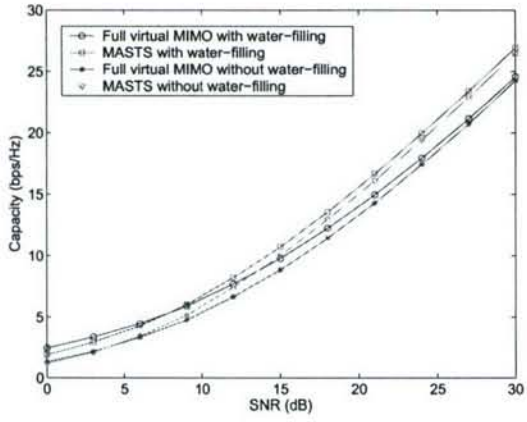

Fig. 5. Capacity for full / MASTS 4×4 virtual MIMO

Due to the randomness, 10000 times Monte Carlo simulation are applied to obtain the expectation of capacity for both MASTS and full 4×4 virtual MIMO at different SNR, which are plotted in Fig. 5. It shows when SNR is larger than 8dB, MASTS achieves larger capacity than that of full virtual MIMO. This is because the same total power have been optimally allocated to the best set of channels in spite of less channel number.

Sometimes in order to reduce the cost and complexity, instead of using water-filling power optimization, people simply allocate equal power to each transmitters. In that case, the capacity becomes

$$C = \sum_{i=1}^{r} B \log_2(1 + \frac{SNR_i}{M_t}) \tag{6}$$

Here we also apply 10000 time Monte Carlo simulation to obtain the expectation of capacities, which are also plotted in Fig. 5. It shows when SNR is larger than 5dB, MASTS achieves larger capacity than that of full virtual MIMO.

B. Diversity Gain and Multiplexing Gain

Intuitively, diversity gain corresponds to the number of independently faded paths that a symbol passes through [24]. In general, based our assumption of independent fading channel model, if finally M channels are selected, the maximal diversity gain provided is M. Since MASTS select M_t+M_r-1 channels, its maximal diversity gain is M_t+M_r-1, compared to that of M_tM_r on full virtual MIMO. Therefore, MASTS can not provide as much as full virtual MIMO on maximal diversity gain. This is illustrated in Fig. 6.

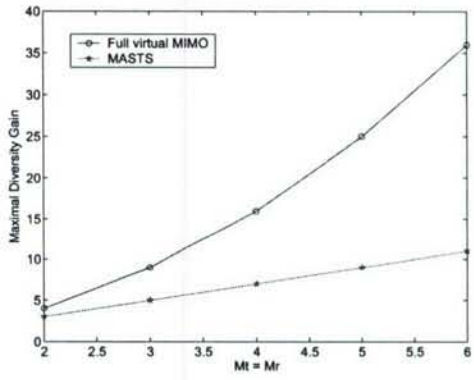

Fig. 6. Maximal diversity comparison

If BPSK and maximal ratio combining (MRC) are employed at maximal diversity gain, then the bit error rate (BER) is [25]

$$P_b = (\frac{1-\mu}{2})^L \sum_{k=0}^{L-1} \binom{L-1+k}{k} (\frac{1+\mu}{2})^k \tag{7}$$

where

$$\mu = \sqrt{\frac{\frac{P}{\sigma^2}}{1+\frac{P}{\sigma^2}}} \tag{8}$$

and L is the diversity gain. Based on (7) (8), we get Fig. 7 for 2×2 virtual MIMO.

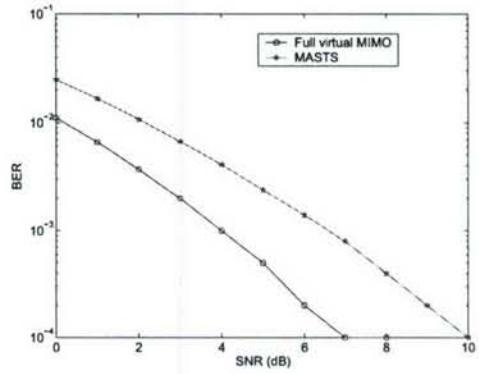

Fig. 7. BER for Full / MASTS 2×2 virtual MIMO

Normally, in order to increase the data rate, different transmitters simultaneously transmit different symbols, so in this case diversity for full and MASTS virtual MIMO are M_r and $(M_t + M_r - 1)/M_t$ respectively.

As for maximal multiplexing gain, it is the number of equivalent multiple parallel spatial channels [26], and also it is referred to as degrees of freedom to communicate [24], which is related with the row and column number of $\mathbf{H}$ and $\hat{\mathbf{H}}$. It has been derived in [24] that the maximal multiplexing gain provided by $M_t \times M_r$ MIMO is $\min(M_t, M_r)$. However, the accurate multiplexing gain is $r = rank(\mathbf{H})$ since it is possible that $\mathbf{H}$ is not full rank. The maximal multiplexing gain offered by MASTS is $\hat{r} = rank(\hat{\mathbf{H}})$. Under the premise that $\mathbf{H}$ is full rank, we ran 10000 times Monte Carlo simulation to obtain the multiplexing gain On MASTS in Fig. 8.

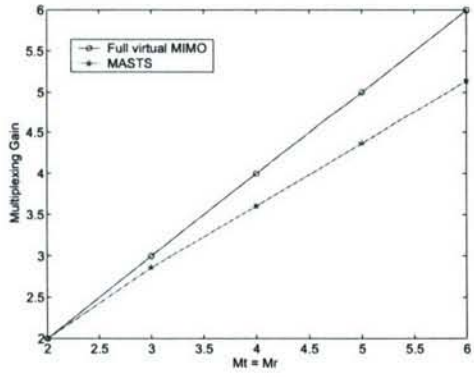

Fig. 8. Multiplexing Gain full / MASTS virtual MIMO

It shows when $Mt = Mr \leq 6$, the difference of Multiplexing Gain between full and MASTS virtual MIM can be less than 1.

In general, MASTS provide satisfying performances compared to that of full virtual MIMO.

V. Conclusion and Future Work

This paper is a preliminary work on practical virtual MIMO channel selection algorithm. MASTS approach with a concrete example is proposed from respect of cross-layer design. By means of Monte Carlo simulation, we approve that MASTS virtual MIMO can achieve even better capacity with/without water-filling, less diversity gain and similar multiplexing gain as those of full virtual MIMO. We not only propose the channel selection algorithm in practice, but also provide the detailed approach on performance analysis with Monte Carlo simulation. Future research tracks might concern the extension of the proposed algorithm to integrate with space time coding (STC) so as to further optimize the system performance.

Acknowledgement

This work was supported by the Office of Naval Research (ONR) Young Investigator Award under Grant N00014-03-1-0466, and ONR Award under Grant N00014-07-1-0395.

References

[1] S. Cui and A. Goldsmith "Energy-efficiency of MIMO and Cooperative MIMO Techniques in Sensor Networks" , *IEEE Journal on selected areas in communications*, vol. 22, Aug 2004, pp. 1089 - 1098

[2] S. K. Jayaweera "Virtual MIMO-based cooperative communication for energy-constrained wireless sensor networks" , *IEEE Transactions on Wireless Communications*, vol. 5, May 2006, pp. 984 - 989

[3] Y. Yuan; Z. He and M. Chen "Virtual MIMO-based cross-layer design forwireless sensor networks" , *IEEE Transactions on Vehicular Technology*, vol. 55, May 2006, pp. 856 - 864

[4] M. Bengtsson and B. Ottersten, "Optimal and suboptimal transmit beamforming", *Handbook of Antennas in Wireless Communications*, L. C. Godara, Ed. Boca Raton, Fl, CRC, 2001

[5] D. A. Gore and A. J. Paulraj, "MIMO antenna subset selection with space-time coding", *IEEE Transactions on Signal Processing*, vol. 50, Oct. 2002

[6] A. Gorokhov, D. A. Gore and A. J. Paulraj, "Receive antenna selection for MIMO flat-fading channels: theory and algorithms", *IEEE Transactions on Information Theory*, vol. 49, Oct. 2003

[7] A. F. Molisch, M. Z. Win and J. H. Winters, "Capacity of MIMO systems with antenna selection", in *Proc. Int. Conf. Communications*, 2001, pp. 570-574

[8] "Selecting an optimal set of transmit antennas for a low rank matrix channel", in *Proc. Int. Conf. Acoustics, Speech, and Signal Processing*, 2000, pp. 2785-2788

[9] "Near optimal antenna selection of transmit antennas for a MIMO channel based on Shannon capacity", in Proc. 34th Asilomar Conf., Nov. 1999, pp. 567-571

[10] "Antenna Selection for spatial multiplexing systems based on minimum error rate", in *Proc. IEEE Int. Control Conf.*, 2001, pp. 2276-2280

[11] Y. J. Choi, J. Kim and S. Bahk, "Downlink scheduling with fairness and optimal antenna assignment for MIMO cellular systems", *Global Telecommunications Conference, 2004*, Vol. 5, 2004 Page(s):3165 - 3169

[12] Y. J. Choi, J. Kim and S. Bahk, "Optimal antenna assignment considering QoS under MIMO environments", *IEEE International Conference on Communications, 2004*, Vol.7, June 2004, pp. 4216 - 4221

[13] S. Sanayei and A. Nosratinia, "Antenna selection in MIMO systems", *IEEE Communications Magazine*, vol. 42, Oct. 2004

[14] J. B. Kruskal "On the shortest spanning subtree and the traveling salesman problem", *Proceedings of the American Mathematical Society*, vol. 7, 1956, pp. 48C50.

[15] A. Goldsmith, *Wireless Communications*, Cambridge University Press, NJ 2001.

[16] D. B. West, *Introduction to Graph Theory (2 Ed.)*, Prentice-Hall of India, NY 2005.

[17] Chen, S., S. A. Billings and W. Luo, "Orthogonal Least Squares Methods and their Application to Nonlinear System Identification," *Int. J. Control*, vol. 50, 1989, pp. 1873-1896.

[18] G. H. Golub, and C. F. Van Loan, *Matrix Computations*, Johns Hopkins University Press, MD 1983.

[19] G. C. Mouzouris and J. M. Mendel, "Designing fuzzy logic systems for uncertain environments using a singular-value-QR decomposition method" , *Proc of IEEE 5th Intl. Conf. on Fuzzy Systems*, pp.295-301, 1996, New Orleans, LA.

[20] G. C. Mouzouris and J. M. Mendel, "A singular-value-QR decomposition based method for training fuzzy logic systems in uncertain environments", *J Intell Fuzzy Systems*, vol. 5, 1997, pp.367-374.

[21] Q. Liang and J. M. Mendal, "Designing interval type-2 fuzzy logic systems using an SVD-QR method: Rule reduction" , *International Journal of Intelligent Systems*, vol. 15, 2000, pp.939-957.

[22] Q. Liang and L. Wang, "Redundancy Reduction in Wireless Sensor Networks Using Singular-Value-QR Decomposition" , *IEEE Military Communication Conference*, Oct. 2005, Atlantic City, NJ.

[23] M.-S. Alouini and A. J. Goldsmith, " Capacity of Rayleigh fading channels under different adaptive transmission and diversity combining techniques", *IEEE Trans. Veh. Tech*, pp. 1165-1181, July. 1999

[24] L. Zheng, D. N. C. Tse, "Diversity and multiplexing: a fundamental tradeoff in multiple-antenna channels", *IEEE Trans. on Information Theory*, vol. 49, pp. 1073-1096, May 2003

[25] G. L. Stuber, *Principles of Mobile Communication*, 2nd ed., Kluwer Academic Publishers, 2001

[26] Jr. R. Heath and A. Paulraj, "Switching between multiplexing and diversity based on constellation distance", in *Proc. Allerton Conf. Communication, Contril and Computing*, Oct 2000.

Channel Selection Algorithms in Virtual MIMO Wireless Sensor Networks

Jing Liang and Qilian Liang, Senior Member, IEEE

Department of Electrical Engineering

University of Texas at Arlington

Arlington, TX 76019-0016 USA

E-mail: jliang@wcn.uta.edu, liang@uta.edu

Abstract

In this paper, we present two practical algorithms to select a subset of channels in virtual MIMO wireless sensor networks (WSN) in order to reduce its complexity and cost. One is Singular-Value Decomposition-QR with Threshold (SVD-QR-T) approach that select best subset of transmitters while keeping all receivers active. The threshold is adaptive by means of Fuzzy C-Mean (FCM). The other is Maximum Spanning Tree Searching (MASTS) algorithm on a basis of graph theory in respect of cross-layer design, which potentially provides a path connecting all sensors that benefits routing and QoS of networks. The MASTS algorithm keeps all sensors active but selects $M_t + Mr - 1$ subchannels, where M_t and M_r are the number of transmitters and receivers respectively. These two approaches are compared against the case without channel selection in terms of capacity, bit error rate (BER) and multiplexing gain in the presence of water-filling as well as the circumstance of without water-filling under the same total transmission power constraint. Despite less multiplexing gain, when water-filling is applied, MASTS achieves higher capacity and lower BER than virtual MIMO without channel selection at moderate to high SNR while SVD-QR-T FCM provides the lowest BER at high SNR; in case of no water-filling and equal transmission power allocation, MASTS still offers the highest capacity at moderate to high SNR but SVD-QR-T FCM achieves the lowest BER. Both algorithms provide satisfying performances compared to the case without channel selection but reduced cost and resource.

Index Terms : SVD-QR, FCM, maximal spanning tree, channel selection, antenna selection, virtual MIMO, wireless sensor networks (WSN).

1 Introduction

1.1 Channel selection in virtual MIMO

Virtual multiple-input-multiple-output (MIMO) has been studied intensively in recent years in order to improve the energy-efficiency in wireless sensor networks (WSN) [1][2][3]. Constrained by its physical size and limited battery, individual sensor is allowed to contain only one antenna. Numerical results show that if these individual sensors jointly form the MIMO system, tremendous energy will be saved while satisfying the required performance. However, a natural drawback of virtual MIMO is the increased complexity and the cost of multiple radio frequency (RF) chains. One technique to reduce the complexity and cost while providing similar capacity and performance is channel selection, or antenna selection.

The knowledge of channels can be obtained by various channel estimation techniques, such as reciprocity principle and feedback channel [4]. When channel side information (CSI) is known to transmitters or receivers, antenna selection can be applied through subset selection algorithms by switchers either at transmitters or receivers, or jointly working at both ends. Therefore the best set of channels are selected to be active while remaining ones are not employed. These switchers typically cost much less than RF chains so that low-cost and low-complexity can be achieved with the benefits of multiple antennas [5] [6]. This system is illustrated in Fig. 1.

Recent years have seen an explosion of interest in MIMO antenna selection and various criteria have been used:

1. Capacity Maximization: In the previous work of [7] [8] [9], channel capacity is used as the optimality criterion, i.e., antennas that achieve the largest capacity are active. [7] demonstrated that in case of no CSI at transmitter (CSIT) but receiver (CSIR), close capacity to that of the MIMO system can be achieved as far as the number of selected receivers is no less than the number of transmitters. [8] and [9] considered CSI at transmitter and proposed an

exhaustive search algorithm.

2. Minimum Error rate: Apart from maximization of capacity based on Shannon theory, [10] derived another criteria from the respect of minimum error rate when coherent receivers, either maximum likelihood (ML), zero-forcing (ZF) or the minimum mean-square error (MMSE) linear receiver is employed.

3. SNR Maximization: In [11], antenna selection is performed only at the receiver on a basis of largest instantaneous SNR using space-time coding. It is analytically shown that full diversity advantage promised by MIMO can be fully exploited using this criteria as long as the space-time code employed has full spatial diversity.

4. Cross-layer optimal scheduling: Besides physical layer, some related works have adopted graph theory approach to consider cross-layer design. [12] performed the optimal antenna assignment for spatial multiplexing by Hungarian algorithm using weighted bipartite matching graph, and [13] took into account users' QoS requirement with clique-searching algorithm for antenna selection.

Although there have been dazzling mathematical studies on antenna selection criteria, practical algorithms of joint transmit and receive antenna selection, i.e., *channel selection* is still open and the problem of corresponding performance analysis require more investigations.

1.2 Contributions and Organization of This Paper

In this paper, under the assumption of quasi-static Rayleigh fading, we propose two practical algorithms to perform channel selection. One is singular-value decomposition-QR with threshold (SVD-QR-T) employing Fuzzy C-Mean (FCM) to virtually provide adaptive threshold ; the other approach is Maximum Spanning Tree Searching (MASTS) algorithm on a basis of Kruskal's theory [14] in respect of graph theory, which potentially offers route connectivity of all sensors for network layer. The former is pure physical design, which selects rt (see section 3) best subset of transmitters while keeping all receivers active. The latter is a cross-layer method, which selects $M_t + Mr - 1$ subset of channels while keeping all transmitters and receivers active. Examples are presented to

illustrate each step. Their performances are estimated in terms of capacity, BER and multiplexing gain by means of Monte Carlo simulations, which is an efficient approach to illustrate the tendency of practical results. In general, it is shown that in spite of less multiplexing gain, when water-filling is applied, MASTS achieves higher capacity and lower BER than virtual MIMO without channel selection at moderate to high SNR while SVD-QR-T FCM provides the lowest BER at high SNR; in case of no water-filling and equal transmission power allocation, MASTS still offers the highest capacity at moderate to high SNR but SVD-QR-T FCM achieves the lowest BER. Both algorithms provide satisfying performances compared to the case without channel selection but reduced cost and resource.

We organize the remainder of this paper as follows. In Section 2, we introduce virtual MIMO channel model in respect of matrix as well as graph theory. Section 3 and 4 propose SVD-QR-T FCM and MASTS algorithms respectively. Section 5 compares the performance of these two algorithms with virtual MIMO and Section 6 draws the conclusion and presents future work.

2 Channel Model

Virtual MIMO channel model with M_t transmitters and M_r receivers (M_t+M_r sensors) is illustrated in Fig. 2, where each receiver observes a superposition of the M_t transmitted signals corrupted by Rayleigh flat fading and additive white gaussian noise. Each h_{ji}, $i = 1, 2, \cdots, M_t$ and $j = 1, 2, \cdots, M_r$ represents the channel gain from transmitter i to receiver j [15], which is assumed to be Rayleigh independent and identically distributed (i.i.d.). The additive noise also has i.i.d entries $n_j \sim \mathcal{CN}(0, \sigma^2)$.

We may denote this virtual MIMO channel graph with discrete time model:

$$\begin{bmatrix} Y_1 \\ Y_2 \\ \vdots \\ Y_{Mr} \end{bmatrix} = \begin{bmatrix} h_{11} & h_{12} & \cdots & h_{1Mt} \\ h_{21} & h_{22} & \cdots & h_{2Mt} \\ \vdots & \vdots & \vdots & \vdots \\ h_{Mr1} & h_{Mr2} & \cdots & h_{MrMt} \end{bmatrix} \begin{bmatrix} X_1 \\ X_2 \\ \vdots \\ X_{Mt} \end{bmatrix} + \begin{bmatrix} n_1 \\ n_2 \\ \vdots \\ n_{Mr} \end{bmatrix} \tag{1}$$

The above equation can be simplified as $\mathbf{Y} = \mathbf{HX} + \mathbf{n}$, where $\mathbf{H}$ is a $Mr \times Mt$ independent

Rayleigh random matrix and $\mathbf{n}$ denotes random noise.

From the respect of graph theory, Fig. 2 is a connected graph [16], i.e., there is a path connecting any two sensors with antennas and channels making up vertex set and edge set respectively while h_{ji} denotes edge weight. This gives rise to the graph theoretical approach on virtual MIMO study. However, integration of graph theory into wireless communication systems is still neonatal and deserves much more attention and development.

3 SVD-QR-T Virtual MIMO

3.1 SVD-QR-T in virtual MIMO channel selection

SVD has been applied to MIMO channel decomposition in [15], [17], and sensor node selection in [18]. However, these studies are on theoretical analysis only and no algorithm has been proposed on which channels will be physically selected in practice.

We propose SVD-QR-T as follows:

1. Given channel gain matrix $\mathbf{H} \in R^{Mr \times Mt}$ and $r = rank(\mathbf{H}) \leq \min(Mt, Mr)$, determine a numerical estimate rt of the rank r by calculating the singular value decomposition

$$\mathbf{H} = \mathbf{U}\Sigma\mathbf{V}^T, \tag{2}$$

where $\mathbf{U}$ is an $Mr \times Mr$ matrix of orthonormalized eigenvectors of $\mathbf{H}\mathbf{H}^T$, $\mathbf{V}$ is an $Mt \times Mt$ matrix of orthonormalized eigenvectors of $\mathbf{H}^T\mathbf{H}$, and Σ is the diagonal matrix $\Sigma = diag(\sigma_1, \sigma_2, \ldots, \sigma_i, \sigma_r)$, where $\sigma_i = \sqrt{\lambda_i}$ and λ_i is the ith eigenvalue of $\mathbf{H}\mathbf{H}^T$ and $\sigma_1 \geq \sigma_2 \geq \cdots \geq \sigma_r > 0$. σ_i is the singular value of $\mathbf{H}$. In many practical cases, σ_1, σ_1, $\cdots$, σ_{rt} are much larger than $\sigma_{rt+1}, \cdots, \sigma_r$; thus we may set threshold to pick up valuable $\sigma_i, i = 1, 2, \cdots, \sigma_{rt}$ and discard those trivial singular values in order to save resource but maintain satisfying performance. Sometimes rt can be chosen much smaller than the rank r, even 1. In this paper, we propose to use fuzzy c-means (FCM) to determine rt. Details will be discussed in section 3.2.

2. Partition

$$\mathbf{V} = \begin{bmatrix} \mathbf{V}_{11} & \mathbf{V}_{12} \\ \mathbf{V}_{21} & \mathbf{V}_{22} \end{bmatrix} \tag{3}$$

where $\mathbf{V}_{11} \in R^{rt \times rt}$, $\mathbf{V}_{12} \in R^{rt \times (Mt-rt)}$, $\mathbf{V}_{21} \in R^{(Mt-rt) \times rt}$, and $\mathbf{V}_{22} \in R^{(Mt-rt) \times (Mt-rt)}$.

3. Using QR decomposition with column pivoting, determine $\mathbf{E}$ such that

$$[\mathbf{V}_{11}^T, \mathbf{V}_{21}^T]\mathbf{E} = \mathbf{QR}, \tag{4}$$

where $\mathbf{Q}$ is a unitary matrix, and $\mathbf{R} \in R^{rt \times Mt}$ forms an upper triangular matrix with decreasing diagonal elements; and $\mathbf{E}$ is the permutation matrix. The positions of 1 in the first rt columns of $\mathbf{E}$ correspond to the rt ordered *most-significant* transmitters.

3.2 Fuzzy C-Means – Unsupervised Clustering for Adaptive Threshold

In order to keep the balance between performances and cost, we propose FCM clustering approach to divide singular value $(\sigma_1, \sigma_2, \ldots, \sigma_r)$ into two clusters, and thus provides virtual adaptive threshold, so the cluster with higher center would remain for active channels.

FCM clustering is a data clustering technique where each data point belongs to a cluster to a degree specified by a membership grade. This technique was originally introduced by Bezdek [19] as an improvement on earlier clustering methods. Here we briefly summarize it.

Definition 1 (Fuzzy c-Partition) *Let $\mathbf{X} = x_1, x_2, \cdots, x_n$ be any finite set, $\mathbf{V}_{cn}$ be the set of real $c \times n$ matrices, and c be an integer, where $2 \leq c < n$. The* Fuzzy c-partition space *for $\mathbf{X}$ is the set*

$$M_{fc} = U \in V_{cn} | u_{ik} \in [0,1] \ \forall i,k; \ \textit{where} \sum_{i=1}^{c} u_{ik} = 1 \ \forall k \ \textit{and} 0 < \sum_{k=1}^{n} u_{ik} < n \ \forall i \tag{5}$$

The row i of matrix $U \in M_{fc}$ contains values of the ith membership function, u_i, in the fuzzy c-partition U of $\mathbf{X}$.

Definition 2 (Fuzzy c-Means Functionals) *[19] Let $J_m : M_{fc} \times \mathcal{R}^{cp} \rightarrow \mathcal{R}^+$ be*

$$J_m(\mathbf{U}, \mathbf{v}) = \sum_{k=1}^{n} \sum_{i=1}^{c} (u_{ik})^m (d_{ik})^2 \tag{6}$$

where $\mathbf{U} \in M_{fc}$ *is a fuzzy c-partition of X;* $\mathbf{v} = (\mathbf{v}_1, \mathbf{v}_2, \cdots, \mathbf{v}_c) \in \mathcal{R}^{cp}$*, where* $\mathbf{v}_i \in \mathcal{R}^p$*, is the cluster center of prototype* u_i*,* $1 \leq i \leq c$*;*

$$(d_{ik})^2 = ||\mathbf{x}_k - \mathbf{v}_i||^2 \tag{7}$$

where $||\cdot||$ *is any inner product induced norm on* $\mathcal{R}^p$*; weighting exponential* $m \in [1, \infty)$*; and,* u_{ik} *is the membership of* $\mathbf{x}_k$ *in fuzzy cluster* u_i*.* $J_m(\mathbf{U}, \mathbf{v})$ *represents the distance from any given data point to a cluster weighted by that point's membership grade.*

The solutions of

$$\min_{\mathbf{U} \in M_{fc}, \mathbf{v} \in \mathcal{R}^{cp}} J_m(\mathbf{U}, \mathbf{v}) \tag{8}$$

are least-squared error stationary points of J_m. An infinite family of fuzzy clustering algorithms — one for each $m \in (1, \infty)$ — is obtained using the necessary conditions for solutions of (8), as summarized in the following:

Theorem 1 *[19] Assume* $||\cdot||$ *to be an inner product induced norm: fix* $m \in (1, \infty)$*, let* $\mathbf{X}$ *have at least* $c < n$ *distinct points, and define the sets* $(\forall k)$

$$I_k = \{i | 1 \leq i \leq c; d_{ik} = ||\mathbf{x}_k - \mathbf{v}_i|| = 0\} \tag{9}$$

$$\tilde{I}_k = \{1, 2, \cdots, c\} - I_k \tag{10}$$

Then $(\mathbf{U}, \mathbf{v}) \in M_{fc} \times \mathcal{R}^{cp}$ *is globally minimal for* J_m *only if* (ϕ *denotes an empty set)*

$$I_k = \phi \Rightarrow u_{ik} = 1 \Big/ [\sum_{j=1}^{c} (\frac{d_{ik}}{d_{jk}})^{2/(m-1)}] \tag{11}$$

or

$$I_k \neq \phi \Rightarrow u_{ik} = 0 \ \forall i \in \tilde{I}_k \text{ and } \sum_{i \in I_k} u_{ik} = 1, \tag{12}$$

and

$$\mathbf{v}_i = \sum_{k=1}^{n} (u_{ik})^m \mathbf{x}_k \Big/ \sum_{k=1}^{n} (u_{ik})^m \ \forall i \tag{13}$$

Bezdek proposed the following iterative method [19] to minimize $J_m(\mathbf{U}, \mathbf{v})$:

1. Fix c, $2 \leq c < n$; choose any inner product norm metric for $\mathcal{R}^p$; and fix m, $1 \leq m < \infty$. Initialize $\mathbf{U}^{(0)} \in M_{fc}$ (e.g., choose its elements randomly from the values between 0 and 1). Then at step l $(l = 1, 2, \cdots)$:

2. Calculate the c fuzzy cluster centers $\mathbf{v}_i^{(l)}$ using (13) and $\mathbf{U}^{(l)}$.

3. Update $\mathbf{U}^{(l)}$ using (11) or (12).

4. Compare $\mathbf{U}^{(l)}$ to $\mathbf{U}^{(l-1)}$ using a convenient matrix norm, i.e., if $||\mathbf{U}^{(l)} - \mathbf{U}^{(l-1)}|| \leq \varepsilon_L$ stop; otherwise, return to step 2.

3.3 Example of SVD-QR-T with FCM in virtual MIMO channel selection

We use the following example to illustrate the SVD-QR-T with FCM application in MIMO-WSN channel selection.

1. *Step 1.* Assume the estimated channel gain is

$$\mathbf{H} = \begin{bmatrix} 0.6211 & 0.7536 & 0.6595 \\ 0.5602 & 0.6596 & 0.1834 \\ 0.2440 & 0.2141 & 0.6365 \\ 0.8220 & 0.6021 & 0.1703 \\ 0.2632 & 0.6049 & 0.5396 \end{bmatrix}$$

By matrix computation, we get:

$$\mathbf{V} = \begin{bmatrix} -0.5856 & -0.5075 & -0.6321 \\ -0.6574 & -0.1589 & 0.7366 \\ -0.4743 & 0.8469 & -0.2406 \end{bmatrix}$$

$diag(\Sigma) = (2.0017, 0.6347, 0.2572)$. Use FCM to divide $diag(\Sigma)$ into 2 clusters, we get

$$\mathbf{v} = \begin{bmatrix} 2.0010 \\ 0.4445 \end{bmatrix}$$

$$\mathbf{U} = \begin{bmatrix} 1.0000 & 0.0190 & 0.0114 \\ 0.0000 & 0.9810 & 0.9886 \end{bmatrix}$$

where entry 1.0000 at $\mathbf{U}$ is the membership that 2.0017 belongs to the cluster with center 2.0010. Therefore, the cluster with higher center is composed of only 2.0017, then 2.0017 is

chosen and $rt = 1$.

2. *Step 2.* Obtain $\mathbf{V}_{11}$ and $\mathbf{V}_{21}$ from $\mathbf{V}$:

$$\mathbf{V}_{11} = -0.5856$$

$$\mathbf{V}_{21} = \begin{bmatrix} -0.6574 \\ -0.4743 \end{bmatrix}$$

Based on $[\mathbf{V}_{11}^T \mathbf{V}_{21}^T]$ get $\mathbf{E}$ by QR:

$$\mathbf{E} = \begin{bmatrix} 0 & 1 & 0 \\ 1 & 0 & 0 \\ 0 & 0 & 1 \end{bmatrix}$$

As $rt = 1$, choose the first column of $\mathbf{E}$

$$\mathbf{E}(:, rt) = \begin{bmatrix} 0 \\ 1 \\ 0 \end{bmatrix}$$

3. *Step 3.* Analyze $\mathbf{E}(:, rt)$, 1 appears on the $2nd$ row, and thus the $2nd$ column of $\mathbf{H}$ is selected to construct $\mathbf{H}_s$, which is:

$$\mathbf{H}_s = \begin{bmatrix} 0 & 0.7536 & 0 \\ 0 & 0.6596 & 0 \\ 0 & 0.2141 & 0 \\ 0 & 0.6021 & 0 \\ 0 & 0.6049 & 0 \end{bmatrix}$$

This implies that the channel to be selected are those that connect $2nd$ transmitter and all receivers, i.e., transmitter 2 and all the receivers are selected to be active while other transmitters are not employed to save their battery.

As we may see, the row index in which 1 appears in $\mathbf{E}(:, rt)$ particularly decide which transmitters to be selected, so with regard to SVD-QR-T, $rt \times M_r$ channels are selected to be active.

4 MASTS virtual MIMO

4.1 MASTS

As mentioned in Section 2, we may use a graph of vertices and edges to represent the virtual MIMO communication scenario. From this aspect, essentially channel selection is to remove some of edges while keep those remaining. However, global connectivity is usually required for WSN [20][21]. Spanning tree [16] suggests such an algorithm that in an arbitrary graph, all the vertices are connected with the minimum necessary edges, i.e., there is no isolated vertice under the condition of the least possible edge number. For example, when $Mt = 3$ and $Mr = 5$, some of the possible spanning trees are drawn in Fig. 3.

Note that for an arbitrary graph of n vertices, its spanning tree is of n vertices and $n-1$ edges [16]. Since there are $Mt + Mr$ vertices, the number of edges to be selected by MASTS algorithm is a fixed $Mt + Mr - 1$, which means MASTS always chooses $Mt + Mr - 1$ channels.

Given Mt and Mr, the ways to construct a spanning tree (not necessarily with maximum sum of weight) is $Mt^{Mr-1} \times Mr^{Mt-1}$. We prove this conclusion by Matrix Tree Theorem [16] as follows:

1. Adjacency matrix of virtual MIMO graph shown in Fig. 2 is

$$
\begin{array}{c}
 \\
X_1 \\
X_2 \\
\vdots \\
X_{Mt} \\
Y_1 \\
Y_2 \\
\vdots \\
Y_{Mr}
\end{array}
\begin{array}{c}
\begin{array}{cccccccc} X_1 & X_2 & \cdots & X_{Mt} & Y_1 & Y_2 & \cdots & Y_{Mr} \end{array} \\
\left[\begin{array}{cccccccc}
0 & 0 & \cdots & 0 & 1 & 1 & \cdots & 1 \\
0 & 0 & \cdots & 0 & 1 & 1 & \cdots & 1 \\
\vdots & \vdots & \vdots & \vdots & \vdots & \vdots & \vdots & \vdots \\
0 & 0 & \cdots & 0 & 1 & 1 & \cdots & 1 \\
1 & 1 & \cdots & 1 & 0 & 0 & \cdots & 1 \\
1 & 1 & \cdots & 1 & 0 & 0 & \cdots & 1 \\
\vdots & \vdots & \vdots & \vdots & \vdots & \vdots & \vdots & \vdots \\
1 & 1 & \cdots & 1 & 0 & 0 & \cdots & 0
\end{array}\right]
\end{array}
$$

2. Degree matrix of the above MIMO graph is:

$$\begin{array}{c} \\ X_1 \\ X_2 \\ \vdots \\ X_{Mt} \\ Y_1 \\ Y_2 \\ \vdots \\ Y_{Mr} \end{array} \begin{array}{c} \begin{array}{ccccccccc} X_1 & X_2 & \cdots & X_{Mt} & Y_1 & Y_2 & \cdots & Y_{Mr} \end{array} \\ \begin{bmatrix} Mr & 0 & \cdots 0 & 0 & 0 & \cdots & 0 \\ 0 & Mr & \cdots 0 & 0 & 0 & \cdots & 0 \\ \vdots & \vdots & \vdots & \vdots & \vdots & \vdots & \vdots \\ 0 & 0 & \cdots Mr & 0 & 0 & \cdots & 0 \\ 0 & 0 & \cdots 0 & Mt & 0 & \cdots & 0 \\ 0 & 0 & \cdots 0 & 0 & Mt & \cdots & 0 \\ \vdots & \vdots & \vdots & \vdots & \vdots & \vdots & \vdots \\ 0 & 0 & \cdots 0 & 0 & 0 & \cdots & Mt \end{bmatrix} \end{array}$$

3. Degree matrix minus adjacency matrix, we get matrix $\mathbf{D}$ which is:

$$\mathbf{D} = \begin{bmatrix} Mr & 0 & \cdots 0 & -1 & -1 & \cdots & -1 \\ 0 & Mr & \cdots 0 & -1 & -1 & \cdots & -1 \\ \vdots & \vdots & \vdots & \vdots & \vdots & \vdots & \vdots \\ 0 & 0 & \cdots Mr & -1 & -1 & \cdots & -1 \\ -1 & -1 & \cdots -1 & Mt & 0 & \cdots & 0 \\ -1 & -1 & \cdots -1 & 0 & Mt & \cdots & 0 \\ \vdots & \vdots & \vdots & \vdots & \vdots & \vdots & \vdots \\ -1 & -1 & \cdots -1 & 0 & 0 & \cdots & Mt \end{bmatrix} \tag{14}$$

4. Delete both an arbitrary row and an arbitrary column of $\mathbf{D}$ and take the determinant of remaining matrix, the result comes to $Mt^{Mr-1} \times Mr^{Mt-1}$, which is the number of ways to form a spanning tree on a basis of MIMO graph.

In general, MASTS algorithm is to compute a spanning tree with the maximum sum of weight of edge, i.e., to select the maximum sum of channel gain while realizing the connectivity of all the sensors. Our contributions mainly lie in applying the graph theoretical concept on maximum spanning tree into virtual MIMO channel selection and program the algorithm.

MASTS algorithm is:

1. *Step 1*: Select 3 edges with the highest weight including their vertices at first.

2. *Step 2*: Enlarge the subgraph by edges with high weight in decreasing manner and make sure no cycles are formed.

3. *Step 3*: Continue *step 2* until the edge number of enlarged subgraph is equal to $Mt+Mr-1$. This final subgraph is the spanning tree with the maximum sum of weight.

4.2 Example of MASTS in virtual MIMO channel selection

As virtual MIMO graph contains the same information as that of channel gain matrix $\mathbf{H}$, we illustrate MASTS algorithm by matrix entry selection procedure using Fig. 4 and matrix $\mathbf{H}_b$ $\mathbf{H}_c$ $\mathbf{H}_d$ $\mathbf{H}_e$ $\mathbf{H}_g$.

Fig. 4 (a) is the original virtual MIMO graph. Here we assume $\mathbf{H}$ is the same as that in SVD-QR example. Fig. 4 (b) shows the subgraph with 3 highest weight. These edges are denoted by $\langle\rangle$ in matrix $\mathbf{H}_b$. This is the *step 1*.

$$\mathbf{H}_b = \begin{bmatrix} 0.6211 & \langle 0.7536 \rangle & 0.6595 \\ 0.5602 & \langle 0.6596 \rangle & 0.1834 \\ 0.2440 & 0.2141 & 0.6365 \\ \langle 0.8220 \rangle & 0.6021 & 0.1703 \\ 0.2632 & 0.6049 & 0.5396 \end{bmatrix}$$

Note that among the selected 3 entries, 0.8220 have the different row index either with 0.7536 or 0.6595, so enlarging this subgraph with any of the remaining edges will absolutely not form a cycle.

Thus, the second step starts with selecting the edge with the fourth highest weight, which is shown in Fig. 4 (c) and Matrix $\mathbf{H}_c$.

$$\mathbf{H}_c = \begin{bmatrix} 0.6211 & \langle 0.7536 \rangle & \langle 0.6595 \rangle \\ 0.5602 & \langle 0.6596 \rangle & 0.1834\times \\ 0.2440 & 0.2141 & 0.6365 \\ \langle 0.8220 \rangle & 0.6021 & 0.1703 \\ 0.2632 & 0.6049 & 0.5396 \end{bmatrix}$$

Note that after selection of entry 0.6595, the entry 0.1834 will no longer be selected, or there is going to form a cycle $X_2Y_1X_3Y_2$, so we note the entry 0.1834 with "×" and use dash line to represent the unavailability of corresponding edge in Fig. 4(c). This implies following criteria:

Criteria *Any four entries with index (i,j) (i,q) (p,j) (p,q), where* $i, p \leq Mr$, $i \neq p; j, q \leq Mt$, $j \neq q$ *form a cycle. If any three have been selected, the remaining one should be eliminated.*

Based on this condition, we continually select entries as shown in Fig. 4 (d) (e) (f) and matrix $\mathbf{H}_d$ $\mathbf{H}_e$ $\mathbf{H}_f$. As we only have to select $3 + 5 - 1 = 7$ edges, edges in graph (f) represented by none-zero entries in matrix $\mathbf{H}_g$ are the channels finally selected.

$$\mathbf{H}_d = \begin{bmatrix} 0.6211 & \langle 0.7536 \rangle & \langle 0.6595 \rangle \\ 0.5602 & \langle 0.6596 \rangle & 0 \\ 0.2440 & 0.2141\times & \langle 0.6365 \rangle \\ \langle 0.8220 \rangle & 0.6021 & 0.1703 \\ 0.2632 & 0.6049 & 0.5396 \end{bmatrix}$$

$$\mathbf{H}_e = \begin{bmatrix} \langle 0.6211 \rangle & \langle 0.7536 \rangle & \langle 0.6595 \rangle \\ 0.5602\times & \langle 0.6596 \rangle & 0 \\ 0.2440\times & 0 & \langle 0.6365 \rangle \\ \langle 0.8220 \rangle & 0.6021\times & 0.1703\times \\ 0.2632 & 0.6049 & 0.5396 \end{bmatrix}$$

$$\mathbf{H}_g = \begin{bmatrix} 0.6211 & 0.7536 & 0.6595 \\ 0 & 0.6596 & 0 \\ 0 & 0 & 0.6365 \\ 0.8220 & 0 & 0 \\ 0 & 0.6049 & 0 \end{bmatrix}$$

It is worth mentioning that $\mathbf{H}_g$ obtained through MASTS is different from $\mathbf{H}_s$ derived by SVD-QR-T. We shall analyze their performances in the next section.

5 Performance Analysis

Due to the randomness of channel gain matrix, we employ Monte Carlo simulations to analyze the performances on our algorithms in terms of capacity, multiplexing gain and bit error rate (BER). Following steps are applied:

1. Use Jake's Model [22] to randomly generate independent $M_t \times M_r$ Rayleigh channels, take their channel gains at a particular the same time as entries for matrix $\mathbf{H}$.

2. Follow the SVD-QR-T FCM and MASTS channel selection algorithms respectively to select channels.

3. Obtain eigenvalue λ_{is} and its rank r_s for $\mathbf{H}_s$. Note that λ_{is} is totally different with λ_i of $\mathbf{H}$. Similarly, we can obtain λ_{ig}, r_g for $\mathbf{H}_g$.

4. Here we assume $B = 1Hz$. Through 10,000 times Monte Carlo simulations to obtain capacity, BER for QPSK modulation and multiplexing gain with and without water-filling.

5.1 Channel Known At the Transmitter: Water-Filling

When both of CSIT and CSIR are known, water-filling technique can be utilized to optimally allocate power P_i at independent parallel channel i. The sum of capacities on each of these independent parallel channels is the maximal capacity of virtual MIMO [15]. This capacity can be expressed as

$$C = \max_{\sum P_i \leq P} \sum_{i=1}^{r} B \log_2(1 + \frac{P_i}{\sigma^2}\lambda_i) \tag{15}$$

where P is total power constraint for transmitters, r is the rank of $\mathbf{H}$ and λ_i is the eigenvalue of $\mathbf{H}\mathbf{H}^T$. Since the SNR at the ith channel at full power is $SNR_i = \lambda_i P/\sigma^2$, the capacity (15) can also be given in terms of the power allocation P_i as

$$C = \max_{\sum P_i \leq P} \sum_{i=1}^{r} B \log_2(1 + \frac{P_i}{P} SNR_i) \tag{16}$$

where

$$\frac{P_i}{P} = \begin{cases} 1/SNR_0 - 1/SNR_i & SNR_i \geq SNR_0 \\ 0 & SNR_i < SNR_0 \end{cases} \tag{17}$$

for some cutoff value SNR_0. The final capacity is given as

$$C = \sum_{SNR_i \geq SNR_0} B \log_2(\frac{SNR_i}{SNR_0}) \tag{18}$$

The value of SNR_0 must be found numerically, owning to no existence of closed-form solution for continues distributions of SNR [24]. This results in Monte Carlo simulations to analyze the capacity performances on SVD-QR-T FCM and MASTS virtual MIMO, which is illustrated in Fig. 5. When SNR is lower than 5dB, SVD-QR-T FCM provides larger capacity than that of MASTS. However, MASTS grow larger than virtual MIMO when SNR reaches around 8.5 dB. It clearly shows that MASTS can offer the largest capacity at high SNR, due to the feature on singular value of $\mathbf{H}_g$. We shall illustrate it using following example:

Suppose

$$\mathbf{H} = \begin{bmatrix} 0.7733 & 1.3614 & 1.2254 & 0.3695 \\ 0.6867 & 0.2879 & 1.2014 & 1.7755 \\ 1.2381 & 0.5776 & 1.5719 & 0.2469 \\ 0.6749 & 1.4501 & 0.4248 & 0.6060 \end{bmatrix}$$

We can get λ = [13.4770 2.0235 1.1696 0.0743]; λ_g = [7.7490 3.7149 2.3701 0.2236]; λ_s = [10.6485 2.0002 1.0406]. With the increase of P/σ^2, MASTS capacity in (18) will increase faster then that of virtual MIMO without channel selection.

Although SVD-QR-T FCM does not seem to provide any advantage in the above figure, it offers lower BER than virtual MIMO without channel selection when SNR is higher than about 7dB as well as lowest BER after SNR grows to 13dB, which is shown in Fig. 6. This is because SVD-QR-T FCM chooses the best subset of equivalent parallel channels so that SNR allocated at each parallel is larger than that of MASTS and virtual MIMO as P/σ^2 grows larger. Here we employ QPSK modulation with multiplexing but no space-time coding (STC). Since no diversity gain is obtained, maximal multiplexing does exist.

Maximal multiplexing gain is the number of equivalent multiple parallel spatial channels [25], and also it is referred to as degrees of freedom to communicate [26], which is related with the row and column number of $\mathbf{H}$, $\mathbf{H}_s$ and $\mathbf{H}_g$. It has been derived in [26] that the maximal multiplexing gain provided by $M_r \times M_t$ MIMO is $\min(M_t, M_r)$. However, the accurate multiplexing gain is $r = rank(\mathbf{H})$ since it is possible that $\mathbf{H}$ is not full rank. As SVD-QR-T FCM select rt transmitters and all receivers, the maximal multiplexing gain offered by SVD-QR-T FCM is $\min(rt, M_r)$. Note that $rt \leq r \leq M_r$, therefore the accurate multiplexing gain for SVD-QR-T FCM is rt. Concerning MASTS, all transmitters and receivers are active and the maximal multiplexing gain is $rank(\mathbf{H}_g)$. However, these values are applicable only for no water-filling. If water-filling are applied, less multiplexing gain will be offered as some singular values with SNR lower than SNR_0 will be cut off.

Under the premise that $\mathbf{H}$ is full rank, we obtain the multiplexing gain on SVD-QR-T FCM and MASTS in Fig. 7 and Fig. 8 respectively. When $M_t = M_r = 10$, multiplexing gain for SVD-QR-T FCM and MASTS are 3.5 and 4 respectively if SNR is 0dB while they grow to 5 and 8.2 if SNR becomes 20dB. Note that although along the increase of SNR, the multiplexing gain of both algorithms will grow larger, this characteristic is more obvious for MASTS.

Fig. 5$\sim$8 implies that MASTS generally outweighs SVD-QR-T FCM on performances under the circumstances of water-filling, nevertheless it is worth mentioning that less multiplexing gain implies less transmitters are applied for SVD-QR-T FCM, so less resource are consumed. As for MASTS, it always employs all transmitters and receivers, which cost more resource than SVD-QR-T FCM.

5.2 Channel Unknown At Transmitter: Uniform Power Allocation

it is not always the case that both CSIT and CSIR are known. In case of only CSIR, water-filling power optimization can not be applied and people simply allocate equal power to each transmitters, therefore its capacity becomes

$$C = \sum_{i=1}^{r} B \log_2(1 + \frac{SNR_i}{M_t}) \tag{19}$$

Here we also apply 10,000 time Monte Carlo simulations to obtain the expectation of capacity for SVD-QR-T FCM / MASTS and 4×4 virtual MIMO at different SNR in Fig. 9.

It is shown that SVD-QR-T FCM provides higher capacity than that of virtual MIMO without channel selection if SNR is less than 10dB and higher capacity than that of MASTS if SNR is less than 2.5dB. MASTS outweighs virtual MIMO without channel selection in capacity from 0dB and this advantage is more obvious along the increase of SNR.

However, MASTS can not provide better performance in BER while SVD-QR-T FCM performs best, which is illustrated in Fig. 10. This is because SNR allocated at each equivalent parallel channel by means of SVD-QR-T FCM is larger than that of MASTS and virtual MIMO from 0dB.

In the mean time, Fig. 11 illustrates that MASTS can achieve larger multiplexing gain than that of SVD-QR-T FCM but that means more resource consumption, which is the same situation as in case of water-filling. As no-water-filling is used, here multiplexing gain is not associate SNR.

6 Conclusions

This paper is a preliminary work on virtual MIMO channel selection problem in practice. Two approaches with concrete examples are proposed from respect of pure physical design and cross-layer consideration respectively. We not only present the channel selection algorithms, but also provide the detailed approach on performance analysis with Monte Carlo simulations. We demonstrate that with the same total transmission power constraint, MASTS can offer highest capacity (either with water-filling or without) than that of virtual MIMO while SVD-QR-T FCM can provide best BER performance. Future research tracks might concern the extension of the proposed algorithm to integrate with space time coding (STC) so as to further optimize the system performances.

Acknowledgement

This work was supported by the Office of Naval Research (ONR) Young Investigator Award under Grant N00014-03-1-0466, and ONR Award under Grant N00014-07-1-0395.

References

[1] S. Cui and A. Goldsmith "Energy-efficiency of MIMO and Cooperative MIMO Techniques in Sensor Networks" , *IEEE Journal on selected areas in communications*, vol. 22, Aug 2004, pp. 1089-1098

[2] S. K. Jayaweera "Virtual MIMO-based cooperative communication for energy-constrained wireless sensor networks" , *IEEE Transactions on Wireless Communications*, vol. 5, May 2006, pp. 984 - 989

[3] Y. Yuan; Z. He and M. Chen "Virtual MIMO-based cross-layer design forwireless sensor networks" , *IEEE Transactions on Vehicular Technology*, vol. 55, May 2006, pp. 856 - 864

[4] M. Bengtsson and B. Ottersten, "Optimal and suboptimal transmit beamforming", *Handbook of Antennas in Wireless Communications*, L. C. Godara, Ed. Boca Raton, Fl, CRC, 2001

[5] D. A. Gore and A. J. Paulraj, "MIMO antenna subset selection with space-time coding", *IEEE Transactions on Signal Processing*, vol. 50, Oct. 2002

[6] A. Gorokhov, D. A. Gore and A. J. Paulraj, "Receive antenna selection for MIMO flat-fading channels: theory and algorithms", *IEEE Transactions on Information Theory*, vol. 49, Oct. 2003

[7] A. F. Molisch, M. Z. Win and J. H. Winters, "Capacity of MIMO systems with antenna selection", in *Proc. Int. Conf. Communications*, 2001, pp. 570-574

[8] D. A. Gore, R. U. Nabar and A. Paulraj, "Selecting an optimal set of transmit antennas for a low rank matrix channel", in *Proc. Int. Conf. Acoustics, Speech, and Signal Processing*, 2000, pp. 2785-2788

[9] S. Sandhu, R. U. Nabar, D. A. Gore and A. Paulraj, "Near optimal antenna selection of transmit antennas for a MIMO channel based on Shannon capacity", in Proc. 34th Asilomar Conf., Nov. 1999, pp. 567-571

[10] R. W. Heath Jr. and A. Paulraj, "Antenna Selection for spatial multiplexing systems based on minimum error rate", in *Proc. IEEE Int. Control Conf.*, 2001, pp. 2276-2280

[11] I. Bahceci, T. M. Duman and Y. Altunbasak "Antenna Selection for Multiple-Antenna Transmission Systems: Performance Analysis and Code Construction *IEEE Transctions on Information Theory*, vol. 49, oct. 2003

[12] Y. J. Choi, J. Kim and S. Bahk, "Downlink scheduling with fairness and optimal antenna assignment for MIMO cellular systems", *Global Telecommunications Conference, 2004*, Vol. 5, 2004 Page(s):3165-3169

[13] Y. J. Choi, J. Kim and S. Bahk, "Optimal antenna assignment considering QoS under MIMO environments", *IEEE International Conference on Communications, 2004*, Vol.7, June 2004, pp. 4216-4221

[14] J. B. Kruskal "On the shortest spanning subtree and the traveling salesman problem", *Proceedings of the American Mathematical Society*, vol. 7, 1956, pp. 48-50.

[15] A. Goldsmith, *Wireless Communications*, Cambridge University Press, NJ 2001.

[16] D. B. West, *Introduction to Graph Theory (2 Ed.)*, Prentice-Hall of India, NY 2005.

[17] Chen, S., S. A. Billings and W. Luo, "Orthogonal Least Squares Methods and their Application to Nonlinear System Identification," *Int. J. Control*, vol. 50, 1989, pp. 1873-1896.

[18] Q. Liang and L. Wang, "Redundancy Reduction in Wireless Sensor Networks Using Singular-Value-QR Decomposition" , *IEEE Military Communication Conference*, Oct. 2005, Atlantic City, NJ.

[19] J. C. Bezdek, *Pattern Recognition with Fuzzy Objective Function Algorithms*, Plenum Press, New York, 1981.

[20] "Xiuzhen Cheng, et al, Strong Minimum Energy Topology: NP-Completeness and Heuristics , IEEE Transaction on Mobile Computing", Vol. 2, No. 3, pp. 248-256, July-September 2003.

[21] Xiuzhen Cheng, et al, "Polynomial-Time Approximation Scheme for Minimum Connected Dominating Set in Ad Hoc Wireless Networks", Networks, Vol. 42, No. 4, pp. 202-208, 2003.

[22] G. Stüber, *Mobile Communications*, 2nd ed., Kluwer Academic Publishers, 2001

[23] M. K. Simon and M. S. Alouini, *Digital Communication over fading channels*, 2nd ed., John Wiley & Sons, 2005

[24] M.-S. Alouini and A. J. Goldsmith, " Capacity of Rayleigh fading channels under different adaptive transmission and diversity combining techniques", *IEEE Trans. Veh. Tech*, pp. 1165-1181, July. 1999

[25] Jr. R. Heath and A. Paulraj, "Switching between multiplexing and diversity based on constellation distance", in *Proc. Allerton Conf. Communication, Contril and Computing*, Oct 2000

[26] L. Zheng, D. N. C. Tse, "Diversity and multiplexing: a fundamental tradeoff in multiple-antenna channels", *IEEE Trans. on Information Theory*, vol. 49, pp. 1073-1096, May 2003

List of Figures

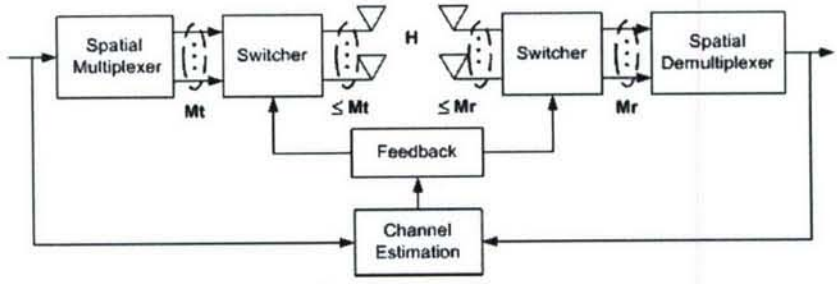

Figure 1: system diagram for virtual MIMO channel selection

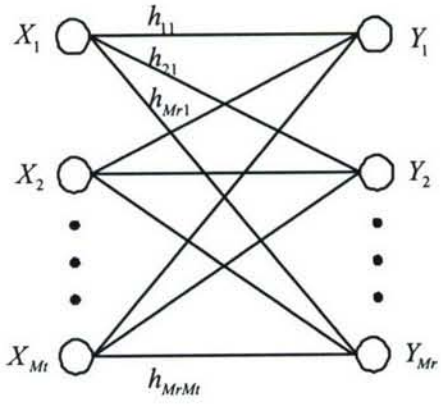

Figure 2: Graphic channel model for virtual MIMO

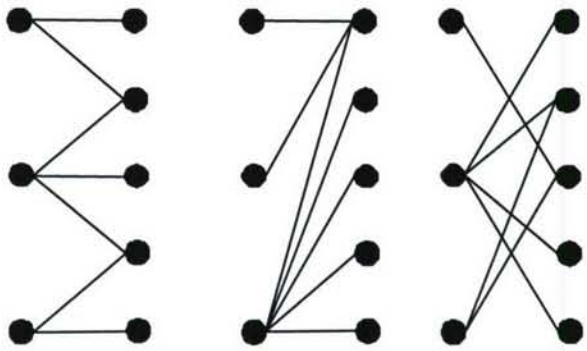

Figure 3: Examples of spanning trees for 5×3 MIMO

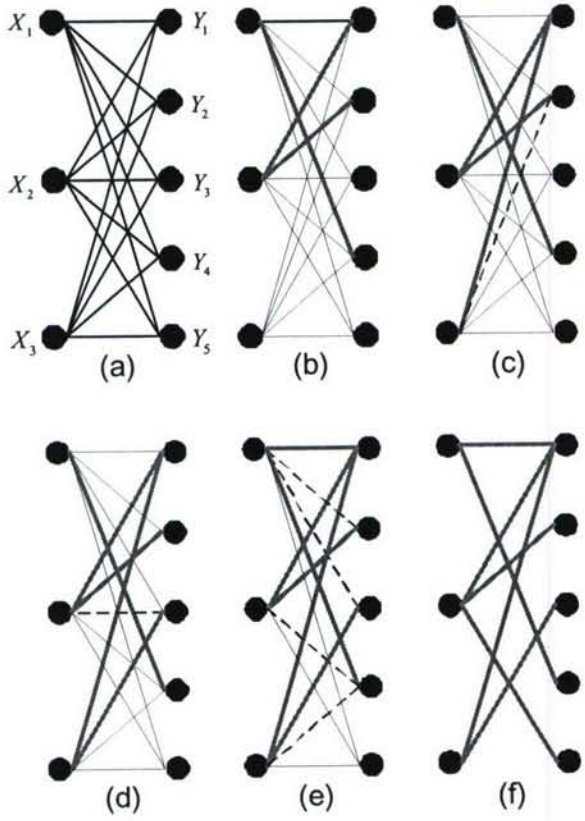

Figure 4: MASTS algorithm

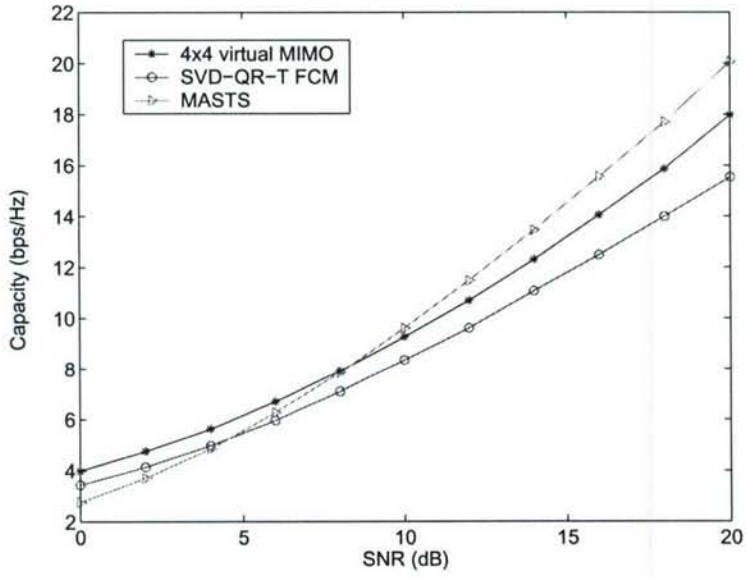

Figure 5: Capacity of SVD-QR-T FCM / MASTS / virtual MIMO with water-filling

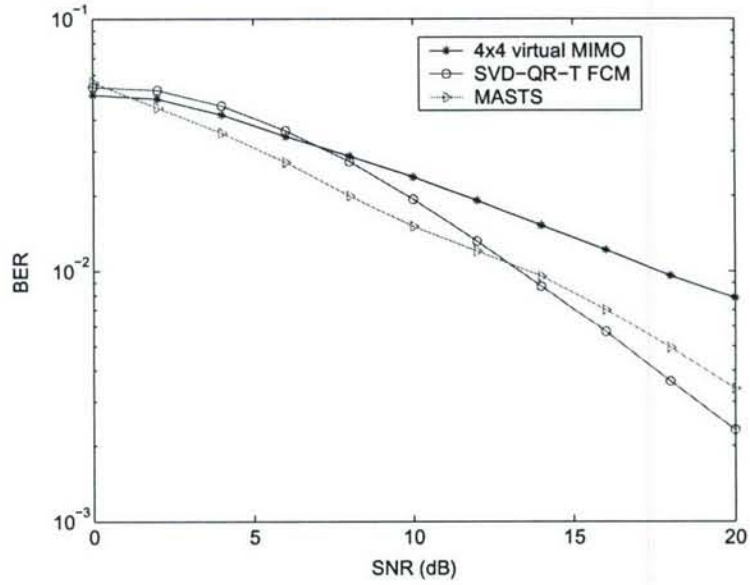

Figure 6: BER of SVD-QR-T / MASTS / 4×4 virtual MIMO with water-filling

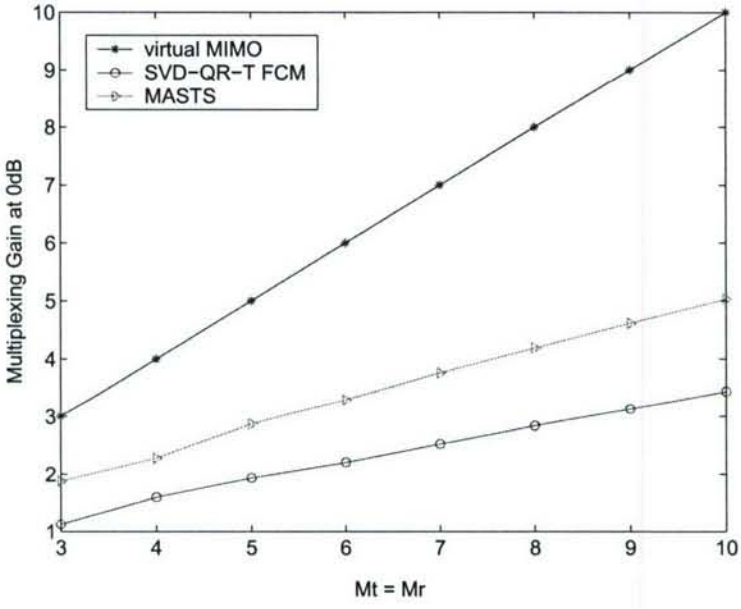

Figure 7: Multiplexing gain of SVD-QR-T FCM/ MASTS / virtual MIMO with water-filling at SNR=0dB

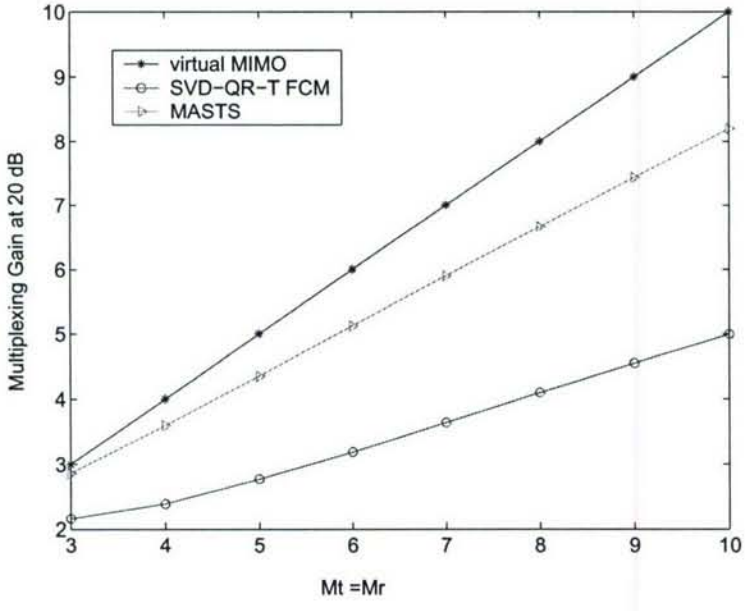

Figure 8: Multiplexing gain of SVD-QR-T FCM/ MASTS / virtual MIMO with water-filling at SNR=20dB

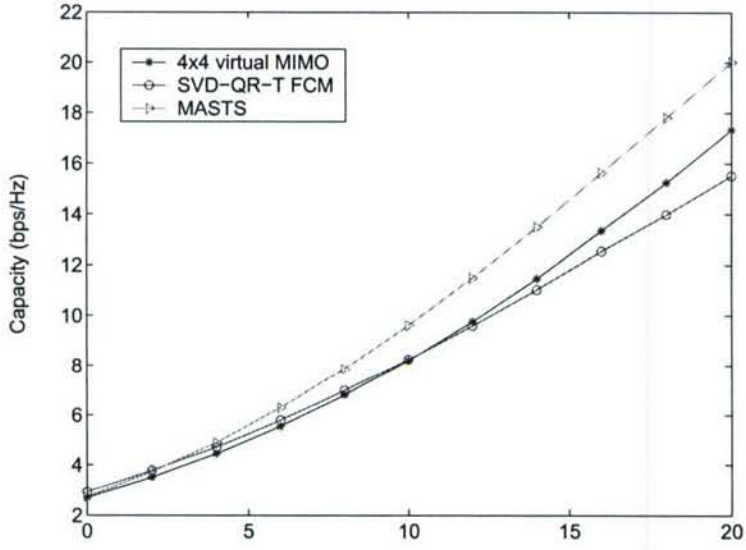

Figure 9: Capacity of SVD-QR-T FCM / MASTS / virtual MIMO without water-filling

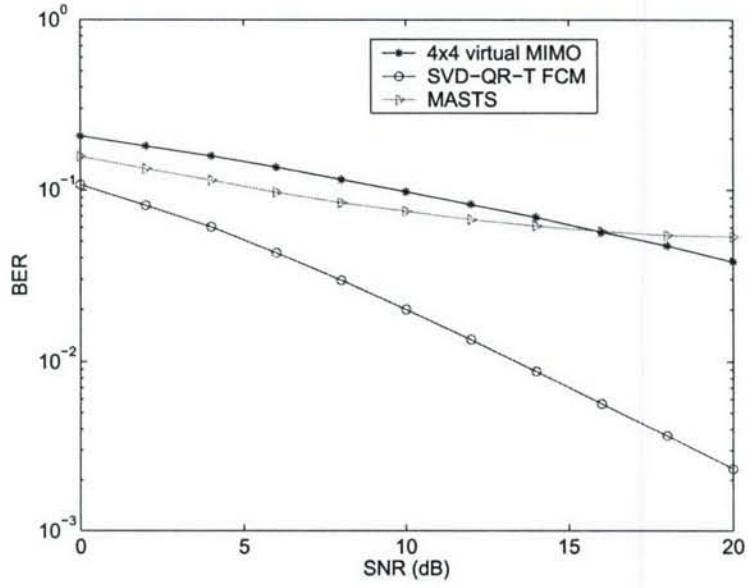

Figure 10: BER of SVD-QR-T / MASTS / 4×4 virtual MIMO without water-filling

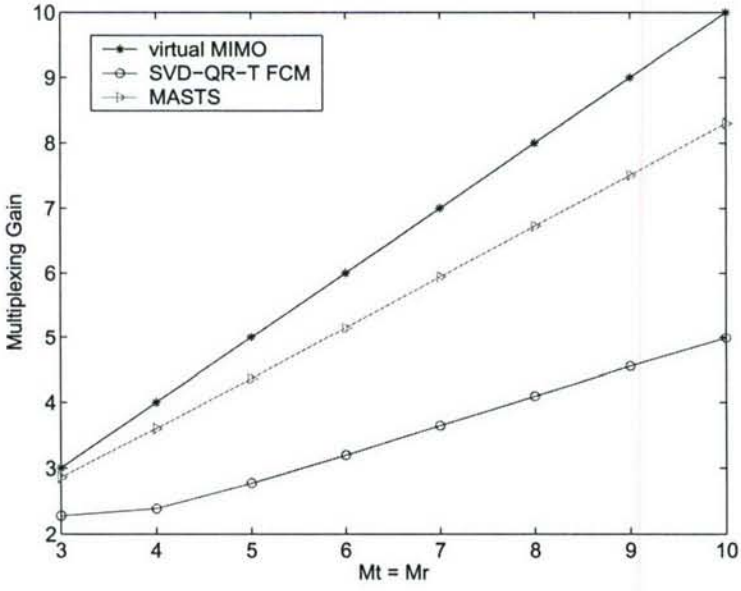

Figure 11: Multiplexing gain of SVD-QR-T FCM/ MASTS / virtual MIMO without water-filling

Image Fusion on Radar Sensor Networks

Jing Liang and Qilian Liang
Department of Electrical Engineering
University of Texas at Arlington
416 Yates Street
Nedderman Hall, Rm 518
Arlington, TX 76019
Email: jliang@wcn.uta.edu, liang@uta.edu

***Abstract*— Owning to Rician fading and white gaussian noise, the scattered back image signal of radar sensors would be distorted to some extend. In this paper, we apply two schemes named Equal Gain Combination (EGC) and Maximal Ration Combination (MRC) respectively for RSN image fusion. Simulation results show that image fusion by means of MRC can provide much better image quality based on both minimum mean squared error (MMSE) and the mean of structural similarity (MSSIM) index if the channel estimation offers satisfying channel side information at receiver (CSIR). However, EGC itself does not require any channel estimation scheme and thus more simple to implement.**

I. Introduction

Enhancing homeland security demands challenging accuracy to detect unauthorized intrusion. For some applications, information provided by single radar may be imprecise or incomplete [1] [2]. A network of multiple radar sensors can been utilized to combat performance degradation of single radar [3]. By employing Radar Sensor Networks (RSN), we are able to protect critical infrastructure from terrorist activities [4].

Image fusion on RSN is that radars are managed by an intelligent clusterhead which combines image diversity in order to satisfy the common goals of the network other than each radar operates independently.

There have been intensive study on radar image fusion, which can be mainly categorized into 3 applications. The first application uses a pair of antennas to obtain an elevation map of the observed scene to resolve the problem of Synthetic Aperture Radar (SAR) Interferometry [5]; the second considers fusion of multisensor images of the same site at different time by means of neural networks [6] [7]; the third refers to a processor to fuse multifrequency, multipolarization and multiresolution images on a basis of wavelet transform and multiscale Kalman filter [8] [9]. However, to this date, the concept of RSN have rarely been employed during the exiting research on radar image fusion. Instead, attention has been mainly given to image fusion on the same single radar. Furthermore, in the previous studies, image processing and physical layer characteristics are usually studied mutually independently to each other. The joint study on both fields demands further exploration besides joint source-channel coding [10] [11].

In this paper, we apply two schemes named Equal Gain Combination (EGC) and Maximal Ratio Combination (MRC) respectively for RSN image fusion. Simulation results show that image fusion by means of MRC can provide much better image quality based on both minimum mean squared error (MMSE) and the mean of structural similarity (MSSIM) index if the channel estimation offers satisfying channel side information at receiver (CSIR). However, EGC itself does not require any channel estimation scheme and thus more simple to implement.

The remainder of this paper will be organized as follows: Section II describes EGC and MRC image fusion schemes respectively. Section III shows image fusion result and Section IV draws conclusion and future work.

II. Theory Of Operation

Radar operates by radiating energy into space and detecting echo signals reflected back from a target [12]. When the non-fluctuating target is constructed from many independently positioned scatterers, the probability density function (PDF) of its radar cross section (RCS) can usually be described by Rician PDF [13] and thus the channel through which the signal is scattered back is usually described by corruption of Rician fading.

As radar sensors are environment dependent [14], it may provide better image quality if different neighboring radars work collaboratively to perform image fusion. For example, consider a system of two radars. When the signal of either radar unfortunately experience a severe fading, if two radars are spaced sufficiently far apart, it is not likely that both of the radars experience deep fade at the same time. By selecting better image pixel from the two radar image candidates, it is unlikely that the image information will be lost as much as that of single radar image. Fig.1 illustrates this scenario. The solid line represents the transmitted signal of radar member while the dash line represents the echo signal which is corrupted with Rician fading and noise.

Fig. 2 shows the diagram of image fusion we have applied to RSN. As the fine details that accurately describes target is critical for reliable detection and classification of targets, before image fusion, the processing for resolution enhancement is required [15]. $\underline{R_1}, \underline{R_2}, \cdots, \underline{R_n}$ represent pixel matrices of images obtained from radar sensor 1, radar sensor

2, $\cdots$, sensor n respectively. $a_1, a_2, \cdots, a_n$ is pixel weighting employed by image fusion. The main purpose of EGC and MRC image fusion schemes is to coherently combine the independent faded images so that the effects of fading and noise are mitigated.

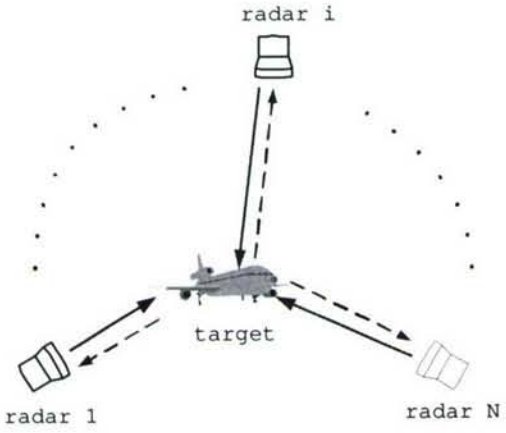

Fig. 1. Radar Sensor Network (RSN)

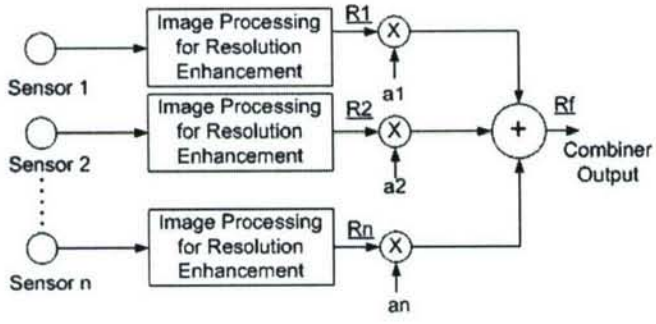

Fig. 2. Diagram of Image Fusion for RSN

EGC is a simple technique which co-phases the image signals on each radar sensor and then combines them using equal weighting, therefore each $a_1, a_2, \cdots, a_n$ equals to the same 1. The pixel matrix after EGC image fusion is

$$\underline{R_f} = (\underline{R_1} + \underline{R_2} + \cdots + \underline{R_n})/n \tag{1}$$

In this case, the output equals to the average of each radar image.

In MRC, the output image is a weighted sum of all radars, the pixel matrix after MRC image fusion is

$$\underline{R_f} = \frac{(\sum_{i=1}^{n} a_i \underline{R_i})^2}{\sum_{i=1}^{n} a_i^2} \tag{2}$$

We can find a_i that maximize $\underline{R_f}$ by taking partial derivatives of (2) or employing the Cauchy-Schwartz inequality [16]. The optimal weights yields $a_i^2 = \underline{R_i}^2$. This implies that radar with good image quality should be weighted more. MRC requires knowledge of time-varying Rician channel fading on each radar, i.e., channel side information at receiver (CSIR) is necessary. CSIR can be obtained through various channel estimation techniques, which are out of the scope of this paper. However, EGC does not have this requirement and thus is more simple to be implemented.

III. Simulation

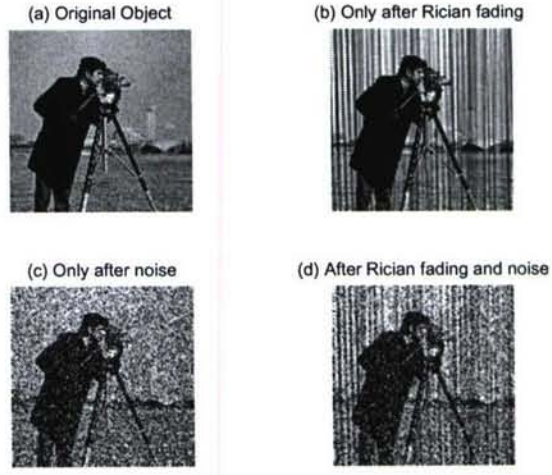

Fig. 3. radar images illustration: (a) Original Object, (b) Only corrupted by Rician fading without noise, (c) Only corrupted by noise without Rician fading, (d) Corrupted by both Rician fading and noise

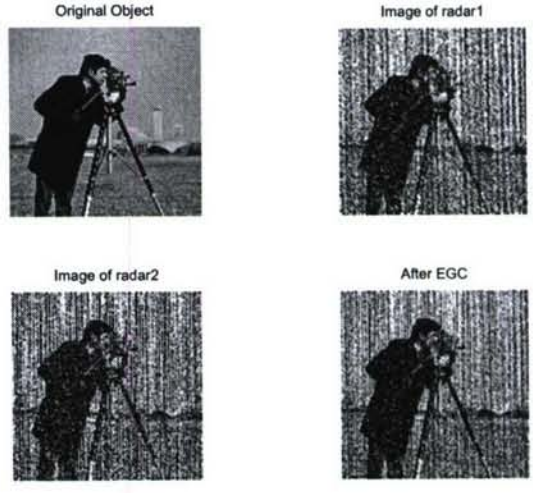

Fig. 4. EGC image fusion: (a) Original Object, (b) image obtained by radar sensor 1, (c) image obtained by radar sensor 2, (d) image obtained by means of EGC

For simplicity, we assume the RSN consist of 2 radars. Of course, the situation of larger number of radar members can be easily extended from this simple case. Jake's Model [17] is

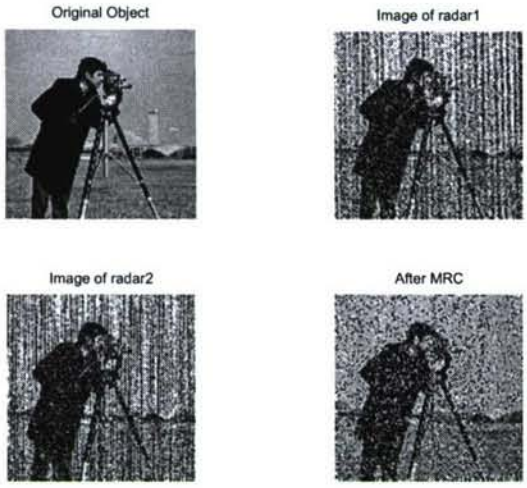

Fig. 5. MRC image fusion: (a) Original Object, (b) image obtained by radar sensor 1, (c)image obtained by radar sensor 2, (d) image obtained by means of MRC with poorer channel estimation

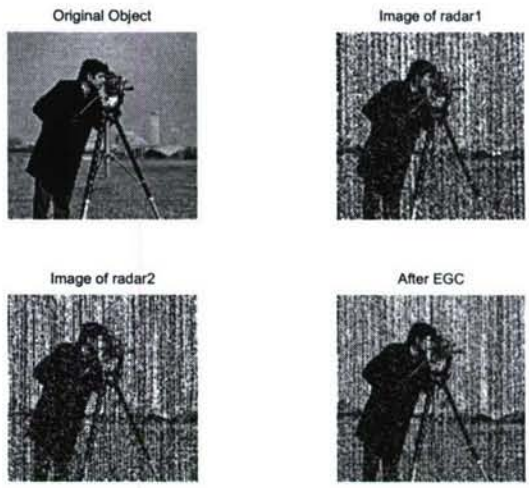

Fig. 6. EGC image fusion: (a) Original Object, (b) image obtained by radar sensor 1, (c) image obtained by radar sensor 2, (d) image obtained by means of EGC

applied to generate Rician fading channel by means of Matlab. As mentioned before, EGC is simply average all images, so no channel estimation technique is required by EGC. However, MRC is on a basis of CSI and thus different channel estimation performance would result in different quality of image fusion. we employ block phase estimation (BPE) raised by Viterbi [18] to estimate Rician channel. This estimation is only used in MRC simulation.

Fig. 3 illustrate image distortion result from Rician fading and white gaussian noise. Fig. (a) is the image of the original object. Fig. (b) is the image corrupted only by Rician fading channels without white gaussian noise. Fig. (c) is the image corrupted only by noise without rician fading. (d) is the image corrupted by both Rician fading and noise, which is practical, as in the real world, fading and noise always coexist. Note that if fading and noise become more inclement, the quality of image can be drastically reduced.

Fig. 4 illustrates the EGC image fusion result compared with the original object and images obtained by independent sensors. Fig (b) and (c) are images obtained by radar sensor 1 and sensor 2 respectively, both are corrupted by white gaussian noise and Rician fading with different fading factor $K = 10$ and $K = 5$, doppler shift $f_d = 100Hz$ and $f_d = 200Hz$ and variance of noise = 0.04 (double size). It is shown that quality of EGC infused image (d) is better than both (b) and (c), this can be particularly analyzed through the jacket of cameraman. However, the improvement on background is not easy to tell by human eyes. The Minimum Mean Squared Error (MMSE) of image (b) and (c) are 0.0541 and 0.0706 respectively, while the MMSE of EGC fused image is 0.0316. Besides MMSE, we also calculate the mean of structural similarity (MSSIM) index [19] by comparing (b)(c)(d) with (a) respectively and get

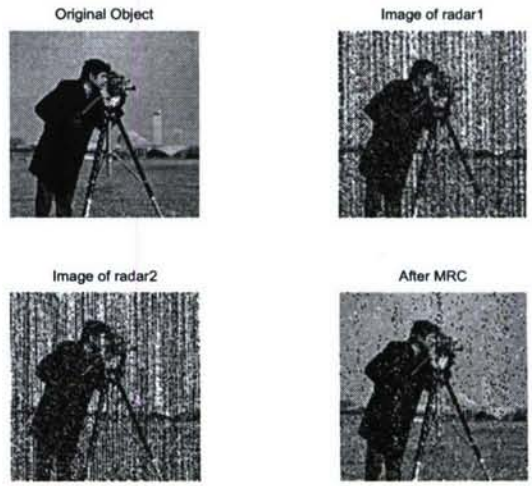

Fig. 7. MRC image fusion: (a) Original Object, (b) image obtained by radar sensor 1, (c)image obtained by radar sensor 2, (d) image obtained by means of MRC with better channel estimation

0.9979, 0.9972 and 0.9988. All MMSE and MSSIM employ "double" size. Both MMSE and MSSIM illustrate that the image obtained through EGC offers better quality then that obtained by independent member.

Similarly, MRC image fusion result is shown in Fig. 5. Fig (b) and (c) are the same images in Fig. 4 (b) and (c). Fig. 5 (d) is the fused image obtained by means of MRC when the performance of channel estimation is bad. Due to the large error in the channel knowledge, we can see that MRC could

not provide good quality of fused image, even the fused image look worse than (b) and (c) to some extend in this case. The MMSE and MSSIM of (d) is 0.0406 and 0.9984 respectively, compared to 0.0316 and 0.9988 of EGC.

Under the condition that the performance of channel estimation is good, we obtain a new group of images in Fig. 6 and 7 with the same fading factor, doppler shift and variance of noise. Note that Fig. 6 is different with Fig. 4. Although channel estimation would not result in the difference between performances of EGC, as EGC itself does not require any knowledge of channel, for better comparison, Fig. 6 is generated in the way that (b) an (c) are the same as those in Fig. 7 with MMSE 0.0510 and 0.0691, MSSIM 0.998 and 0.9973. MMSE of Fig. 6 (d) and Fig. 7 (d) are 0.0298 and 0.0153 respectively while their MSSIM are 0.9988 and 0.9994. These values further illustrate that MRC under good channel estimation can definitely offer better quality of fused image than that of EGC.

IV. Conclusion and Future Works

This paper is a preliminary work on image fusion on RSN. We applied EGC and MRC to fuse images and the result shows that both EGC and MRC are capable of offering better image quality than that of single radar.

Acknowledgement

This work was supported by the Office of Naval Research (ONR) Young Investigator Award under Grant N00014-03-1-0466, and ONR Award under Grant N00014-07-1-0395.

References

[1] P. K. Varshney, "Multisensor data fusion" , *Electronics & Communication Engineering Journal*, pp.245-263Dec. 1997.

[2] D. L. Hall and J. Llinas, "An Introduction to Multisensor Data Fusion", *Proceedings of the IEEE* vol. 85, No. 1, pp.6-23, Jan. 1997

[3] S. Haykin, "Cognitive radar networks" , *2005 1st IEEE International Workshop on Computational Advances in Multi-Sensor Adaptive Processing*, pp.1-3, Dec 2005.

[4] S. Haykin, "Towards Radar-Enabled Sensor Network" , *ISPN'06* , April 19-21, 2006.

[5] M. Costantini, A. Farina and F. Zirilli "A Fast Phase Unwrapping Algorithm for SAR Interferometry" , *IEEE Transactions on Geoscience and Remote Sesning*, vol. 37, No.1 pp.452-469, Jan. 1999

[6] S. B. Serpico and F. Roli, "Classification of Multisensor Remote Sensing Images by Structured Neural Networks", *IEEE Transactions on Geoscience and Remote Sensing*, vol. 33, No.3, pp.562-578, May 1995

[7] L. Bruzzone, D. F. Prieto and S. B. Serpico, "A Neural Statistical Approach to Multitemporal and Multisensor and Multisource Remote Sensing Image Classification", *IEEE Transactions on Geoscience and Remote Sensing*, vol. 37, No. 3, pp. 1350-1359, May 1999

[8] A. M. Signorini, A. Farina and G. Zappa, "Application of multiscale estimation algorithm to SAR images fusion", *International Symposium on Radar* IRS98, Munich, pp. 1341-1352, Sept. 15-17, 1998

[9] P. W. Feieguth et al, "Multiresolution Optimal Interpolation and Statistical Analysis of TOPEX/POSEIDON Statellite Altimetry", *IEEE Transactions on Geoscience and Remote Sensing*, vol. 33. No.2, pp. 280-292, March 1995

[10] J. Cai and C. W. Chen "Robust joint source-channel coding for image transmission over wireless channels", *IEEE Transactions on Circuits and Systems for Video Technology*, vol. 10. No.2, pp. 962-996, Sept. 2000

[11] E. Arikan and N. Merhav "Joint source-channel coding and guessing with application to sequential decoding " *IEEE Transactions on Information Theory* vol. 44, pp. 1756-1759, Sept. 1998

[12] M. I. Skolnik, *Introduction to Radar Systems* , 3rd ed, New York, McGraw Hill, 2001.

[13] N. Levanon, *Radar Principles*, New York, Wiley, 1988.

[14] R. A. Johnson and E. L. Titlebaum, "Range Doppler Uncoupling in the Doppler Tolerant Bat Signal", *Proc. of IEEE Ultrasonics Symposium* , New York, pp.64-67, 1972.

[15] M. K. Sundareshan and S. Bhatacharjee, "Super-Resolution of Tractical Surveillance and Tracking Data for Fusion of Images" *Data fusion for Situation Monitoring, Incident Detection, Alert and Response Management* pp.448-463, IOS Press 2005

[16] A. Goldsmith, *Wireless Communications*, Cambridge University Press, NJ 2001.

[17] G. Stüber, *Mobile Communications*, 2nd ed., Kluwer Academic Publishers, 2001

[18] A. J. Viterbi and A. M. Viterbi "Nonlinear Estimation of PSK-Modulated Carrier Phase with Application to Burst Digital Transmission" *IEEE Transcations on Information Theory* no.4, pp. 543-551, July 1983

[19] Z. Wang, A. C. Bovik, H. R. Sheikh and E. P. Simoncelli, "Image quality assessment: From error visibility to structural simalrity" *IEEE Transactions on Image Processing* vol.13, no.4, pp. 600-612, April, 2004

Cross-Layer Design for Image Transmission in Wireless Sensor Networks

Xinsheng Xia and Qilian Liang
Department of Electrical Engineering
The University of Texas at Arlington
416 Yates Street, Rm 518
Arlington, TX 76010-0016

***Abstract*— Wireless sensor networks need to support image traffic. However, existing wireless sensor networks provide only limited quality of service (QoS) for image application. Hence, We could consider cross-layer design for image transmission in wireless sensor networks. We combine application layer, MAC layer and physical layer together. According to analysis and simulation, high priority service will achieve better PSTR performance. Low priority service achieve better performance at the first stage, and it become worse later. The application level QoS is a tradeoff with the energy consumption between high priority service and low priority service.**

I. INTRODUCTION

The demand for image transmission in wireless sensor networks is growing in a rapid speed. A strict layered design is not flexible enough to cope with the dynamics of the wireless sensor networks [1]. To enhance the QoS(Quality of Service) for multimedia transmission, we consider the cross-layer design. Cross-layer design could introduce the layer interdependencies to optimize overall network performance.

Lots of previous works have focused on cross-layer design for QoS provision. Liu [2] combine the AMC at physical layer and ARQ at the data link layer. Ahn [3] use the info from MAC layer to do rate control at network layer for supporting real-time and best effort traffic. Akan [4] propose a new adaptive transport layer suite including adaptive transport protocol and adaptive rate control protocol based on the lower layer information.

Some works related to energy efficiency have been reported. Banbos proposes a power-controlled multiple access schemes in [5]. This protocol reveals the trade-off of the transmitter power cost and backlog/delay cost in power control schemes. Zhu [6] proposes a minimum energy routing scheme, which consider the energy consumption for data packets as well as control packets of routing and multiple access. In [7], Sichitiu proposes a cross-layer scheduling method. Through combining network layer and MAC layer, a deterministic, schedule-based energy conservation scheme is proposed. This scheme drives its power efficiency from eliminating idle listening and collisions.

In our paper, we propose a cross-layer design to combine the application layer, MAC layer and physical layer together. We use image as traffic and SPIHT (Set Partitioning in Hierarchical Trees) is the image-compressed algorithm in application layer. In MAC layer and physical layer, we select MAC layer retransmission times and AMC (adaptive modulation and coding) as the cross-layer design parameters. For WSNs, the energy is critical parameters. We will also consider the energy consumption in different designs.

We use peak signal to noise ratio (PSNR) and Structural Similarity(SSIM) [8] to evaluate the application-level QoS for the cross-layer design. We also use packet successful transmission ratio, average delay to evaluate the communcation systems. Remaining energy is used to evaluate the energy consumption.

The remainder of this paper is structured as following. In section II, we introduce the preliminaries. In section III, we make an overview of cross-layer design. Simulation and analysis are in section IV. We make conclusion in section V.

II. PRELIMINARIES

A. IEEE 802.11a OFDM PHY

The physical layer is the interface between the wireless medium and the MAC [9]. The principle of OFDM is to divide a high-speed binary signal to be transmitted over a number of low data-rate subcarriers. A key feature of the IEEE 802.11a PHY is to provide 8 PHY modes with different modulation schemes and coding rates, making the idea of link adaptation feasible and important, as listed in Table I. BPSK, QPSK, 16-QAM and 64-QAM are the supported modulation schemes. The OFDM provides a data transmission rates from 6 to 54MBPS. The higher code rates of 2/3 and 3/4 are obtained by puncturing the original rate 1/2 code.

TABLE I
EIGHT PHY MODES OF THE IEEE802.11A PHY

Mode	*Modulation*	*CodeRate*	*DataRate*	*Bps*
1	*BPSK*	1/2	$6Mbps$	3
2	*BPSK*	3/4	$9Mbps$	4.5
3	*QPSK*	1/2	$12Mbps$	6
4	*QPSK*	3/4	$18Mbps$	9
5	$16-QAM$	1/2	$24Mbps$	12
6	$16-QAM$	3/4	$36Mbps$	18
7	$64-QAM$	2/3	$48Mbps$	24
8	$64-QAM$	3/4	$54Mbps$	27

B. IEEE 802.11 MAC

The 802.11 MAC uses Carrier-Sense Multiple Access with Collision Avoidance (CSMA/CA) to achieve automatic medium sharing between compatible stations. In CSMA/CA, a station senses the wireless medium to determine if it is idle before it starts transmission. If the medium appears to be idle, the transmission may proceed, else the station will wait until the end of the in-progress transmission. A station will ensure that the medium has been idle for the specified inter-frame interval before attempting to transmit.

Besides carrier sense and RTS/CTS mechanism, an acknowledgment (ACK) frame will be sent by the receiver upon successful reception of a data frame. Only after receiving an ACK frame correctly, the transmitter assumes successful delivery of the corresponding data frame. The sequence for a data transmission is: RTS-CTS-DATA-ACK.

A mobile node will retransmit the data packet when finding failing transmission. Retransmission of a signal packet can achieve a certain probability of delivery. There is a relationship between the probability of delivery p and retransmission times n:

$$n = 1.451n\frac{1}{1-p} \tag{1}$$

The IEEE 802.11 standard requires that the transmitter's MAC discard a data frame after certain number of unsuccessful transmission attempts. According to the requirement of probability of delivery, we choose the minimum number of retransmission. The advantage is we can save energy through avoiding unnecessary retransmission, and ensure probability of delivery.

C. Application Layer

Set Partitioning in Hierarchical Trees (SPIHT) is an image compression algorithm that exploits the inherent similarities across subbands in a wavelet decomposition of an image. The algorithm codes the most important (in the sense of MSE reduction) wavelet transform coefficients in priority, so we could apply service differential in application layer.

D. Energy

A mobile node consumes significant energy when it transmits or receives a packet. But we will not consider the energy consumed when the mobile node is idle.

The distance between two nodes are variable in the mobile ad hoc networks and the power loss model is used. To send the packet, the sender consumes [10],

$$P_{tx} = P_{elec} + \epsilon_{fs} \cdot d^2 \tag{2}$$

and to receive the packet, the receiver consumes,

$$P_{rx} = P_{elec} \tag{3}$$

where P_{elec} represents the power that is necessary for digital processing, modulation, and ϵ_{fs} represents the power dissipated in the amplifier for the free space distance d transmission.

A joint characteristic of most application scenarios of mobile ad hoc networks is that mobile nodes only have a limited energy supply which

might not even be rechargeable, hence they have to be energy-efficient as possible. Transmitter power control allows interfering communication links sharing the same channel to achieve their required QoS levels, minimizing the needed power, mitigating the channel interference, and maximizing the network user/link capacity.

E. Delay

The packet transmission delay between the mobile nodes includes three parts: the wireless channel transmission delay, the Physical/MAC layer transmission delay, and the queuing delay [11].

Defining D as the distance between two nodes and C as the light speed, the wireless channel transmission delay as:

$$Delay_{ch} = \frac{D}{C} \tag{4}$$

The Physical/MAC layer transmission delay will be decided by interaction of the transmitter and the receive channel, the node density and the node traffic intensity etc.

The queuing delay is decided by the mobile node I/O system-processing rate, the subqueue length in the node.

F. Node Mobility and Channel Fading

Mobility of a mobile node generates a doppler shift, which is a key parameter of fading channel. The doppler shift is

$$f_d = \frac{v}{c} f_c \tag{5}$$

where v is the ground speed of a mobile node, c is the speed of light ($3 \times 10^8 m/s$), and f_c is the carrier. In our simulation, we used the carrier is $6GHz$. For reference, if a node moves with speed $10m/s$, the doppler shift is $200Hz$.

We model channel fading in ad hoc networks as Rician fading. Rician fading occurs when there is a strong specular (direct path or line of sight component) signal in addition to the scatter (multipath) components. For example, in communication between two infraed sensors, there exist a direct path. The channel gain,

$$g(t) = g_I(t) + j g_Q(t) \tag{6}$$

can be treated as a wide-sense stationary complex Gaussian random process, and $g_I(t)$ and $g_Q(t)$ are Gaussian random processes with non-zero means $m_I(t)$ and $m_Q(t)$, respectively; and they have same variance σ_g^2, then the magnitude of the received complex envelop has a Rician distribution,

$$p_\alpha(x) = \frac{x}{\sigma^2} \exp\{-\frac{x^2 + s^2}{2\sigma^2}\} I_0(\frac{xs}{\sigma^2}) \quad x \geq 0 \tag{7}$$

where

$$s^2 = m_I^2(t) + m_Q^2(t) \tag{8}$$

and $I_0(\cdot)$ is the zero order modified Bessel function. This kind of channel is known as Rician fading channel. A Rician channel is characterized by two parameters, Rician factor K which is the ratio of the direct path power to that of the multipath, i.e., $K = s^2/2\sigma^2$, and the Doppler spread (or single-sided fading bandwidth) f_d. We simulate the Rician fading using a direct path added by a Rayleigh fading generator. The Rayleigh fade generator is based on Jakes' model [12] in which an ensemble of sinusoidal waveforms are added together to simulate the coherent sum of scattered rays with Doppler spread f_d arriving from different directions to the receiver. The amplitude of the Rayleigh fade generator is controlled by the Rician factor K.

BPSK, QPSK, 16-QAM and 64-QAM are the supported modulation schemes for IEEE 802.11a OFDM physical layer. We can show their performance curves with Rician fading in Fig.1.

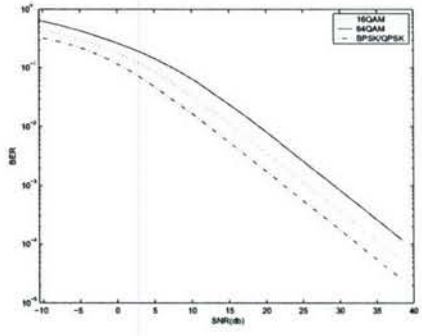

Fig. 1. Modulation Curves with Rician Fading

After we introduce the channel coding and node mobility into the modulation schemes, the mudualtion curves will change a lot. For the same SNR,

channel coding will improve the BER performance and the mobility will degrade the BER performance.

G. One-step Markov Path Model

The mobile nodes are roaming independently with variable ground speed. The mobility model is called one-step Markov path model [13]. The probability of moving in the same direction as the previous move is higher than other directions in this model, which means this model has memory. Fig.2 shows the probability of the six directions.

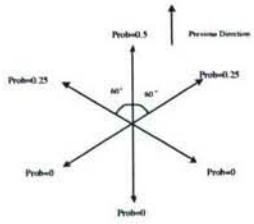

Fig. 2. One-step Markov Path Model

III. Overview of Cross-layer Design

In our cross-layer design, we consider three layers: application layer, MAC layer and Physical layer. Fig.3 shows the structure of this design.

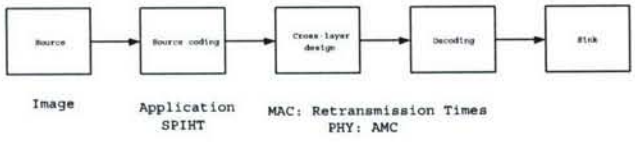

Fig. 3. Structure of Cross-layer design

As we know, SPIHT codes the most important wavelet transform coefficients in priority, and put them in the front of the coded data. We could apply service differential in application layer. We divide the data into two priorities and the service differentiation aims at improving the service of high-priority classes. We set the first part of data as high priority and the remaining data as low priority.

For the MAC layer, the maximum retransmission times will manage the frame loss ratio and the energy consumption. We set large number for high priority service and small number for low priority service. Large retransmission times will decrease frame loss ratio, however small retransmission times will decrease delay and energy consumption.

In the 802.11A protocol, eight AMC modes are used in physical layer. We set small mode number for high priority service. This is also a tradeoff. Small mode number, good BER performance, large delay. On the contrast, large mode number, high speed, cost less energy to overcome interference and noise.

IV. Simulation

We implemented the SPIHT using Matlab, and implemented communication system using the OPNET modeler. The simulation region was 300×300 meters. There were 9 mobile nodes in the simulation model, and the nodes were roaming independently with variable ground speed between 1 to 10 meters per second. The mobility model was called one-step Markov path model. The movement would change the distance between mobile nodes.

Table II showed simualtion parameters setting in application layer. We could see there is no cross-layer design in case 1 and case 4. In case 2 and case 3, we applied cross-layer design and we divided the data into different portion for high priority service and low priority service.

TABLE II
Design Cases

Design	*HighPriority*	*LowPriority*	*Total*
1	26199	0	26199
2	20000	6199	26199
3	4000	22199	26199
4	0	26199	26199

Table III showed simulation parameters settings in MAC layer, physical layer and energy consumption. Retransmission times is the maxium retransmission times in MAC layer.

TABLE III
Parameters Setting

	MACRetransmissionTimes	*AMC*	*Power*
HighPriority	8	1	0.20
LowPriority	3	8	0.10

1) Packet Successful Transmission Ratio: Because we increased the maximum retransmission time and transmitted power to overcome noise and interference, we could achieve better performance in packet successful transmission ratio for high priority. Simulation result in fig.4 showed high priority design could have better PSTR performance. Fig.4 also showed if we selected large portion of data as high priority, we could achieve better PSTR performance. Comparing design 2 with 3, the PSTR performance in design 2 was up to 25.4% larger.

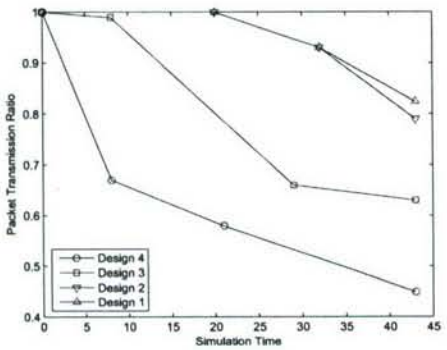

Fig. 4. Packet Successful Transmission Ratio

2) Average Delay: For the image transmission, the delay/time jitter was not important. We used the average delay to evaluate the delay performance. K was the received packets number.

$$d_{average} = \frac{\sum_{i=1}^{k} d_i}{k} \tag{9}$$

According to analysis, small retransmission times would decrease delay. Fig.5 showed the delay performance of the high priority was worse than that of low priority at the first stage. However the delay performance of high priority would be better than that of low priority when the the communication model finished transmitting the whole image. This was because low priority had low PSTR and it ruined its delay performance. As showed in fig.5., we conclued that desin 2 achieve the best delay performance, which meant the portion of high priority data was large than that of low priority data could achieve the best delay performance.

3) Energy Efficiency: It was not convenient to recharge the battery, so the energy efficiency was extremely important for wireless sensor networks. For

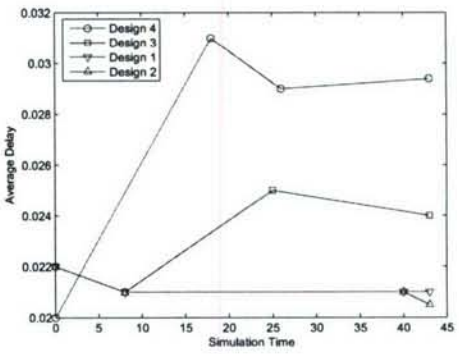

Fig. 5. Average Delay

high priority service, it would cost more energy than low priority service. For low priority service, they will cost less energy because it was less important according to SPIHT image compressed algorithm. Simulation result in Fig.6 matched our analysis. There was a tradoff between the QoS performance and the energy efficiency.

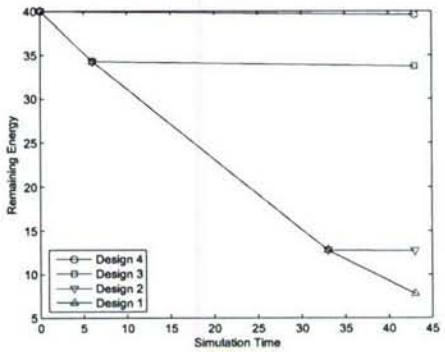

Fig. 6. Remaining Energy

4) Image Quality: PSTR could only indicate packet level QoS. Application level QoS was more important in case of image transmission. We use 0.1 as the SPIHT compressed ratio. According to our analysis, we knew that high priority service would achievce better QoS quality for both application level and packet level. The simulation result was same as the analysis. We listed the PSTR and SSIM index for four designs in table IV. It was interesting that the application QoS was exactly a tradeoff with the energy consumption.

Fig.7 showed the images for four designs. Design

TABLE IV
IMAGE QUALITY

Design	*PSNR*	*SSIM*
1	29.31	0.8027
2	27.75	0.7683
3	23.08	0.6007
4	19.59	0.4699

4 had the worst application level QoS performance, but it consumed the least energy.

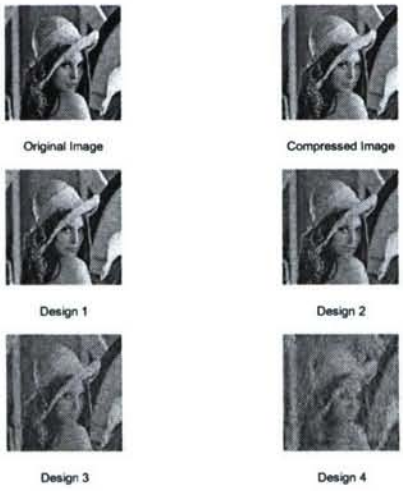

Fig. 7. The Image Results

We introduced the cross-layer design for image transmission in wireless sensor networks. Comparing the performance of QoS and energy efficiency, the cross-layer design could be flexible and simpler to implement and the performance outputs were also impressive.

V. CONCLUSION

Cross-layer design is a effective approach for image transmission in wireless sensor networks. In this paper, we introduce the cross-layer design for application layer, MAC layer and physical layer. Analysis and simulation results shows the cross-layer design could benefit image transmission in wireless sensor networks. High priority service will achieve better PSTR performance. Low priority service achieve better performance at the first stage, and it become worse later. The application level QoS is a tradeoff with the energy consumption between high priority service and low priority service.

ACKNOWLEDGMENT

This work was supported by the U.S. Office of Naval Research (ONR) Young Investigator Award under Grant N00014-03-1-0466.

REFERENCES

[1] Goldsmith A.J.; Wicker, S.B.; " Design Challenges for Energy-Constrained Ad Hoc Wireless Networks," *IEEE Wireless Comm.,*, vol. 9, No. 4 ,2002 , pp. 8-27.

[2] Q.Liu, S.Zhou and G.Giannakis; " Cross-Layer Combining of Adaptive Modulation and Coding with Truncated ARQ over Wireless Links ," *Wireless Communications, IEEE Transactions on*, Volume: 3 , Issue: 5 , Sept. 2004 Pages:1746 - 1755.

[3] G. Ahn, A. Campbell, A. Veres and L. Sun; " Support Service Differentiation for Real-Time and Best-Effort Traffic in Stateless Wireless Ad Hoc Networks (SWAN)," *Mobile Computing, IEEE Transactions on*, Volume: 1 , Issue: 3 , July-Sept. 2002 Pages:192 - 207.

[4] O.B.Akan and I.F.Akyildiz; " ATL, An Adaptive Transport Layer Suite for Next Generation on Wireless Internet ," *IEEE Journal on Selected Areas in Communcations*, June 2004.

[5] N.Bambos, S.Kandukuri " Power-Controlled Multiple Access Schemes for Next-Generation Wireless Packet Networks ," *IEEE Wireless Communications*, June 2002.

[6] J.Zhu, C.Qiao and X.Wang " A Comprehensive Minimum Energy Routing Scheme for Wireless Ad Hoc Networks ," *IEEE INFOCOM2004*.

[7] M.L.Sichitiu " Cross-Layer Scheduling for Power Efficiency in Wireless Sensor Networks ," *IEEE INFOCOM2004*.

[8] Wang, Z.; Bovik, C.; et al " Image Quality Assessment: From Error Visibility to Structural Similarity," *IEEE Transactions On Image Processing*, Vol. 13, No. 4. April 2004..

[9] D.Qiao, S. Choi, and K.G. Shin " IEEE Trans. On Mobile Computing ,", *IEEE Trans. On Mobile Computing*, Oct. 2002.

[10] Heinzelman, W.B.; Chandrakasan, A.P.; Balakrishnan, H.; " An application-specific protocol architecture for wireless microsensor networks ," *IEEE Transactions on Wireless Communications*, Volume: 1 Issue: 4, Oct 2002.

[11] Xia, X.;Liang, Q.; "Latency-aware and energy efficiency tradeoffs for sensor networks" *Accepted by Personal, Indoor and Mobile Radio Communications, 2004. PIMRC 2004. 15th IEEE* .

[12] G.L. Stuber; "Principles of Mobile Communcation" *Kluwer Academic Press*, 2001.

[13] Hou T. C., and Tsai T. J.; "Adaptive clustering in a hierarchical ad hoc network" *Proc. Int. Computer Symp.,Tainan, Taiwan,R.O.C.*, Dec.1998, pp.171-176..

Performance Analysis of Energy Detection for Cognitive Radio Wireless Networks

Qingchun Ren and Qilian Liang

Department of Electrical Engineering

University of Texas at Arlington

E-mail: ren@wcn.uta.edu, liang@uta.edu

Abstract

While energy detection has been extensively studied in the past, hidden terminal and exposed node problems are ignored through assuming that the environment is same for transmitters and receivers. In this paper, considering hidden terminal and exposed node problems, we make a theoretical analysis on the performance of commonly used energy detection methods, such as ideal method, transmitter-independent method and transmitter/receiver-cooperated method, in terms of detection probability. Corresponding analytical models are provided. Performance theoretical curves are acquired to compare the characteristics for individual energy detection methods under various scenarios. Moreover the upper bound for detection probability is achieved and is compared under various system traffic intensity and sensing capability. From the theoretical results, we found that it is easy to correctly detection the channel status when primary systems are heavily occupied for ideal energy detection method and tansmitter/receiver-cooperated energy detection method. Otherwise, transmitter-independent method is a better scheme to monitor the primary systems. Commonly, increasing the sensitivity of secondary users can upgrade the detection performance. However, in our analysis, it is not true for transmitter-independent method and transmitter/receriver-cooperated method under certain situations. We have concluded those special cases in this paper. Therefore, the theoretical results can supply a reference on the choosing of energy detection method according to system scenario, such as traffic load, sensing capability, etc..

1 Introduction

Today's wireless networks are regulated by a fixed spectrum assignment policy, i.e. the spectrum is regulated by governmental agencies and is assigned to license holder or services on a long term basis for larger geographical regions. In addition, according to Federal Communications Commission (FCC)[1], temporal and geographical variations in the utilization of the assigned spectrum range from 15% to 85%. Although the fixed spectrum assignment policy generally served well in the past, there is a dramatic increase in the access to the limited spectrum for mobile services in the recent years. By adapting radios' operating characteristics to the real-time conditions of the environment, CR enable flexible, efficient and reliable spectrum use. Hence, CRs (secondary users) have the potential to utilize a large amount of unused spectrum in an intelligent way while not interfering with other legacy license holders (primary users) in frequency bands already licensed for specific users.

In order to ensure cognitive radio network (CRN), which is consisting of CRs, working smoothly, one of important requirements is to sense the spectrum holes successfully. The most efficient detection method is to detect the primary users that are receiving data within the communication range of an secondary user. In reality, however, it is difficult for a CR to have a direct measurement of a channel between a primary receiver and a primary transmitter. Thus, the most recent work focuses on primary transmitter detection based on local observations of secondary users. Generally, the spectrum sensing techniques can be classified into matched filter[2], energy detector and cyclostationary feature detector[3].

One common method for detection of unknown signals is energy detection, which measures the energy in the received waveform over an observation time window[4][5]. In [6], energy detection of unknown deterministic signals are studied. Detection performance in terms of detection probability and false alarm probability is formulated. In [7] and [8], multiband/wavelet approach and blind adaptive minimum output energy detection were proposed for capturing the AM-FM components of modulated signals immersed in noise and for DS/CDMA[9] over multipath fading channel separately. Performance of energy detection under channel randomness has been considered in [10] and [11]. In order to improve spectrum sensing, several authors have recently proposed collaboration among secondary users[12][13]. A group of unlicensed deices were exploited for spectrum sensing, which leads to more efficient spectrum utilization from a system-level point of view while decreasing computational complexity of detection algorithms at individual nodes.

However energy detection has been extensively studied in the past, hidden terminal and exposed node problems are ignored through assuming that the environment is same for transmitters and receivers. While this assumption does not always held, especially in high node-density scenarios. In this paper, considering hidden terminal and exposed node problems, we make a theoretical analysis on the performance of energy detection in terms of detection probability. An analytical model is provided for ideal energy detection, transmitter-independent energy detection for CSMA[14]/ALOHA[15]/Schedule-based systems and transmitter/receiver-cooperated energy detection. Theoretical curves are acquired to compare the characteristics for individual energy detection methods under various situations. Moreover the upper bound for detection probability is achieved and compared under various system traffic and sensing error. The theoretical results we acquired can supply a reference on the method selection.

The remainder of this paper is organized as follows. In Section 2, we summarize motivations for our work. We summary all definitions used through this paper in Section 3. Section 4 and Section 5 describe our theoretical analysis on different energy detection methods. Simulation results are given in Section 6. Section 7 concludes this paper.

2 Our Motivations

Two nodes are said to be hidden from one another (out of signal range) when both attempt to send information to the same receiving node, resulting in a collision of data at the receiver node. On the other hand, overhearing a data transmission from neighboring nodes can inhibit one node from transmitting to other noes. Those are very well-known hidden terminal problem and exposed node problem for contention-based MAC protocols[16]. Hidden terminal problem causes failure communication with collision, while exposed node problem decreases frequency utilization due to unnecessarily blocking some communications. RTS-CTS method is one of the most popular solutions to the hidden terminal problem, such as in IEEE80.2.11[17]. In CRNs, hidden terminal

problem and exposed node problem also should be considered for energy detection, since the strength of received signal is various at transmitter side and receiver side for CRs. To the best of our knowledge, it is the first paper to study the influence of hidden and exposed problems on energy detection capability.

2.1 Hidden Terminal Problem

As shown in Fig. 1, in a primary system there are two primary users (PUs) A and B. When communication is processing between A and B, there are two secondary users (SUs) C and D appeared in the same region. According to most of existing energy detection methods, before deciding working spectrum, C will sense spectrum hole around it. Since C is hidden from A, C cannot detect the transmission between A and B, then C will decide to pick up the same spectrum band to process communication to D, which will destroy the communication between A and B as shown in Fig. 1(a). This is the hidden terminal problem for energy detection in CRNs. This hidden problem breaks one of the most important rules for CRNs: the SUs should not generate unacceptable interference to PUs.

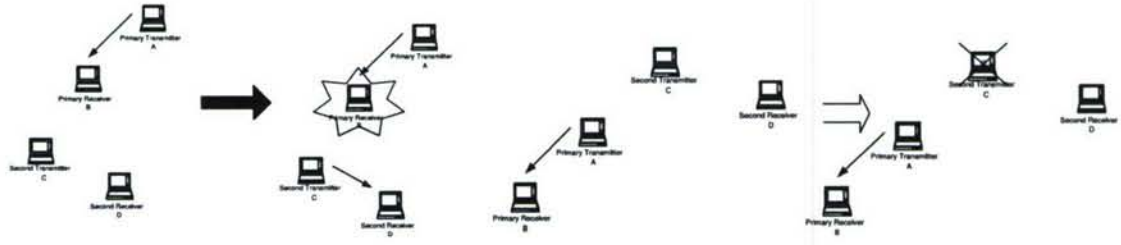

(a) (b)

Figure 1: (a)The illustration of hidden terminal problem and (b) The illustration of exposed node problem

2.2 Exposed Node Problem

As shown in Fig. 1(b), in a primary system there are two PUs A and B. When communication is processing between A and B, there are two SUs C and D appeared in the same region. According to most of existing energy detection methods, before deciding working spectrum, secondary user C will sense spectrum hole around it. Since C is exposed to A, C will detect the transmission between A and B, then C will decide to block its transmission or pick up different spectrum band to process communication to D, even though in fact the communication between C and D on the same frequency band won't cause any interference to primary receiver B. This is the exposed node problem for energy detection in CRNs. This exposed problem breaks another most important rules for CRNs: in order to enhance the spectrum utilization, CRNs allow more SUs to work on spectrum holes of primary systems.

3 Main Definitions

We classify the frequency band/channel state into three categories:

- *Idle:* When both secondary transmitter and receiver do not sense any signal, we claim the channel is idle. In this case, secondary communication pair can utilize the channel for communications.

- *Busy:* Once a secondary transmitter senses the beacon from a primary receiver and/or a secondary receiver senses the beacon from a primary transmitter, we claim a channel is busy. In this case, secondary communication pair should not utilize the busy channel for communications, since their communication might destroy primary users' or be destroyed by primary users'. item*Fake Busy:* Just a secondary transmitter senses the beacon from a primary transmitter and/or a secondary receiver senses the beacon from a primary receiver, we claim the channel is fake busy. In this case, secondary communication pair still can utilize the channel for communication, since there is no any unacceptable interference among them.

Generally, network topology, traffic type and communication capability of primary user system determine channel state. In this paper, we exploit p_{id}, p_{bs} and p_{fd} to express the chance of channel state might be at certain point of time. They are always satisfy $p_{id} + p_{bs} + p_{fd} = 1$. The definitions are:

- p_{id} is the probability of a channel being *Idle*;
- p_{bs} is the probability of a channel being *Busy*; and
- p_{fd} is the probability of a channel being *Fake Busy*.

During energy detection, the sensed signal can come from primary transmitters and, for some cases, primary receivers, which is not determined. We use p_{tx} and p_{rx} to stand the probability that the sensed signal coming from primary transmitters and from primary receivers.

The sensing probabilities are defined as:

$$P\{no\ signal\ sensed \mid no\ signal\ exsiting\} = P_{00};$$
$$P\{signal\ sensed \mid signal\ exsiting\} = P_{11};$$
$$P\{no\ signal\ sensed \mid signal\ exsiting\} = P_{10}; and$$
$$P\{signal\ sensed \mid no\ signal\ exsiting\} = P_{01}.$$

Studies in [6][10][11] showed that the detection probability and false alarm probability were the functions of signal-to-noise ratio (SNR, γ). Hence we note those sensing probabilities as $P_{00}(\gamma)$, $P_{01}(\gamma)$, $P_{10}(\gamma)$ and $P_{11}(\gamma)$.

The probability of correct decision (P_{cd}) is the probability that a SU makes a correct decision on utilizing or not utilizing a particular frequency band when sensing a particular frequency band is *Idle/Fake Busy* or *Busy*, defined as:

$$\begin{aligned} P_{cd} &= P\{communication\ is\ blocked \mid channel\ is\ Busy\}P\{channel\ is\ Busy\} \\ &+ P\{communication\ is\ processed \mid channel\ is\ Idle/Fake\ Busy\}P\{channel\ is\ Idle/Fake\ Busy\} \end{aligned} \quad (1)$$

4 Generic Environment for Secondary Transmitter and Receiver

While energy detection has been extensively studied in the past, hidden terminal and exposed node problems are ignored through assuming that the environment is often same for transmitters and receivers. However, this assumption can not always hold in the real world. In this section, we use the generic model, in which the signal sensed by secondary transmitters (STs) might not be identical for secondary receivers (SRs). Moreover, in real

world, there is always error for signal sensing, i.e., $0 < P_{00}, P_{11}, P_{01}, P_{10} < 1$. In this case, for real system design, we evaluate the performance in terms of detection probability for ideal energy detection method, transmitter-independent energy detection method and transmitter/receiver-cooperated energy detection method.

4.1 Ideal Energy Detection

In this case, the primary transmitter (PT) and primary receiver (PR) have the capability to send out special messages such as beacons to indicate they are doing communications. Moreover, for energy detection, not only ST but also SR participate sensing task. Based on the detection results both from STs and SRs, the secondary communication pairs decide their working frequency bands.

We define a 2×2 matrix ($S = \begin{pmatrix} s_{r1} & s_{r2} \\ s_{t1} & s_{t2} \end{pmatrix}$) to express the detection results for secondary communication pairs. s_{r1} and s_{r2} are the detection results referring to PR and PT individually at the SR side. Similarly, s_{t1} and s_{t2} are the detection results referring to PT and PR individually at the ST side. The value for s_{r1}, s_{r2}, s_{t1} and s_{t2} can be 1 or 0 based on signals detected or not. There are totally 16 statuses for S (See Table 1). Note that the signal strength s_{t1} and the signal strength s_{r2} reflect the hidden problem degree and exposed problem degree individually. Therefore, combining the detection at STs and SRs, the detection errors caused by hidden problem and exposed problem can be solved successfully at the same time.

Table 1: Channel state classification according to S for ideal energy detection

Channel State	S
Idle	$\begin{pmatrix} 0 & 0 \\ 0 & 0 \end{pmatrix}$
Fake Busy	$\begin{pmatrix} 0 & 0 \\ 0 & 1 \end{pmatrix}, \begin{pmatrix} 1 & 0 \\ 0 & 0 \end{pmatrix}, \begin{pmatrix} 1 & 0 \\ 0 & 1 \end{pmatrix}.$
Busy	$\begin{pmatrix} 0 & 0 \\ 1 & 0 \end{pmatrix}, \begin{pmatrix} 0 & 0 \\ 1 & 1 \end{pmatrix}, \begin{pmatrix} 0 & 1 \\ 0 & 0 \end{pmatrix}, \begin{pmatrix} 0 & 1 \\ 0 & 1 \end{pmatrix}, \begin{pmatrix} 0 & 1 \\ 1 & 0 \end{pmatrix}, \begin{pmatrix} 0 & 1 \\ 1 & 1 \end{pmatrix}, \begin{pmatrix} 1 & 0 \\ 1 & 0 \end{pmatrix}, \begin{pmatrix} 1 & 0 \\ 1 & 1 \end{pmatrix}, \begin{pmatrix} 1 & 1 \\ 0 & 0 \end{pmatrix}, \begin{pmatrix} 1 & 1 \\ 0 & 1 \end{pmatrix}, \begin{pmatrix} 1 & 1 \\ 1 & 0 \end{pmatrix}, \begin{pmatrix} 1 & 1 \\ 1 & 1 \end{pmatrix}.$

Based on the definition on detection probability (P_{cd}), we derive (2) as following:

$$\begin{aligned} P_{cd} &= (p_{id} + p_{fbs})p_{00}(\gamma_{r2})p_{00}(\gamma_{t1}) + \frac{1}{9}p_{bs}[p_{01}(\gamma_{t1}) + p_{01}(\gamma_{r2}) + p_{10}(\gamma_{r2})p_{11}(\gamma_{t1}) \\ &+ p_{11}(\gamma_{r2})p_{10}(\gamma_{t1}) + 3p_{11}(\gamma_{r2})p_{00}(\gamma_{t1}) + 3p_{11}(\gamma_{r2})p_{11}(\gamma_{t1}) + 3p_{11}(\gamma_{r2})p_{11}(\gamma_{t1})] \end{aligned} \quad (2)$$

Note that:

- Even though PT, PR, ST and SR participate spectrum sensing, incorrect decision is still possible that for sensing errors of STs and SRs.

- Although both ST and SR implement energy detection according to messages exchanged between PTs and PRs, detection performance in terms of detection probability P_{cd} has nothing with $p(\gamma_{r1})$ and $p(\gamma_{t2})$. That is, only the detection capability referring to PRs of STs, and detection capability referring to PTs of SRs together determines the performance of this ideal energy detection method. This implies that, during detection, to ensure the detection performance the STs only need to monitor the signal from PRs, and the STs need to monitor the signal from PTs. Consequently, the overhead brought by energy detection for STs and STs in CRNs can be safely reduced through making STs/SRs ignore the signal from PTs/PRs.

- Moreover, assuming CRs can correctly detect whether there is transmission processing around them on a particular frequency band, i.e., $p_{00} = 1$, $p_{11} = 1$, $p_{01} = 0$ and $p_{10} = 0$. In this case according to (2), we have $P_{cd} = 1$, which are consisting with our above analysis. For this reason, this ideal energy detection method is an optimal detection way for CRNs.

However, it is too good to be true in real world since overhead caused by transmitting beacons both form primary transmitters and receivers is too heavy to be acceptable or feasible for some systems that utilize certain MAC methods, in which there is no confirmation/response from receivers during data transmission process.

4.2 Transmitter-Independent Energy Detection

In transmitter-independent energy detection method, only STs processes spectrum sensing task. Therefore, the matrix S is reduced into a scalar whose value can be 0 or 1. When a ST senses there is no primary communication pairs doing communication, i.e., $S = 0$, it will decide to use this channel for its communication, otherwise it will not. Generally, there are two categories of primary system based on whether there is confirmation/response from primary receivers. In CSMA/CA primary systems, since besides RTS control packets and data packets transmitted by PTs, another control packets - CTS and ACK are transmitted by PRs[17]. The decision can be done according to the detection with PTs or PRs, in this case, P_{cd} is modified as follows.

$$\begin{aligned} P_{cd} &= p_{tx}\{p_{id}p_{00}(\gamma_{t2}) + \frac{1}{3}p_{fbs}[p_{00}(\gamma_{t2}) + 2p_{10}(\gamma_{t2})] + \frac{1}{2}p_{bs}p_{11}(\gamma_{t2})\} \\ &+ p_{rx}\{(p_{id} + p_{fbs})p_{00}(\gamma_{t1}) + \frac{2}{3}p_{bs}p_{11}(\gamma_{t1})\} \end{aligned} \tag{3}$$

Compared with ideal energy detection methods, follows are observed:

- P_{cd} is not only the functions of $p_{\gamma_{t1}}$, but also the functions of $p_{\gamma_{t2}}$ when the detected signal coming from PTs.

- Assuming CRs can correctly detect whether there is transmission processing around them on a particular frequency band, i.e., $p_{00} = 1$, $p_{11} = 1$, $p_{01} = 0$ and $p_{10} = 0$. In this specific case, $P_{cd} = p_{tx}(p_{id} + \frac{1}{3}p_{fbs} + \frac{1}{2}p_{bs}) + p_{rx}(p_{id} + p_{fbs} + \frac{2}{3}p_{bs})$. Since it always has $p_{tx} + p_{rx} = 1$ hold, the upper bound of P_{cd} is given in (4). It is achieved when the detected signals all come from PRs, i.e., $p_{tx} = 0$ and $p_{rx} = 1$.

$$P_{cd,max} = p_{id} + p_{fbs} + \frac{2}{3}p_{bs} \tag{4}$$

- Even though only STs are exploited for energy detection in CSMA/CA-based primary system, it can be an optimal energy detection method when channel status only be *Idle* or *Fake Busy*. That is, when $p_{bs} = 0$, $P_{cd,max} = 1$. Otherwise, the performance of transmitter-independent energy detection methods is always $\frac{1}{3}p_{bs}$ worse than the ideal energy detection methods.

- For other primary systems, such as TDMA systems, CSMA systems and ALOHA systems, in which there is no response/confirmation from receivers during data transmission processes, i.e., $p_{tx} = 1$ and $p_{rx} = 0$. In this case, there is

$$P_{cd,max} = p_{id} + \frac{1}{3}p_{fbs} + \frac{1}{2}p_{bs} \tag{5}$$

  Comparing (5) with (4), note that if more signal from PRs can be detected by STs, better detection performance can be achieved under same system scenario, i.e., same p_{id}, p_{fbs}, p_{bs}.

4.3 Transmitter/Receiver-Cooperated Energy Detection

Considering the spectrum environment sensed by receiver and transmitter due to different location of them, receiver aiding spectrum sensing method is one of feasible mechanisms to improve the detection performance. Consequently, the detection matrix S is changed into $\begin{pmatrix} 0 \\ 0 \end{pmatrix}$, $\begin{pmatrix} 0 \\ 1 \end{pmatrix}$, $\begin{pmatrix} 1 \\ 0 \end{pmatrix}$ and $\begin{pmatrix} 1 \\ 1 \end{pmatrix}$. Only ST doing frequency sensing, it is impossible to identify the channel is *Busy* or *Fake Busy* when $S = \begin{pmatrix} 0 \\ 1 \end{pmatrix} / \begin{pmatrix} 1 \\ 0 \end{pmatrix}$. Hence, there are two alternative ways to infer the channel state. One is claiming the channel is *Idle* when $S = \begin{pmatrix} 0 \\ 0 \end{pmatrix}$, claiming the channel is *Fake Busy* when $S = \begin{pmatrix} 0 \\ 1 \end{pmatrix}$, $\begin{pmatrix} 1 \\ 0 \end{pmatrix}$ *and* $\begin{pmatrix} 1 \\ 1 \end{pmatrix}$ (See Table 2).

Table 2: Channel state classification according to S for transmitter/receiver-cooperated method

Channel State	S
Idle	$\begin{pmatrix} 0 \\ 0 \end{pmatrix}$
Busy	$\begin{pmatrix} 0 \\ 1 \end{pmatrix}$, $\begin{pmatrix} 1 \\ 0 \end{pmatrix}$, $\begin{pmatrix} 1 \\ 1 \end{pmatrix}$

Then, the P_{cd} is calculated through

$$\begin{aligned} P_{cd} &= p_{tx}\{p_{id}p_{00}(\gamma_{r2})p_{00}(\gamma_{t2}) + \frac{1}{3}p_{fbs}[p_{00}(\gamma_{r2})p_{00}(\gamma_{t2}) + 2p_{00}(\gamma_{r2})p_{10}(\gamma_{t2})] \\ &+ \frac{1}{6}p_{bs}[p_{11}(\gamma_{t2}) + 4p_{11}(\gamma_{r2}) + 2p_{10}(\gamma_{r2})p_{01}(\gamma_{t2}) + 2p_{10}(\gamma_{r2})p_{11}(\gamma_{t2}) + p_{01}(\gamma_{r2}) \\ &+ p_{00}(\gamma_{r2})p_{01}(\gamma_{t2})]\} + p_{rx}\{p_{id}p_{00}(\gamma_{r1})p_{00}(\gamma_{t1}) + \frac{1}{3}p_{fbs}[p_{00}(\gamma_{r1})p_{00}(\gamma_{t1}) \\ &+ 2p_{10}(\gamma_{r1})p_{00}(\gamma_{t1})] + \frac{1}{6}p_{bs}[4p_{11}(\gamma_{t1}) + p_{11}(\gamma_{r1}) + 2p_{01}(\gamma_{r1})p_{10}(\gamma_{t1}) \\ &+ 2p_{11}(\gamma_{r1})p_{10}(\gamma_{t1}) + p_{10}(\gamma_{r1})p_{01}(\gamma_{t1})]\} \end{aligned} \tag{6}$$

The other is One is claiming the channel is *Idle* when $S = \begin{pmatrix} 0 \\ 0 \end{pmatrix}$, claiming the channel is *Fake Busy* when $S = \begin{pmatrix} 0 \\ 1 \end{pmatrix} / \begin{pmatrix} 1 \\ 0 \end{pmatrix}$, and claiming the channel is Busy when $S = \begin{pmatrix} 1 \\ 0 \end{pmatrix} / \begin{pmatrix} 0 \\ 1 \end{pmatrix}$ *and* $\begin{pmatrix} 1 \\ 1 \end{pmatrix}$ (See Table 3).

Table 3: channel state classification according to S for transmitter/receiver-cooperated method

Channel State	S
Idle	$\begin{pmatrix} 0 \\ 0 \end{pmatrix}$
Fake Busy	$\begin{pmatrix} 0 \\ 1 \end{pmatrix} / \begin{pmatrix} 1 \\ 0 \end{pmatrix}$
Busy	$\begin{pmatrix} 1 \\ 0 \end{pmatrix} / \begin{pmatrix} 0 \\ 1 \end{pmatrix}, \begin{pmatrix} 1 \\ 1 \end{pmatrix}$

In this case, the P_{cd} is calculated through

$$\begin{aligned} P_{cd} &= p_{tx}\{p_{id}[p_{00}(\gamma_{r2})p_{00}(\gamma_{t2}) + p_{00}(\gamma_{r2})p_{01}(\gamma_{t2})] + \frac{1}{3}p_{fbs}[p_{00}(\gamma_{r2})p_{00}(\gamma_{t2}) \\ &+ 2p_{00}(\gamma_{r2})] + \frac{1}{3}p_{bs}[2p_{11}(\gamma_{r2}) + p_{01}(\gamma_{r2})]\} + p_{rx}\{p_{id}[p_{00}(\gamma_{r1})p_{00}(\gamma_{t1}) \\ &+ p_{01}(\gamma_{r1})p_{00}(\gamma_{t1})] + \frac{1}{3}p_{fbs}[p_{00}(\gamma_{r1})p_{00}(\gamma_{t1}) + 2p_{00}(\gamma_{t1}) + \frac{1}{3}p_{bs}[2p_{11}(\gamma_{t1}) \\ &+ p_{01}(\gamma_{t1})]\} \end{aligned} \tag{7}$$

Follows are discussed based above formulas:

- Compared with transmitter-independent energy detection methods, since both STs and SRs participate the detection process, the detection performance is same whatever the detection is based on the signal from PTs or PRs. It is a good news for CRNs that are coexisting with primary systems, in which no response/confirmation from PRs during data transmission processes.

- Assuming CRs can correctly detect whether there is transmission processing around them on a particular frequency band, i.e., $p_{00} = 1$, $p_{11} = 1$, $p_{01} = 0$ and $p_{10} = 0$. In this specific case, the upper bound for detection probability is:

$$P_{cd,max} = p_{id} + \frac{1}{3}p_{fbs} + \frac{5}{6}p_{bs} \tag{8}$$

and

$$P_{cd,max} = p_{id} + p_{fbs} + \frac{2}{3}p_{bs} \tag{9}$$

Note that when $p_{bs} < 4p_{fbs}$, the performance of treating $\begin{pmatrix} 0 \\ 1 \end{pmatrix}$ as *Fake Busy* is worse than treating $\begin{pmatrix} 0 \\ 1 \end{pmatrix}$ as *Busy*.

- Using transmitter/receiver-cooperated energy detection methods, it can acquire better performance for TDMA primary systems, ALOHA systems and CSMA systems. However, for CSMA/CA systems, the transmitter/receiver-cooperated energy detection method treating $\begin{pmatrix} 0 \\ 1 \end{pmatrix}$ as *Busy* achieves better performance when $p_{tx} \geq \frac{4p_{fbs}-p_{bs}}{4p_{fbs}p_{bs}}$, and treating $\begin{pmatrix} 0 \\ 1 \end{pmatrix}$ as *Fake Busy* can always achieve better performance.
- Even though only PTs and PRs are exploited for energy detection, it can be an optimal energy detection method when channel status only be *Idle* or *Fake Busy*. That is, when $p_{bs} = 0$, $P_{cd,max} = 1$. Otherwise, the performance is always $\frac{1}{3}p_{bs}$ worse than the one of ideal energy detection method.

5 Identical Environment for Secondary Transmitter and Receiver Scenario

When the environment for secondary transmitters and receivers are same. In this case, all possible values for S are shown in Table 4. We will obtain P_{cd} for various energy detection methods separately.

Table 4: channel state classification according to S for ideal method

Channel State	S
Idle	$\begin{pmatrix} 0 & 0 \\ 0 & 0 \end{pmatrix}$
Busy	$\begin{pmatrix} 0 & 1 \\ 0 & 1 \end{pmatrix}, \begin{pmatrix} 1 & 0 \\ 1 & 0 \end{pmatrix}, \begin{pmatrix} 1 & 1 \\ 1 & 1 \end{pmatrix}.$

5.1 Ideal Energy Detection

Since the situation for STs and SRs is same, it is validate to make correct decision only according to the detection by STs or SRs. Moreover, for ideal energy detection, PTs and PRs have the capability to send message out, which can be detected by secondary users. In this case, the detection probability P_{cd} is as follows.

$$\begin{aligned} P_{cd} &= p_{id}p_{00}(\gamma_1)p_{00}(\gamma_2) + \frac{1}{3}p_{bs}[p_{01}(\gamma_1) + p_{11}(\gamma_1) + p_{01}(\gamma_2) + p_{00}(\gamma_1)p_{11}(\gamma_2) \\ &+ p_{10}(\gamma_1)p_{11}(\gamma_2) + p_{11}(\gamma_1)p_{00}(\gamma_2)] \end{aligned} \tag{10}$$

p_{γ_1} is the detect probability according to the signal from PRs, and p_{γ_2} is the detect probability according to the signal from PTs. Compared with ideal energy detection performance in generic environment, i.e., the situation for SRs might not be identical with the one for STs, they are same when there are only *Busy* or *Ideal* status existed for channel (i.e., $p_{fbs} = 0$) and the detection results at SRs are same as the one at STs (i.e., $p(\gamma_{r2}) = p(\gamma_2)$ and $p(\gamma_{t1}) = p(\gamma_1)$).

5.2 Transmitter-Independent Energy Detection

When the environment is same for STs and SRs, using the transmitter-independent detection method the detection performance is as following:

$$\begin{aligned} P_{cd} &= p_{tx}\{p_{id}p_{00}(\gamma_2) + \frac{1}{3}p_{bs}[2p_{11}(\gamma_2) + p_{01}(\gamma_2)]\} + p_{rx}\{p_{id}p_{00}(\gamma_1) \\ &+ \frac{1}{3}p_{bs}[2p_{11}(\gamma_1) + p_{01}(\gamma_1)]\} \end{aligned} \tag{11}$$

Following characteristics are observed:

- When the situations for STs and SRs are identical, the upper bound of detection performance is same. It is $P_{cd,max} = p_{id} + \frac{2}{3}p_{bs}$.
- Since the situations at STs and SRs are same, it is unnecessary to exploit both secondary transmitter and receiver for better detection performance for CRNs. Therefore, for the special case that there is identical environment for STs and SRs, traditional energy detection method - transmitter-independent energy detection - is an optimal choice.
- Since the situations at STs and SRs are same, obviously, detection probability can be enhanced. However, compared with the performance in generic environment, the upper bound is same as the ones when only monitoring PRs' signals for energy detection, but always better than the ones when only monitoring PTs' signals. It inspired us that some wrong detections are generated for the difference between STs and SRs. That is, in that case, traditional transmitter-independent energy detection is not the best choice. If more signal from PRs can be detected by STs, even for different situation for STs and SRs, better detection performance can be achieved.

6 Simulation and Performance Analysis

6.1 Surface of detection probability P_{cd} for ideal energy detection

Assuming STs and SRs own same sensing capability, that is, $p_{00}(\gamma_{r2}) = p_{11}(\gamma_{r2})$ and $p_{00}(\gamma_{t1}) = p_{11}(\gamma_{t1})$. Moreover, $p_{10}(\gamma_{r2}) = p_{01}(\gamma_{r2}) = 1 - p_{00}(\gamma_{r2})$ and $p_{10}(\gamma_{t1}) = p_{01}(\gamma_{t1}) = 1 - p_{00}(\gamma_{t1})$. Based on (2) and (10), Fig.2 shows the surfaces for P_{cd} under various combinations of traffic load intensity p_{bs}, sensing capability of STs/SRs $p(\gamma_{r2})/p(\gamma_{t1})$. Here, the range for $p(\gamma_{r2})$ and $p(\gamma_{t1})$ is [0.5 0.6 0.7 0.8 0.9 1.0], as well as the candidates for p_{bs} are [0.0 0.3 0.5 0.8 1.0]. In those two figures, with p_{bs} the maximum value and minimal value of P_{cd} are shown for each surface. Note that:

- Fixing the traffic intensity of primary systems (i.e., fixing p_{bs}), with the increase of signal detection capability for STs/SRs (i.e., increasing $p(\gamma_{r2})/p(\gamma_{t1})$) there is higher chance to make correct decision for secondary users. It inspire us that enhance the detection capability for secondary users can reduce the interference to primary systems and increase the frequency utilization.
- Fixing the signal detection capability of STs/SRs (i.e., fixing the value for $p(\gamma_{r2})/p(\gamma_{t1})$), when primary system is more often being truly busy (i.e., with higher value for p_{bs}) there is higher chance to make correct decision for secondary users. That is, it is more easy for secondary users to successfully monitor

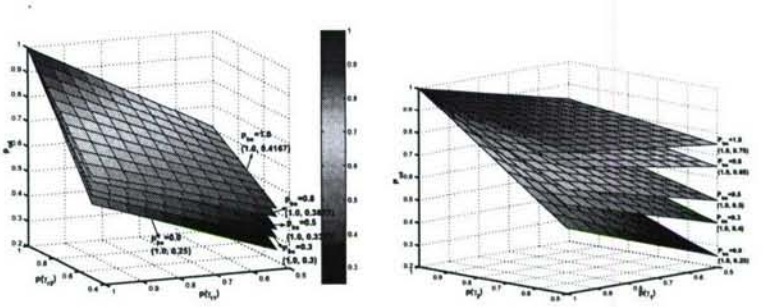

(a) (b)

Figure 2: Detection probability P_{cd} for ideal energy detection method for (a) generic environment for secondary transmitters/receivers scenario and (b) identical environment for secondary transmitters/receivers scenario.

the primary system, which is busy exchanging information. Otherwise, more error will be made for detection.

- Identical environment for STs and SRs can improve the detection performance for CRNs even under same situation, such as same p_{bs}, $p(\gamma_{r2})$ and $p(\gamma_{t1})$, since there is no chance for channel being *Fake Busy*. Therefore, the improvement due to identical environment is reduced when the detection error caused by exposed node problem is less (i.e., less chance for channel being *Fake Busy*). For example, when $p_{bs} = 0.0$, the minimal successful detection probability is same as 0.25 for generic scenario and identical scenario, while when $p_{bs} = 1.0$, the minimal successful detection probability for identical environment is 44.44% ($\frac{0.75-0.4167}{0.75} = 44.44\%$) higher than the one for generic environment.

6.2 Surface of detection probability P_{cd} for transmitter-independent energy detection method

Assuming there is same sensing probability for STs, that is, $p_{00}(\gamma_{t1}) = p_{11}(\gamma_{t1})$ and $p_{10}(\gamma_{t1}) = p_{01}(\gamma_{t1}) = 1 - p_{00}(\gamma_{t1})$. When sensed signal comes from primary transmitters and receivers both, we assume the sensing probability at STs is same. Here, the range for $p(\gamma_{t1})$ is [0.5 0.6 0.7 0.8 0.9 1.0], as well as the candidates for p_{bs} are [0.0 0.3 0.5 0.8].

According to (3), Fig.3 shows the surfaces for P_{cd} under various combinations of traffic load intensity p_{bs}, p_{fbs} and sensing capability of secondary transmitter $p(\gamma_{t1})$ when sensed signal come from PTs or PRs. In above two figures, with p_{bs}, the maximum value and minimal value for P_{cd} are shown for each surface. Note that

- From Fig. 3(a), compared with ideal energy detection method, the more the chance for channel being truly occupied by primary users is, the more the detection error becomes both for generic and identical scenarios. It inspires us that the behavior of primary systems, in which the channel is less often occupied, can be more easy to be monitored by secondary systems only through STs.

- Also from Fig. 3(a), since the channel status can not be accurately monitored only by STs, the chance for channel being *Fake Busy* directly impacts on the detection performance. Fixing the chance for channel being truly busy, the chance for STs to successfully detect the channel status is decreased with the detection error introduced by exposed node problem becoming bigger (i.e., higher value for P_{fbs}). While, in this

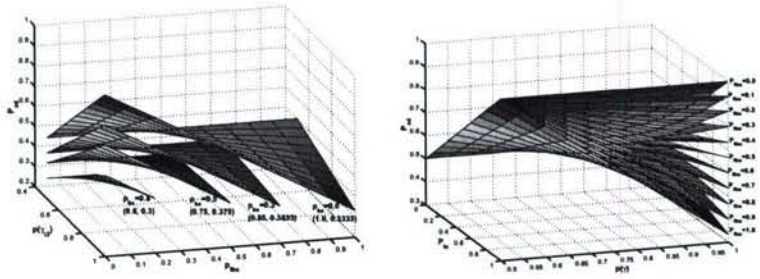

(a) (b)

Figure 3: Detection Probability of P_{cd} for Transmitter Independent Energy Detection when Sensed Signal from (a) Primary Transmitter only and (b) Primary Transmitter or Receiver

case, the detection performance can be improved through enhance the sensing capability for STs (i.e., higher value for $p(\gamma_{t2})$).

- When sensed signal comes from PTs or PRs (See Fig. 3(b)), it is a negative influence of sensing capability for STs on the detection performance.

- From Fig. 3(b), if more sensed signal comes from PRs, the performance for transmitter-independent detection method can be improved when fixing channel status. Moreover the influence degree of P_{tx} on P_{cd} is changed with the chance for channel being *Fake Busy*. That is, the more the chance for channel being *Fake Busy*, the less the improvement on detection performance caused by more sensed signal coming from PRs. Even more, this positive impact becomes a negative impact when p_γ and P_{fbs} locate in a certain range. The turning points are: $p(\gamma) \geq 0.9$ when $P_{fbs} = 1.0$, $p(\gamma) \geq 0.95$ when $P_{fbs} = 0.9$ and $p(\gamma) = 1.0$ when $P_{fbs} = 0.8$.

6.3 Surface of detection probability P_{cd} for transmitter/receiver-cooperated energy detection

Assuming there is same sensing probability for secondary transmitters and receivers, that is, $p_{00}(\gamma_{t2}) = p_{11}(\gamma_{t2})$ and $p_{00}(\gamma_{r2}) = p_{11}(\gamma_{r2})$. Moreover, $p_{10}(\gamma_{t2}) = p_{01}(\gamma_{t2}) = 1 - p_{00}(\gamma_{t2})$ and $p_{10}(\gamma_{r2}) = p_{01}(\gamma_{r2}) = 1 - p_{00}(\gamma_{r2})$. When sensed signal comes from PRs and PTs both, we assume the sensing probability at STs is same. Here, the range for $p(\gamma_{t1})$ is [0.5 0.6 0.7 0.8 0.9 1.0], as well as the candidates for p_{bs} are [0.0 0.3 0.5 0.8].

Based on (6), Fig. 4, Fig. 5, Fig. 6 and Fig. 7 show the surfaces for P_{cd} under various combinations of traffic load intensity p_{bs}, p_{fbs} and sensing capability of STs/SRs $p(\gamma_{t2})/p(\gamma_{r2})$ when sensed signal come from PTs/PRs.

Note that

- Similarly with ideal energy detection method, the more the chance for channel being truly occupied by primary users is, the less the detection error becomes both for generic and identical scenarios. It inspires us that the behavior of primary systems, in which the channel is more often occupied, can be more easy to be monitored by secondary systems both through STs and SRs.

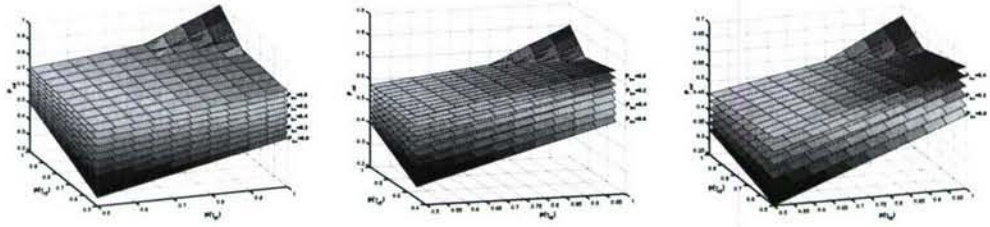

(a) (b) (c)

Figure 4: In Generic Scenario, Detection Probability of P_{cd} for Transmitter/Receiver-Cooperated Energy Detection for (a) $P_{fbs} = 0.0$, (b) $P_{fbs} = 0.3$ and (c) $P_{fbs} = 0.5$

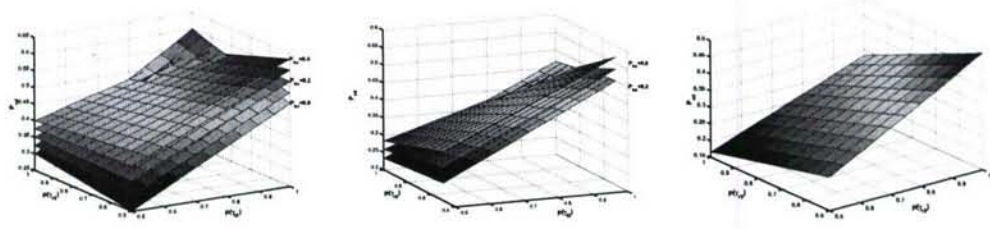

(a) (b) (c)

Figure 5: In Generic Scenario, Detection Probability of P_{cd} for Transmitter/Receiver-Cooperated Energy Detection for (a) $P_{fbs} = 0.6$, (b) $P_{fbs} = 0.8$ and (c) $P_{fbs} = 1.0$

- Fixing the chance for channel being *Busy* and *Fake Busy*, the chance for secondary users to successfully detect the channel status is enhanced for utilizing more sensitive STs (i.e., higher value for $p(\gamma_{t2})$).
- There is a watershed for the influence of sensing capacity of SRs on detection performance when the environment for STs and SRs is not identical. When $P_{fbs} \leq 0.5$, the detection performance can be improved through using more sensitive receivers, otherwise when $P_{fbs} \geq 0.5$, less sensitive receivers should be exploited to reduce detection errors. However, this watershed is disappeared when identical environment for STs and SRs.
- Both using STs and SRs for detection, it is still impossible to accurately monitor the operation for

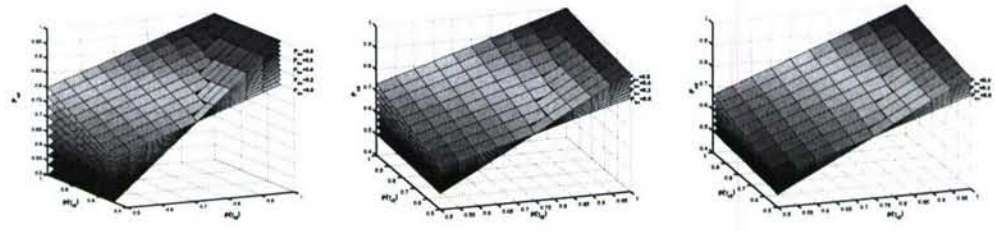

(a) (b) (c)

Figure 6: In Identical Scenario, Detection Probability of P_{cd} for Transmitter/Receiver-Cooperated Energy Detection for (a) $P_{fbs} = 0.0$, (b) $P_{fbs} = 0.3$ and (c) $P_{fbs} = 0.5$

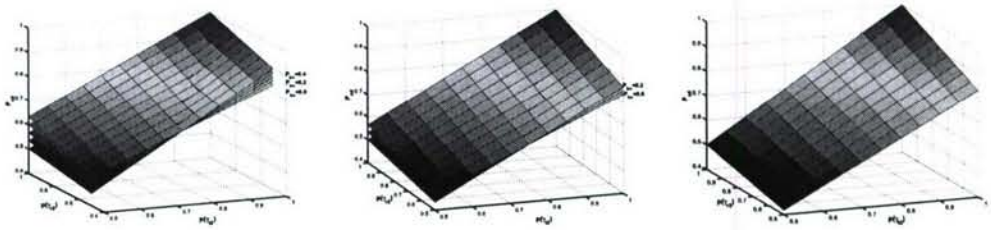

(a) (b) (c)

Figure 7: In Identical Scenario, Detection Probability of P_{cd} for Transmitter/Receiver-Cooperated Energy Detection for (a) $P_{fbs} = 0.6$, (b) $P_{fbs} = 0.8$ and (c) $P_{fbs} = 1.0$

primary users for exposed node problem and hidden terminal problem. Identical environment for secondary transmitters and receivers can improve the detection performance

7 Conclusions

While energy detection has been extensively studied in the past, hidden terminal and exposed node problems are ignored through assuming that the environment is same for transmitters and receivers. In this paper, considering hidden terminal and exposed node problems, we make a theoretical analysis on the performance of commonly used energy detection methods, such as ideal method, transmitter-independent method and transmitter/receiver-cooperated method, in terms of detection probability. Corresponding analytical models are provided. Performance theoretical curves are acquired to compare the characteristics for individual energy detection methods under various scenarios. Moreover the upper bound for detection probability is achieved and is compared under various system traffic intensity and sensing capability. From the theoretical results, we found that it is easy to correctly detection the channel status when primary systems are heavily occupied for ideal energy detection method and tansmitter/receiver-cooperated energy detection method. Otherwise, transmitter-independent method is a better scheme to monitor the primary systems. Commonly, increasing the sensitivity of secondary users can upgrade the detection performance. However, in our analysis, it is not true for transmitter-independent method and transmitter/receriver-cooperated method under certain situations. We have concluded those special cases in this paper. Therefore, the theoretical results can supply a reference on the choosing of energy detection method according to system scenario, such as traffic load, sensing capability, etc..

Acknowledgement

This work was supported by the U.S. Office of Naval Research (ONR) Young Investigator Program Award under Grant N00014-03-1-0466, and ONR Award under Grant N00014-07-1-0395.

References

[1] FCC, "Spectrum policy task force report," in *ET Docket No. 02-155*, Nov. 2002.

[2] J. G. Proakis, *Digital Communications.* NY: Mc Graw Hill, 2001.

[3] D. Cabric, S. M. Mishra, and R. W. Brodersen, "Implementation issues in spectrum sensing for cognitive radios," in *38th Asilomar Conference on Signals, Systems and Computers*, Nov. 2004, pp. 772–776.

[4] G. Ganesan and Y. Li, "Cooperative spectrum sensing in cognitive radio networks," in *Proc. First IEEE International Symposium on New Frontiers in Dynamic Spectrum Access Networks 2005 (DySPAN2005)*, Nov. 2005, pp. 137–143.

[5] M. P. Wylie-Green, "Dynamic spectrum sensing by multiband ofdm radio for interference mitigation," in *Proc. First IEEE International Symposium on New Frontiers in Dynamic Spectrum Access Networks 2005 (DySPAN2005)*, Nov. 2005, pp. 619–625.

[6] H. Urkowitz, "Energy detection of unknown deterministic signals," *Proceedings of the IEEE*, vol. 55, no. 4, pp. 523–531, 1967.

[7] A. C. Bovik, P. Maragos, and T. F. Quatieri, "Am-fm energy detection and separation in noise using multiband energy operators," *IEEE Trans. Signal Processing*, vol. 41, no. 12, pp. 3245–3265, 1993.

[8] J. F. Weng and T. Le-Ngoc, "Rake receiver using blind adaptive minimum output energy detection for ds/cdma over multipath fading channels," *Proceedings of the IEE*, vol. 148, no. 6, pp. 385–392, 2001.

[9] M. Schwartz, *Mobile Wireless Communications.* NY: Cambridge University Press, 2005.

[10] F. F. Digham, M. Alouini, and M. K. Simon, "On the energy detection of unknown signals over fading channels," in *Proc. IEEE International Conference on Communications 2003 (ICC'03)*, May 2003, pp. 3575 – 3579.

[11] A. Ghasemi and E. S. Sousa, "Collaborative spectrum sensing for opportunistic access in fading environments," in *Proc. First IEEE International Symposium on New Frontiers in Dynamic Spectrum Access Networks 2005 (DySPAN 2005)*, Nov. 2005, pp. 131–136.

[12] T. Kamakaris, M. M. Buddhikot, and R. Iyer, "A case for coordinated dynamic spectrum access in celluar networks," in *Proc. First IEEE International Symposium on New Frontiers in Dynamic Spectrum Access Networks 2005 (DySPAN2005)*, Nov. 2005, pp. 289–298.

[13] E. Visotsky, S. Kuffner, and R. Peterson, "On collaborative detection of tv transmissions in support of dynamic spectrum sharing," in *Proc. First IEEE International Symposium on New Frontiers in Dynamic Spectrum Access Networks 2005 (DySPAN2005)*, Nov. 2005, pp. 338–345.

[14] A. S. Tanenbaun, *Comupter Networks.* NJ: Prentice-Hall, 1996.

[15] B. Sklar, *Digital Communications.* NJ: Prentice-Hall, 2001.

[16] C. K. Toh, *Ad Hoc Mobile Wireless Networks: Protocols and Systems.* Prentice-Hall, 2002.

[17] P802.11, "Ieee standard for wireless lan medium access control (mac) and physical layer (phy) specifications," Nov. 1997.

Superimposed Code Based Channel Assignment in Multi-Radio Multi-Channel Wireless Mesh Networks

Kai Xing & Xiuzhen Cheng & Liran Ma

Department of Computer Science
The George Washington University
Washington, DC 20052, USA
{kaix,cheng,lrma}@gwu.edu

Qilian Liang

Department of Electrical Engineering
The University of Texas at Arlington
Arlington, TX 76019, USA
liang@uta.edu

ABSTRACT

Motivated by the observation that channel assignment for multi-radio multi-channel mesh networks should support both unicast and local broadcast[1], should be interference-aware, and should result in low overall switching delay, high throughput, and low overhead, we propose two flexible localized channel assignment algorithms based on s-disjunct superimposed codes. These algorithms support the local broadcast and unicast effectively, and achieve interference-free channel assignment under certain conditions. In addition, under the primary interference constraints[2], the channel assignment algorithm for unicast can achieve 100% throughput with a simple scheduling algorithm such as the maximal weight independent set scheduling, and can completely avoid hidden/exposed terminal problems under certain conditions. Our algorithms make no assumptions on the underlying network and therefore are applicable to a wide range of MR-MC mesh network settings. We conduct extensive theoretical performance analysis to verify our design.

Categories and Subject Descriptors

C.2.1 [**Network Architecture and Design**]: Wireless Communication

General Terms

Algorithms, Design

Keywords

Multi-radio multi-channel wireless mesh networks, interference, channel assignment, superimposed codes

1. INTRODUCTION

With recent advances in wireless technology, the utilization of multiple radios as well as non-overlapping channels provides an opportunity to reduce interference and increase network capacity. Equipped with multiple radios, nodes can communicate with multiple neighbors simultaneously over different channels, and thus can significantly improve the network performance by exploring concurrent transmissions [1].

In a multi-radio multi-channel (MR-MC) mesh network, a key challenging problem for capacity optimization is *channel assignment*. Since practically the number of radios at each node is always much smaller compared to that of orthogonal channels due to reasons such as cost and small form factors, it may be prohibitive to assign one fixed channel to each radio. In other words, a radio may need to switch to different channels as time goes for better performance. This radio constraint makes the channel assignment in MR-MC mesh networks much harder. In this paper, we propose two channel assignment algorithms for interference mitigation and throughput maximization. Our research is motivated by the following observations.

- Current channel assignment approaches lack a support to local broadcast in MR-MC mesh networks. As neighboring nodes tend to use different channels for transmissions, the broadcast packet has to be separately transmitted by the sender on multiple channels. Thus, broadcast can be more expensive than that in single-radio single-channel (SR-SC) networks.

- A number of current channel assignment approaches rely heavily on solving complex optimization problems, which might be impractical for many MR-MC mesh network scenarios. In addition, techniques based on default radio/channel degrade network throughput when the number of radios is much smaller than that of channels.

- Channel switching delay is an important parameter that should be counted in channel assignment. Since the number of radios per node is usually much smaller than that of orthogonal channels, allowing a radio switch among the full range of channels results in higher overall delay since the radio may switch back and forth frequently when multiple different flows traverse the same node simultaneously.

- CSMA/CA is believed to be inadequate to meet the high traffic demand in mesh networks [2]. Any channel assignment that requires RTS/CTS for channel reservation is unfavored due to the high overhead. Since co-channel interference is one of the major reasons for capacity degradation in MR-MC mesh networks, interference-aware channel assignment for throughput optimization should be sought.

[1] A broadcast to be heard by all immediate neighbors.

[2] Under the primary interference constraints, each radio can talk with at most one single neighbor at any instant of time. Namely the set of active links supported the same channel at any point of time is a matching.

MobiCom'07, September 9–14, 2007, Montréal, Québec, Canada.

In this paper, we propose two channel assignment algorithms based on s-disjunct superimposed codes. The basic idea is sketched as follows. For each node, all available orthogonal channels are labelled as either primary or secondary via a binary channel codeword. This labelling is controlled by an s-disjunct superimposed $(s, 1, N)$-code. The codeword of the transmitting node, together with those of the interferers, determine the channel. Note that primary channels are always preferred during channel assignment. Our analysis indicates that by exploring the s-disjunct property of the $(s, 1, N)$-code, it is possible to achieve interference-free channel assignment for both unicast and broadcast. Comparing with the related literature in Section 2, we have identified the following unique contributions of our paper.

- We have designed two localized simple algorithms that can effectively support both local broadcast and unicast. Under certain conditions, interference-free broadcast and unicast can be achieved.
- Since our algorithms assign channels to transmitters for both unicast and broadcast, and because the channels are selected from a small subset of primary channels whenever possible, our algorithms can effectively decrease the overall switching delay caused by the oscillation of switching back and forth due to the large difference between the numbers of radios and channels.
- With a very simple scheduling algorithm, our channel assignment for unicast is proved to be able to achieve 100% throughput under the primary interference constraints. We also identifies the conditions when hidden and exposed terminal problems are completely avoided with our channel assignment.
- We have conducted extensive theoretical performance analysis to verify our algorithm design. In addition, our algorithms are localized, and have low computation and communication overheads.
- Our algorithms support dynamic, static, and adaptive channel assignment without requesting any complex scheduling and/or channel coordination. These algorithms make no assumptions on the underlying network settings such as traffic patterns and MAC/routing protocols. Therefore they are applicable to a wide range of mesh networks.

The rest of the paper is organized as follows: Section 2 discusses the related work in channel assignment for MR-MC mesh networks. In Section 3, we present our network model and assumptions. Section 4 introduces the s-disjunct superimposed code and links it to the problem of channel assignment in MR-MC mesh networks. In Section 5, we present our channel assignment algorithms for both unicast and broadcast, and analyze their performance theoretically. In Section 6, we discuss a number of related issues. Section 7 summarizes the work and concludes the paper.

2. RELATED WORK

In this section, we survey the most related research in channel assignment for MR-MC mesh networks.

The benefits of using multiple radios and channels have been theoretically studied in [1,3–5] by jointly considering routing, scheduling, and channel assignment. Load-aware channel assignment is studied in [6, 7]. Marina and Das jointly consider channel assignment and topology control in [8].

In Kyasanur and Vaidya [9], the multiple radios at each node are divided into two groups, with one assigned fixed channels for packet reception and ensuring connectivity, and the other assigned switchable channels for capacity increase. This multiple channel management actually handles the channel allocation at the receiver side. Each switchable radio switches to the fixed channel of the destination radio when data transmission needs to be launched. For fixed channel assignment, a node selects random channels for its fixed interfaces initially. To balance the utilization of all channels, nodes collect two-hop neighborhood information and change their fixed channels accordingly. Obviously this fixed channel assignment takes time to converge. In addition, the number of switchable channels is relatively large when the number of radios per node is small, which may cause a large overall switching delay when the node has to switch back and forth in order to simultaneously relay multiple flows to different neighbors. Furthermore, the receiver-based channel assignment does not support broadcast efficiently and each broadcast packet has to be transmitted separately on one of the fixed channels for each neighbor. Our work differs in that we consider transmitter channel assignment, which is expected to incur low overall switching delay and can trivially support efficient broadcast.

A common default channel is introduced in [10–14] to handle the network partition caused by dynamic channel assignment, and to facilitate channel negotiation for data communications. To assign channels to the interfaces other than the default radio, [10] presents a localized greedy heuristic based on an interference cost function defined for pairs of channels. Refs. [11, 12] consider the mesh networks with main traffic flowing to and from a gateway, which is also in charge of the channel computation. In their channel assignment to a non-default radio, nodes closer to the gateway and/or bearing higher traffic load get a better quality channel. In DCA [14], the default channel is used as a control channel. For each node, one of the radios stays on the control channel for exchanging control messages, and other radios dynamically switch to the data channels for transmission. In this case, the utilization of the control channel could be small even though the data channels can be fully utilized. A multi-channel MAC is proposed in [13] for single-radio networks. This MAC protocol requires all nodes to meet at the common channel periodically to negotiate the channels for data communication.

The default channel does not have to be the same for all nodes in the network. In [15], each node fixes one radio on some channel but different nodes possibly use different fixed channels. This channel assignment actually fixes the reception channel for each node, and therefore the remaining radios of the node dynamically switch to its neighbors' fixed channels for data transmission. The same idea is adopted in [9]. In SSCH [16], radios switch among channels following some pseudo-random sequences such that neighboring nodes meet periodically at a common channel. This approach is simple but it requires clock synchronization.

Compared to the works mentioned above, our work does not require any special radio. We consider the channel assignment to all radios in a static fashion. In addition, our channel assignment algorithms are localized and are designed for a mesh network with a more general peer-to-peer traffic pattern.

Another important category of related work is code assignment for hidden terminal interference avoidance in CDMA packet radio networks. Bertossi and Bonuccelli [17] presents a centralized greedy algorithm to assign CDMA codes to vertices such that every pair of nodes at two-hop distance is assigned with a couple of different codes and the number of orthogonal codes utilized is minimized. This is a NP-Complete problem, and therefore the proposed

algorithm is an approximate heuristic. The distributed implementation of the algorithm, which results in a high overhead, is also proposed in [17]. The same code assignment problem is considered in [18] too, where a distributed heuristic is proposed. Note that to ensure hidden terminal interference-free communications, different codes should be assigned to every pair of nodes that are two-hop away. Our work differs from [17, 18] in that we intend to assign channels to nodes with an objective of interference-free unicast and broadcast to their immediate neighbors. In addition, the number of available orthogonal channels in our study is much smaller than that of the CDMA codes in a packet radio network. Furthermore, our localized algorithms are much simpler and results in much lower overhead.

Our work focuses on channel assignment for general MR-MC mesh networks. Each node is associated with a binary channel codeword, and computes its channels based on the codewords of the interferers. The algorithms involved are simple, has very low computation and communication overheads, and can support both unicast and local broadcast effectively.

3. NETWORK MODEL

In this section, we introduce the underlying network model, assumptions, and terminologies employed in the paper.

3.1 Basics

We consider a stationary multi-radio multi-channel (MR-MC) wireless mesh network with $|V|$ nodes. There exist N orthogonal (non-overlapping) frequency channels labelled by $k_1, k_2, \cdots, k_N$. Each node is equipped with Q radio interfaces. In our consideration, $Q \ll N$. This is a practical assumption since the number of radios per node is constrained by cost and form factors. For example, in an IEEE 802.11a based mesh network, each node may have 2 or 3 radios but the number of orthogonal channels is 12. We assume that the footprint of a radio is a disk resulting from an omni-directional antenna. In addition, we assume that each radio supports the same set of non-overlapping channels. Note that the number of radios equipped on each mesh node could be different.

For each node, the N available orthogonal channels are divided into two categories: *primary channels* and *secondary channels*. A binary column vector $\vec{c_u}$ of length N, called a *channel codeword*, is associated with each node u to label its channels, with a value 1 representing a primary channel and a value 0 secondary. For example, $\vec{c_u} = (1,0,0,1,0,0,0,1,0,1,0,0)'$ means that channels k_1, k_4, k_8, and k_{10} are primary to u, and k_2, k_3, k_5, k_6, k_7, k_9, k_{11} and k_{12} are secondary to u for a network that can support 12 orthogonal channels. Note that partitioning the channels into two sets can facilitate our algorithm design. Intuitively, a node should favor a channel that is secondary to all its interferers. Therefore for each node, the number of primary channels should be smaller than that of the secondary.

We require that for any two channel codewords $\vec{c_u}$ and $\vec{c_v}$, there exist at least two channels k_1 and k_2 such that k_1 is primary to u but secondary to v, and k_2 is secondary to u but primary to v. In other words, we can always find out a channel that is primary to one node and secondary to another node when the two corresponding channel codewords are different. For simplicity, we assume all nodes have the same number of primary channels. Let this number be w. Then the number of channel codewords satisfying the above condition is $\binom{N}{w}$ for N available orthogonal channels, which reaches its maximum when $w = \frac{N}{2}$. For example, when $N = 12$, there are 66, 495, and 924 available channel codewords for $w = 2, 4, 6$ respectively. We assume that the channel codewords assigned to each node is unique. As explained in Section 6, this assumption can be relaxed when the cellular grid architecture is introduced for salability considerations.

In our study, the network is modelled by a directed graph $G(V, E)$, where V is the set of nodes, and E is the set of directed links. A *channel code*, denoted by a $N \times |V|$ binary matrix $\mathcal{C}$, is associated with G. Therefore sometime G is denoted by $G(V, E, \mathcal{C})$. Each column of $\mathcal{C}$ represents a channel codeword pertaining to a node in the network. For example, the uth column is the channel codeword $\vec{c_u}$ for node u. The purpose of this paper is to assign channels to a node u based on $\vec{c_u}$ and the channel codewords of its interferers in order to mitigate co-channel interference for network capacity maximization, an optimization problem requiring the joint consideration of routing, channel assignment, and packet scheduling. Nevertheless, we focus on channel assignment in this paper, and propose to study joint routing and scheduling based on our channel assignment as a future research.

We assume that a DATA packet sending from u to v is acknowledged with an ACK message from v to u. Therefore even though we use a directed graph to model the network, only bidirectional links are considered. A directed link from node u to v is denoted by $(u \rightarrow v)$. In addition, we use $N_1(u)$ and $N_2(u)$ to represent the sets of neighbors of u within one-hop and two-hop away. We have $u \notin N_1(u)$ and $u \notin N_2(u)$.

3.2 Interference Model

For any node $u \in V$, denoted by $\mathcal{N}(u)$ the set of interferers of u. A node $v \in V$ is an *interferer* of u if v's transmission interferes with u's transmission. Therefore when two-way handshake (DATA-ACK) is adopted for successful packet delivery, the interferers for the unicast from u to v include $N_1(u)$ and $N_1(v)$. For a local broadcast by u, the interferers include all nodes in $N_2(u)$.

4. LINKING SUPERIMPOSED CODES WITH MR-MC NETWORKS

In this section, we first give a brief introduction on *superimposed codes*. Then we link the superimposed $(s, 1, N)$-code, also called the *s-disjunct code*, to channel assignment in MR-MC mesh networks.

4.1 Superimposed codes

Superimposed codes were introduced by Kautz and Singleton [19] in 1964. Since then, they have been extensively studied and applied to various fields, such as multi-access communications [20], [21], cryptography [22], pattern matching [23], circuit complexity [24], and many other areas of computer science. For convenience, we first introduce the basic definitions and properties of superimposed codes.

Let N, t, s, and L be integers such that $1 < s < t$, $1 \leq L \leq t - s$, and $N > 1$. Given a $N \times t$ binary matrix $\mathcal{X}$, denote the ith column of $\mathcal{X}$ by $X(i)$, where $X(i) = (x_1(i), x_2(i), \cdots, x_N(i))'$. We call $X(i)$ a codeword i of $\mathcal{X}$ with a length N. In other words, $\mathcal{X}$ is a *binary code* with each column corresponding to a codeword. Let w and λ be defined as:

$$w_i = \sum_{k=1}^{N} x_k(i), \quad (1)$$

$$\lambda_j = \sum_{k=1}^{t} x_j(k). \quad (2)$$

Therefore w and λ are called the *column weight* and *row weight* of $\mathcal{X}$, respectively. We have $w_{min} = \min_{i=1}^{t} w_i$, $w_{max} = \max_{i=1}^{t} w_i$, $\lambda_{min} = \min_{j=1}^{N} \lambda_j$, and $\lambda_{max} = \max_{j=1}^{N} \lambda_j$. Note that w_i and

$$\begin{pmatrix} 1 & 0 & 0 & 0 & 1 & 0 & 0 & 0 & 0 & 0 & 1 & 0 & 1 \\ 1 & 1 & 0 & 0 & 0 & 1 & 0 & 0 & 0 & 0 & 0 & 1 & 0 \\ 0 & 1 & 1 & 0 & 0 & 0 & 1 & 0 & 0 & 0 & 0 & 0 & 1 \\ 1 & 0 & 1 & 1 & 0 & 0 & 0 & 1 & 0 & 0 & 0 & 0 & 0 \\ 0 & 1 & 0 & 1 & 1 & 0 & 0 & 0 & 1 & 0 & 0 & 0 & 0 \\ 0 & 0 & 1 & 0 & 1 & 1 & 0 & 0 & 0 & 1 & 0 & 0 & 0 \\ 0 & 0 & 0 & 1 & 0 & 1 & 1 & 0 & 0 & 0 & 1 & 0 & 0 \\ 0 & 0 & 0 & 0 & 1 & 0 & 1 & 1 & 0 & 0 & 0 & 1 & 0 \\ 0 & 0 & 0 & 0 & 0 & 1 & 0 & 1 & 1 & 0 & 0 & 0 & 1 \\ 1 & 0 & 0 & 0 & 0 & 0 & 1 & 0 & 1 & 1 & 0 & 0 & 0 \\ 0 & 1 & 0 & 0 & 0 & 0 & 0 & 1 & 0 & 1 & 1 & 0 & 0 \\ 0 & 0 & 1 & 0 & 0 & 0 & 0 & 0 & 1 & 0 & 1 & 1 & 0 \\ 0 & 0 & 0 & 1 & 0 & 0 & 0 & 0 & 0 & 1 & 0 & 1 & 1 \end{pmatrix}$$

Figure 1: An example of a superimposed $(3, 1, 13)$-code of size 13

λ_j record the number of 1's in column i and in row j of $\mathcal{X}$, respectively. Hence w_{min} and w_{max} are the minimum and the maximum column weights of $\mathcal{X}$, respectively; and λ_{min} and λ_{max} are the minimum and the maximum row weights of $\mathcal{X}$, respectively.

The Boolean sum

$$Y = \bigvee_{i=1}^{s} X(i) = X(1) \bigvee X(2) \bigvee \cdots \bigvee X(s)$$

of codewords $X(1), X(2), \cdots, X(s)$ is the binary codeword $Y = (y_1, y_2, \cdots, y_N)'$ such that

$$y_j = \begin{cases} 0, & \text{if } x_j(1) = x_j(2) = \cdots = x_j(s) = 0, \\ 1, & \text{otherwise,} \end{cases}$$

for $j = 1, 2, \cdots, N$. We say that *a binary codeword Y covers a binary codeword Z if the Boolean sum $Y \bigvee Z = Y$.*

Superimposed code (SC): A $N \times t$ binary matrix $\mathcal{X}$ is called a superimposed code of length N, size t, strength s, and $listsize \leq L - 1$ if the Boolean sum of any s-subset[3] of the codewords of $\mathcal{X}$ covers no more than $L - 1$ codewords that are not components of the s-subset. This code is also called a (s, L, N)-code of size t. Fig. 1 shows an example of a superimposed $(3, 1, 13)$-code of size 13.

s-disjunct Code: A binary matrix $\mathcal{X}$ is called an s-disjunct code if and only if it has the property that the Boolean sum of any s codewords in $\mathcal{X}$ does not cover any codeword not in that set of s codewords.

Based on the definitions, a superimposed $(s, 1, N)$-code is a s-disjunct code. Taking the $(3, 1, 13)$-code shown in Fig. 1 as an example, the Boolean sum of the first 3 codewords of $\mathcal{X}$ is $X(1) \bigvee X(2) \bigvee X(3) = (1, 1, 1, 1, 1, 1, 0, 0, 0, 1, 1, 1, 0)'$, which doesn't cover any other codeword of $\mathcal{X}$ but themselves.

According to the s-disjunct characteristic of the superimposed $(s, 1, N)$-code, we can derive the following important property:

LEMMA 4.1. *Given an $(s, 1, N)$ superimposed code $\mathcal{X}$, for any s-subset of the codewords of $\mathcal{X}$, there exists at least one row at which all codewords in the s-subset contains the value 0.*

PROOF. For contradiction we assume that there is no row at which all codewords in the s-subset contain a common value 0. Then the Boolean sum of the s codewords equals $(1, 1, \cdots, 1)'$, which can cover all other codewords in $\mathcal{X}$, contradicting to the fact that $\mathcal{X}$ is a superimposed s-disjunct code. □

[3] An s-subset is a subset of s codewords.

4.2 Superimposed $(s, 1, N)$-codes and Channel Assignment in MR-MC Networks

As elaborated in Subsection 3.1, an MR-MC network is modelled by a directed graph $G(V, E, \mathcal{C})$, where $\mathcal{C}$ is the corresponding channel code. For any given node $u \in V$, $\vec{c}_u \in \mathcal{C}$ is a binary vector with each element corresponding to a channel and its $1/0$ value representing this channel being a primary channel or a secondary channel of node u. This observation helps us to build a direct mapping between a superimposed s-disjunct code $\mathcal{X}$ (represented by a $N \times t$ matrix), and the channel code $\mathcal{C}$ of a network G: N represents the number of available orthogonal channels, and each codeword of $\mathcal{X}$ indicates a possible channel codeword to a node in G. Then the column weight w_i of $\mathcal{X}$ represents the number of primary channels a node i has, and the row weight λ_j represents the number of nodes that take channel k_j as a primary channel.

In this paper, we will design algorithms for channel assignment based on superimposed codes. This research is motivated by the following observation: if the channel code $\mathcal{C}$ of a network G is a superimposed s-disjunct code $\mathcal{X}$, the nice s-disjunct property of $\mathcal{X}$ can be applied to derive the conditions for interference-free channel assignment.

Therefore we assume that the channel code $\mathcal{C}$ of network G is an s-disjunct superimposed code. From now on, we will use $\mathcal{X}$ to represent the channel code. We require that each node gets a unique codeword from $\mathcal{X}$ before participating in the network. In our algorithms, codewords from one-hop or two-hop neighbors are required for channel computation. A natural question is: how to obtain the codewords from neighboring nodes before channel assignment is complete? In this study, we assume that each node broadcasts its channel codeword once on each of its primary channels, or on all channels, to inform the neighbors of its codewords.

5. CHANNEL ASSIGNMENT BASED ON SUPERIMPOSED CODES

In this section, we first propose a generic channel assignment algorithm for MR-MC mesh networks. The generic algorithm assigns channels to nodes instead of links. This can facilitate channel selection for broadcast traffic. Then we propose an algorithm for link channel assignment targeting the unicast traffic. We also analyze the performances of both algorithms in detail.

5.1 The Generic Channel Assignment Algorithm

Let G be an MR-MC wireless mesh network with N available orthogonal channels, and $\mathcal{X}$ be the superimposed $(s, 1, N)$-code for its channel assignment. For any node u in G, a unique codeword $X(u) \in \mathcal{X}$ is associated with u indicating u's primary and secondary channel sets. Denote by $\mathcal{N}(u)$ the set of interferers of u. Algorithm 1 is a generic one that computes a set of channels for node u's transmissions.

Intuitively, u should choose only those channels not being used by any of its interferers from its primary channel set. If none of these primary channels is available, u should choose the secondary channels that are not primary to any of the nodes in $\mathcal{N}(u)$, the set of interferers of u. Since all nodes intend to utilize their primary channels whenever possible, choosing a channel that is secondary to all interferers is a reasonable choice. If u can not find out a channel that is secondary to all interferers, it picks up the primary channels that are primary to the least number of nodes in $\mathcal{N}(u)$.

These primary channels have the smallest row weight in $\mathcal{X}(\mathcal{N}(u))$, the set of codewords of $\mathcal{N}(u)$. Let $CH(u)$ be the set of channels assigned to u.

Algorithm 1 Channel Assignment for Node u

Input: Codewords $X(u)$ and $\mathcal{X}(\mathcal{N}(u))$.
Output: $CH(u)$, the set of channels assigned to u.

1: **function** $CH(u)$=**ChannelSelect**($X(u)$, $\mathcal{X}(\mathcal{N}(u))$)
2: $CH_1(u) \leftarrow Channels(BoolSum(\mathcal{X}(\mathcal{N}(u) \cup \{u\})) \oplus BoolSum(\mathcal{X}(\mathcal{N}(u))))$ ▷ Find the set of primary channels that are secondary to all nodes in $\mathcal{N}(u)$.
3: **if** $CH_1(u) \neq \emptyset$ **then**
4: $CH(u) \leftarrow CH_1(u)$
5: **else**
6: $CH_2(u) \leftarrow Channels(\overline{BoolSum(\mathcal{X}(\mathcal{N}(u) \cup \{u\}))})$ ▷ Find the set of secondary channels that are secondary to all nodes in $\mathcal{N}(u)$.
7: **if** $CH_2(u) \neq \emptyset$ **then**
8: $CH(u) \leftarrow CH_2(u)$
9: **else**
10: $CH_3(u) \leftarrow$ Select $Channels(X(u))$ with the smallest row weight in $\mathcal{X}(\mathcal{N}(u))$ ▷ Select the primary channels with the least row weight in $\mathcal{N}(u)$.
11: $CH(u) \leftarrow CH_3(u)$
12: **end if**
13: **end if**
14: **end function**

The basic idea for Algorithm 1 can be sketched below. Given $X(u)$ and $\mathcal{X}(\mathcal{N}(u))$, the Boolean sum of $\mathcal{X}(\mathcal{N}(u))$ and $\mathcal{X}(\mathcal{N}(u) \cup \{X(u)\})$ are first computed. Then the algorithm computes $CH_1(u)$, the set of u's primary channels that are secondary to all nodes in $\mathcal{N}(u)$. If $CH_1(u) \neq \emptyset$, assign $CH_1(u)$ to u; Otherwise, check $CH_2(u)$, the set of channels that are secondary to all nodes in $\mathcal{N}(u) \cup \{u\}$. If $CH_2(u) \neq \emptyset$, assign $CH_2(u)$ to u; otherwise, assign $CH_3(u)$, the set of primary channels whose corresponding row weights in the set $\mathcal{X}(\mathcal{N}(u))$ are minimum, to u.

Note that the set of primary channels of u are those favored by u. Therefore, $CH_1(u)$ contains the channels favored by u only, and $CH_3(u)$ is the set of channels favored by u and the least number of interferers of u. For $CH_2(u)$, since it contains the set of channels nobody likes to utilize in u's interference range, u should take this advantage. These channel assignment criterions reflect our design principle: *a node always selects a channel that causes the least interference to its neighborhood.*

Also note that Algorithm 1 is a localized one with each node u running a copy and making its channel assignment independently. We will prove in Lemma 5.1 that if there is an unused channel in $CH_1(u)$ for a radio r of u, r's transmission is guaranteed to be interference free.

Since each node may be equipped with multiple radios, the channels in $CH_1(u)$ may not be enough. In this case, assign all channels from $CH_1(u)$ first, then use the channels from $CH_2(u)$, and then from $CH_3(u)$.

Remarks: Algorithm 1 is a generic one that takes the codewords of u and its interferers as inputs. Therefore, Algorithm 1 does not rely on any interference model, as long as the set of u's interferers can be defined. Additionally, since Algorithm 1 assigns channels to the node, or the transmitters of the node, Algorithm 1 is a static channel allocation method. If roles of radios (the role of transmission or reception) are fixed, Algorithm 1 can help to decrease the number of channel switchings significantly compared to dynamic channel assignment. However, Algorithm 1 is dynamic when the set of interferers are collected on-line. Therefore, Algorithm 1 is flexible in that it can support both static and dynamic channel assignments.

Note that the channels determined by Algorithm 1 can be used for both unicast and local broadcast simultaneously. Since Algorithm 1 intends to pick up channels that may not be used by the interferers based on the local knowledge, it is superior in supporting local broadcast compared to existing research (Section 2). We plan to conduct extensive simulations to study the performance of Algorithm 1 when utilized to support broadcast in MR-MC mesh networks.

Example: Take the superimposed 3-disjunct code $\mathcal{X}$ in Fig. 1 as an example. Given a node u and $\mathcal{N}(u) = \{v, w, y\}$. Let $X(u) = X(1)$. If $X(v) = X(2)$, $X(w) = X(3)$, and $X(y) = X(4)$, Algorithm 1 yields $CH_1(u) = \{1, 10\}$, which means that channels 1 and 10 can be assigned to u. In this case, u picks up its primary channels. Since both channels are primary to u, based on Lemma 5.1, the transmission from u will not interfere with any other on-going traffic. If $\mathcal{N}(u) = \{v, w, y, z\}$, and $X(v) = X(3)$, $X(w) = X(10)$, $X(y) = X(12)$, and $X(z) = (13)$, no primary channels of u can be assigned to u but u can get channels $\{5, 7\}$ that are secondary to all nodes in $\mathcal{N}(u) \cup \{u\}$. When $\mathcal{N}(u) = \{v, w, y, z\}$, and $X(v) = X(4)$, $X(w) = X(10)$, $X(y) = X(12)$, and $X(z) = X(13)$, no channel that is secondary to all nodes in $\mathcal{N}(u)$ can be assigned to u. Therefore u picks up channels from its primary channel set $\{1, 2, 4, 10\}$ since all of them have the same row weight of 1 in $\mathcal{N}(u)$.

5.1.1 *Conditions for Interference-Free Channel Assignment*

In this subsection, we study the conditions for interference-free channel assignment based on Algorithm 1. Note that Algorithm 1 does not require a node u to collect the codewords of all interferers. If u knows nothing about its neighborhood, one of its primary channels will be picked for transmission. However, if $\mathcal{N}(u)$ is the complete set of interferers of node u, interference-free channel assignment is possible. In the following, we will first study the two scenarios when the channels assigned to u based on Algorithm 1 do not conflict with those of any other node in $\mathcal{N}(u)$. Then we study the conditions when interference-free communication in the whole network can be achieved. For simplicity, we assume that each node u in the network is equipped with two radios: one for transmission and one for reception. The results can be generalized to the case of more than two radios.

LEMMA 5.1. *If $CH_1(u) \neq \emptyset$, node u does not interfere with any other node in $\mathcal{N}(u)$.*

PROOF. When $CH_1(u) \neq \emptyset$, node u picks up channels from $CH_1(u)$, a subset of u's primary channel set, for transmission. $CH_1(u)$ contains channels that are primary to u but secondary to all nodes in $\mathcal{N}(u)$. For $\forall v \in \mathcal{N}(u)$, v can't use any channel from $CH_1(u)$ based on Algorithm 1 since v is assigned with either its own primary channels (from $CH_1(v)$ or $CH_3(v)$), which can't be in $CH_1(u)$, or channels that are secondary to all interferers in $\mathcal{N}(v)$ ($CH_2(v)$), which are secondary to u too since $u \in \mathcal{N}(v)$. □

Note that based on Lemma 5.1, if $\mathcal{N}(u)$ is the complete set of interferers of node u, u's transmissions on the channels from $CH_1(u)$ do not cause any interference to other on-going traffic.

THEOREM 5.1. *If $CH_1(u) \neq \emptyset$ holds for $\forall u \in V$ and $\mathcal{N}(u)$ is the complete set of interferers of u in the network $G(V, E)$, the channel assignment based on Algorithm 1 guarantees interference free communications in the network.*

PROOF. The theorem holds from Lemma 5.1. □

Theorems 5.1 indicates that if each node can compute a primary channel that is secondary to all its interferers based on Algorithm 1, interference-free communications in the whole network can be achieved. In the following, we identify another scenario to accomplish interference-free transmission.

LEMMA 5.2. *Given a node u with $CH_1(u) = \emptyset$ and $CH_2(u) \neq \emptyset$, if $CH_1(v_i) \neq \emptyset$ holds for all its interferers $v_1, v_2, \cdots, v_{|\mathcal{N}(u)|}$, node u's transmissions do not interfere with any other node in $\mathcal{N}(u)$.*

PROOF. Since $CH_1(u) = \emptyset$ and $CH_2(u) \neq \emptyset$, the set of channels assigned to u contains u's secondary channels that are secondary to all other nodes in $\mathcal{N}(u)$. If $CH_1(v_i) \neq \emptyset$ holds for all its interferers $v_1, v_2, \cdots, v_{|\mathcal{N}(u)|}$ in $\mathcal{N}(u)$, the set of channels assigned to v_i for $i = 1, 2, \cdots, |\mathcal{N}(u)|$ include v_i's primary channels only. Therefore, u's and its interferers' transmission channels do not overlap, and thus u's transmissions do not interfere with its interferers, and are not interfered by its interferers. □

Note that Theorem 5.1 does not place any restrictions on the size of the interferer set for any node. In the following, we prove that when $s \geq |\mathcal{N}(u)|$ holds for $\forall u \in V$ in the network $G(V, E)$, interference-free communication is guaranteed.

THEOREM 5.2. *If $s \geq |\mathcal{N}(u)|$ and $\mathcal{N}(u)$ is the complete set of interferers of u for $\forall u$ in G, the channel assignment based on Algorithm 1 guarantees interference free communications in the network.*

PROOF. Since $\mathcal{X}$ is an s-disjunct code, $BoolSum(\mathcal{X}(\mathcal{N}(u)))$ does not cover $X(u)$, which means that there exists at least one row in $\mathcal{X}$ at which $X(u)$ has the value 1 and all $\mathcal{X}(\mathcal{N}(u))$ have the value 0 (see Lemma 4.1). Therefore condition $CH_1(u) \neq \emptyset$ holds. Based on Theorem 5.1, the claim holds. □

Theorem 5.2 reports another condition for interference-free communications in the whole network based on Algorithm 1. In other words, if s upper-bounds the cardinality of the complete interferer set of each node in the network, interference-free communications can be achieved. This condition sounds very rigorous. However, for a stationary multi-radio multi-channel mesh network where the mesh routers can be carefully placed, the set of interferers could be small to provide sufficient coverage. In this scenario, channel assignment based on Algorithm 1 yields an interference-free network.

5.1.2 *Probabilities for interference-Free Channel Assignment*

Note that Lemma 5.1 and Lemma 5.2 report two conditions to achieve interference-free communications with no restrictions on the size of $\mathcal{N}(u)$. In this subsection, we conduct further analysis to derive the probabilities for interference-free channel assignment when $|\mathcal{N}(u)| > s$ based on Algorithm 1. In other words, we will study the probability that a node u can find out a channel to achieve interference-free communication in its local neighborhood when $s' > s$, where $s' = |\mathcal{N}(u)|$.

Let P_1 be the probability that Lemma 5.1 holds for some node u, and P_2 be the probability that Lemma 5.2 holds. Let $\mathcal{N}(u)$ be the complete set of interferers of node u. Under the protocol interference model, $\mathcal{N}(u) = N_2(u)$. We have

$$\begin{aligned} P_1 &= p(CH_1(u) \neq \emptyset), \quad (3) \\ P_2 &= p(CH_2(u) \neq \emptyset, CH_1(u) = \emptyset, \\ &\quad CH_1(v_i) \neq \emptyset, \forall v_i \in \mathcal{N}(u)) \\ &= p(CH_2(u) \neq \emptyset, CH_1(u) = \emptyset) \cdot \\ &\quad p(CH_1(v_i) \neq \emptyset, \forall v_i \in \mathcal{N}(u)) \\ &= p(CH_2(u) \neq \emptyset, CH_1(u) = \emptyset) \cdot \\ &\quad \prod_{i=1}^{|\mathcal{N}(u)|} p(CH_1(v_i) \neq \emptyset) \quad (4) \end{aligned}$$

The last two equalities hold because the channel codeword for each node is randomly and independently assigned. Based on Eq. (3) and (4), to compute P_1 and P_2, we need to first compute the probability that $CH_1(u) \neq \emptyset$ for $\forall u \in V$, and the probability that $CH_1(u) = \emptyset$ and $CH_2(u) \neq \emptyset$ hold simultaneously.

Let m be the number of rows in $BoolSum(\mathcal{X}(\mathcal{N}(u)))$ with a value 0. Given the condition $CH_1(u) \neq \emptyset$ or $CH_2(u) \neq \emptyset$, it implies that $m > 0$. Denote these m rows by $row_1, row_2, \cdots, row_m$. Let λ_{max} be the maximum row weight among $row_1, row_2, \cdots, row_m$. We have $t - s' - \lambda_{max} \geq 0$.

Note that the boolean sum $BoolSum(\mathcal{X}(\mathcal{N}(u)))$ can cover a codeword $X(v)$ in the set $\mathcal{X} \setminus \mathcal{X}(\mathcal{N}(u))$ **iff** $X(v)$ has a value 0 at all the m rows $row_1, row_2, \cdots, row_m$. Therefore, the probability that the boolean sum of $\mathcal{X}(\mathcal{N}(u))$ covers an arbitrary codeword $X(v)$ in $X \setminus \mathcal{X}(\mathcal{N}(u))$ is

$$\begin{aligned} p_{cover|m>0} &= \prod_{i=1}^{m} \frac{|\mathcal{X}| - s' - \lambda_{row_i}}{|\mathcal{X}| - s'} \\ &= \prod_{i=1}^{m} (1 - \frac{\lambda_{row_i}}{|\mathcal{X}| - s'}) \quad (5) \end{aligned}$$

Thus the probability that the boolean sum of $\mathcal{X}(\mathcal{N}(u))$ does not cover any arbitrary codeword $X(v)$ in the set $\mathcal{X} \setminus \mathcal{X}(\mathcal{N}(u))$ is

$$\begin{aligned} p_{uncover|m>0} &= 1 - p_{cover|m>0} \\ &= 1 - \prod_{i=1}^{m} (1 - \frac{\lambda_{row_i}}{|\mathcal{X}| - s'}). \quad (6) \end{aligned}$$

Based on the above analysis, we conclude that a good superimposed code for our channel assignment should have a larger s and larger row weights λ since the higher the probability $p_{uncover}$, the less interference our channel assignment causes. Methods of constructing superimposed (s, L, N)-codes have been extensively studied in [21] [23] [25] [26] [27] [28] [29] [30]. Ref. [31] reports some optimal designs to construct an s-disjunct code with different N, s, t.

Let $p(m > 0|\mathcal{N}(u))$ denote the probability that there exists at least one row with a value 0 in $BoolSum(\mathcal{X}(\mathcal{N}(u)))$. Assuming that each codeword in $\mathcal{X}$ is independent, we have

$$\begin{aligned} p(m > 0|\mathcal{N}(u)) &= 1 - p(m = 0|\mathcal{N}(u)) \\ &= 1 - \prod_{i=1}^{N} (1 - \frac{\binom{t-\lambda_i}{s'}}{\binom{t}{s'}}) \quad (7) \end{aligned}$$

Therefore the probability that $CH_1(u) \neq \emptyset$ is

$$p(CH_1(u) \neq \emptyset) = p(m > 0|\mathcal{N}(u)) \cdot p_{uncover|m>0} \quad (8)$$

Now let's compute the probability that both $CH_1(u) = \emptyset$ and $CH_2(u) \neq \emptyset$ hold. Based on the definition of m, $CH_2(u) \neq \emptyset$ and $CH_1(u) = \emptyset$ hold **iff** the Boolean sum $BoolSum(\mathcal{X}(\mathcal{N}(u)))$

covers the codeword $X(u)$ and $m > 0$. According to Eq.(5), the probability that node u can find a secondary channel for communication is

$$p(CH_2(u) \neq \emptyset, CH_1(u) = \emptyset) = p(m > 0|\mathcal{N}(u)) \cdot p_{cover|m>0} \quad (9)$$

For completeness, we provide the probability that a channel from $CH_3(u)$ is picked. Note that both $CH_1(u) = \emptyset$ and $CH_2(u) = \emptyset$ hold **iff** the boolean sum $BoolSum(\mathcal{X}(\mathcal{N}(u)))$ covers the codeword $X(u)$ and $X(u)$ cannot have a value 0 at any row of the m rows, namely $m = 0$. According to Eq.(7), the probability that $CH_1(u) = \emptyset$ and $CH_2(u) = \emptyset$ is

$$p(CH_1(u) = \phi, CH_2(u) = \phi) = p(m = 0|\mathcal{N}(u)) = \prod_{i=1}^{N}(1 - \frac{\binom{t-\lambda_i}{s'}}{\binom{t}{s'}}) \quad (10)$$

The probability that P_2 holds and the probabilities that u picks up a channel from $CH_1(u)$, $CH_2(u)$, and $CH_3(u)$ with respect to s' for the superimposed $(3, 1, 13)$-code of size 13 (Fig. 1) are illustrated in Fig. 2. Notice that when $s' \leq s$, Algorithm 1 guarantees to choose a channel from $CH_1(u)$ is 1.

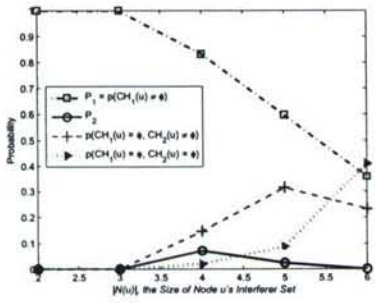

Figure 2: The probabilities that u picks up a channel from $CH_1(u)$, $CH_2(u)$, and $CH_3(u)$, respectively, and the probability that P_2 holds. Here $s = 3, t = N = 13$.

5.2 Channel Assignment for Broadcast Traffic

When a channel for broadcast is needed, we can apply Algorithm 1 directly. Let u be any node in a network $G(V, E)$. Let $\mathcal{N}(u)$ be the set of interferers of u. In the topology interference model, $\mathcal{N}(u)$ contains all two-hop neighbors of u, i. e. $\mathcal{N}(u) = N_2(u)$. Let $X(u)$ and $\mathcal{X}(N_2(u))$ be the codewords of u and its interferers. For broadcast channel assignment at node u the inputs to Algorithm 1 are $X(u)$ and $\mathcal{X}(N_2(u))$.

Note that Algorithm 1 does not care whether $\mathcal{N}(u)$ is a complete set of interferers or not. However, if $\mathcal{N}(u)$ is the complete set of interferers of u, and $|\mathcal{N}(u)| \leq s$ holds for $\forall u \in V$, broadcast does not cause any interference (see Theorem 5.2).

In reality, broadcast and unicast coexist. However, broadcast is inferior to unicast, as assumed by IEEE 802.11 standard. Therefore, when applying Algorithm 1 for broadcast channel assignment, u selects an unused channel in $CH_1(u) \neq \emptyset$ first. If fails, u picks up an unused channel in $CH_2(u) \neq \emptyset$. If no channels in $CH_1(u)$ and $CH_2(u)$ is available for u's broadcast, u picks up an unused primary channel from $CH_3(u)$.

5.3 Channel Assignment for Unicast Traffic

In this section, we consider the channel assignment for the unicast traffic from node u to node v, where u and v reside in each other's transmission range. In our consideration, it is u's responsibility to compute the channel for the link $(u \rightarrow v)$. For simplicity, we use $N(u)$ to denote $N_1(u)$, the one-hop immediate neighbor set of u. We have $u \in N(v)$ and $v \in N(u)$.

A simple idea would be to plug-in $X(u)$ and $\mathcal{X}(N(v)) \cup \{X(v)\}$ into Algorithm 1 to compute a channel for $(u \rightarrow v)$. However, since $\mathcal{X}(N(u))$ is available to u too, it is reasonable to use both $\mathcal{X}(N(u))$ and $\mathcal{X}(N(v))$ for $(u \rightarrow v)$ channel assignment. This is our motivation for designing Algorithm 2 for the unicast traffic from u to v. Note that in Algorithm 2 we consider $N(u)$ and $N(v)$ instead of $N_2(u)$ and $N_2(v)$ as the interferers for the unicast traffic from u to v. We will prove that the channel codewords from one-hop neighbors of both the sender and the receiver suffice for Algorithm 2 to achiever 100% throughput with a very simple scheduling algorithm.

Algorithm 2 Channel Assignment for unicast from u to v

Input: Codewords $\mathcal{X}(N(u))$, and $\mathcal{X}(N(v))$
Output: $CH(u \rightarrow v)$, a channel to the link from u to v.

1: **function** $CH(u \rightarrow v)$=**UnicastChannelSelect**($\mathcal{X}(N(u))$, $\mathcal{X}(N(v))$)
2: $CH_1(u) \leftarrow SelectAChannel(BoolSum(\mathcal{X}(N(v) \cup \{v\})) \oplus BoolSum(\mathcal{X}(N(v) \cup \{v\} \setminus \{u\})))$ ▷ Find a primary channel that is secondary to all nodes in $N(v) \cup \{v\} \setminus \{u\}$.
3: **if** $CH_1(u) \neq \emptyset$ **then**
4: $CH(u \rightarrow v) \leftarrow CH_1(u)$
5: **else**
6: $CH_2(u) \leftarrow SelectAChannel(\overline{BoolSum(\mathcal{X}(N(u) \cup \{u\}))} \bigwedge BoolSum(\mathcal{X}(N(v))))$ ▷ Find a secondary channel that is secondary to all nodes in $N(u) \cup \{u\}$ but primary to at least one node in $N(v)$.
7: **if** $CH_2 \neq \emptyset$ **then**
8: $CH(u \rightarrow v) \leftarrow CH_2(u)$
9: **else**
10: $CH_3(u) \leftarrow SelectAChannel(X(u) \bigwedge \overline{X(v)})$ ▷ Select a channel that is primary to u and secondary to v.
11: $CH(u \rightarrow v) \leftarrow CH_3(u)$
12: **end if**
13: **end if**
14: **end function**

The basic idea for Algorithm 2 is sketched below. Node u, the unicast source, first computes a channel that is primary to u but secondary to all nodes in $N(v) \cup \{v\} \setminus \{u\}$. In this case, the channel selected corresponds to a row with a value 1 in $X(u)$ and all 0's in $\mathcal{X}(N(v) \cup \{v\} \setminus \{u\})$. If this primary channel does not exist, u computes a channel that is secondary to all nodes in $N(u) \cup \{u\}$ but primary to at least one node in $N(v)$. If fails again, u picks up a primary channel that is secondary to v. As shown in Theorem 5.6, this channel selection criteria intends to minimize interference and accordingly maximize throughput.

The design motivation for Algorithm 2 is stated as follows. A node should utilize its primary channels if possible; Otherwise, it should choose a secondary channel that is secondary to all nodes in its closed neighborhood, but not secondary to all nodes in the receiver's neighborhood, since otherwise, the receiver may choose the same channel for its own unicast, causing interference.

Note that each node u runs a copy of Algorithm 2 to compute a channel k for the unicast link $(u \rightarrow v)$, where $v \in N(u)$. Therefore Algorithm 2 is a localized transmitter-oriented channel assignment algorithm.

5.3.1 *Interference Analysis*

An interesting problem is whether Algorithm 2 can compute an interference-free channel for u's transmission to v. Note that there are two different kinds of interferences for the unicast traffic: the direct interference caused by immediate neighbors and the indirect interference caused by the neighbors of the receiver. The first one results in the *exposed terminal problem* while the second one results in the *hidden terminal problem*.

The hidden and exposed terminal problems are well-known phenomenons in wireless networks due to the broadcast nature of the wireless media. For example, in Fig. 3, when node u is transmitting data to node v, the hidden terminal problem occurs when node x, which is unaware of the ongoing transmission, attempts to transmit, thus causing collision at node v. In Fig. 4, when node v is transmitting data to node u, the exposed terminal problem occurs when node x, which is aware of the ongoing transmission, refrains to communicate with y, thus causing degraded network throughput.

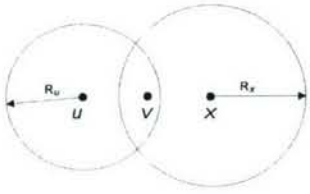

Figure 3: The hidden terminal problem in wireless networks.

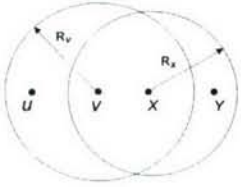

Figure 4: The exposed terminal problem in wireless networks.

In the following we prove that when the number of immediate neighbors of any node in the network is upper-bounded by s, the hidden/exposed problems can be solved and the network communication is free of interference. Note that in the following analysis, we assume that there is no broadcast traffic that can potentially interfere with the unicast traffic.

THEOREM 5.3. *Let u and v be any pair of immediate neighbors in the network $G(V, E)$. If $|N(w)| \leq s$ holds for $\forall w \in V$, Algorithm 2 yields* **hidden** *terminal interference-free channel assignment for the unicast traffic from u to v.*

PROOF. Let x be any hidden terminal, as shown in Fig. 3. We have $x \in N(v)$. Since $|N(v)| \leq s$, $|N(v) \cup \{v\} \setminus \{u\}| \leq s$. Therefore the Boolean sum of all codewords owned by $N(v) \cup \{v\} \setminus \{u\}$ does not cover the codeword of u due to the s-disjunct property of the superimposed code $\mathcal{X}$ used for channel assignment. Thus $CH_1(u) \neq \emptyset$ holds in Algorithm 2 and u can choose one of its primary channels that are secondary to all nodes in $N(v) \cup \{v\} \setminus \{u\}$. Let k be the channel selected by u for the unicast from u to v.

We claim that it is impossible for any node $x \in N(v) \cup \{v\} \setminus \{u\}$ to choose k for unicast based on Algorithm 2. Assume x needs a channel to unicast to y. Since $|N(y)| \leq s$, $CH_1(x) \neq \emptyset$. Therefore x will choose one of its primary channels that are secondary to all nodes in $N(y) \cup \{y\} \setminus \{x\}$ based on Algorithm 2. However, k is secondary to x since $x \in N(v)$. Therefore the unicasts from u to v and from x to y do not interfere since they use different channels.

Note that any node w in $N(u)$ but not in $N(v)$ may choose the same channel as that of u for unicast. But this unicast does not cause interference at v since v is out of w's transmission range. □

THEOREM 5.4. *Let v and u be any pair of immediate neighbors in the network $G(V, E)$. If $|N(w)| \leq s$ holds for $\forall w \in V$, Algorithm 2 yields* **exposed** *terminal interference-free channel assignment for the unicast traffic from v to u.*

PROOF. Let x be any exposed terminal to the unicast from v to u, as shown in Fig. 4. Let y be the destination of the unicast traffic from x. We have $x \in N(v)$, $x \notin N(u)$, and $y \notin N(v) \cup N(u)$. Thus the ACK from y to x does not reach v. For the same reason, the ACK from u to v does not reach x. Therefore, no matter which channels the links $(u \rightarrow v)$ and $(y \rightarrow x)$ receive from Algorithm 2, the two ACKs do not collide at v and x.

Since v and y are hidden with respect to x, based on Theorem 5.3,v and y choose different channels when $|N(w)| \leq s$ holds for $\forall w \in V$ in the network. Therefore, the ACK from y to x and the data from v to u do not collide at x. For the same reason, the ACK from u to v and the data from x to y do not collide at v.

Based on this analysis, Algorithm 2 yields **exposed** terminal-free channel assignment. □

Note that Theorems 5.3 and 5.4 hold when $|N(w)| \leq s$ for $\forall w \in V$ for a network $G(V, E)$. Assuming no interference caused by broadcast traffic (see Subsection 5.2), these two theorems indicate that Algorithm 2 yields interference-free communications in the network G when the maximum node degree (the number of one-hop neighbors) is $\leq s$.

THEOREM 5.5. *If $|N(w)| \leq s$ for $\forall w \in V$ holds for a network $G(V, E)$, Algorithm 2 yields interference-free communications in G.*

PROOF. Proof follows from Theorems 5.3 and 5.4. □

5.3.2 *Throughput Analysis*

It is interesting to observe that the induced graph of the edges being assigned the same channel via Algorithm 2 is a forest. Recent research [32, 33] indicates that with a simple scheduling algorithm (maximal weight independent set scheduling), a tree graph can achieve 100% throughput under the primary interference constraints. This result can be applied to analyze the achievable throughput via Algorithm 2.

Let's study Algorithm 2 again. It has the following nice feature:

LEMMA 5.3. *Let $(w \rightarrow u)$ and $(u \rightarrow v)$ be two adjacent edges in $G(V, E)$. Assume k_1 is the channel assigned to $(w \rightarrow u)$ and k_2 is the channel to $(u \rightarrow v)$ by Algorithm 2. We have $k_1 \neq k_2$.*

PROOF. Channels k_1 and k_2 are computed by w and u respectively. If $CH_1(w) \neq \emptyset$, $k_1 \in CH_1(w)$. Therefore k_1 is primary to w but secondary to $N(u) \cup \{u\} \setminus \{w\}$. In this case, since k_1 is secondary to u, $k_1 \notin CH_1(u)$ and $k_1 \notin CH_3(u)$. Also because k_1 is primary to w, k_1 can not be in $CH_2(u)$ since $w \in N(u)$ and all channels in $CH_2(u)$ are secondary to $N(u) \cup \{u\}$. Thus channel k_1 can not be selected by u for the edge $(u \rightarrow v)$ if $k_1 \in CH_1(w)$.

If $CH_1(w) = \emptyset$ and $CH_2(w) \neq \emptyset$, k_1 is selected from $CH_2(w)$ by w, which means that k_1 is secondary to all nodes in $N(w) \cup \{w\}$ but primary to at least one node in $N(u)$. Therefore k_1 can not be in $CH_2(u)$ since it contains channels secondary to all nodes in $N(u) \cup \{u\}$. $k_1 \notin CH_1(u)$ and $k_1 \notin CH_3(u)$ hold too since k_1

is secondary to u as $u \in N(w)$. Therefore channel k_1 can not be selected for the edge $(u \rightarrow v)$ if $k_1 \in CH_2(w)$.

If k_1 is selected from $CH_3(w)$, k_1 is primary to w and secondary to u, therefore $k_1 \notin CH_1(u)$ and $k_1 \notin CH_3(u)$. We claim that $k_1 \notin CH_2(u)$ too since otherwise k_1 would be secondary to w because $w \in N(u)$ and all channels in $CH_2(u)$ are secondary to the nodes in $N(u) \cup \{u\}$.

Therefor the channel k_1 assigned to the link $(w \rightarrow u)$ by Algorithm 2 could not be assigned to the link $(u \rightarrow v)$. We have $k_1 \neq k_2$. □

Note that the proof of Lemma 5.3 utilizes the fact that CH_3 is always non-empty. This is guaranteed by the following requirement on the channel codewords: for any two channel codewords $X(u)$ and $X(v)$, there exists two channels k_1 and k_2 such that k_1 is primary to u and secondary to v, and k_2 is primary to v and secondary to u.

COROLLARY 5.1. *Let k_1 and k_2 be the channels assigned to the edges $(u \rightarrow v)$ and $(v \rightarrow u)$, respectively, by Algorithm 2. Then $k_1 \neq k_2$.*

PROOF. Claim follows from Lemma 5.3. □

Corollary 5.1 indicates that the channels used for DATA and for ACK are always different. Lemma 5.3 indicates that two adjacent links can transmit DATA or ACK concurrently. Therefore, a multihop path can achieve maximum throughput in MR-MC networks since all nodes can transmit simultaneously without causing any collision.

Let $G_k(V, E_k)$ be the induced graph containing all edges receiving channel k based on Algorithm 2. We have

LEMMA 5.4. *For $\forall k \in C$, where C is the set of orthogonal channels, G_k is a forest.*

PROOF. For contradiction we assume that G_k is not a forest. In other words, G_k contains a circle $\mathcal{O}$. Consider any two adjacent edges $(w \rightarrow u)$ and $(u \rightarrow v)$ in $\mathcal{O}$. Based on Lemma 5.3, the channels assigned to $(w \rightarrow u)$ and $(u \rightarrow v)$ must be different. Therefore only one of them can appear in G_k. A contradiction to the assumption that $(w \rightarrow u)$ and $(u \rightarrow v)$ both appear in G_k. Thus no circle $\mathcal{O}$ exists in G_k. □

Lemma 5.3 indicates that each tree in G_k has a star-shaped topology[4], and the number of concurrent transmissions supported equals the total number of stars in all G_k.

COROLLARY 5.2. *Each tree in G_k is a star.*

PROOF. Proof follows from that of Lemma 5.3. □

COROLLARY 5.3. *The number of concurrent transmissions supported by the network equals the total number of stars in all G_k for all $k \in C$.*

PROOF. Since each star topology can support only one unicast at any time, claim follows. □

Brzezinski, Zussman, and Modiano [32] has proved the following lemma:

LEMMA 5.5. *A maximal weight independent set scheduling algorithm achieves 100% throughput for a tree network.*

[4]Since we consider directed links, this topology actually is a star-shaped DAG (Directed Acyclic Graph).

Therefore we have

THEOREM 5.6. *There exists a simple scheduling algorithm such that Algorithm 2 yields 100% throughput.*

PROOF. Proof follows from Lemma 5.4 and Lemma 5.5. □

Brzezinski, Zussman, and Modiano [32] presents multiple algorithms based on matroid intersection to partition the network into subnetworks with large capacity regions to maximize the throughput of each of the subnetwork. Algorithm 2, which is much simpler, maximizes the throughput if each node has a unique channel codewords satisfying the condition elaborated in Section 3.1.

5.3.3 *Simulation Study*

In this subsection, we conduct simulation to evaluate Algorithm 2 in terms of channel utilization and usage fairness. Our goal is to investigate: 1. the number of concurrent transmissions; 2. the channel usage fairness.

In the simulation we have considered an area of a 100×100 square units with 13 randomly deployed nodes. The simulation settings are listed as follows:

- All simulation results are averaged over 100 different topologies.
- The number of available channels in the network is set to $N = 13$.
- The superimposed $(3, 1, 13)$-code $\mathcal{X}$, as shown in Fig. 1, is applied in the simulation.
- Each node randomly picks a unique codeword from $\mathcal{X}$ as its channel codeword.
- The average node degree is denoted by d, where d varies from 2 to 6.
- The number of radios equipped by each node is denoted by Q, where $Q \in \{2, 4, 6, 8, 10, 12\}$. Q varies under different topologies.

Note that the number of channels utilized by a node can be measured by the number of concurrent transmissions supported by that node. Therefore for an arbitrary node u, we denote its channel utilization by the number of supported concurrent transmissions.

Fig. 5 describes the relationship among the number of concurrent transmissions supported by each node, the average node degree d, and the number of radios Q. For each settings of d and Q, the results are averaged on all the nodes in the network over 100 different topologies. As shown in Fig. 5, when the number of radios is fixed in the network, the smaller the average node degree, the larger the number of concurrent transmissions supported by each node. This is because the smaller the average node degree, the less number of interferers a node may have, namely the more number of channels available for concurrent transmissions.

When the average node degree is fixed, the larger the number of radios, the more the number of concurrent transmissions supported by each node. This result is intuitive since the number of concurrent transmissions is bounded by the number of radios in the network. Comparing the six curves in Fig. 5, we find that the smaller the number of radios, the smaller the number of concurrent transmissions supported by each node. We also find that when $d \leq s$ and Q is fixed, the number of concurrent transmissions supported by each node reaches its maximum, that is Q.

Fairness in channel usage is another important issue in wireless networks. Note that in our simulation study, the channel assignment matrix $\mathcal{X}$ has a constant column weight, which means that

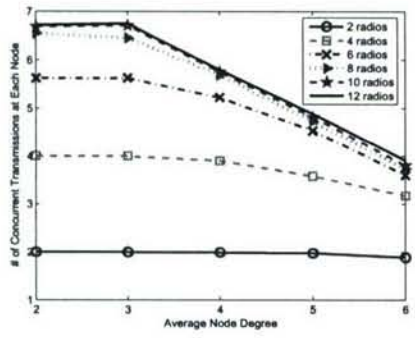

Figure 5: The average number of concurrent transmissions supported by each node.

each node in the network has the same numbers of primary channels and secondary channels. Since the channel codeword is picked randomly and independently for each node, intuitively the channel usage should be fair. This has been validated by our simulation result reported in Fig. 6.

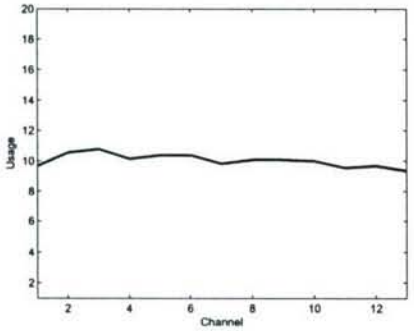

Figure 6: The channel usage of each channel when average node degree is 3.

6. DISCUSSION

6.1 Strength of Algorithms 1 and 2

Note that Algorithms 1 and 2 are both localized. They require the availability of the channel codewords from one or two-hop neighborhood, which results in low communication overhead since the binary codewords are short. In addition, both algorithms have low computation overhead since only simple Boolean algebraic is involved.

Algorithm 1 is generic. It is suitable for both unicast and broadcast traffic. As long as the codewords of the set of interferers are available, an interference-aware channel can be computed. Under certain conditions, this channel causes no interference.

The underlying design principle for unicast channel assignment (Algorithm 2) is the same as that of Algorithm 1: a node always selects a channel that causes the least interference to its neighborhood based on its current knowledge. With a simple scheduling algorithm, Algorithm 2 can achieve 100% throughput.

Neither of the two algorithms relies on the s-disjunct superimposed code, which is introduced to identify the scenarios when interference free communications are possible. However, if the channel codewords form an s-disjunct code, Algorithms 1 and 2 can compute a channel for better interference mitigation. In addition, the larger the s, the better the performance.

Both algorithms can be uploaded to the same node for broadcast and unicast channel computation. However, broadcast may be inferior to unicast, as in IEEE 802.11 standard. In this case, a channel has a higher priority to be assigned for unicast. If the probability of a channel being primary or secondary is the same for all nodes, the channel usage is fair.

Note that even though we assume the frequency channels in our discussion, both algorithms work with any kind of orthogonal channels: time slots, orthogonal codes, etc., as long as the channels can be labelled by a binary string indicating their primary and secondary roles to each node.

6.2 Superimposed Codes

The s-disjunct property elaborated in Lemma 4.1 plays a significant role in interference-free channel assignment. It is clear that the strength s should be strong and the size t should be large for a superimposed code $\mathcal{X}$ of length N to be applicable to a MR-MC network with N available orthogonal channels. Given N, computing a satisfiable superimposed s-disjunct code is non-trivial. As reported by D'yachkov and Rykov in [31], the following relationship of N, t, s, and λ_{max} holds.

LEMMA 6.1. *Let $t > \lambda_{max} > s \geq 1$ and $N > 1$ be integers.*

1. *For any superimposed $(s, 1, N)$-code of length N, size t, and maximum row weight λ_{max}:*

$$N \geq \lceil \frac{(s+1)t}{\lambda_{max}} \rceil \tag{11}$$

2. *If $\lambda_{max} \geq s + 2$, $(s + 1)t = \lambda_{max} N$, and there exists a superimposed $(s, 1, N)$-code $\mathcal{X}$ with size t and maximum row weight λ_{max}, then*

   - *Code $\mathcal{X}$ has a constant column weight $w = s + 1$, and a constant row weight $\lambda = \lambda_{max}$, and the maximal dot product of any two codewords in $\mathcal{X}$ is 1.*
   - *The following inequality holds true:*

$$\lambda^2 - \frac{\lambda(\lambda - 1)}{s + 1} \leq t \tag{12}$$

Note that for a superimposed $(s, 1, N)$-code, the upper bound of s is limited by N. Therefore s cannot be a large number if the number of available channels N in the network is small. However, this should not be a restriction on the application of superimposed codes in IEEE 802.16e based stationary MR-MC wireless mesh networks. The OFDMA technique in IEEE 802.16e [34] [35] allows bandwidth to be divided into many lower-speed sub-channels to increase resistance to multi-path interference. Typically a large number of non-overlapping orthogonal sub-channels are available for simultaneous transmissions. Therefore in this case, s can be large since N is large.

However, the non-overlapping channels in 802.11 standards are limited (3 non-overlapping channels in IEEE 802.11b/g; 12 non-overlapping channels in original IEEE 802.11a). Therefore s in 802.11-based wireless mesh networks is limited to some small number, which may affect the effectiveness of channel assignment.

A good news is that it is very likely that we still have disjunct property with more than s codewords. Let's introduce the definition for α-almost s-disjunct code proposed in [29] [36]: *A binary matrix*

is α-almost s-disjunct if for any randomly selected set of s columns, the probability that they cover no other column is at least α. In [29], authors proposed a study on a 3-disjunct superimposed code of size 30, where the number of codewords is much larger than s. The results indicate that this superimposed code is 0.95-almost 15 disjunct, and 0.6-almost 30 disjunct. This study tells us that a less powerful s-disjunct superimposed code could work well in our channel assignment.

6.3 Scalability Considerations

In superimposed codes, although t increases superlinearly compared to N [31], it is still a bounded number. Therefore, when applying a superimposed code in a MR-MC network, the network size is restricted because a superimposed code can only accommodate at most t nodes. To overcome this problem, we propose the following scalability enhancement.

As shown in Fig. 7, we map the network by cellular grids (regular hexagonal grids). The side length of each grid is R_{max}, where R_{max} is the maximum interference range a node can have in the network. Since the chromatic number of face coloring of such a graph is 3, the cellular grids of the network can be easily classified into 3 categories denoted by A, B, and C.

Given a superimposed $(s, 1, N)$-code $\mathcal{X}$, we evenly divide $\mathcal{X}$ into 3 subsets: t_A, t_B and t_C. Each subset exclusively contains about $1/3$ codewords of $\mathcal{X}$, representing a possible channel assignment for a grid category. For example, nodes belonging to the grids of category A are assigned channels based on t_A; nodes belonging to grids of category B are assigned channels based on t_B; and nodes belonging to grids of category C are assigned channels based on t_C, as shown in Fig. 7.

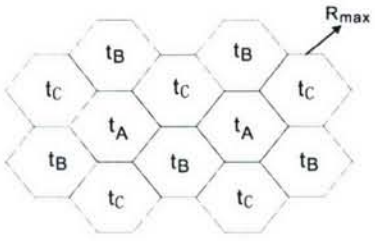

Figure 7: Channel assignment in a scalable network under a cellular grid topology.

Facilitated with a cellular grid topology, the network can scale to infinite size, though the superimposed $(s, 1, N)$-code has a bounded size t.

6.4 Applications to Mobile Mesh Networks

Since both algorithms are localized, and the communication overhead for a node to obtain the channel codewords from its neighborhood is low, channel assignment for mobile MR-MC wireless mesh networks can be easily supported. We will quantitatively study the performance of our algorithms in a mobile mesh network and test their support to popular mobile routing protocols in our future research.

6.5 Future Research

This paper presents our exploratory work toward capacity improvement in MR-MC mesh networks. We will study the performance of our algorithms in an mobile environment and test their capability of simultaneously supporting both unicast and broadcast. Additionally, we will design a MAC protocol based on these two algorithms to efficiently utilize the network resource for throughput maximization. Furthermore, we will explore the impact of channel codeword on the performance of channel assignment based on our algorithms.

7. CONCLUSION

In this paper, we have designed two localized channel assignment algorithms based on s-disjunct superimposed codes for multi-radio multi-channel wireless mesh networks. Our algorithms can effectively support channel allocation for both unicast and local broadcast since channels are pertained to transmitters instead of links even though the interferers at the destination affects channel selection. The selected channels are expected to cause low overall switching delay and low interference to the local neighborhood. In addition, we have identified the conditions when interference-free channel assignment can be achieved and when hidden/exposed terminal problems can be avoided. For unicast, our algorithm results in 100% network throughput with a simple scheduling algorithm. Since we do not make any assumptions on the underlying network settings such as traffic patterns and MAC/routing protocols, our channel assignment algorithms are applicable to a wide range of MR-MC mesh networks.

8. ACKNOWLEDGMENTS

The research of Xing, Cheng, and Ma is supported in part by the NSF CAREER award CNS-0347674. The research of Liang is supported in part by ONR under grant N00014-07-1-0395 and N00014-07-1-1024.

We are grateful to Dr. Lili Qiu, our shepherd, for her help in revising this paper. We are also grateful to the anonymous reviewers for their invaluable and constructive comments and suggestions.

9. REFERENCES

[1] P. Kyasanur and N. H. Vaidya, "Capacity of multi-channel wireless networks: impact of number of channels and interfaces," in *MobiCom '05: Proceedings of the 11th annual international conference on Mobile computing and networking*. ACM Press, 2005, pp. 43–57.

[2] G. Brar, D. M. Blough, and P. Santi, "Computationally efficient scheduling with the physical interference model for throughput improvement in wireless mesh networks," in *MobiCom '06: Proceedings of the 12th annual international conference on Mobile computing and networking*. ACM Press, 2006, pp. 2–13.

[3] M. Alicherry, R. Bhatia, and L. E. Li, "Joint channel assignment and routing for throughput optimization in multi-radio wireless mesh networks," in *MobiCom '05: Proceedings of the 11th annual international conference on Mobile computing and networking*. ACM Press, 2005, pp. 58–72.

[4] M. Kodialam and T. Nandagopal, "Characterizing the capacity region in multi-radio multi-channel wireless mesh networks," in *MobiCom '05: Proceedings of the 11th annual international conference on Mobile computing and networking*. ACM Press, 2005, pp. 73–87.

[5] A. P. Subramanian, R. Krishnan, S. R. Das, and H. Gupta, "Minimum-interference channel assignment in multi-radio wireless mesh networks."

[6] A. Raniwala, K. Gopalan, and T. cker Chiueh, "Centralized channel assignment and routing algorithms for multi-channel wireless mesh networks," *SIGMOBILE Mob. Comput. Commun. Rev.*, vol. 8, no. 2, pp. 50–65, 2004.

[7] A. Raniwala and T. Chiueh, "Architecture and algorithms for an ieee 802.11-based multi-channel wireless mesh network," in *IEEE Infocom*, 2005.

[8] M. K. Marina and S. R. Das, "A topology control approach for utilizing multiple channels in multi-radio wireless mesh networks," in *2nd International Conference on Broadband Networks*, 2005, pp. 381– 390.

[9] P. Kyasanur and N. H. Vaidya, "Routing and link-layer protocols for multi-channel multi-interface ad hoc wireless networks," *SIGMOBILE Mob. Comput. Commun. Rev.*, vol. 10, no. 1, pp. 31–43, 2006.

[10] B.-J. Ko, V. Misra, J. Padhye, and D. Rubenstein, "Distributed channel assignment in multi-radio 802.11 mesh networks," in *Wireless Communications and Networking Conference (WCNC)*, 2007, pp. 3978–3983.

[11] K. N. Ramachandran, E. M. Belding, K. C. Almeroth, and M. M. Buddhikot, "Interference-aware channel assignment in multi-radio wireless mesh networks," in *Infocom*, 2006.

[12] H. Skalli, S. K. Das, L. Lenzini, and M. Conti, "Traffic and interference aware channel assignment for multi-radio wirelesss mesh networks," in *Technical Report*, 2006.

[13] J. So and N. H. Vaidya, "Multi-channel mac for ad hoc networks: handling multi-channel hidden terminals using a single transceiver," in *MobiHoc '04: Proceedings of the 5th ACM international symposium on Mobile ad hoc networking and computing*. ACM Press, 2004, pp. 222–233.

[14] S.-L. Wu, C.-Y. Lin, Y.-C. Tseng, and J.-P. Sheu, "A new multi-channel mac protocol with on-demand channel assignment for multi-hop mobile ad hoc networks," in *ISPAN '00: Proceedings of the 2000 International Symposium on Parallel Architectures, Algorithms and Networks (ISPAN '00)*. IEEE Computer Society, 2000, p. 232.

[15] P.Kyasanur and N.H.Vaidya, "Routing and interface assignment in multi-channel multi-interface wireless networks," in *Wireless Communications and Networking Conference, 2005 IEEE*, vol. 4, 2005, pp. 2051–2056.

[16] P. Bahl, R. Chandra, and J. Dunagan, "Ssch: slotted seeded channel hopping for capacity improvement in ieee 802.11 ad-hoc wireless networks," in *MobiCom '04: Proceedings of the 10th annual international conference on Mobile computing and networking*. ACM Press, 2004, pp. 216–230.

[17] A. A. Bertossi and M. A. Bonuccelli, "Code assignment for hidden terminal interference avoidance in multihop packet radio networks," *IEEE/ACM Trans. Netw.*, vol. 3, no. 4, pp. 441–449, 1995.

[18] J. Garcia-Luna-Aceves and J. Raju, "Distributed assignment of codes for multihop packet-radio networks," in *Milcom '97: Proceedings of the 1997 Military Communications Conference*. IEEE Computer Society, 1997, pp. 450–454.

[19] W. H. Kautz and R. C. Singleton, "Nonrandom binary superimposed codes," in *IEEE Trans. Inform. Theory*, vol. IT-10, 1964, pp. 363–377.

[20] D. Du and F. Hwang, "Combinatorial group testing and its applications," *2nd Edition, World Scientific*, 2000.

[21] A. E. F. Clementi, A. Monti, and R. Silvestri, "Selective families, superimposed codes, and broadcasting on unknown radio networks," in *SODA '01: Proceedings of the twelfth annual ACM-SIAM symposium on Discrete algorithms*. Society for Industrial and Applied Mathematics, 2001, pp. 709–718.

[22] D. Stinson, T. van Trung, and R. Wei, "Secure frameproof codes, key distribution patterns, group testing algorithms and related structures," in *Journal of Stat. Planning and Inference*, vol. 86, no. 2, 2000, pp. 595–617.

[23] P. Indyk, "Deterministic superimposed coding with applications to pattern matching," in *FOCS '97: Proceedings of the 38th Annual Symposium on Foundations of Computer Science (FOCS '97)*. IEEE Computer Society, 1997, p. 127.

[24] S. Chaudhuri and J. Radhakrishnan, "Deterministic restrictions in circuit complexity," in *STOC '96: Proceedings of the twenty-eighth annual ACM symposium on Theory of computing*. ACM Press, 1996, pp. 30–36.

[25] A. D. Bonis and U. Vaccaro, "Constructions of generalized superimposed codes with applications to group testing and conflict resolution in multiple access channels," in *Theoretical Computer Science 306*, vol. 1, no. 3, 2003, pp. 223–243.

[26] A. D'yachkov, V. Lebedev, P. Vilenkin, and S. Yekhanin, "Cover-free families and superimposed codes: Constructions, bounds, and applications to cryptography and group testing," in *IEEE International Symposium on Information Theory*, 2001.

[27] D. Danev, "Some constructions of superimposed codes in euclidean spaces," *Discrete Appl. Math.*, vol. 128, no. 1, pp. 85–101, 2003.

[28] A. D. yachkov, A. M. Jr, and V.V.Rykov, "New constructions of superimposed codes," in *Information Theory, IEEE Transactions on*, vol. 46, no. 1, 2000, pp. 284–290.

[29] D. C. Engelhart and A. Sivasubramaniam, "Almost disjunct codes in large scale multihop wireless network media access control," in *MASCOTS '05: Proceedings of the 13th IEEE International Symposium on Modeling, Analysis, and Simulation of Computer and Telecommunication Systems*. IEEE Computer Society, 2005, pp. 453–463.

[30] A. J. Macula, "A simple construction of d-disjunct matrices with certain constant weights," *Discrete Math.*, vol. 162, no. 1-3, pp. 311–312, 1996.

[31] A. G. D'yachkov and V. V. Rykov, "Optimal superimposed codes and designs for renyi's search model," *Journal of Statistical Planning and Inference*, vol. 100, no. 2, pp. 281–302, 2002.

[32] A. Brzezinski, G. Zussman, and E. Modiano, "Enabling distributed throughput maximization in wireless mesh networks - a partitioning approach," in *MobiCom '06: Proceedings of the 12th annual international conference on Mobile computing and networking*. ACM Press, 2006, pp. 26–37.

[33] A. Dimakis and J. Walrand, "Sufficient conditions for stability of longest queue first scheduling: Second order properties using fluid limits," *Advances of Applied Probability*, vol. 38, no. 2, pp. 505–521, 2006.

[34] "Wimax/802.16 revealed." [Online]. Available: http://www.wi-fiplanet.com/tutorials/article.php/3550476

[35] "What is ieee 802.16e." [Online]. Available: http://www.wimax.com/education/faq/faq45

[36] A. J. Macula, V. V. Rykov, and S. Yekhanin, "Trivial two-stage group testing for complexes using almost disjunct matrices," *Discrete and Applied Mathematics*, vol. 137, pp. 97–107, 2004.